

Advanced course on low-pressure plasmas : technology and applications, Eindhoven University of Technology, Eindhoven, the Netherlands, June 26-28, 1985 : lecture notes

Citation for published version (APA):

Massee, P., & Merck, W. F. H. (1985). *Advanced course on low-pressure plasmas : technology and applications, Eindhoven University of Technology, Eindhoven, the Netherlands, June 26-28, 1985 : lecture notes*. Eindhoven University of Technology.

Document status and date:

Published: 01/01/1985

Document Version:

Publisher's PDF, also known as Version of Record (includes final page, issue and volume numbers)

Please check the document version of this publication:

- A submitted manuscript is the version of the article upon submission and before peer-review. There can be important differences between the submitted version and the official published version of record. People interested in the research are advised to contact the author for the final version of the publication, or visit the DOI to the publisher's website.
- The final author version and the galley proof are versions of the publication after peer review.
- The final published version features the final layout of the paper including the volume, issue and page numbers.

[Link to publication](#)

General rights

Copyright and moral rights for the publications made accessible in the public portal are retained by the authors and/or other copyright owners and it is a condition of accessing publications that users recognise and abide by the legal requirements associated with these rights.

- Users may download and print one copy of any publication from the public portal for the purpose of private study or research.
- You may not further distribute the material or use it for any profit-making activity or commercial gain
- You may freely distribute the URL identifying the publication in the public portal.

If the publication is distributed under the terms of Article 25fa of the Dutch Copyright Act, indicated by the "Taverne" license above, please follow below link for the End User Agreement:

www.tue.nl/taverne

Take down policy

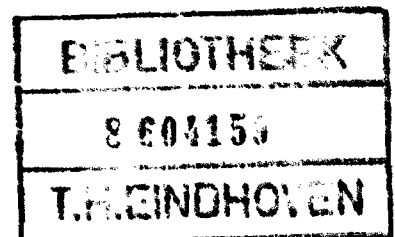
If you believe that this document breaches copyright please contact us at:

openaccess@tue.nl

providing details and we will investigate your claim.

**ADVANCED COURSE ON
LOW-PRESSURE PLASMAS
TECHNOLOGY AND APPLICATIONS**

**EINDHOVEN UNIVERSITY OF TECHNOLOGY
EINDHOVEN, THE NETHERLANDS
JUNE 26-28, 1985**



LECTURE NOTES

VOLUME 1

EDITED BY P. MASSEE and W.F.H. MERCK

Address of the editors:

Massee/Merck
Department of Electrical Engineering
Division EG
Eindhoven University of Technology
P.O. Box 513
5600 MB Eindhoven, The Netherlands.

© EINDHOVEN UNIVERSITY OF TECHNOLOGY

All right reserved. No part of this publication may be reproduced or used in any form or by any means - graphic, electronic or mechanical, including photocopying, recording, taping or information storage and retrieval systems - without the prior, written permission of the editor.

CIP-GEGEVENS KONINKLIJKE BIBLIOTHEEK, DEN HAAG

Advanced

Advanced course on low-pressure plasmas: technology and applications. Eindhoven, the Netherlands, June 26-28, 1985. Lecture notes. Vol. 1. / ed. by P. Massee and W.F.H. Merck. - Eindhoven: University of Technology. -
Fig., tab
Met lit. opg., reg.
ISBN 90-6144-998-7
SISO 655.7 UDC 533.9:621.794 UGI 650
Trefw.: plasmatechnologie.

Table of Contents

	page
1. Plasma technology-Introduction (D.C Schram)	1-1
2. Basics of gas discharges (A.J. van Roosmalen and C.A.M. de Vries)	2-1
3. Plasma chemistry and physics (D.L. Flamm)	3-1
4. Plasma-wall interactions (P.C. Zalm)	4-1
5. Basics of reactor design (C.A.M. de Vries and A.J. van Roosmalen)	5-1
6. Diagnostics for research and application	
6.1. Surface and thin film analysis (P.C. Zalm)	6.1-1
6.2. Mass spectroscopy (G. Turban)	6.2-1
6.3. Optical spectroscopy (J.P.M. Schmitt)	6.3-1
7. Survey of applications in plasma etching and plasma deposition (G.K. Herb)	7-1
8. Surface treatments and plasma polymerization (J. Amouroux)	8-1

1. PLASMA TECHNOLOGY - INTRODUCTION

Dr. Daniel C. Schram, Professor of Physics at the Eindhoven University of Technology, The Netherlands. His principal interests range from low density plasmas as used in plasma etching, plasma deposition, moderately dense magnetized plasmas, to high density (super) atmospheric arc physics.

Plasma as a medium for processing

Daniel C. Schram
 Department of Physics, Eindhoven University of Technology,
 Eindhoven, The Netherlands

A general introduction to two subsequent plasmacourses:

1. Course on thermal plasmas
2. Course on low pressure plasmas

1. Introduction

Plasmas are increasingly used for processes to modify surfaces, for chemical processing, and to cover surfaces with specific layers. To illustrate the specific use of plasmas we will first briefly list several applications, and to arrive at some specific characteristic features of plasma processing.

1.a. Examples of plasma treatments

The applications can be roughly divided into three classes:

- 1.a.1. Volume chemistry
- 1.a.2. Surface modification
- 1.a.3. Heating and acceleration of particulate matter

1.a.1. In Volume Chemistry the plasma is used to enhance the reactivity in the medium. In normal chemistry this is achieved by increasing the temperature and pressure. As a consequence particles with a higher energetic state are produced, which serve as intermediate in the chemical reaction. If the chemical process is exothermic, then energy is produced whence the reactions are started and the temperature is kept high by the process itself. In this case the initial temperature rise is only required to start the process which can be explosive if the energy input by the reactions is larger than the energy loss. A pertinent example is the diesel-engine.

In endothermic processes energy has to be added to compensate for the increase in internal energy and for the energy loss.

In these processes the reactivity of the medium can be determined on the basis of chemical equilibrium considerations, a situation which is usually not present in plasma chemistry. Here, the reactivity of the medium is artificially enhanced above the level at the prevailing heavy particle temperature by the use of a discharge. A pertinent example is the production of ozone in ozone-synthesis apparatus. A well known method is the use of a (negative) corona discharge.

It will be clear, that here the emphasis will be to reach a high specific reactivity, i.e. reactivity per unit volume at a minimum of electrical energy. The reactivity can be characterized by the number density of radicals. A radical is defined as a particle which has a larger internal energy than the gas particles present at normal conditions.

So, in this definition the nitrogen atom: N is a radical in a nitrogen molecules gas. Other examples are oxygen atoms, nitrogen oxide NO, etc. in air atmosphere.

The number density, i.e. the number of particles per unit volume, of radicals is directly related to the specific reactivity of the medium. If this number density is not in chemical equilibrium then kinetic models have to be used to calculate the reactivity of the medium.

1.a.2. The second application area is surface modification. Here the surface of a substrate is modified. Reasons may be deposition and etching of several layers of different materials on substrates, the alteration of the surface to allow adhesion, the hardening of surface layers and to improve corrosion resistance of the substrate. In many of these applications it is essential that the temperature of the substrate can be controlled and be much lower than the temperature needed for the reaction. So the plasma serves here to provide the reactive gases and so to promote the chemical reaction on the surface whereas the substrate may remain cold. We will list here several examples of such surface modifications.

- cleaning of the surface

It can be important to release from the surface adsorbed gases and to remove any impurities from the surface. This can be achieved by using plasmas, in the so-called discharge cleaning technique. Usually the surface to be cleaned forms a part of an electrode; if it is an isolator a RF discharge is advantageous. Depending in the application the process effectivity can be varied, by proper choice of power density in the plasma and the employed filling pressure.

- wetting of the surface

For some applications it may be necessary to provide a wettability of a surface made of smooth material. This may be necessary for writing (bank cards) or to improve adhesive properties.

etching

Another important technique of this second class is the so called dry etching of surfaces. This is an attractive alternative for the wet etching techniques and has several additional features. An important advantage is the possibility of anisotropic etching, i.e. vertical etching and no horizontal etching. Another important item is the selectivity of the etching process. One substance must be etched (e.g. SiO_2) whereas the other exposed substances must remain intact (e.g. photoresist, Si). Both items are of great relevance in (sub)micron technology.

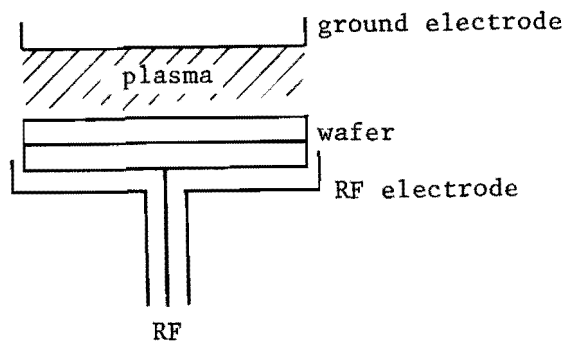


Fig.1. Schematic view of a single wafer etch apparatus

deposition

With plasmas it is also possible to deposit layers of all kind of materials on substrates. Plasma assisted chemical vapour deposition (PACVD) may be a good alternative to the well known chemical vapour deposition (CVD)-methods. Advantages are controllable substrate conditions, pressure, large freedom in choice of materials. Also the morphology of the layer can be influenced by the plasma and substrate conditions. Amorphous hydrogenated, polychrystalline etc. are possible. This technique is also of significance for sub-micron technology. Other important applications are a.o. solar cell fabrication, single mode glasfiber production (with profiled index of refraction), corrosion- and wear resistant layers.

polymerization

A related process is the procurement of layers of polymers. With appropriate materials and under specific conditions polymerization at the surface takes place during the deposition process. A polymer layer is the result. These techniques are a.o. being used in the optical and electronic industry.

boriding, carbonizing, nitriding

With the diffusion of several kinds of atoms into the surface of a substrate its surface properties can be changed. Well known examples are the hardening of steel by carbon or nitrogen. Also here plasma assisted techniques offer an attractive alternative for convential technologies.

They also have the advantage of a clean process.

"Ionitriding", i.e. nitriding by plasmas, is already used a long time. By the availability of new plasma techniques, the larger freedom of choice of materials and by conditioning, also here a further development is to be expected.

General features of surface modification processes are: the fluxes of radicals, atoms and ions to the surface, the relation of these fluxes to the number densities in the

plasmas and the discharge parameters. Also the surface condition, the absorbed layers, surface damage, are pertinent problems in this area.

Often limits are imposed to the fluxes of particles which eventually determine the rates of the processes, deposition rates, etching rates. This may be related to the surface conditions and adsorbed layers, to induced photon-damage or to the demand of anisotropy of the process.

1.a.3. Surface covering, joining, cutting, wetting.

In this third subclass of plasma processing the plasma is primarily used to provide heat and momentum. The reactive properties are of less importance; the plasma is a source of heat, to melt the material.

Plasmaspraying is one of the major applications here.

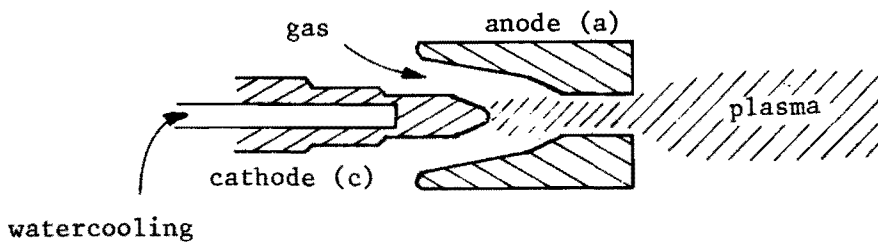


Fig.2. Schematic view of a plasma gun used for plasmaspraying

In the plasma gun, gas (argon with hydrogen, nitrogen) is ionized, heated and accelerated. In the resulting plasmajet with temperatures in excess of 10.000 K and velocities of 400 m/sec, spray particles are introduced.

These particles are accelerated and heated to the melting temperature during the distance to the substrate. They are finally splashed onto the surface and adhere by subsequent processes in the droplet and substrate. At first sight this process resembles plasma deposition, but it is quite different in procedure, process and result. In plasma deposition the layer is deposited atom by atom, whereas in plasmaspraying particulate matter of typically 50 μ size is sprayed as a whole on the surface.

Plasmamelting is another important example. Here plasmaguns are used which are similar in principle to the one described above. Again heat is used to melt the material and momentum is used to transport the energy away from the source. Other examples are plasma cutting, welding.

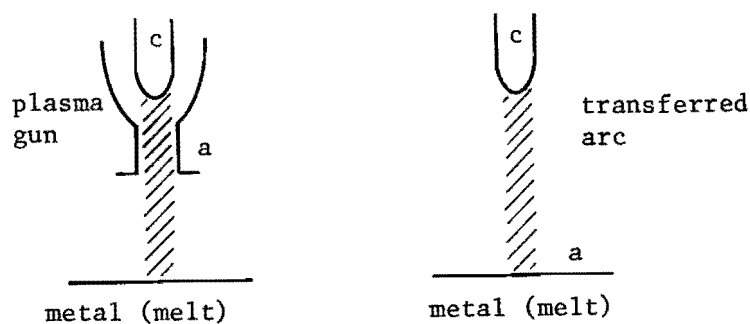


Fig.3. Schematic view of a plasma gun and a transferred arc used for plasma melting.

Another related area is plasma spectrochemical analysis. Here there is a chemical use of the internal energy of the plasma for the ionization and excitation of the

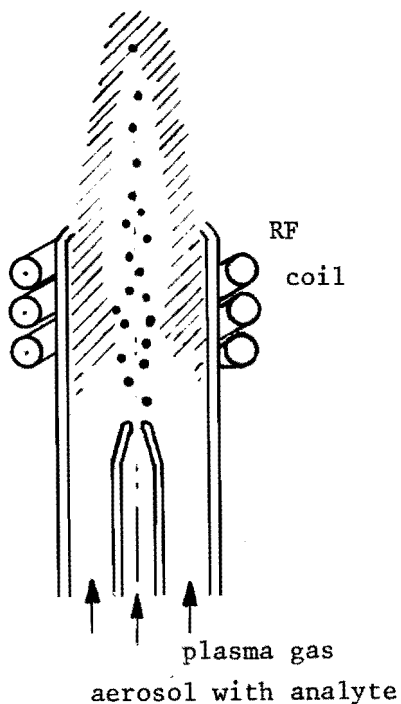
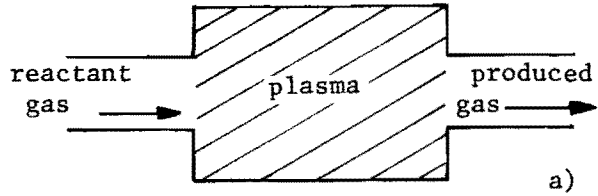


Fig.4. Schematic view of an ICP plasma used for spectrochemical analysis.

material to be analysed. However, the relative content of the sample in the plasma is small and the primary use of the plasma is again as a source of energy and momentum. One of the most important designs is the so-called Inductively Coupled Plasma (ICP). This has the advantage of clean operation and is also potentially useful for preparational techniques as plasma deposition.

To summarize, we have:

1.a.1. Volume chemistry



important parameters: Fig.5a

- volume of the plasma
- specific plasma reactivity
 - number density of radicals
 - (a.o. free atoms, ions, electrons)
- flow, throughput

1.a.2. Surface modification

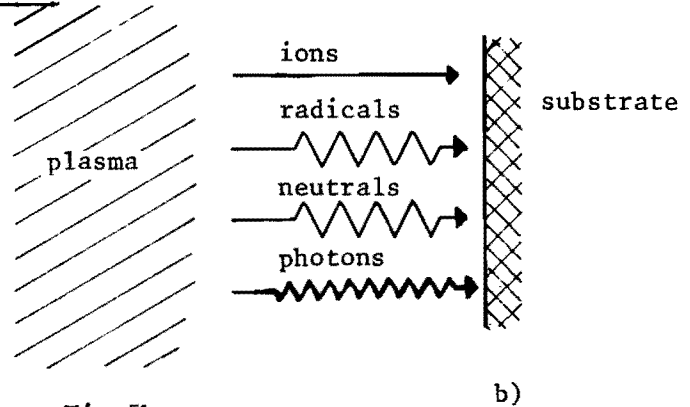


Fig.5b

- fluxes to substrate
- directionality of ion fluxes
- determined by power, pressure, flow

1.a.3. Surface covering and melting

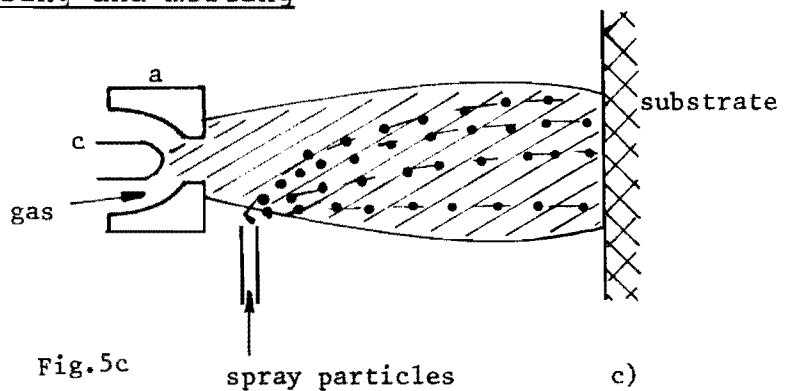


Fig.5c

- energy flow/content
- temperature
- momentum/velocity
- determined by power, pressure, flow

1.b. Why the use of plasmas

From the quoted examples of plasma treatments it is evident that the primary reason of the use of plasmas is the provision of a high temperature. Of course a high temperature does not necessarily require a plasma. In fact usually the plasma is electrically heated and this may not be the cheapest form of

energy.

Special advantages accompany the use of plasmas; generally plasma processing can be done in relatively small units without increasing the price significantly. More important is the large specific reactivity achievable in plasmas. This relates as well to reactivity per unit volume as per particle (atom or molecule). The reactivity is usually determined by the electron temperature, T_e , which does not need to be in equilibrium with the heavy particle temperature. In most discharges T_e is in the range of a few eV* ($1\text{eV} \Delta 11.600\text{ K}$), whereas the heavy particle, or gas temperature is close to ambient temperature. Even though, particularly at low pressure, the system is not in chemical equilibrium, the reactivity is appreciably higher than the one of a gas at the gas temperature. So even though the reactivity is usually lower than the one in chemical equilibrium at the electron temperature, the reactivity is very large since T_e is high. This is probably the most pertinent advantage of the use of a plasma.

This feature enables one to have a high reactivity without necessarily the associated bulk heat content of a system in chemical equilibrium. The background gasparticles which may be the majority may have a low temperature and also the density of the background gas can be low. The latter has a definite side advantage for e.g. deposition where the ambient pressure may be an important parameter.

Another related quality of plasma assisted methods is, that the temperature of the substrate to be treated or covered can be low. An independent variation and control of the substrate temperature is of importance to improve the quality of the product, e.g. the adhesion of deposited layers.

A definite advantage of plasmas is the large freedom of choice of materials. The easiest form of introduction of the desired materials is in gaseous form and though there are limitations here still a large variety is possible. But the material can also be introduced as a liquid in droplets or aerosols, or as a solid by sputtering or vaporization.

A lot of attention is paid to the material efficiency in plasma processing.

In some cases hazardous or environmentally problematic materials and/or products have to be dealt with. Then the high reactivity per particle (atom or molecule) is an advantage as this tends to improve the material efficiency and to reduce environmental waste production. However, as the plasma is a nonequilibrium system careful modelling and testing is required to optimize the system also for this aspects.

Finally the achievable quality of the product is one of the major reasons to use plasma assisted technologies. Again, to optimize, skillful handling and careful treatment on the basis

*The unit eV is commonly used in plasmachemistry.
 $1\text{eV} \Delta 11.6000\text{ Kelvin}$. The unit eV can also be used
 as energy unit; then it is aequivalent to $1.6 \cdot 10^{-19}$ Joule

of models and diagnosis helps to obtain the best achievable quality.

In the subsequent lectures one will touch in detail many of the mentioned aspects of plasma treatments.

1.c. Plasma appearances

Depending on the power density absorbed by the plasma, on the type gas used and on the discharge geometry the plasma appearance shows a wide variety. The type of gas is of great influence as the atomic and molecular processes depend on it. As electrons and ions must be produced by ionization it is evident that ionization potential, and the reaction rates for these processes determine partly the plasmaparameters and the plasmacomposition. As loss of electrons has to be compensated for by sufficiently fast production a minimum electron temperature is required. A reasonably first guess for this important quantity is 1/4 of the ionization potential at low pressures down to 1/10 or lower at high pressures.

As the ionization potential differs for many gases also T_e will vary. In part also dependent on the power density are the electron density, n_e , and the ionization degree, n_e/n_g here defined as the ratio of electron density and gas density, n_g . In the second section we will argue that characterization of the plasma by n_e and n_e/n_g is a good guide in plasma chemistry.

Other important factors which determine the plasma appearance are the discharge geometry and the way the power is applied to the plasma. We will limit ourselves here to electrical discharges. One can distinguish between DC, RF and microwave discharges.

Tabel 1.

		typical values for			
D.C. discharges	type	current density	n_e	n_e/n_g	p
	Townsend discharge	10^{-1} A/m ²	10^{14} /m ³	10^{-7}	around 10^{-3} at
	positive column normal glow	10 A/m ²	10^{17} /m ³	10^{-4}	
	abnormal glow	10^3 A/m ²	10^{18} /m ³	10^{-3}	
	medium pressure arc	10^6 A/m ²	10^{19} /m ³	10^{-2}	
	atmospheric arc	10^7 A/m ²	10^{23} /m ³	1	
	Penning discharge	10^4 A/m ²	10^{18} /m ³	10^{-3}	10^{-1} Torr
	magnetron discharge	10^4 A/m ²	10^{18} /m ³	10^{-4}	1 Torr
	magnetized arc	10^6 A/m ²	10^{20} /m ³	1	10^{-3} Torr

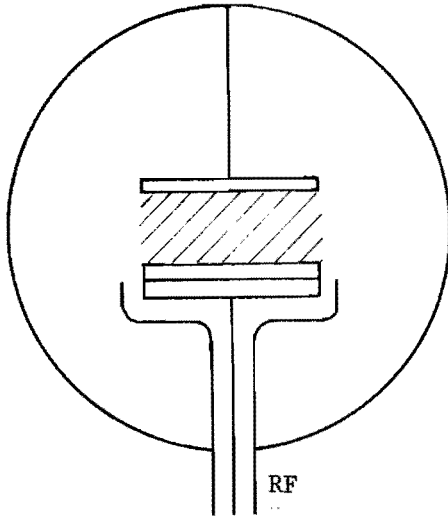
Electrode design is very important and needs much attention.

RF discharges

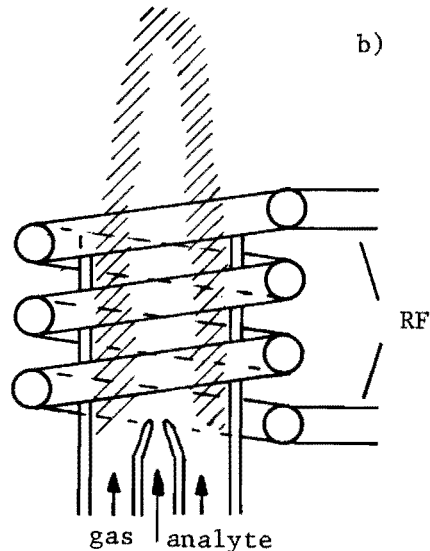
RF plasmas depend primarily on the applied frequency; one uses low frequencies (10kHz - 1MHz), intermediate frequencies

(13.6, 27.2, 54.4 MHz) and ultra high frequencies (UHF; ~ 100 MHz and higher).

At lower and intermediate frequencies usually capacitive coupling is employed. RF discharges have the advantage above D.C. plasmas, that also insulating substrates can be treated.



a)



b)

Fig.6a. Capacitive coupling
(single wafer etcher)

Fig.6b. Inductive coupling
(ICP-plasma)

In fact, potentials are built up which are important for directional (anisotropic) etching. The potential can be varied within certain limits by variation of the discharge geometry, e.g. larger or smaller electrodes, pressure and power.

At intermediate and higher frequencies also inductive coupling is employed. As shown in fig.6b it can be constructed such that the plasma is only bounded by glasswalls.

This enables very low levels of impurities as metals (smaller than ppB) which makes it suitable for plasmaspectrochemistry and for critical preparative applications.

Also microwave plasmas are used. They also can be dimensioned such that no metal walls surround the plasma. They usually burn stable and show somewhat higher electron densities than comparable RF discharges.

Finally, the corona discharge should be mentioned as a special case. At one electrode, field amplification is achieved by using either sharp needles or thin wires with very small radii of curvature. At that electrode rather high field strength exist, also because a large potential difference is applied (several kV).

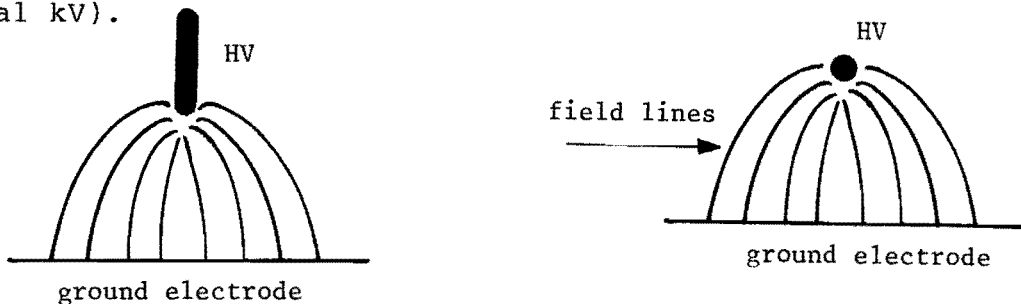


Fig.7. Corona geometries: a) point-plate, b) wire plate.

The needle or wire can be either positive or negative (resp. positive and negative corona). In the latter one a repetitive discharge may exist (the so-called trichel pulses) especially in electronegative gases. In coronas large spatial and temporal variations in plasma density occur and these plasmas are difficult to classify.

Finally, the influence of the chemical processes, either in the volume or at the wall should be mentioned. They may influence the composition, the electron temperature, and give rise to negative ion formation. Also the importance of electrodes has already been referred to; it is also an important item in reliability considerations.

1.c.2. Some essential characteristics

It will be clear from the foregoing that a primary feature of plasmas is the presence of charged particles. As ionization in the majority of cases is primarily induced by electron collisions, electrons are the key characteristic even in very weakly ionized gases. It has already been stated that the presence of electrons leads to all kind of radicals, whose densities can be even higher than n_e . This leads to a large reactivity. Chemical equilibrium is by no means assured; only in high pressure, high power density plasmas the system may be close to local thermodynamic equilibrium (LTE), i.e. the system may be defined by only two thermodynamic variables. But as said, this is more an exception than a rule.

Another characteristic is that plasmas tend to maintain charge neutrality, i.e. to keep the positive charge density (ions) equal to the negative charge density (electrons and sometimes negative ions). Only in a layer adjacent to the wall a substantial electric field strength may be built up caused by very small excess of positive charges in the discharge. Hence, the name quasi neutrality is used:

$$n_e = n_+ \quad (1)$$

but large electric fields may exist in the sheaths because of a small unbalance. Another way to illustrate this, is to follow in time the evolution of a plasma.



Fig. 8. Ambipolar diffusion.

Imagine the charged particles to diffuse freely and independent. Because of the small electron mass and high mobility, electrons tend to diffuse faster out of the discharge than the colder and much heavier ions. Then even a small unbalance, a deficit of electrons, leads immediately to large positive space charges which hampers the electron

diffusion and helps the ion diffusion. This process continues up to the point when ions and electrons diffuse together, the so called ambipolar diffusion. Only in the sheath adjacent to the wall a strong unbalance in electron and ion densities can occur. The thickness of this sheath is related to the Debye shielding length, defined as:

$$\lambda_{DC} = \sqrt{\frac{\epsilon_0 k T_e}{n_e e^2}} \approx 7.10^3 \sqrt{\frac{\hat{T}_e \text{ (eV)}}{n_e}} \approx \frac{10^4}{\sqrt{n_e}} \quad (2)$$

Typical values are 100 μm for low density plasmas and .1 μm for very high density plasmas.

This sheath with associated potential difference which may accelerate ions to the wall is very important for plasma processing. It is an essential factor in the unidirectionality of plasma etching.

2. Plasma characterization

It has been clear from the foregoing that plasmas can appear in a large variety. The particular application of the plasma medium will determine which plasma parameters and which geometry and excitation is most appropriate. In the two subsequent courses several application areas will be covered, so here only a few general remarks will be made.

One of the most important parameters is the electron temperature T_e . For low ionization degrees, $\alpha = n_e/n_g < 10^{-2}$ significant deviations from Maxwell Boltzmann distributions may occur and it is better to use a average electron energy $\langle \epsilon_e \rangle$. However, the electron temperature (or $\langle \epsilon_e \rangle$) does not vary appreciably; it has to be at a certain minimum value for the plasma to exist and it can not rise fast with increasing power because of fast increasing radiation losses. So, at low and intermediate pressures a very reasonable first guess for the electron temperature of active plasmas (where the power is dissipated) is around $1/4 \epsilon_{ion}$, where ϵ_{ion} is the ionisation energy. At higher pressures (around 1 at. $\Delta 10^5 \text{ N/m}^2$) the temperature can be lower, typically around 1 eV ($\sim (1/15) \epsilon_{ion}$). So, the electron temperature is not a very good parametrizing quantity. The relative amount of excitation, which is related to T_e by at least an exponential Boltzmann factor would be a better choice, but is not very convenient in use and is rather abstract. Of course the reactivity is determined by excitation and in view of chemical use it would be appropriate to find a parameter related to reactivity.

To obtain a first insight it is advantageous to use as a first parameter: the electron density, n_e . In practically all cases it determines the reactivity since in any case in some step it takes care of excitation, dissociation and ionization etc.

As a second parameter a quantity related to the gas density n_g , is a good choice. This could be the total pressure, but we will use the ionization degree, defined as n_e/n_g . This choice has a very definite advantage for the division of the plasma into two distinct regimes: of low ionization degree and of "high" ionization degree. The boundary between these two

regimes (the subjects of the two courses) is about at $\alpha \approx 10^{-2}$. There are several reasons to make this distinction useful. The first reason is that of the dominance of either collisions with neutrals or Coulomb collisions. At low ionization degrees (below 1%) the collisions of electrons with neutral gas particles are more frequent than those with ions. As a consequence all transport properties, as e.g. the conductivity, are determined primarily by these electron-neutral collisions. This is the wellknown gasdischarge regime. At the other hand if the ionization degree is sufficiently high ($\alpha > 1\%$) electron-ion Coulomb collisions outweigh the collisions with neutrals. In this regime several transport properties as e.g. the resistivity are determined by Coulomb collisions; the resistivity does not depend on the neutral density and is a function of the electron temperature only.

A (related) second reason for this division into two regimes is found in the form of the electron energy distribution. For high ionization degrees ($\alpha > 1\%$) the electron-electron collisions are frequent and tend to maintain a Maxwell distribution. Hence, the electron energy distribution can be characterized by a temperature, T_e , which facilitates the calculation of rates of inelastic processes.

For low ionization degrees ($< 1\%$) substantial deviations may occur for several reasons and care has to be taken in the calculations. A third reason is the behaviour of the heavy particle temperature or average energies. The energy coupling between electron and heavy particles as ions and neutrals is poor, in view of the large mass ratio. So, for low ionization degrees the neutrals are hardly heated and one speaks about "low temperature" plasmas. However at higher α 's the heating of ions by electrons start to play a role and at even higher α 's the heavy particle temperatures may approach the electron temperature. That is the regime of thermal plasmas, at least at higher pressures. In some literature one refers to this regime as high temperature plasmas, but this name is also used for the very much hotter thermonuclear plasmas.

Also the ion dynamics changes around the discussed boundary for $\alpha \approx 10^{-2}$.

Above that value usually ion-ion Coulomb collisions outweigh ion-neutral collisions and again the ions can be defined by an ion temperature T_i (which does not need to be equal to T_e).

For all plasmas to be discussed ion-neutral collisions dominate the ambipolar diffusion process. This is so, even in the high ionization regime, since the ion-ion collisions do not hamper the particle transport in first order. Like-Like (ion-ion) particle collisions do not change the total momentum of the total (ion) distribution.

There is an exception if a magnetic field is applied and when the electrons gyrate freely around the magnetic field lines. This is however beyond the scope of the present discussion.

In order to elucidate the characterization, plasmas used in several applications are plotted in fig.9, where the coordinates are n_e as abscis and n_e/n_g as ordinate.

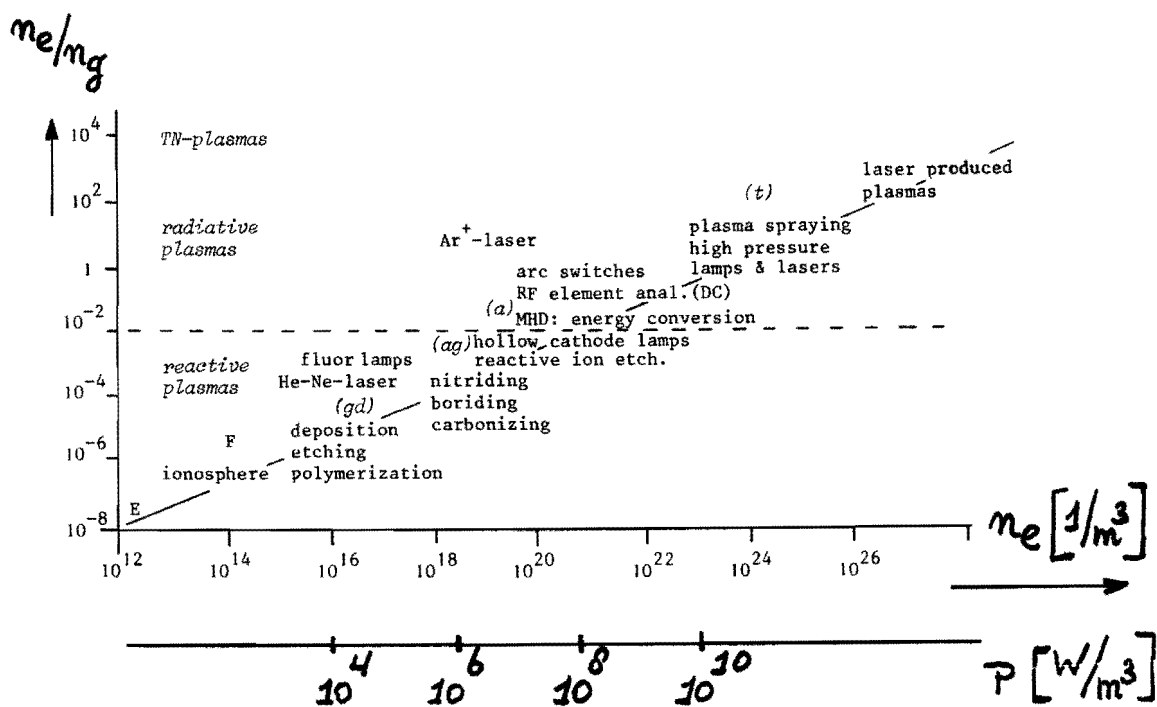


Fig. 9. Plasma characterization; gd: glow discharge; ag: anomalous glow;

a: arc; t: thermal plasmas.

It can be observed that there is a definite alignment in this figure. Apparently, plasma production imposes restraints. Note also, that the Ar^+ -ion laser plasma does appear somewhat higher in this figure. The reason is the application of a magnetic field which helps to cut down on plasma transport. As a consequence the plasma is hotter and the main heavy particle is now the ion rather than the neutral particle. This of course is essential in this application since Ar^+ -ions have to be excited to produce laser emission.

As a rule, however, plasmas group around the line:

$$\frac{n_e}{n_g} \approx (10^{-24} n_e)^{2/3} \tag{3}$$

• where n_e is in units of $[1/m^3]$.

There is a definite relationship between the required power density and the electron density. This can be argued quite easily on the basis of the basic formulation of mass- and energybalances. For simplicity we will assume a simple plasma in the sense that one neutral atom or molecule forms the major neutral particle. Further, in the mass balance we will assume ambipolar diffusion to dominate. Finally, in the energy balance we will take the increase of internal energy as the major energy loss term. Also we will limit ourselves for plasmas which are relatively far out of equilibrium.

Then the mass balance reads:

Net production of charged particles = ambipolar loss

or in formula:

$$n_e n_g K_1 (T_e) = - \nabla \cdot D_A \nabla n_e \sim \frac{D_A n_e}{L^2} \quad (4)$$

in which K_1 stands for the total excitation and ionization rate, D_A for the ambipolar diffusion coefficient and L for a typical dimension of the plasma. If, as usual, ion neutral collisions determine the diffusion (enhanced by the ambipolar factor T_e / T_i) then D_A is primarily dependent on neutral gas density (inversely proportional) and of course the temperature. In fact, from this equation immediately the conclusion can be drawn that the dimensions of the plasma are not free. Extracting the gas density from D_A by using $D_A n_g$ which is independent of the gas density, immediately the following relation results:

$$n_g L \sim \sqrt{\frac{(D_A n_g)}{K_1 (T_e)}} = \text{only a function of temperature} \quad (5)$$

Working out the details for e.g. argon at $T_e \sim 3\text{eV}$ we find $n_g L \sim 10^{19} / \text{m}^2$ which is indeed a typical value for gas discharge plasmas. So, in using plasmas, one has to take care to obey the plasma rules. There are ways to escape them but they are limited and have to be designed with great care.

In fact, the situation is a little bit more complicated as not necessarily all excitations need to lead to ionization. Particularly at low electron densities ($< 10^{19} / \text{m}^3$) radiation back to the ground state may make it necessary to "hit" the neutral several times (typically a number between 1-10) before ionization is successful. We can account for this by the multiplication of the LHS of the mass balance (4) a factor γ which is between .1 and 1.

A similar relation is a "bare" energy balance, in which we assume that all the consumed power is used to excite and ionize particles. In this way radiative losses (at least in the neutral system) are taken care of, since they are accounted for during the excitation:

$$n_e n_g K_1 (\epsilon_{1+} + \frac{5}{2} k T_e) \approx P = \underline{j \cdot E} \quad (6)$$

Note, that the required power density, P , would be even larger if other losses as heat conduction, convection etc., would play a role. The term $\frac{5}{2} k T_e$ stands for the contributions of the required heating of the newborn electrons ($\frac{3}{2} k T_e$) and the expansion energy ($k T_e$).

By now combining the mass balance and energy balance one can write immediately:

$$P \sim \frac{(D_A n_g) (\epsilon_{1+} + \frac{5}{2} k T_e)}{\gamma L^2} \cdot \frac{n_e}{n_g} \quad (7)$$

So we conclude, that as a general rule to obtain more density and more ionization degree more power consumption is required. In fig.9. we have indicated several typical values for P which are in good agreement with the estimates based on eq. (7).

We have stated already, that the use of balances have only an illustrative meaning. We have not treated plasmas which are close to equilibrium where also recombination has to be taken care of. Nevertheless it illustrates two basic rules:

- 1) The size of plasma and its form are also chosen by the plasma itself and in the design this has to be taken into account.
- 2) To arrive at a higher reactivity a larger power density has to be used. Roughly speaking there is a proportionality.

Of course any detail is beyond the scope of this introduction. It illustrates the way the conservation laws in a more elaborate form are used for the modelling of plasmas. To study plasmaflow also the conservation law for momentum has to be used.

Particle balance: diffusion, transport \longleftrightarrow
 ionization/recombination
 (mass)

momentum balance: forces (e.g. $e\mathbf{E}$, ∇p) \longleftrightarrow flow of plasma

energy balance: power consumption \longleftrightarrow plasma heating

3. To summarize, there are two limiting plasma regimes:

1. Low temperature (T_g low), low ionization degree ($\frac{n_e}{n_g}$ low) low electron density plasmas. The electron temperature is substantially higher than the gas temperature which is close to ambient temperature. The plasmas are out of chemical equilibrium; the reactivity is high; it is very much higher than the equilibrium value at gas temperature, but lower than that at electron temperature.

There is a definite relation between power density and radical and ion density, thus specific reactivity.

These plasmas are used for volume chemistry and many applications on surface modification.

2. "high" temperature (T_g "high") plasmas, thermal plasmas, relatively high ionization degree ($> 1\%$), high electron density plasmas. At atmospheric plasmas they are usually referred to as thermal plasmas since they are commonly not too far from local thermodynamic equilibrium.

As a consequence of the higher ionization degrees and relative large electron and thus ion densities the heavy particle (read gas-) temperature is close to the electron temperature. Even though in this plasmas also high reactivities are achieved, the use of the large (kinetic and internal) energy density and/or large momentum is primary here.

So the division into the two subsequent courses finds its basis in this subdivision.

It is however obvious, that the transition between the two regimes is gradually and it is useful to consider for any application the plasma regime as a whole.

To illustrate this we will end this introduction by referring to two examples where within the used classifications both kinds of plasmas are encountered.

The first is the negative corona discharge which is used for a long time for ozone production. In electro-negative coronas there is a definite time structure and the discharge is very inhomogeneous. During the very short discharge pulses (the so called Trichel pulses) relative high electron densities are achieved near the corona wire or point, ^{and} classification as high temperature plasma is appropriate. The dimensions of this initial plasma are small and it starts very soon to expand during the interval between the Trichel pulses. This expanding plasma consumes the energy deposited during the short pulse and there is no need for Joule dissipation; also there is no requirement of stationarity. This decaying plasma (a miniaturized afterglow) could be classified as weakly ionized plasma.

The second example is the use of a thermal plasma (either D.C. or inductively coupled) as a particle source to be used in a surface modification process. Now it is possible to use the thermal plasma in the active domain with high power density, high specific reactivity, but also with high fluxes. This flux is allowed to expand and a low density plasma of large size is produced. Since again this is a flowing afterglow the basic limitations do not apply and more freedom in use of plasmas is achieved.

In both examples use is made of convective energy transport from the high density active regime to the low density "preparation" regime. It is one way to escape some of the limitations of active plasmas, where the power is dissipated at the spot of chemical action.

By the same examples it may have become clear that a thorough knowledge of plasma physics and plasma chemistry is of advantage in optimizing plasma processing.

D.C. Schram

2. BASICS OF GAS DISCHARGES

Dr. Alfred J. van Roosmalen and Ir. Carol A.M. de Vries work at the Philips Research Laboratories, Eindhoven, The Netherlands. Dr. van Roosmalen is in charge of dry-etch process research and development for silicon VLSI. The research interests of Ir. de Vries are in basic studies of R.F. plasmas for dry etching.

BASICS OF GAS DISCHARGES

A.J. van Roosmalen and C.A.M. de Vries
Philips Research Laboratories Eindhoven, The Netherlands

1. Introduction

This introduction to plasma electronics focuses on applications in thin film processing, i.e., dry etching and deposition. The large majority of the systems in practical use is based on low-pressure rf excited plasmas. In the family of plasmas they can be classified as glow discharges - cold gas plasmas with a degree of ionization below $1:10^4$. Typical gas pressures range from 0.2 to 400 Pa. Rf excitation is so wide-spread because it allows the use of non-conducting substrates and electrodes; no net direct current is drawn. In many cases interactions at or near the substrate surface, such as ion bombardment, play an important role. A large part of the text to follow is dedicated, therefore, to the space charge regions ('sheaths') that form between the plasma and its surroundings.

For numeric calculations we define a standard system consisting of a 20 Pa Ar plasma enclosed between two circular plates of radius $r = 30$ cm and spacing $l = 5$ cm. We assume an electron temperature $T_e = 23000$ K (2 eV), an ion temperature equal to that of the neutral gas, $T_i = T_g = 400$ K (0.03 eV), and an electron density $n_e = 10^{16} \text{ m}^{-3}$. For simplicity we consider positive ions only.

The value for the electron temperature is taken from electrostatic probe measurements in rf tube discharges by Cantin and Gagné (1) and rf planar discharges by Mosburg et al. (2). The temperature in dc glow discharges is usually found to be of this same magnitude (1,3). Several authors have reported much higher temperatures for rf than for dc excitation (3,4). Since the data in these references has been obtained without proper prevention of rf interference their conclusions are in our opinion questionable and will not be taken into account here (1). The electron density is a high estimate based on LIFS data from Donnelly et al. (5) and microwave cut-off experiments by de Vries et al. (6).

The Debye length and the average velocity in a Maxwell-Boltzmann distribution are given by

$$\lambda_D = (\epsilon k T_e / e^2 n_e)^{0.5} , \quad (1.1)$$

$$\bar{v} = 1.6 (k T / m)^{0.5} , \quad (1.2)$$

where ϵ is the dielectric constant of vacuum, k Boltzmann's constant, e the electron charge, n_e the electron density, and T and m the particle temperature and mass, respectively (7). For the above conditions we find $\lambda_D = 0.1$ mm, $\bar{v}_e = 10^6 \text{ m s}^{-1}$, and $\bar{v}_i = 9 \times 10^2 \text{ m s}^{-1}$.

2. Floating sheath

The thermal current density current in one direction for any single charged species is

$$J = e n \bar{v} / 4 . \quad (2.1)$$

Because of the large difference in velocity much more electrons than ions pass through a given surface per unit time. For the standard system introduced in the previous section $J_e = 400 \text{ A m}^{-2}$ and $J_i = 0.4 \text{ A m}^{-2}$ under assumption that $n_e = n_i$. Hence, an electrically floating wall charges very rapidly negative with respect to the plasma. The steady-state potential difference is called the floating potential, V_f . We can derive its magnitude from the following argument.

The number of electrons in a Maxwell-Boltzmann distribution that can pass a potential barrier of height V_f is

$$n_e' = n_e \exp (e V_f / k T_e) . \quad (2.2)$$

Because of this exponential decrease in electron density when approaching a negative potential - the wall - the plasma ceases to exist and a positive space charge region - the ion sheath - is built up. The ion sheath can for suitable conditions be observed by eye as a dark space since most gas phase excitation processes involve electrons, and the optical emission of the discharge is largely caused by radiative decay of short-living excited species. The net electron current density to the wall is found by inserting Eq. 1.2 and 2.2 in Eq. 2.1,

$$J_e = 0.4 e n_e (k T_e / m_e)^{0.5} \exp (e V_f / k T_e) . \quad (2.3)$$

To obtain the ion current density at the wall we have to realize that electrons do not screen out potential deviations small relative to their thermal energy, i.e., below $k T_e / e$. These potentials are very large for ions, because $T_i \ll T_e$. Therefore, the electric field in the space charge region can extend somewhat in the plasma. It can be derived from mathematic continuity considerations that the ions must enter the sheath with an energy of $k T_e / 2 e$; this is the Bohm criterion (7). Under assumption of collisionless motion, and neglecting the thermal motion of the ions, the directed ion velocity u follows from energy conservation,

$$m_i u^2 / 2 = e k T_e / 2 e , \quad (2.4)$$

$$u = (k T_e / m_i)^{0.5} . \quad (2.5)$$

The potential at the plasma - ion sheath boundary is $k T_e / 2 e$, or half the electron temperature in volts. According to Eq. 2.2 the electron density is then $n_e \exp (- 0.5) = 0.6 n_e$. The ion density at the boundary is numerically equal to this value, so that the ion current density to the wall is

$$J_i = e n_i u = 0.6 e n_e (k T_e / m_i)^{0.5} . \quad (2.6)$$

For a wall at floating potential $J_e = J_i$. With Eqs. 2.3 and 2.6 we find

$$V_f = 0.5 k T_e / e . \ln (m_i / 2.3 m_e) . \quad (2.7)$$

This means that the floating potential is equal to a few times the electron temperature in volts. In the standard system from Section 1 we calculate $V_f = -10$ V and $J_i = 2$ A m⁻². As we will see in the next section the thickness of the floating wall sheath is of the order of the Debye length.

3. Cathode fall

In Section 2 we analyzed the interaction with a perfect floating wall. In practice there is almost always some applied potential. Here we will describe the cathode fall in a dc-operated 'abnormal' glow discharge. The term abnormal stems from lamp technology (8). It indicates the situation where the negative glow covers the cathode completely. The operating voltage is then a strong function of current. In the usual operating range for cold-cathode lamps this is not the case. Instead, raising the current increases the electrode coverage thereby leaving the voltage across the tube virtually unaffected ('normal' discharge). Figure 1 gives a quick view at the relevant regions in a tube discharge.

A reasonable cathode potential is -500 V. With voltages of this magnitude no plasma electrons can reach the cathode surface, and a net positive ion current is drawn. At the anode on the opposite side of the discharge the electrode potential will be slightly less negative than V_f in order to compensate the cathode current with a net negative electron current.

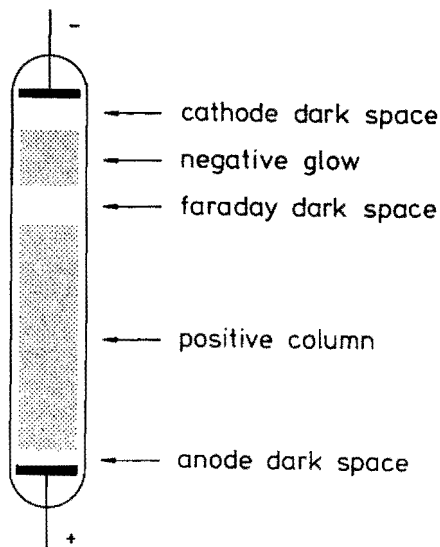


Fig. 1. Bright and dark zones in a dc tube discharge.

We will derive here some expressions with which it is possible to calculate potential and density gradients in the sheath. This knowledge will enable us to understand a number of phenomena in both dc and rf discharges. Consider a positive x-axis perpendicular to the cathode surface and with the origin on the plasma - sheath boundary. Assume that single-charged ions are the only charge carriers, and that they can move without collisions from plasma to wall. Anywhere along the positive x-axis the current density can then be written as

$$J_i = e n_i(x) u(x) , \quad (3.1)$$

where density and velocity are both a function of x. Since we neglect collisions J_i is a constant dictated by the Bohm criterion. By energy conservation

$$m_i u(x)^2 / 2 = e V(x) , \quad (3.2)$$

so that

$$u = (2 e V / m_i)^{0.5} , \quad (3.3)$$

where V is the potential relative to the plasma - sheath boundary. V is, of course, also a function of x. Note the similarity between these expressions and Eqs. 2.4 and 2.5. Eliminating u in Eq. 3.1 with the aid of Eq. 3.3 gives

$$n_i = J_i / e \cdot (m_i / 2 e V)^{0.5} . \quad (3.4)$$

Poisson's equation in one dimension is

$$d^2V/dx^2 = e n_i / \epsilon . \quad (3.5)$$

By substituting Eq. 3.4 for n_i a differential equation in V and x is obtained. With the boundary conditions $dV/dx = 0$ and $V = 0$ at $x = 0$ this equation can be solved by direct integration. After rearranging we find

$$J_i = 0.6 (\epsilon^2 e / m_i)^{0.5} \cdot V^{1.5} / x^2 . \quad (3.6)$$

This is the Child-Langmuir equation for collisionless space-charge limited current (9).

Because the derivation holds for all positive x values we may substitute the wall potential V_s for V and the sheath thickness d for x. With 2 A m^{-2} for J_i , see Eq. 2.6, and -500 V for V_s we find $d = 7 \text{ mm}$, in reasonable agreement with observed dark-space values (10).

For a floating wall we can insert Eqs. 2.6 and 2.7 in Eq. 3.6 which yields, after rearranging

$$d = \lambda_D \cdot 0.6 (\ln (m_i / 2.3 m_e))^{0.75} . \quad (3.7)$$

With the appropriate values for the various constants the ion sheath thickness at floating surfaces appears to be about twice the Debye length, or 0.2 mm.

Density, voltage, and field gradients calculated with Eqs. 3.1, 3.4, and 3.6 are given in Figure 2. The behavior at the plasma - ion sheath boundary is taken from the discussion on the Bohm criterion in the previous section. Note that the ion density rises asymptotically to infinity at $x = 0$. This is caused by the zero potential boundary condition in the integration of Poisson's equation, implying a zero velocity. For a finite ion velocity the differential equation cannot be solved analytically.

For an ion sheath thickness of 7 mm the concept of collisionless ion motion may be doubted. The collision cross section of Ar^+ in Ar is about $5 \times 10^{-19} \text{ m}^2$ which for 20 Pa implies a mean free path of 0.4 mm only (10). This has of course consequences for the ion impact energy. Instead of 500 eV for all ions in this example a wide range of energies is observed, see Figure 3. Hence, a mobility dominated for the ion movement might be

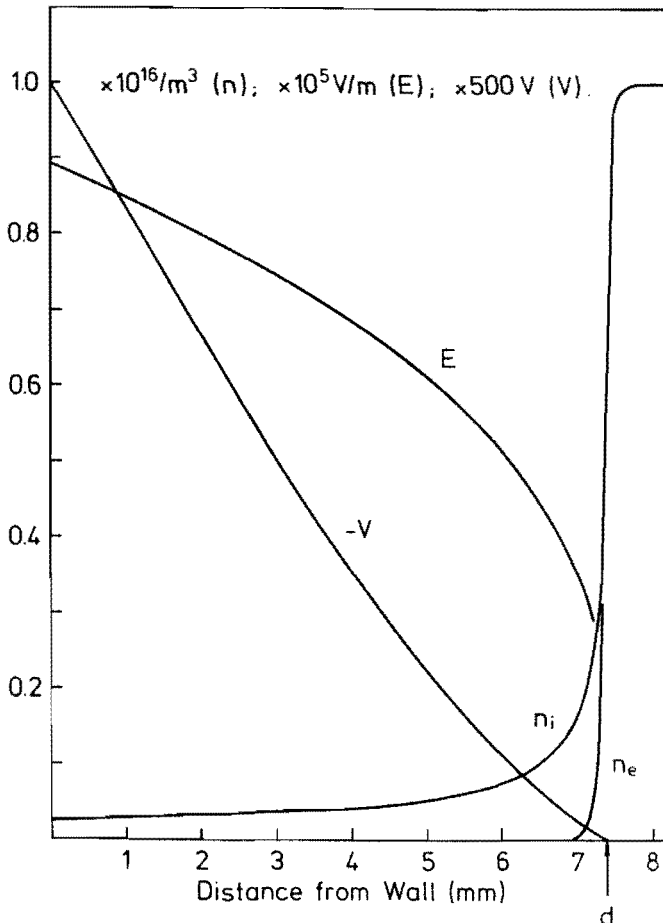


Fig. 2. Potential (V), electric field (E), and electron and positive ion density (n_e , n_i) gradients in a free-fall space-charge region.

more applicable. Using a derivation similar to the one above, but for the ion velocity using the drift equation

$$u = \mu_i dV/dx , \quad (3.8)$$

where μ_i is the ion mobility, we obtain

$$J_i = 1.2 \epsilon \mu_i V^2 / x^3 . \quad (3.9)$$

Surprisingly this expression is qualitatively quite similar to Eq. 3.6 for collisionless current. The voltage varies now as $x^{1.5}$ in stead of $x^{1.33}$, but that difference is small. For our example even the calculated sheath thickness is about the same, viz. 9 mm estimating the mobility of energetic Ar^+ ions in 20 Pa Ar on $0.5 \text{ m}^2 \text{ V}^{-1} \text{ s}^{-1}$ (11). It appears that 20 Pa is already in a transition zone; one has to go to either much higher or much lower pressure to discriminate between the two models.

So far, we have obtained expressions relating the dark space thickness with the current and voltage across it. For a complete description we have to include the effects of gas pressure variations too. The bombardment of the cathode with energetic ions initiates secondary electron emission. These secondary electrons are accelerated back into the plasma and serve there as a major energy input for sustaining the discharge. Increasing the pressure lowers the mean free path and, hence, brings the onset of cascade ionization closer to the cathode surface. In other words, the secondary electrons determine the position of the plasma boundary. It is observed indeed that the length of the cathode dark space in a dc discharge is inversely proportional to the gas pressure (9). As we will see later on other mechanisms have to be taken into account when rf fields are involved.

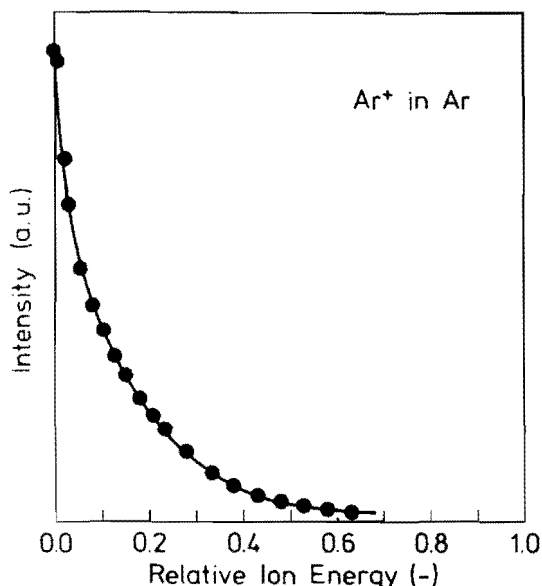


Fig. 3. Energy distribution for Ar^+ from an Ar dc-discharge cathode fall. Conditions: $p = 8 \text{ Pa}$; $V_S = 600 \text{ V}$; $d = 13 \text{ mm}$. Data from ref. (10).

4. Characteristic frequencies

When touching the subject of rf excitation one must realize that plasmas have a large variety of characteristic frequencies and time constants. Relevant are here the electron plasma frequency ω_e , the ion plasma frequency ω_i , the electron - neutral collision frequency ν_e , and the electrical plasma decay time τ . The values for these parameters calculated below are in Hz ($\omega_e / 2\pi$, $\omega_i / 2\pi$, $\nu_e / 2\pi$) to allow direct comparison with the excitation frequency.

The electron plasma frequency is a measure of the response time for perturbation of the charge neutrality in the plasma, and is given by (7)

$$\omega_e = (e^2 n_e / \epsilon m_e)^{0.5} . \quad (4.1)$$

Inserting appropriate values for the various constants we find that an electron density of 10^{16} m^{-3} corresponds to 900 MHz. Note that ω_e is related to \bar{v}_e and λ_D ,

$$\lambda_D \cdot \omega_e = 0.6 \bar{v}_e , \quad (4.2)$$

see Eqs. 1.1 and 1.2. This is consistent with the picture of λ_D as the spatial extent of deviations from neutrality.

A similar expression can be derived for the ion plasma frequency (9). In Eq. 4.1 we then have to replace n_i for n_e and m_i for m_e . With $n_e = n_i$ and our standard Ar plasma we find an equivalent frequency of 3 MHz.

The electron - neutral collision frequency is

$$\nu_e = n_g (\bar{v}\sigma)_e \approx n_g \bar{v}_e \sigma_T, \quad (4.3)$$

where n_g is the neutral gas density, $(\bar{v}\sigma)_e$ the average product of electron velocity and total collision cross section, and σ_T the cross section at T_e . Taking $\sigma_T = 3 \times 10^{-20} \text{ m}^2$ (12) gives us $1.6 \times 10^8 \text{ s}^{-1}$ for ν_e , which corresponds to 25 MHz.

The decay time in low-pressure, high area-to-volume type of plasma considered here is determined mainly by wall recombination of ions and electrons. An estimate can be obtained by dividing the total charge in the system by the loss current. For the geometry of our system

$$\tau = e n_e \pi r^2 l / J_i (2\pi r^2 + 2\pi r l) , \quad (4.4)$$

where J_i is the ion current density at the plasma boundary (Bohm criterion). Inserting $J_i = 2 \text{ A m}^{-2}$ yields $20 \mu\text{s}$ for τ . This is the half-cycle time of a 25 kHz wave.

Figure 4 shows the characteristic frequencies derived above together with the rf bands commonly used for etching and deposition plasmas. Systems not working in the indicated ranges are very rare. We will denote the 50 - 500 kHz band as LF (low

frequency), the 10 - 50 MHz band as HF (high frequency), and the 1 - 50 GHz band as MW (microwave). Note that the use of MHz and GHz frequencies is limited in practice to the industrial frequencies of 13.56 MHz, 2 GHz, and 40 GHz.

5. High-frequency sheath

When an rf voltage is applied between a plasma and a dc-floating wall or electrode basically two effects are possible. For frequencies well below the ion plasma frequency (LF band) ions and electrons follow the field and the system behaves as a dc cathode fall in the cathodic cycle and as an anodic sheath in the anodic cycle, see Figure 5.

Electric fields with a period larger than the decay time cause the discharge to extinguish every half cycle, which results in a switched breakdown with the corresponding high starting fields. We will not discuss such systems here.

Above the ion plasma frequency the ions cannot respond to the field and the electrons become the dominant current carriers (HF band). Since the sheath regions are virtually electron-free they behave now as capacitors and cause large ac potentials to develop between plasma and walls.

As an example we will now analyze the electrode sheath in a 13.56 Mhz system in detail. As this frequency is in the HF band there will be large rf potentials across the sheath. No net direct current can flow in the external circuit. To keep positive and negative particle fluxes equal the average electrode potential will drop to a large negative value. The final steady-state situation is illustrated in Figure 6. The ion current is constant since the ions do not 'see' the rf field, and the decay time is much longer than the rf cycle time. For most of the time the wall potential is much more negative than V_f so that the electron current is negligible. Once every rf cycle the electrode potential approaches zero; there, the plasma electrons break through the ion sheath to neutralize the positive wall charge built up in the previous cycle.

As the positive ions 'see' only the time averaged value of the rf field, it appears as though they are accelerated by a constant potential difference numerically equal to the rf peak voltage (6). This is the so-called dc self-bias. Loosely speaking one could say that the ion sheath acts as a diode rectifier

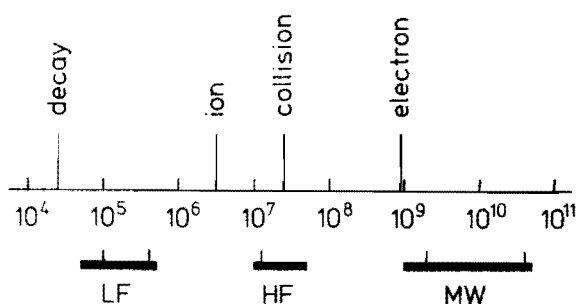


Fig. 4. Characteristic discharge frequencies and operating bands for plasma etching and deposition.

(the electrons) with a parallel resistor (the ions) and a parallel smoothing capacitor (the space-charge region).

With a 500 V peak value for the rf voltage across the sheath it is obvious that a - 500 V dc self-bias is obtained. As ions dominate the sheath for most of the rf period the space charge region will be similar to a 500 V cathode fall, at least to a first approximation. The sheath thickness is then 9 mm again according to Eq. 3.9. Treating the sheath as a perfect capacitor,

$$C_S = \epsilon / d , \quad (5.1)$$

we can calculate its reactive impedance ,

$$Z = 1 / \omega C_S , \quad (5.2)$$

where ω is the excitation angular frequency. For our system we

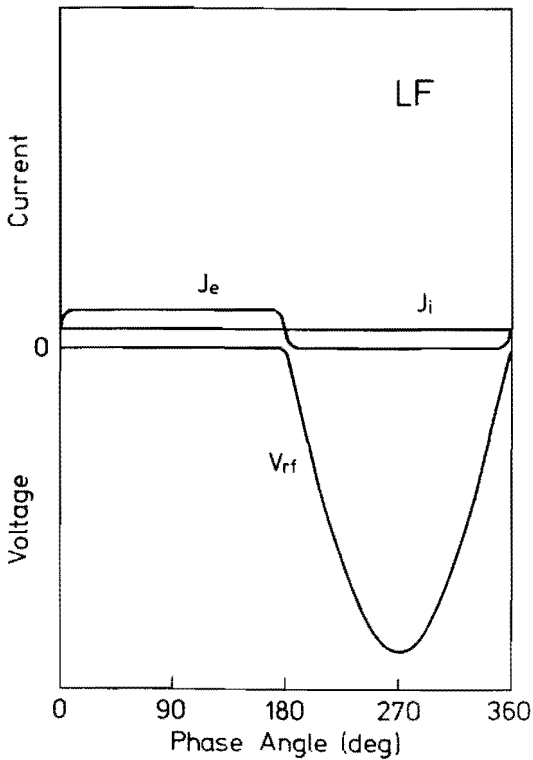


Fig. 5. Voltage (V_{rf}) and ion and electron current density (J_i , J_e) across the electrode sheath in LF operation as a function of time.

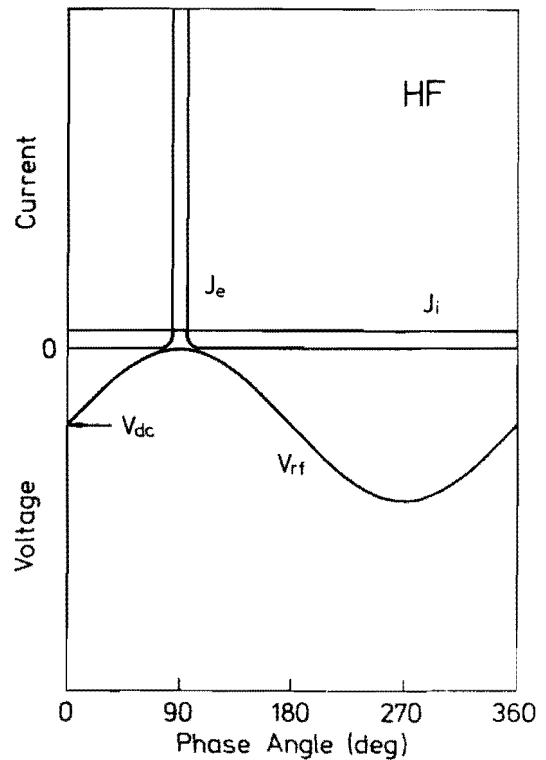


Fig. 6. Voltage (V_{rf}) and ion and electron current density (J_i , J_e) across the electrode sheath in HF operation as a function of time. Arrow indicates ion bombardment energy (V_{dc}).

obtain $C_s = 1.1 \text{ nF m}^{-2}$, so that $Z = -10 \text{ j ohm m}^{-2}$. This agrees well with measured rf impedances (13,14). With a 500 V peak applied voltage the rms current density is 35 A m^{-2} , hence, far more than the dc current density in the sheath, 2 A m^{-2} , but less than the random electron current in the glow, 400 A m^{-2} (Eq. 2.1).

Although the high frequency sheath resembles the cathode fall in some aspects it would be a misunderstanding to believe that they are identical. From Poisson's equation (Eq. 3.5) it follows directly that if the voltage across a space charge region decreases, the net enclosed charge has to decrease. The positive charge density is prescribed by the rf independent ion flux, so that electrons must move back and forth. This implies an oscillatory movement of the plasma - ion sheath boundary. Figure 7 shows the calculated position of the plasma - ion sheath boundary relative to the wall as a function of time. The assumed ion density distribution and electron density cut-off are as per Figure 2.

It should be noted that the high-frequency sheath thickness is prescribed by Poisson's equation, not by the onset of cascade ionization as in the dc case, see Section 3. While the cathode-fall length in a dc discharge varies as p^{-1} ($p = \text{pressure}$), the dependence here is much less pronounced, see Figure 8. It will be clear that for a given pressure the rf sheath is also much thinner than the cathode fall. Finally, the sheath formation mechanism implies that there is no 'anode' sheath.

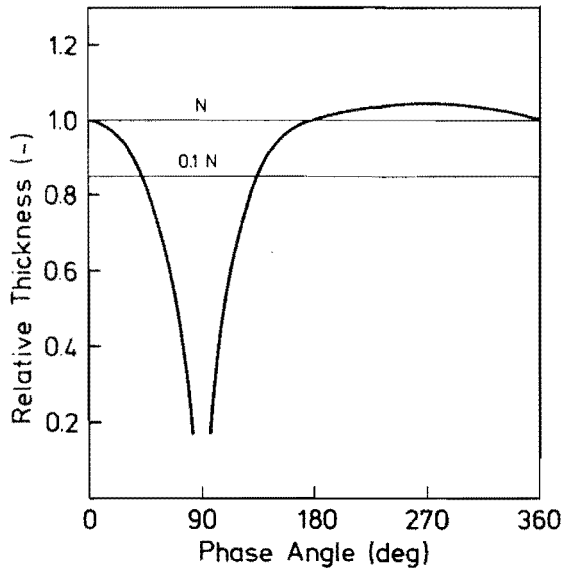


Fig. 7. Position of the plasma - ion sheath boundary relative to the wall as a function of time.

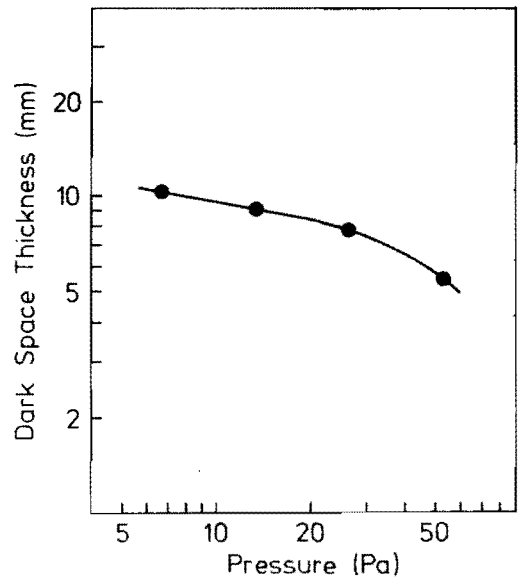


Fig. 8. Optical ion-sheath thickness in an O_2 discharge as a function of pressure. Data from ref. (14).

6. Energy transfer

It is illustrative to have a look at the various energy loss and gain mechanisms in the 13.56 MHz discharge introduced in the previous section (11). Calculations are for a 'half system', i.e., an electrode in the cathodic cycle plus a proportional piece of adjacent plasma. Power dissipation is given per unit of electrode surface, thereby following a common use in thin film processing.

We have already stated that the main charge loss mechanism is wall recombination. The power density needed to replace this loss by ionization is

$$P_1 = J_i / e \cdot \eta_i , \quad (6.1)$$

where η_i is the effective energy per ionizing collision. Note that η_i has to be higher than the ionization energy in order to compensate for non-ionizing inelastic collisions. With $\eta_i = 30$ eV (9) and $J_i = 2 \text{ A m}^{-2}$ it appears that $P_1 = 60 \text{ W m}^{-2}$.

In the discharge large rf currents are flowing. For electron drift velocities small relative to the thermal velocity we may write

$$J_{rf} = e n_e v_d , \quad (6.2)$$

$$v_d = \mu_e E_{rf} , \quad (6.3)$$

where J_{rf} is the rms current, v_d the drift velocity, E_{rf} the effective electric field, and μ_e the electron mobility. Hence the specific plasma resistivity ρ

$$\rho = 1 / e n_e \mu_e . \quad (6.4)$$

For moderate fields the product of mobility and pressure is constant so that ρ can be calculated. The associated energy dissipation

$$P_2 = J_{rf}^2 \rho L , \quad (6.5)$$

where L is the plasma length in the direction of the rf current vector. Taking $l/2 = 2.5 \text{ cm}$ for L , $300 \text{ m}^2 \text{ V}^{-1} \text{ s}^{-1}$ for μ_e in 20 Pa Ar (15), and 35 A m^{-2} for J_{rf} , see the previous section, we find $P_2 = 60 \text{ W m}^{-2}$, just enough to sustain the discharge (P_1).

A much larger contribution to the energy dissipation in the discharge comes from the ion wall bombardment. The energy transferred by the ions is

$$P_3 = J_i V_s , \quad (6.6)$$

which in this example amounts to 1000 W m^{-2} . Secondary electrons liberated by the ion bombardment are accelerated back into the plasma thereby providing an additional high-energetic power

input. As this increases the effective positive current to the wall we have to multiply J_i in Eq. 6.6 by $(1 + \gamma)$, where γ is the secondary emission coefficient. Estimating γ at 0.1 electrons per ion (9) we have to add some 100 W m^{-2} to P_3 . Obviously this input helps to sustain the discharge and raises the high-energy tail of the Maxwell-Boltzmann distribution.

So far we have located 1160 W m^{-2} of work done by the rf field. The total rf power input to obtain the conditions in our example are, however, much larger, typically 5000 W m^{-2} . Rf-impedance measurements also indicate a resistive component much larger than can be accounted for by ion sheath flux and electron drift alone (14). An additional contribution can come from electrons interacting with the oscillating plasma - ion sheath boundary, see Figure 7. Calculations have shown, however, that the dissipation in W m^{-2} is less than the sheath voltage in volts, so that the contribution is not substantial (14). Possibly collective processes are involved, such as wave interaction. Note that the total energy input per electron with 5000 W m^{-2} is rather large; from the collision frequency and the total charge in the system we calculate an average of 1 eV per mean free path.

7. Macroscopic properties

It will be attempted in this Section to summarize the results from the previous sections in a macroscopic description of the rf discharge over a large frequency range. We will focus on the key parameters sheath potential, plasma density, ion wall current, degree of dissociation and discharge impedance.

For a conceptual understanding of rf discharges it is convenient to describe the sheath - plasma system in terms of an electric equivalent circuit, see Figure 9. In this diagram D, R_1 , and C_1 stand for the electron, ion, and capacitive currents in the sheath, while R_2 and C_2 denote the plasma resistance and capacitance. Remember that the ion current in the sheath is always continuous, whereas the electrons can pass the sheath only if the electrode potential is sufficiently close to zero.

For the 13.56 MHz example we saw in the previous section that $R_2 \ll 1 / \omega C_1 \ll R_1$. The admittance of C_2 is negligible here (see below). Obviously the HF discharge is almost completely capacitive.

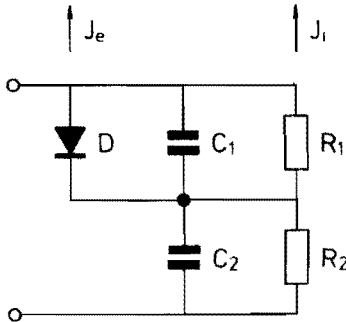


Fig. 9. Electrical equivalent circuit for an rf discharge in contact with an electrode. D, R_1 , C_1 : electron, ion, and capacitive current in the ion sheath; R_2 , C_2 : plasma resistance and capacitance.

In the LF band $1/\omega C_1 \gg R_1$, so that both C_1 and C_2 can be neglected. The system is resistive, and the rf current is about equal to the ion current on the cathode (16). Power dissipation is as given by Eq. 6.6, since there is now no low-impedance bypass through the dark space and $R_1 \gg R_2$. The charge density in the plasma does not appear to depend much on the operating frequency as long as the power density is kept constant (5), see Figure 10. With 5000 W m^{-2} and $J_i = 2 \text{ A m}^{-2}$ we find from Eq. 6.6 that $V_S = 2500 \text{ V}$. It has been observed indeed that the potentials in LF discharges are substantially higher than for HF systems (5), see Figure 10. Toward the low end of the LF band the discharge becomes inductive because time-dependent ionization and transfer processes cannot be neglected anymore (8).

Above the HF band one would expect the discharge to be resistive again, since $1/\omega C_1 \ll R_1, R_2$, were it not that the electron-neutral collision frequency is crossed. This implies that the electrons make many oscillations between two collisions, and that the plasma itself becomes capacitive, $1/\omega C_2 \ll R_2$. This effect is usually accounted for by incorporating an imaginary mobility in the equation for the resistivity, Eq. 6.4. It can be derived that (17)

$$\mu_e' = \mu_e / (1 + j \omega / \nu_e) . \quad (7.1)$$

Frequencies above the electron plasma frequency (MW) can cause

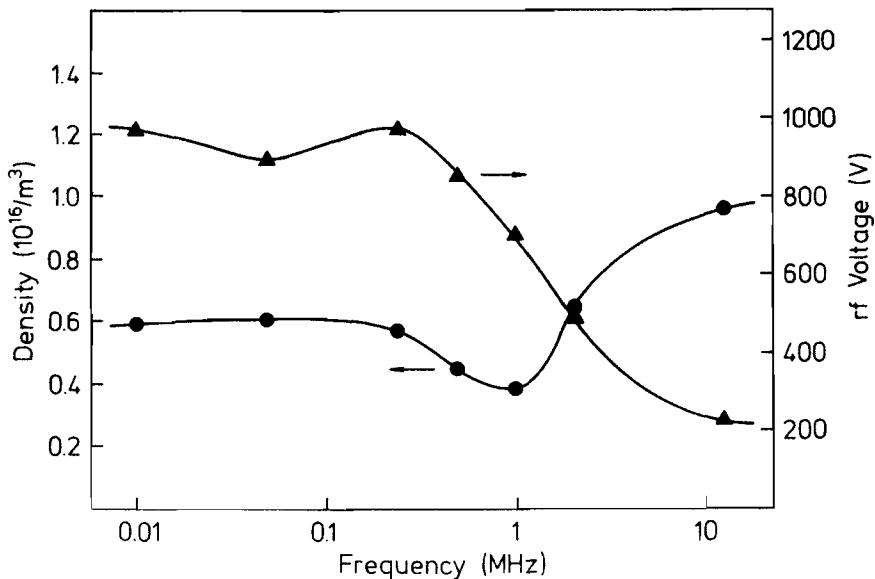


Fig. 10. Density of Cl_2^+ from laser-induced fluorescence, and reactor rf potential (peak-to-peak) as a function of frequency for a Cl_2 discharge. Data from ref. (5).

longitudinal waves as the electrons are too slow to keep the plasma field-free. Actually the discharge reactor at these frequencies takes the shape of a tuned cavity with a small loss angle. Since the sheath reactance ($1 / \omega C_1$) becomes negligible at very high frequencies the rf current will not produce a potential drop across the dark space. Walls and electrodes will all be at or near floating potential, $V_s = V_f = 10$ V.

For discharges in the LF and HF band there exist at the moment no self-consistent models predicting plasma parameters from external variables; only the (less common) MW systems are relatively well-described (17). Even reliable parameter measurements are scarce.

From the existing literature it can be concluded that n_e (hence, J_i ; Bohm criterion) is about proportional to the rf power, although there are indications of upper and lower limits that might be reactor geometry dependent; pressure and frequency appear to have little effect (5,6).

The sheath voltage in HF systems has a power dependence lying roughly between square root and linear (14); in LF systems the influence of rf power is much less pronounced (16). It will be clear that the plasma potential in MW discharges depends on rf power to the extent that the electron temperature does (Eq. 2.7), i.e., very little.

In HF discharges the ion sheath thickness is normally insensitive to the rf power (14). It is difficult to give a statement for the LF sheath because of its pulsating nature. In MW discharges a sheath will not be visible (Eq. 3.7).

A useful empirical observation is that the higher the frequency, the higher the degree of gas dissociation (not ionization!) for a given power level. This can be judged from e.g. the formation of glow polymer and chlorine in a CCl_4 discharge, being negligible in LF systems, significant in the HF band, and almost quantitative in MW excitation (18,19).

References

- 1 A. Cantin and R.R.J. Gagné, Appl. Phys. Lett. 30, 316 (1977).
- 2 E.R. Mosburg, Jr., R.C. Kerns, and J.R. Abelson, J. Appl. Phys. 54, 4916 (1983).
- 3 E. Eser and R.E. Ogilvie, J. Vac. Sci. Technol. 15, 199 (1978).
- 4 M.J. Kushner, J. Appl. Phys. 53, 2939 (1982).
- 5 V.M. Donnelly, D.L. Flamm, and G. Collins, J. Vac. Sci. Technol. 21, 817 (1982).
- 6 C.A.M. de Vries, A.J. van Roosmalen, and G.C.C. Puylaert, J. Appl. Phys. 56 (1985), in press.
- 7 F.F. Chen, "Introduction to Plasma Physics" (Plenum, New York, 1977).
- 8 G.F. Weston, "Cold Cathode Glow Discharge Tubes" (ILIFFE, London, 1968).

- 9 B.N. Chapman, "Glow Discharge Processes" (Wiley, New York, 1980).
- 10 W.D. Davis and T.A. Vanderslice, Phys. Rev. 131, 219 (1963).
- 11 M.A. Biondi and L.M. Chanin, Phys. Rev. 94, 910 (1954).
- 12 R.D. Dubois and M.E. Rudd, J. Phys. B 8, 9, 1474 (1975).
- 13 A.J. van Roosmalen, Appl. Phys. Lett. 42, 416 (1983).
- 14 A.J. van Roosmalen, W.G.M. van den Hoek, and H. Kalter, J. Appl. Phys. 56 (1985), in press.
- 15 J.M. Anderson, Phys. Fluids, 7, 1517 (1964).
- 16 A.J. van Roosmalen, C.A.M. de Vries, and H.T. Arends, to be published.
- 17 G. Francis, "Ionization Phenomena in Gases" (Butterworths, London, 1960).
- 18 R.H. Bruce and B. Gelernt, ECS Ext. Abstr. Vol. 80-1 (1980), p. 307.
- 19 N.P. Armstrong and J. Malehan, Vacuum 33, 291 (1983).

3. PLASMA CHEMISTRY AND PHYSICS

Dr. Daniel L. Flamm is a member of technical staff at AT & T Bell Laboratories, Murray Hill, N.J., USA. His principal research interests include plasma chemistry and processing, engineering of electrical discharge processes and electronic material processing.

INTRODUCTION TO PLASMA CHEMISTRY AND PHYSICS

D. L. Flamm

Copyright 1985

All rights reserved.

References

SURVEYS THE CHEMISTRY COVERED IN THIS LECTURE

- "Basic Principles of Plasma Etching for Silicon Devices," D. L. Flamm, V. M. Donnelly and D. E. Ibbotson, "Chapter 8, pp. 190-246 in VLSI Electronics Microstructure Science, Vol. 8, ed. N. G. Einspruch, D. M. Brown, Academic Press (1984).
- "The Design of Plasma Etchants," D. L. Flamm and V. M. Donnelly, *Plasma Chem. and Plasma Proc.*, *1*, 317 (1981).
- "Basic Chemistry and Mechanisms of Plasma Etching," D. L. Flamm, V. M. Donnelly, D. E. Ibbotson, *J. Vac. Sci. Technol.*, *B1*, 23 (1983).

PLASMA ETCHING WITH EMPHASIS ON LITHOGRAPHY (SOME OF THIS IN LECTURE)

"Dry Etching," C. J. Mogab, in *VLSI Technology*, pps. 303-345, S. M. Sze, ed., (Mc Graw Hill, 1983).

AN INTRODUCTORY OVERVIEW OF PLASMA ETCHING

"Plasma Etching," J. A. Mucha, D. W. Hess, Chapter 5, p. 287 in *Introduction to Microlithography, Theory, Materials and Processing*, L. F. Thompson, C. G. Willson, M. J. Bowden, eds, Amer. Chem. Soc. Symp. Ser. No. 219 (1983).

THIS SURVEY INCLUDES GOOD COVERAGE OF SPUTTER ETCHING

"Plasma-Assisted Etching Techniques for Pattern Delineation," C. M. Melliar-Smith and C. J. Mogab, in *Thin Film Processes*, J. L. Vossen and W. Kern, eds, (Academic, NY, 1979).

REVIEW WITH EMPHASIS ON IBM WORK AND INTERPRETATIONS

"Plasma Assisted Etching," J. W. Coburn, *Plasma Chem. and Plasma Proc.*, *2*, 1 (1982).

BRIEF, SIMPLIFIED DISCUSSION OF PLASMA POTENTIALS AND PROBES

- "Glow Discharge Phenomena in Plasma Etching and Plasma Deposition," J. L. Vossen, *J. Electrochem. Soc.*, *126*, 319 (1979).

READABLE, SIMPLE INTRODUCTION TO PHYSICS OF ELECTRICAL DISCHARGES

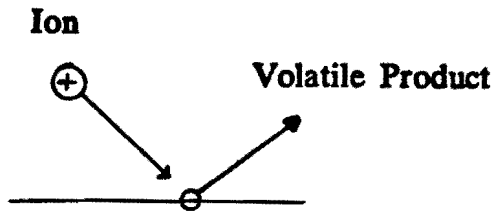
- "An Introduction to Gas Discharges," A. M. Howatson, (Pergamon Press, 1965).

MORE ADVANCED INTRODUCTION TO GASEOUS ELECTRONICS

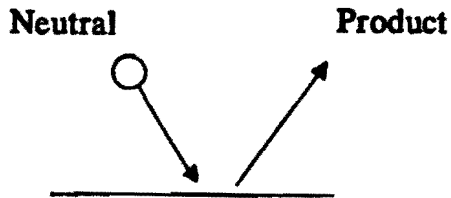
"Introduction to Electric Discharges in Gases," S. C. Brown, (John Wiley, 1966).

No part of this publication may be reproduced in any form without written permission of the author.

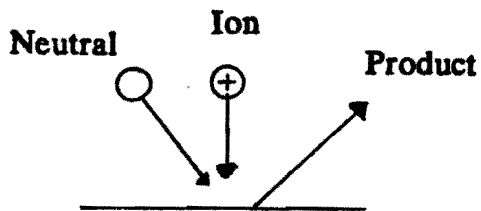
How Does Plasma Etching Take Place



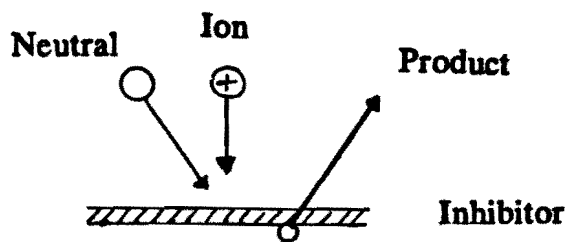
1. Sputtering



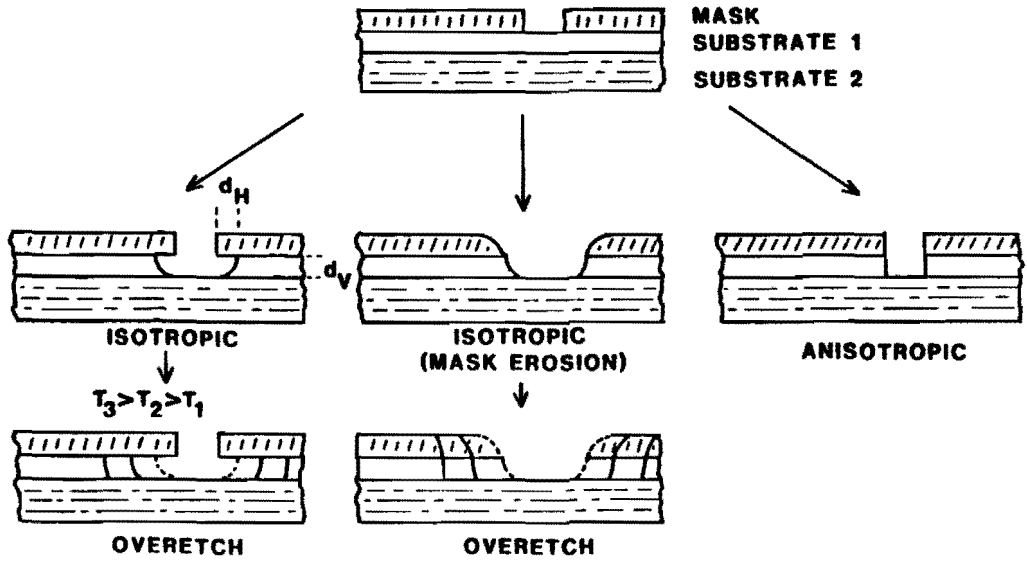
2. Chemical



3. Ion-Enhanced,
Energetic



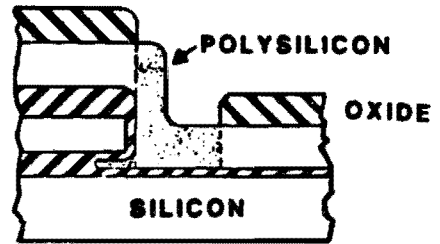
4. Ion-Enhanced,
Protective



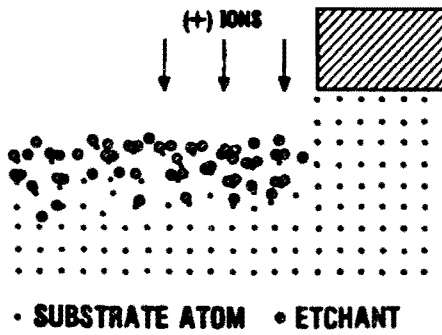
Isotropic and anisotropic etching. The degree of anisotropy is defined as $(1 - d_H/d_V)$. Feature size is limited to the film thickness.

Isotropic etching is useful for:

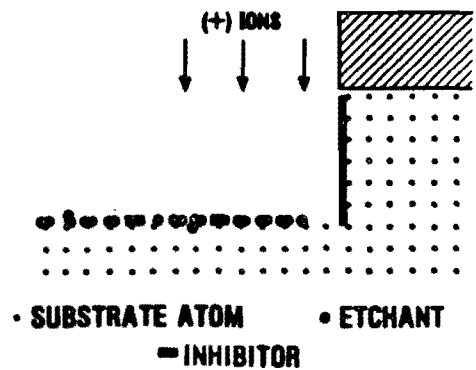
1. High Selectivity
2. Stripping
3. Undercutting (liftoff)
4. Tapering
5. Larger geometries



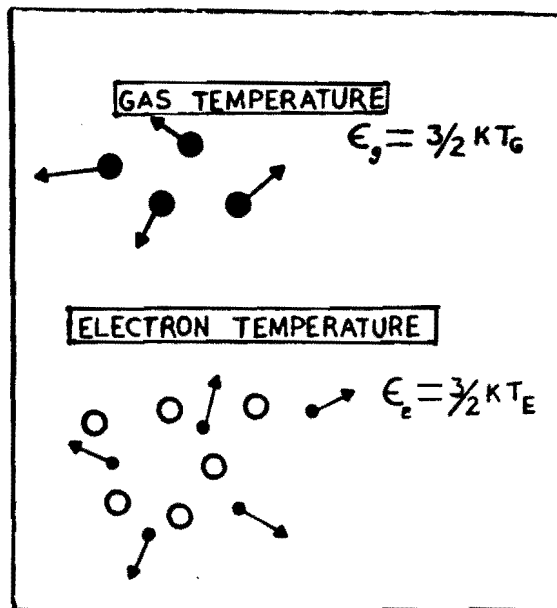
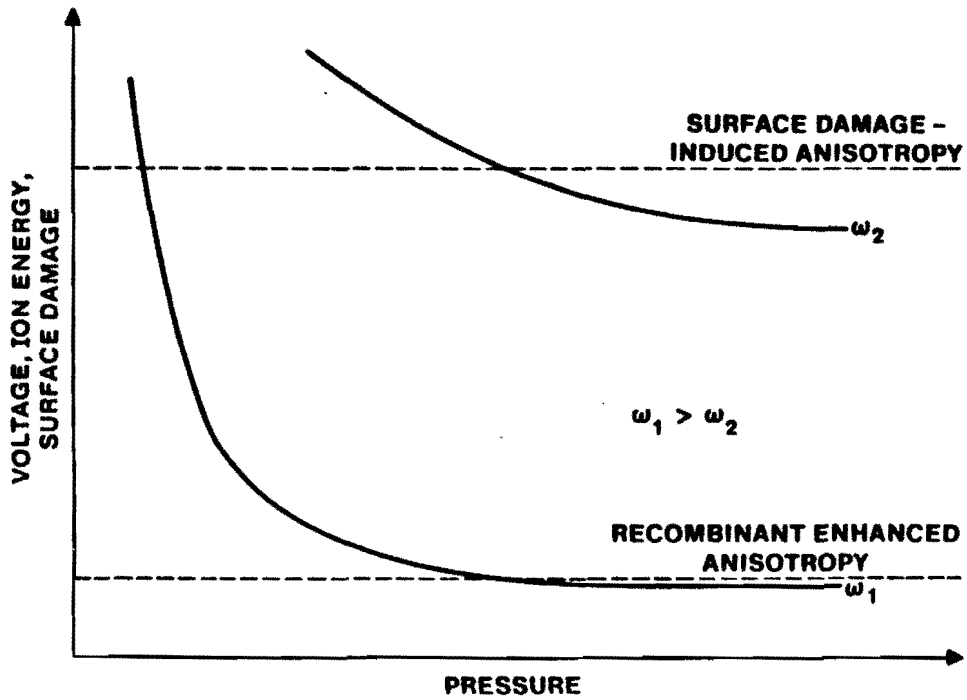
SURFACE DAMAGE INDUCED ANISOTROPY



SURFACE INHIBITOR MECHANISM OF ANISOTROPY



ETCH PROPERTY	PLASMA VARIABLE	SIMILARITY VARIABLE
Rate	Power	E/N
Selectivity	Pressure	Nd
Anisotropy	Frequency	f/N
Morphology	Temperature	T
	Flow	n_e/N
	Gas Composition	

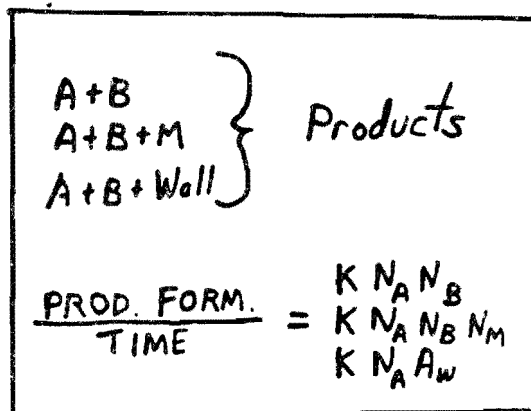


High electron energy in a discharge permits chemical activation at low gas temperature.

CHEMICAL KINETICS: REACTION

FORMS AND RATE EXPRESSIONS

A and B are reactants, M is a non-reactive collision partner that carries away energy, helping the reaction to proceed, and A_w is the wall area in first order reactions. For a fixed composition, N_A , N_B , N_M are proportional to pressure. Since the various reactions forms have different pressure dependencies, pressure can be used to alter the relative importance of competing reactions.



Effect of Pressure on Reactions of Various Order

Overall Reaction	Effective Dependence
$F + Si_{surf} - SiF$	P
$CF_3 + F - CF_4$	P^2
$CF_2 + F_2 - CF_3 + F$	P^2
$CF_2 + CF_2 - C_2F_4$	P^2
$3CF_2 - C_3F_6$	P^3
$4CF_2 - C_4F_8$	P^4

These are typical of etching, recombination and polymerization reactions in fluorocarbon plasmas. The higher the order of a reaction (exponent of pressure), the greater is its relative importance with increasing pressure. Contrarywise, the lower order reactions dominate at low pressure. The above sequence thus illustrates that pressure favors oligimerization of unsaturates to form polymeric precursors relative to etching and saturation (recombination) reactions.

Gas and surface temperatures are also very important since rate constants (K) generally vary exponentially with temperature. Likewise, wall material can control the rate of surface reactions such as recombination.

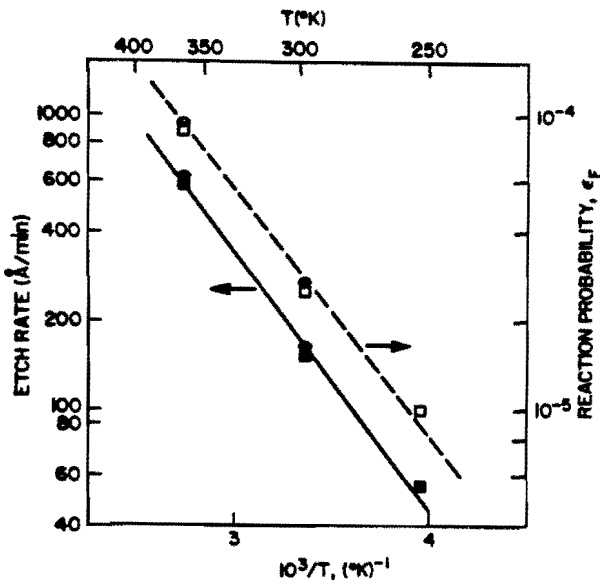
	THESE DIRECTLY AFFECT RATE	
	K'S AFFECTS	N'S
GAS TEMP	✓	
ELEC TEMP	✓	
NET DENSITY (PRESSURE)		✓
REL GAS CONC		✓
REL ELEC CONC		✓
Wall Material	✓	

F-ATOM ETCH RATES

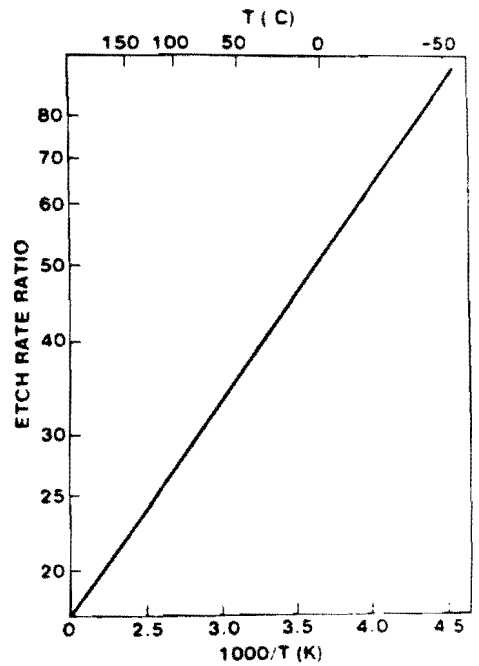
$$ER(\text{angstrom/min}) = A n_F T^{1/2} e^{-E_A/RT}$$

FILM	A	E _A (kcal/mole)	RATE Å/min (298K, n _F = 3 × 10 ¹⁴ cm ⁻³)
Si	2.86 × 10 ⁻¹²	2.48	2250
SiO ₂	0.614 × 10 ⁻¹²	3.76	55
$ER(\text{Si})/ER(\text{SiO}_2) = 4.66 e^{1.27/RT}$ $= 44 \quad (\text{at } 298\text{K})$			

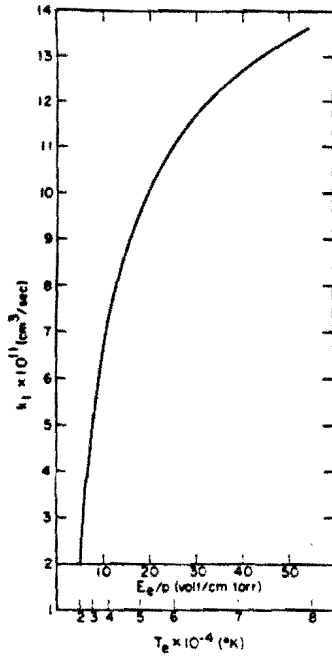
Etching of Si and SiO₂ by F-atoms obey an Arrhenius expression. E_A is called the activation energy. The larger E_A, the more sensitive a reaction is to temperature. Since E_A is material dependent, selectivity is temperature dependent.



Silicon etch rate and reaction probability vs. 1/T. Logarithm of the etch rate is linear in this form, which is called an Arrhenius plot.

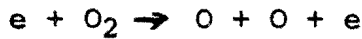


Si/SiO₂ etch rate ratio vs. 1/T.

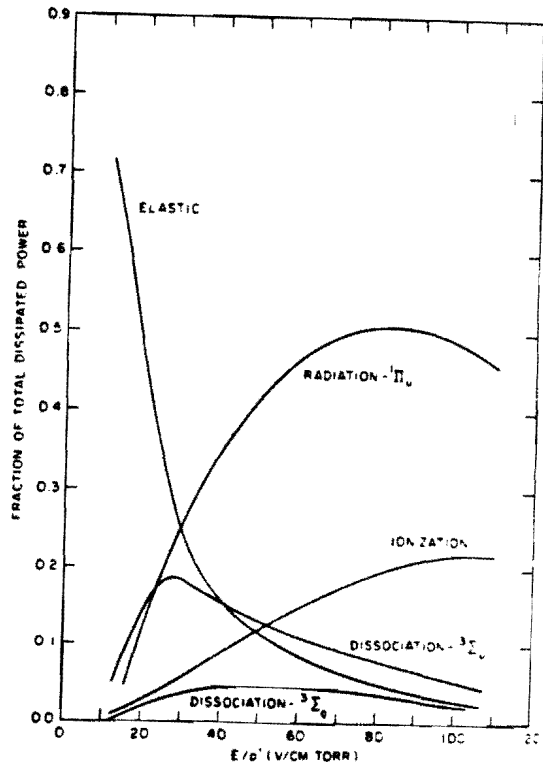


Rate constants for electron-molecule reactions depend primarily on T_e , not T_g when $T_e \gg T_g$. Sometimes the rate goes through a maximum and then decreases with T_e (unlike the curve at left).

Dissociation of molecular oxygen as a function of T_e & E/p .



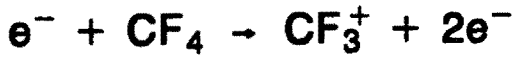
Reaction processes in a hydrogen discharge. Maximum energy is coupled into distinct channels as E/p is changed owing to different individual dependencies of rate constants on T_e . Energy efficiency of H atom production is greatest at $E/p \approx 20-30$.



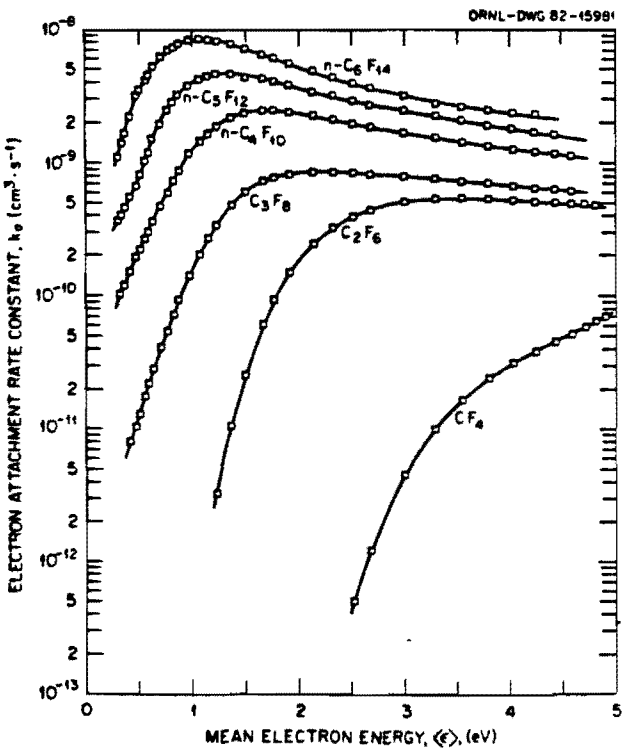
DISTRIBUTION OF DISSIPATED POWER IN HYDROGEN

ELECTRON-MOLECULE REACTIONS IN A CF_4 DISCHARGE

IONIZATION



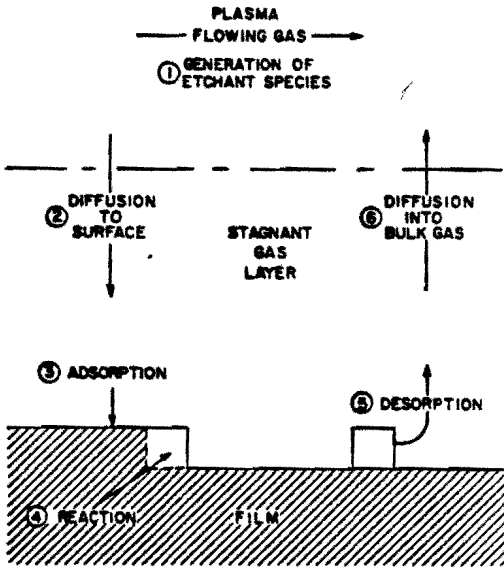
DISSOCIATION



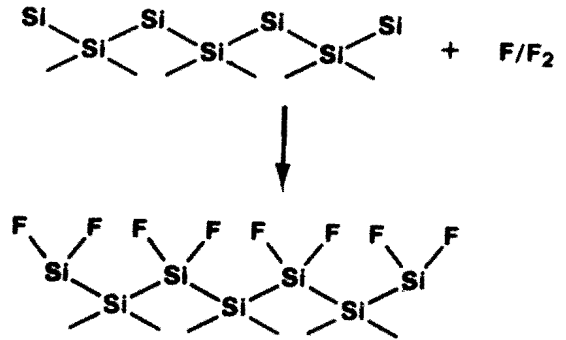
F ATOMS ETCH SILICON. THE RATES OF F-ATOM FORMATION DEPEND MAINLY ON ELECTRON ENERGY SINCE DETACHMENT IS RAPID IN A PLASMA.

MECHANISM FOR A CF₄ DISCHARGE

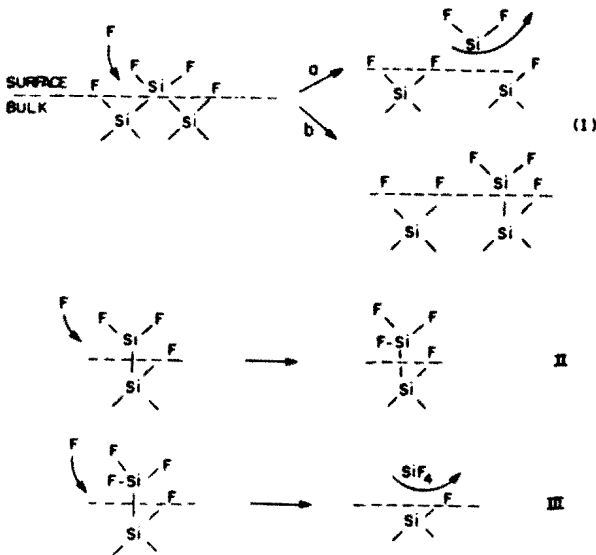
<p>Ionization $e^- + CF_4 \rightarrow CF_3^+ + 2e^- + F$</p> <p>Attachment $e^- + CF_4 \rightarrow CF_3 + F^-$ $e^- + F_2 \rightarrow F + F^-$</p> <p>Detachment $e^- + F^- \rightarrow F + 2e^-$ $CF_3 + F^- \rightarrow CF_4 + e^-$ $F + F^- \rightarrow F_2 + e^-$ $F^- + M \rightarrow F + e^- + M$</p> <p>Ion Recombination $e^- + CF_3^+ \rightarrow CF_3$ $CF_3^+ + F^- \rightarrow CF_3 + F$</p> <p>Diffusion $e^- \rightarrow e^-(S)$ $CF_3^+ \rightarrow CF_3^+(S)$ $F^- \rightarrow F^-(S)$</p>	<p>Surface Recombination $e^-(S) + CF_3^+(S) \rightarrow CF_3(S)$ $F^-(S) + CF_3^+(S) \rightarrow CF_4(S)$</p> <p>Dissociation $e^- + CF_4 \rightarrow CF_3 + F + e^-$ $e^- + C_2F_6 \rightarrow CF_3 + CF_3 + e^-$ $e^- + F_2 \rightarrow F + F + e^-$</p> <p>Recombination $2CF_3 \rightarrow C_2F_6$ $CF_3 + F + M \rightarrow CF_4 + M$ $CF_3 + F_2 \rightarrow CF_4 + F$ $F + F + M \rightarrow F_2 + M$</p> <p>Surface Reactions $CF_3 \rightarrow CF_3(S)$ $F \rightarrow F(S)$ $F + CF_3(S) \rightarrow CF_4(S)$ $CF_3 + CF_3(S) \rightarrow C_2F_6(S)$ $F + Si \rightarrow SiF(Si)$ $F + SiF(Si) \rightarrow SiF_2(Si)$ $F + SiF_2(Si) \rightarrow SiF_3(Si)$ $F + SiF_3(Si) \rightarrow SiF_4(Si)$</p>	<p>Surface Recombination $2F(S) \rightarrow F_2(S)$ $CF_3(S) + F(S) \rightarrow CF_4(S)$ $2CF_3(S) \rightarrow C_2F_6(S)$</p> <p>Polymerization $CF_3(S) \rightarrow CF_2(P) + F(S)$ $CF_2(P) + F(S) \rightarrow CF_3(S)$</p> <p>Desorption $CF_4(S) \rightarrow CF_4$ $C_2F_6(S) \rightarrow C_2F_6$ $F_2(S) \rightarrow F_2$ $F(S) \rightarrow F$ $CF_3(S) \rightarrow CF_3$ $SiF_4(Si) \rightarrow SiF_4$</p>
---	--	---



BEFORE STEADY STATE



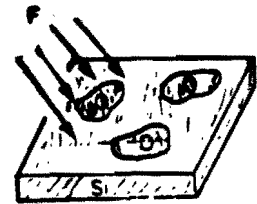
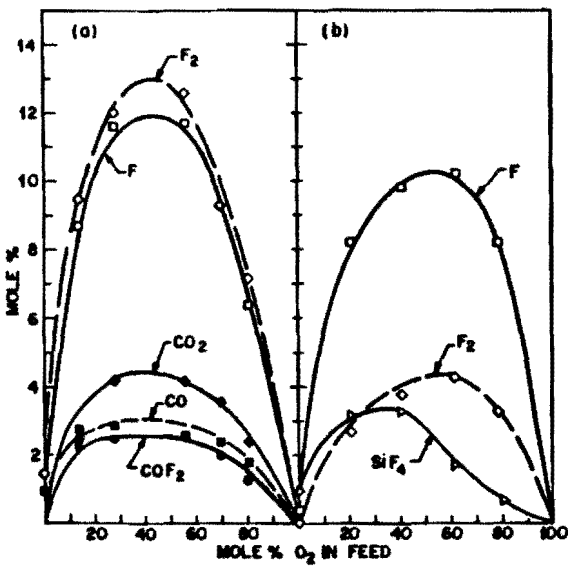
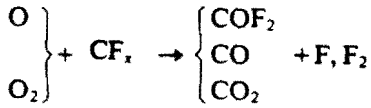
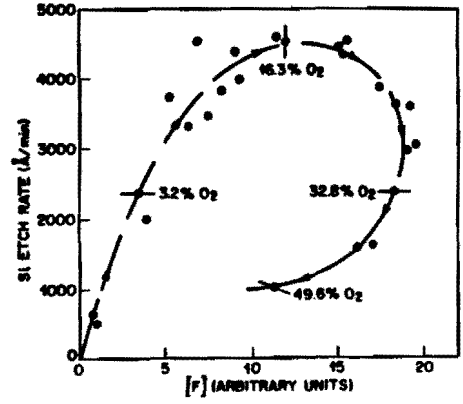
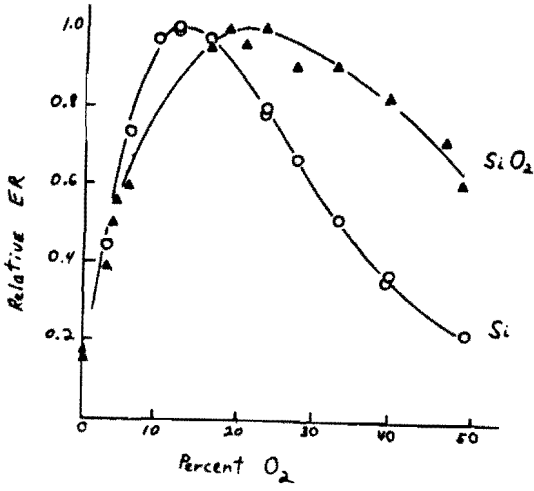
ETCH RATES AND ACTIVATION ENERGIES FOR SILICON ETCHING IN F-SOURCE PLASMAS



Plasma	Etch Rate At 100°C (Å/min)	E _a (eV)
F·/F ₂ [†]	4600	0.108
CF ₄ /O ₂	4600	0.11
CF ₄ /O ₂	3000	0.11
CF ₄	300	0.124
SIF ₄ /O ₂	440	0.11

Some Fluorine Atom-Source Plasmas

- CF₄ CF₄/O₂ SF₆ SF₆/O₂ F₂ NF₃
 C₂F₆/O₂ C_NF_{2N+2}/O₂



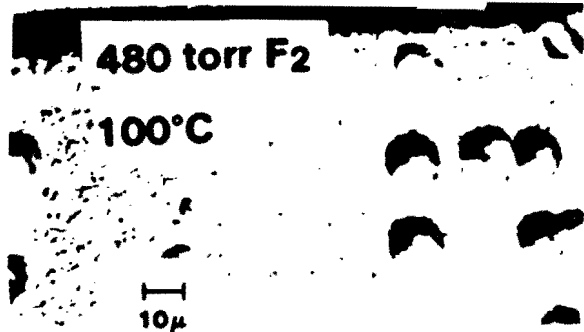
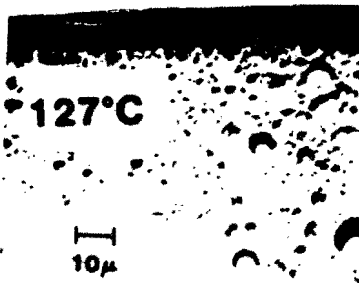
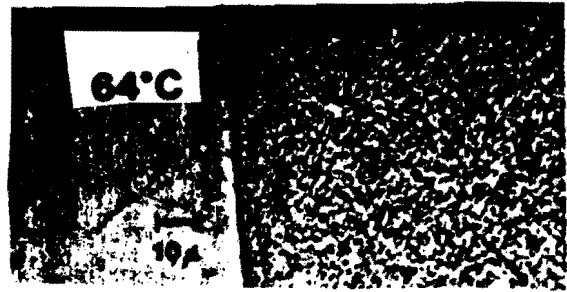
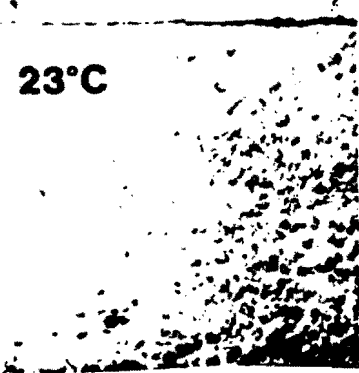
SUMMARY OF PLASMA ETCHING WITH FLUORINE ATOM PLASMAS

Materials	Gases	Anisotropy	Selectivity
Si	F ₂ , CF ₄ -O ₂ , C ₂ F ₆ -O ₂ , C ₃ F ₈ -O ₂ , SF ₆ -O ₂ , SiF ₄ /O ₂ , NF ₃ , ClF ₃	Isotropic	High over SiO ₂ , Si _x N _y , metals
SiO ₂ , Si _x N _y		Isotropic, Anisotropic at high ion energies	∞ over III-V compounds
TiSi ₂ , TaSi ₂ , MoSi ₂ , WSi ₂		Partially anisotropic at high ion energies	High over SiO ₂ , Si _x N _y , ~1:1 over Si
Ti, Ta, Mo, W, Nb		Anisotropic at high ion energies	High over SiO ₂ at high powers
Ta ₂ N		-	-

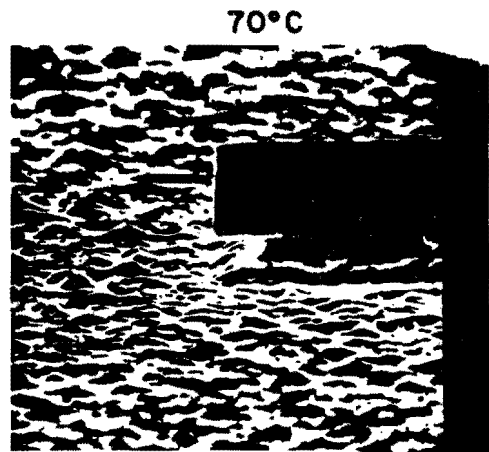
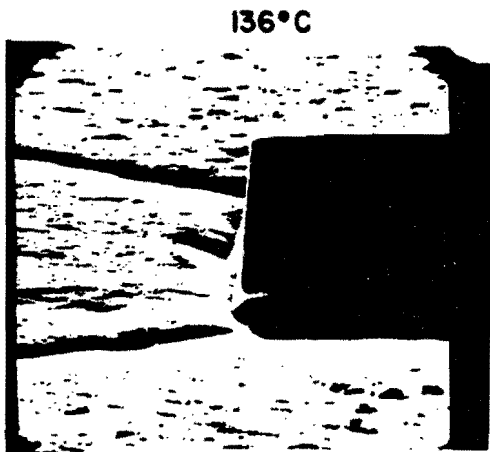
TEMPERATURE INFLUENCES MORPHOLOGY

2.7×10^{15} F-atoms/cm³

1 torr F₂



ROUGHNESS INCREASES WITH TEMPERATURE AND PRESSURE USING FLUORINE ETCHANTS

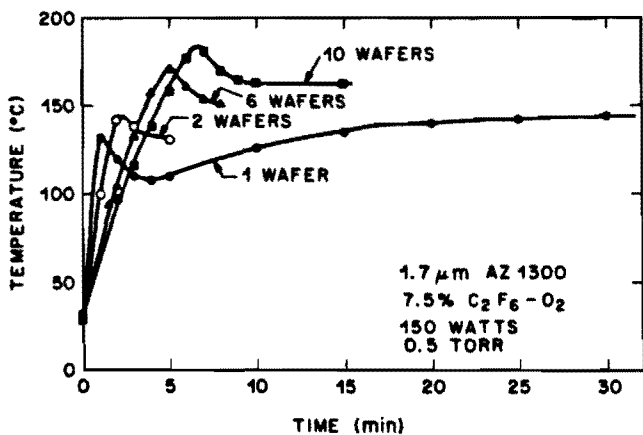
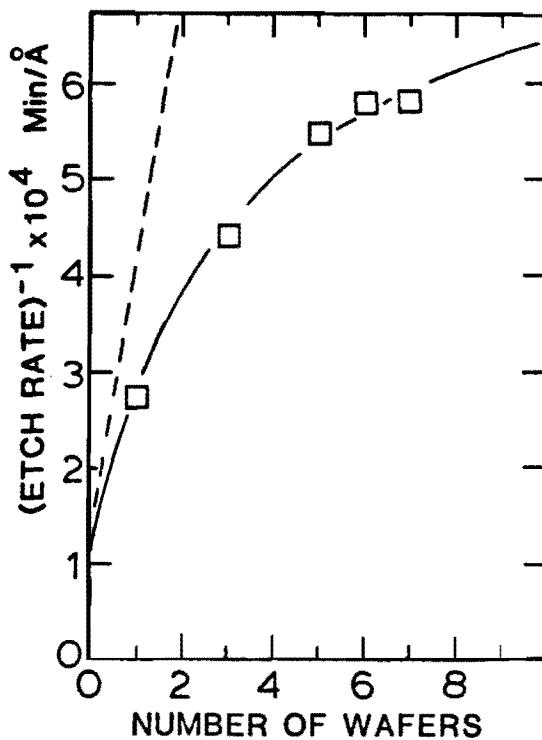
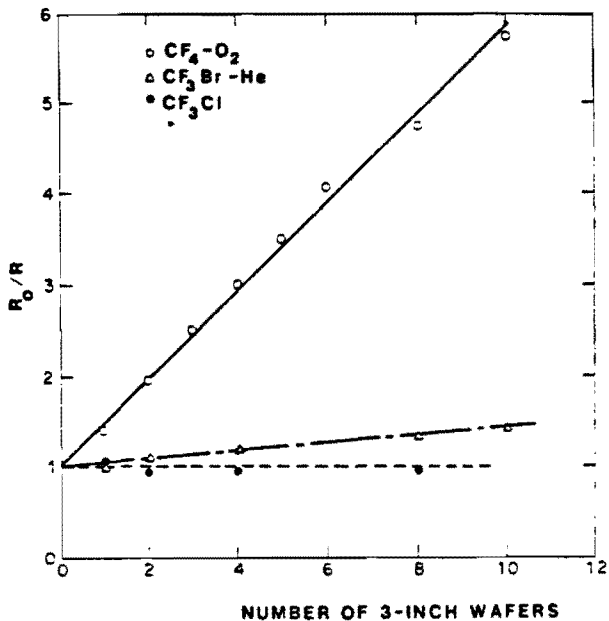


THE III-V COMPOUNDS EXHIBIT A ROUGH TO SMOOTH TRANSITION WHEN ETCHING AT INTERMEDIATE PRESSURE IN Cl₂ PLASMA PLASMAS (GAAs SHOWN).

THE LOADING EFFECT IN PLASMA ETCHING

$$\frac{R_0}{R_m} = 1 + m \frac{A_w R_{WF}}{A R_{SF}}$$

\swarrow species we rate for etching
 \nwarrow Loss of species from all other causes (e.g. recomb.)

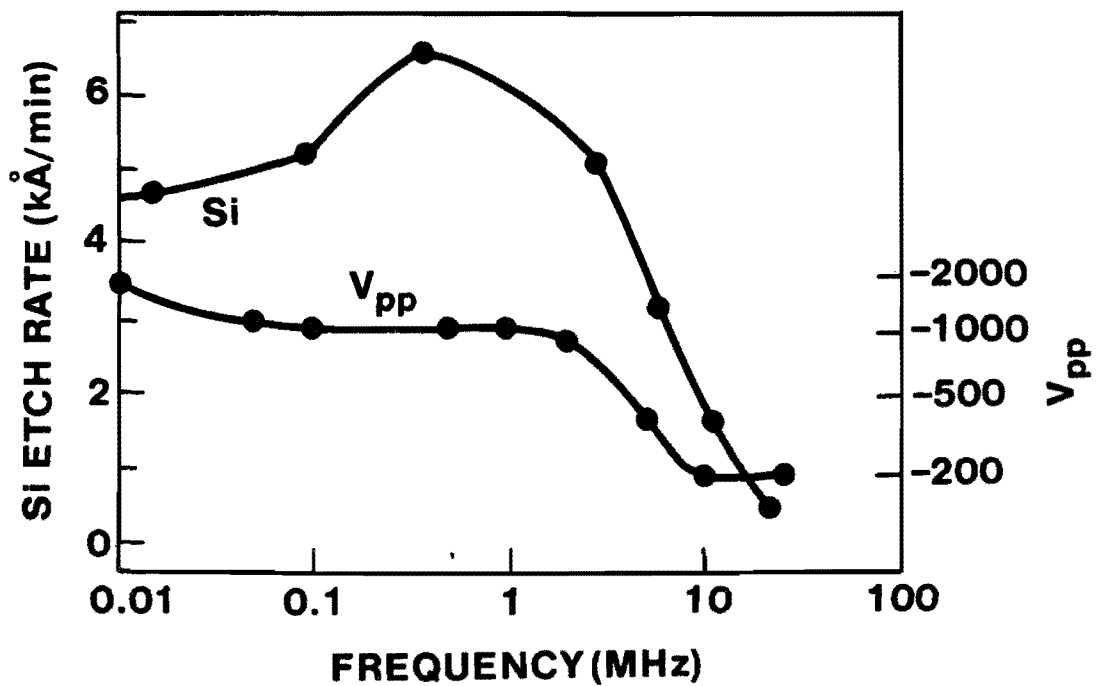


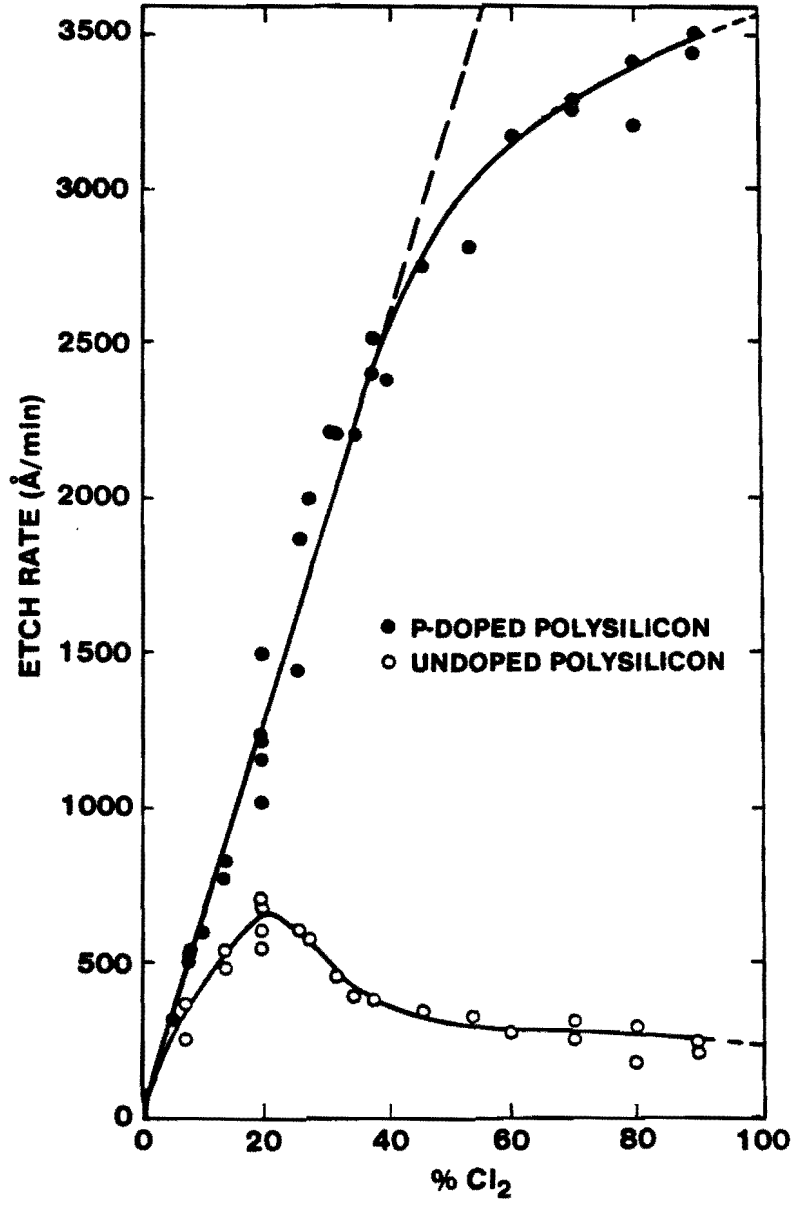
Multicomponent loading effect in ClF_3 . Combination of F and Cl etchants do not obey reciprocal law.

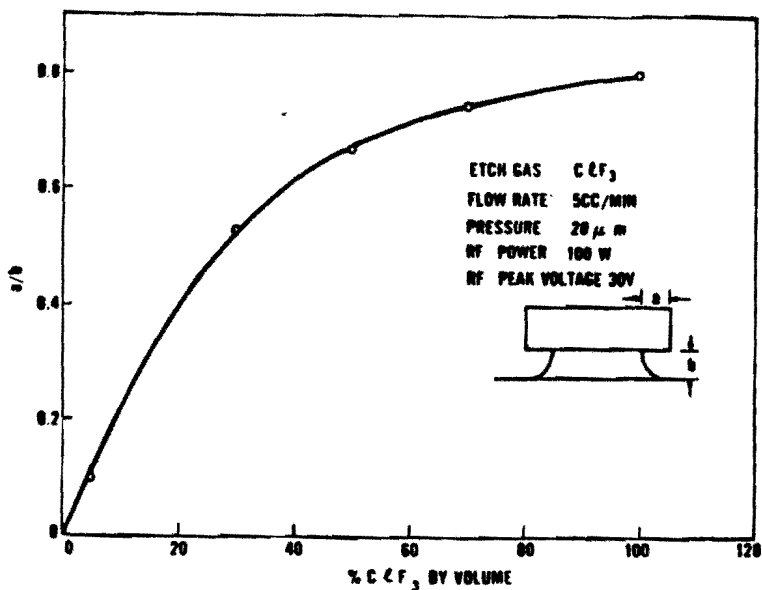
The variation of wafer temperature with time during plasma stripping of a photoresist layer.

CL PLASMA ETCHING

- CL AND CL_2 DO NOT ETCH UNDOPED SILICON SPONTANEOUSLY
ALL ETCHING IS ION-ASSISTED.
- HEAVILY DOPED SILICON IS ETCHED SPONTANEOUSLY BY
CL AND BR ATOMS.
- INHIBITOR CHEMISTRY IS USEFUL FOR ETCHING OF DOPED LAYERS







ClF_3/Cl_2 feed mixtures can be used to achieve controlled degrees of anisotropy.

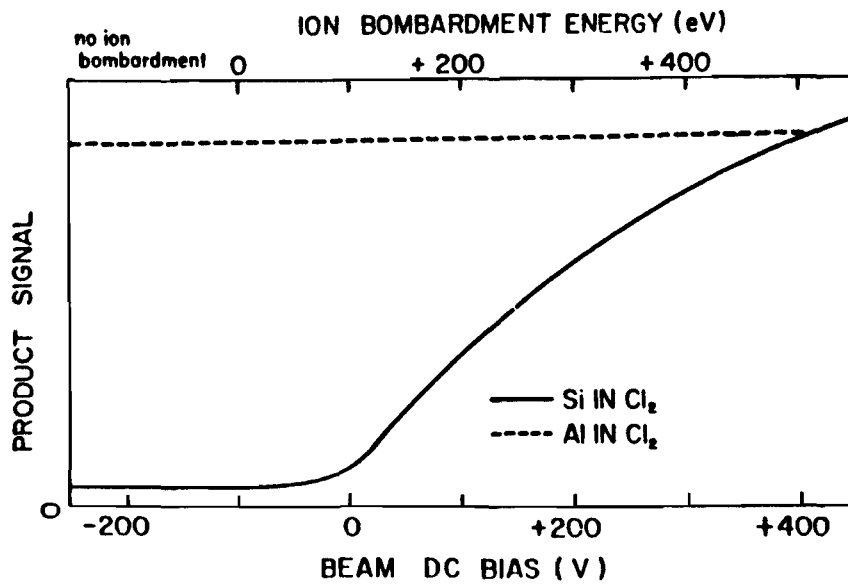
Summary of Plasma Etching in Chlorine and Bromine Containing Plasmas			
Materials	Gases	Anisotropy	Selectivity
Si	$Cl_2, CCl_4, CF_2Cl_2, CF_3Cl, Cl_2/C_2F_6, Cl_2/CCl_4, Br_2, CF_3Br$	anisotropic at high and low ion energies, isotropic for doped Si under high pressure conditions with pure Cl_2	high over SiO_2
III-V Compounds	$Cl_2, CCl_4, CF_2Cl_2, CCl_4/O_2, Cl_2/O_2, Br_2$	anisotropic at high and low ion energies (for chlorocarbon and BCl_3 mixtures), isotropic for Br_2, Cl_2 under some conditions	high over SiO_2, Al_2O_3, Cr, MgO
Al	$Cl_2, CCl_4, SiCl_4, BCl_3, Cl_2/CCl_4, Cl_2/BCl_3, Cl_2/CH_3Cl, SiCl_4/Cl_2$	anisotropic at high and low (for chlorocarbon mixtures and BCl_3) ion energies, isotropic for Cl_2 without surface inhibitor	high over Al_2O_3 and some photoresists
Ti	Br_2	-	-
Cr	$Cl_2/O_2/Ar, CCl_4/O_2/Ar$	anisotropic at low ion energies	1:1 vs. CrO_2 at $\geq 20\% O_2$
CrO_2	$Cl_2/Ar, CCl_4/Ar$	-	high vs. Cr
Au	$C_2Cl_2F_4, Cl_2$	-	-

ALUMINUM ETCHING

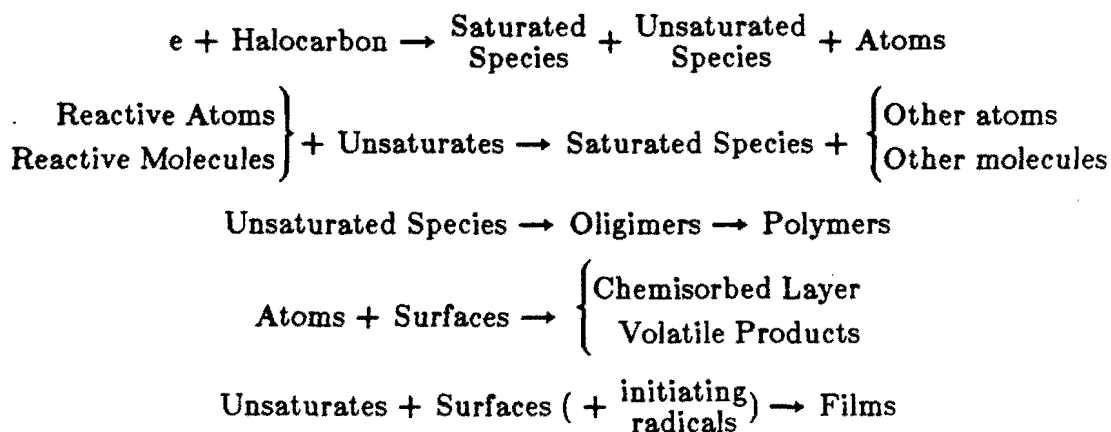
- Anisotropic
- Large Chemical Etch Rate in Cl_2
- Native Oxide Layer
- Copper, CuCl_3 evaporation ~ 33 Kcal/mole
- Unsaturates or other inhibitor
- Hygroscopic Byproducts of Etching
- Fluorine
- Reactor Material and adsorption

Gases

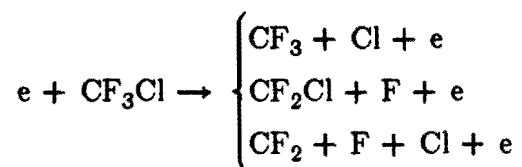
Cl_2 BCl_3 CCl_4 CCl_3H Ar He (C_2F_6)



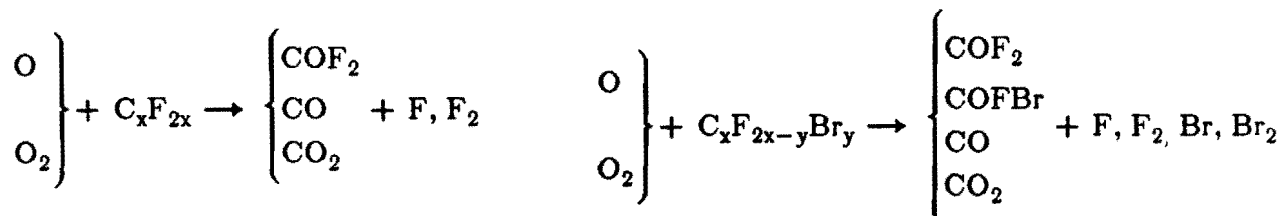
THE ETCHANT-UNSATURATE CONCEPT



Reactions of type (1) are illustrated by the following:



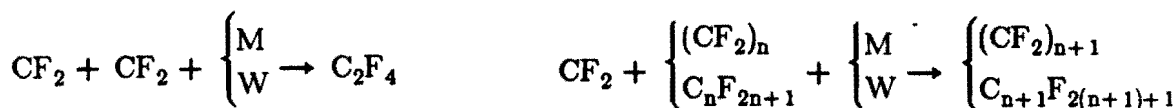
and possible saturation reactions between reactive oxidants and unsaturates are:



The above reactions cause an increase in F, F₂, Br, and Br₂ concentrations. Another example, without oxygen is:



The reaction of unsaturated species to form oligomers and polymers is typified by:



TO ALTER BALANCE

- Add Oxidant (Etchant)

Examples: O_2 , F_2 , NF_3 , Cl_2

Note: There appears to be a displacement effect-

$F \sim O > Cl > Br$

- Remove Oxidant or Add Unsaturates

Examples: Loading (Consume by Etching)

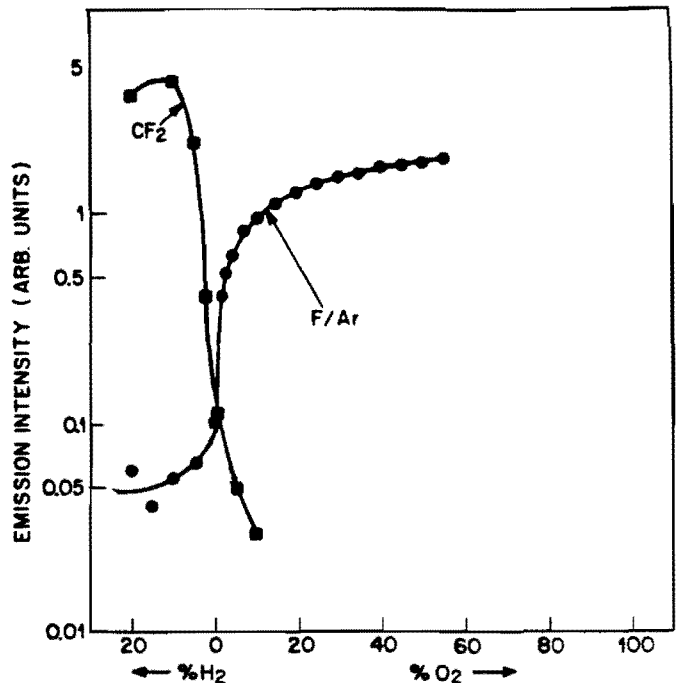
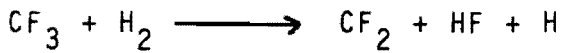
Add Hydrogen

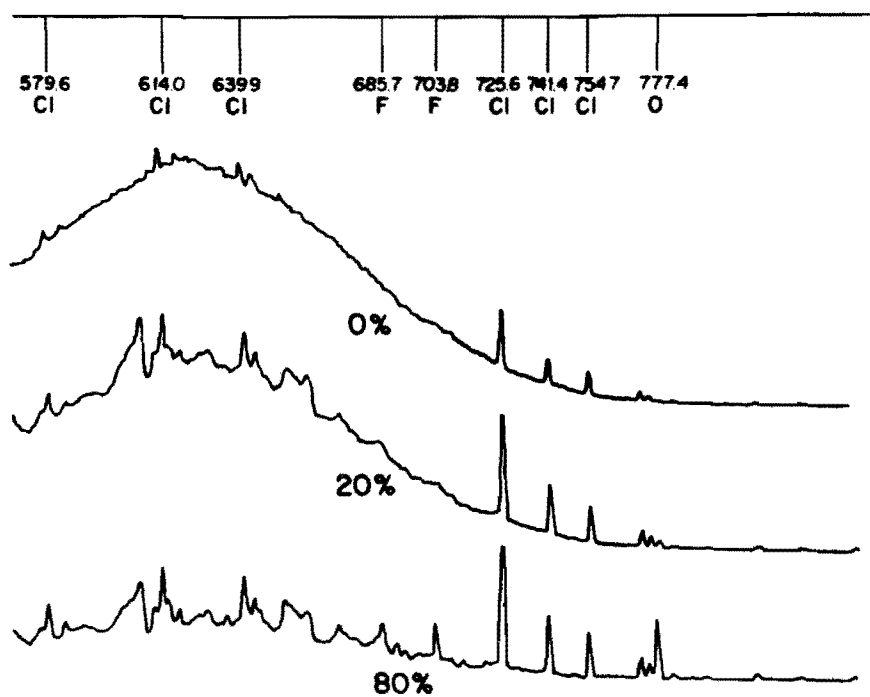
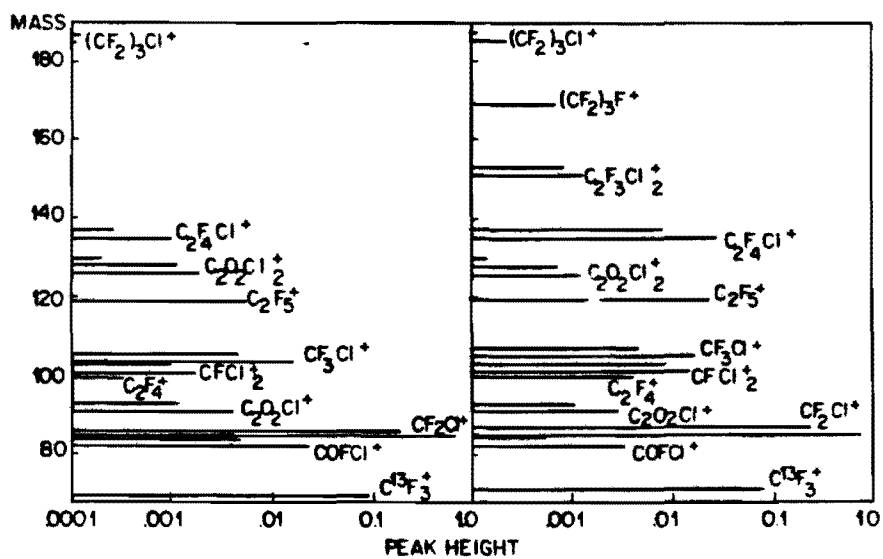
- Surfaces May Play These Roles

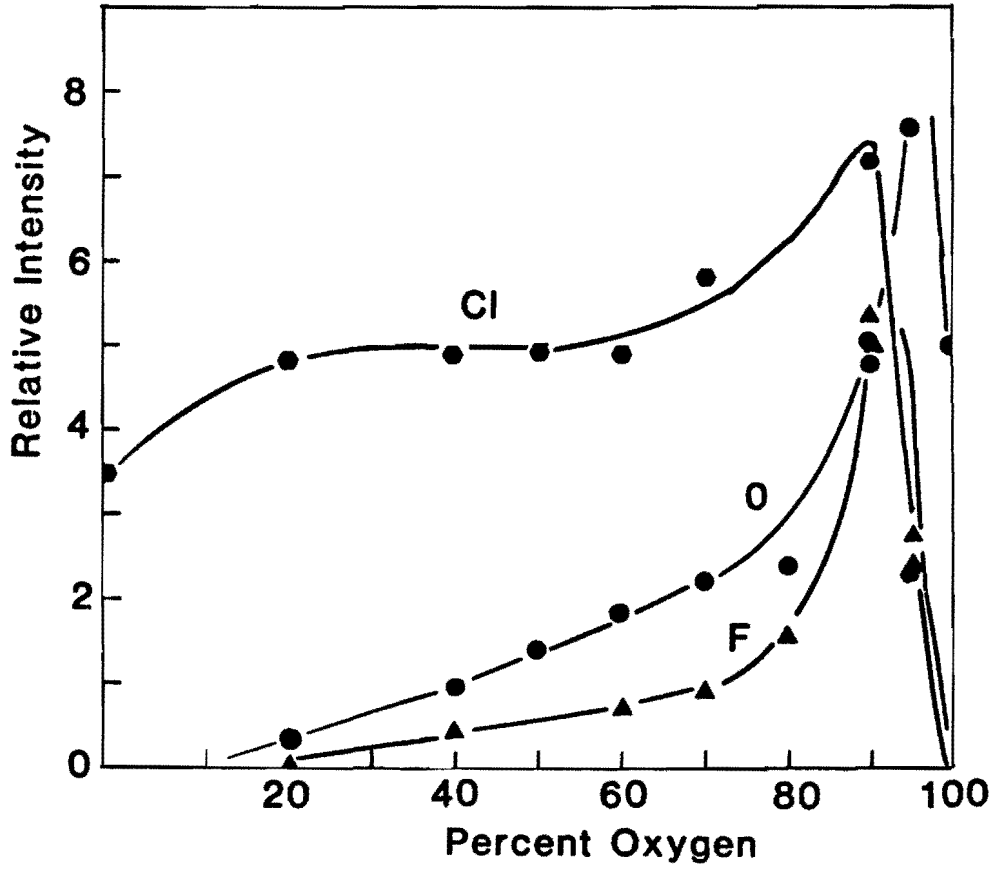
Examples: Carbon electrode $\longrightarrow CF_x$

$SiO_2 \longrightarrow O$

EFFECT OF H_2 ADDED TO A CF_4 DISCHARGE





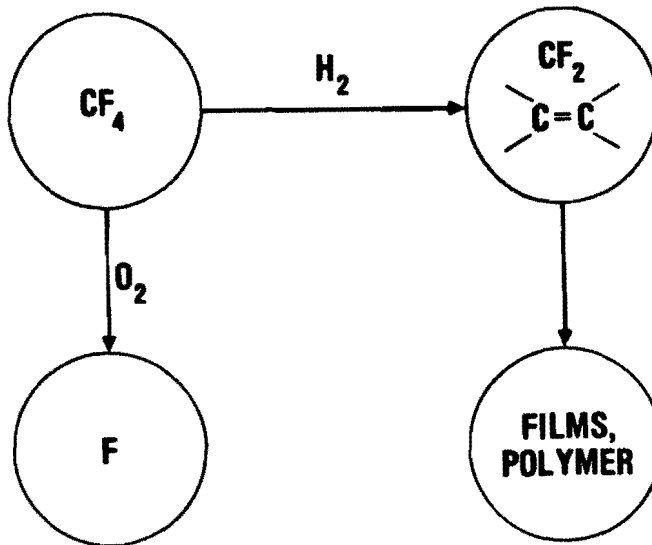


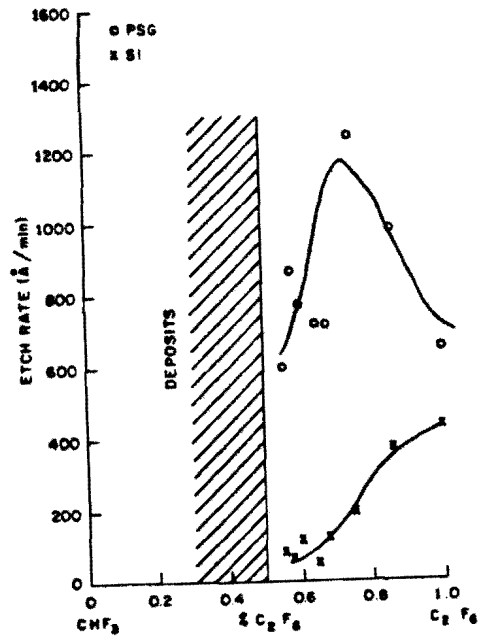
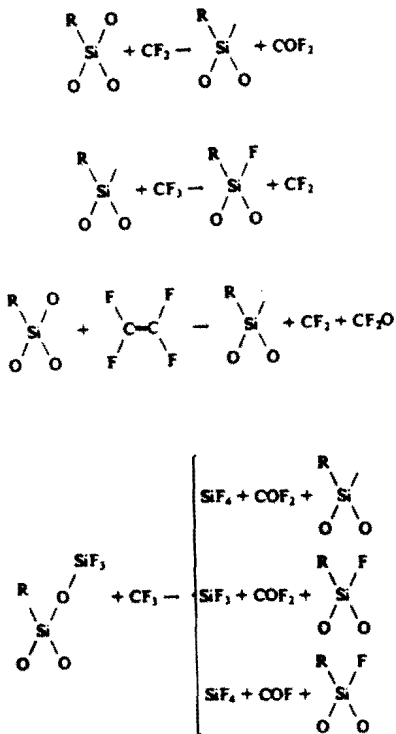
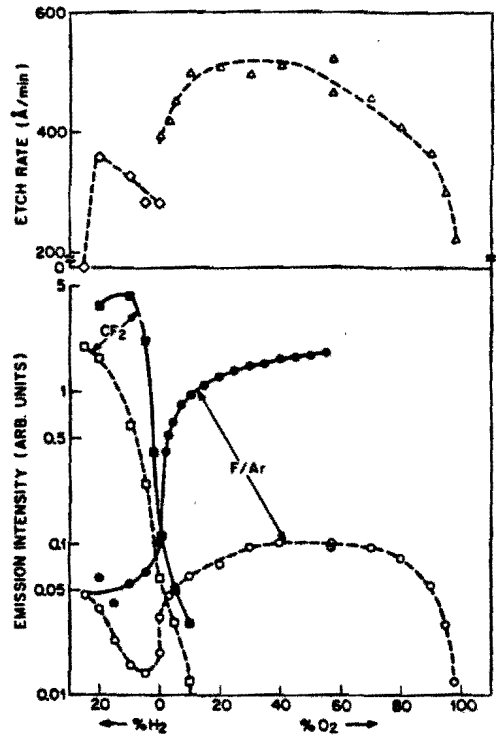
SUMMARY OF ETCHING WITH UNSATURATED FLUOROCARBON PLASMAS

Materials	Gases	Anisotropy	Selectivity
Si	CF ₄ , C ₂ F ₆	Partially anisotropic at low pressure, high ion energy	-
SiO ₂ , Si _x N _y	CF ₄ , C ₂ F ₆ , C ₃ F ₈ , CF ₄ , or C ₂ F ₆ with H ₂ , CH ₄ , C ₂ H ₂ , or C ₂ H ₄ additions	Anisotropic at high ion energies	High over Si and III, V compounds
TiO ₂		-	High over Ti
V ₂ O ₅		-	High over V

PLASMA ETCHING OF SiO_2

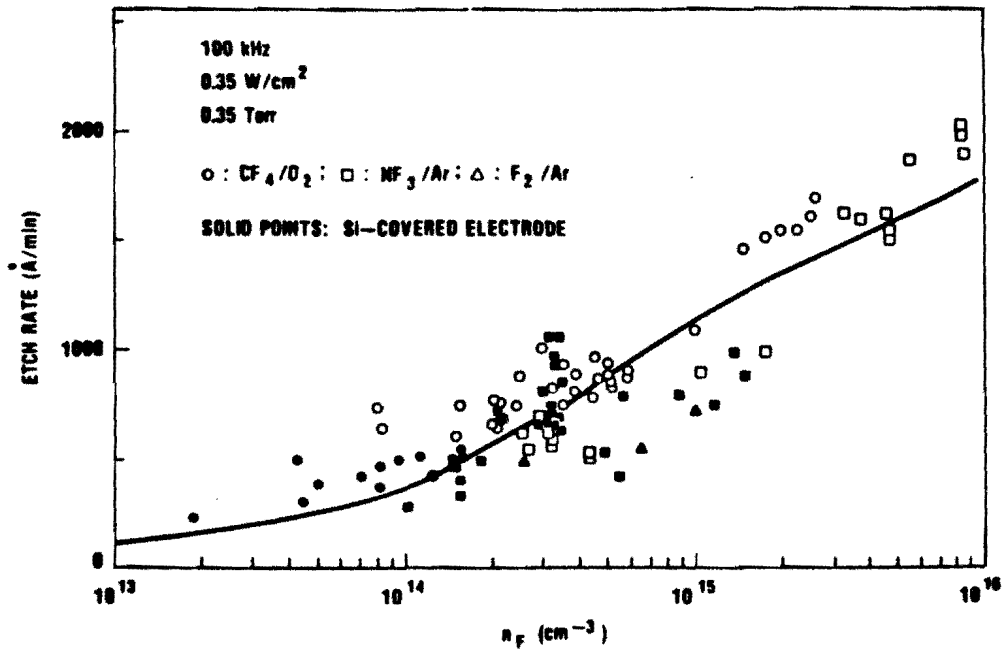
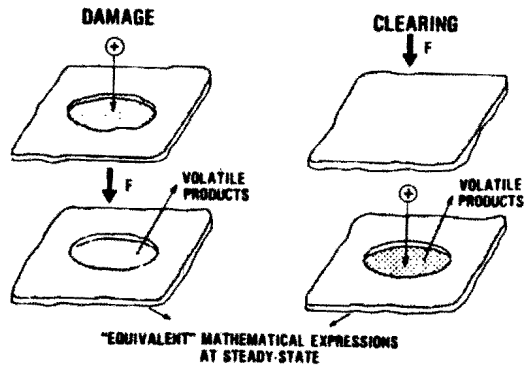
CONDITIONS	ETCHANTS	RATES/PROFILE
CF_4/O_2 HIGH PRESSURE HIGH FREQUENCY	F	~300 Å/min ISOTROPIC
CF_4/O_2 HIGH PRESSURE LOW FREQUENCY (OR LOW PRESSURE HIGH FREQUENCY)	F + IONS	1800 Å/min PARTIALLY ANISOTROPIC
CF_4/H_2 HIGH PRESSURE- LOW FREQUENCY (OR LOW PRESSURE HIGH FREQUENCY)	C_xF_y SPECIES + IONS	~1000 Å/min ANISOTROPIC

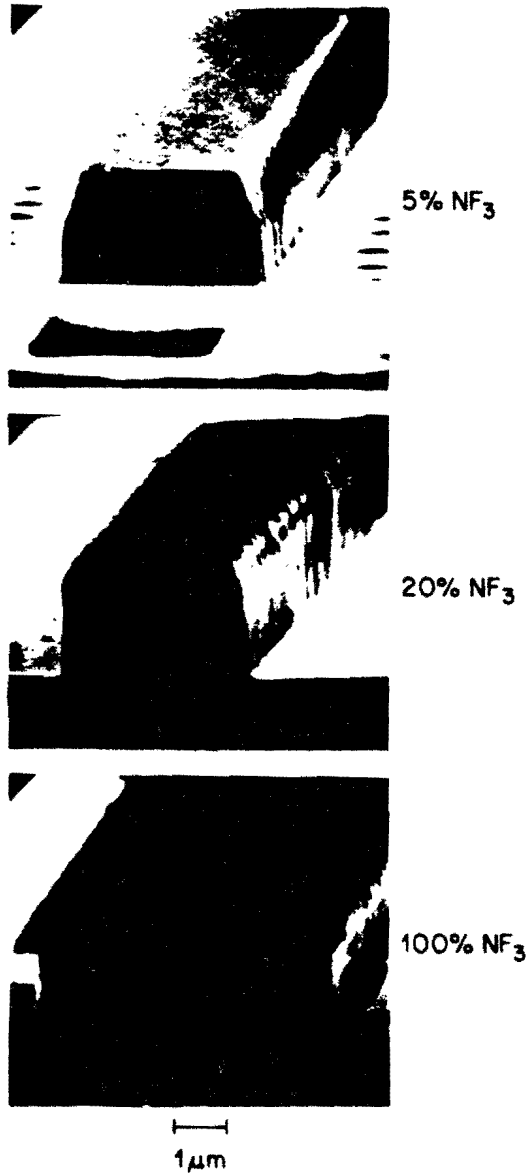




ETCH RATE OF PSG AND Si AS A FUNCTION OF REACTANT GAS MIXTURE

ION-ENHANCED ANISOTROPIC ETCHING OF SiO_2 IN LOW-FREQUENCY F-ATOM PLASMAS

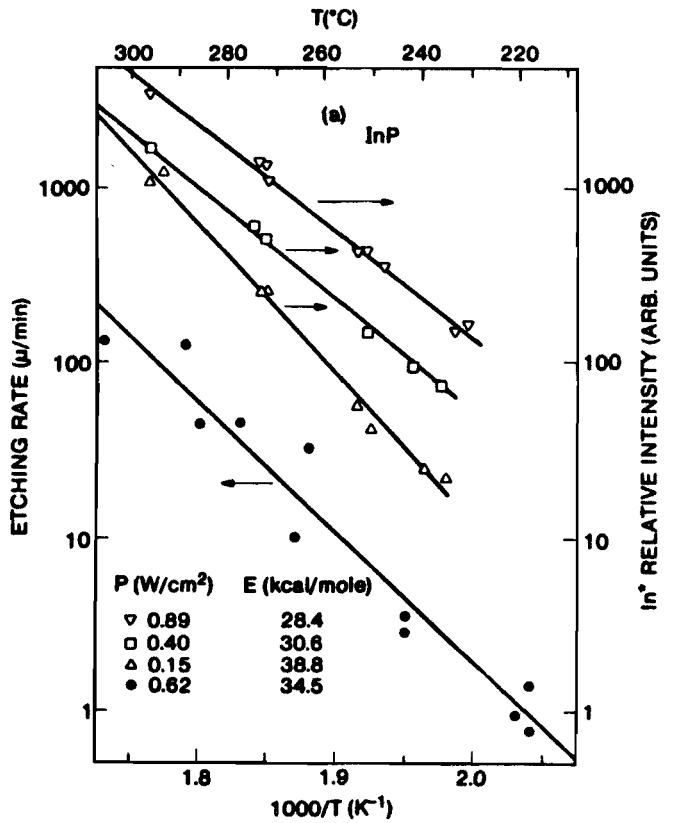
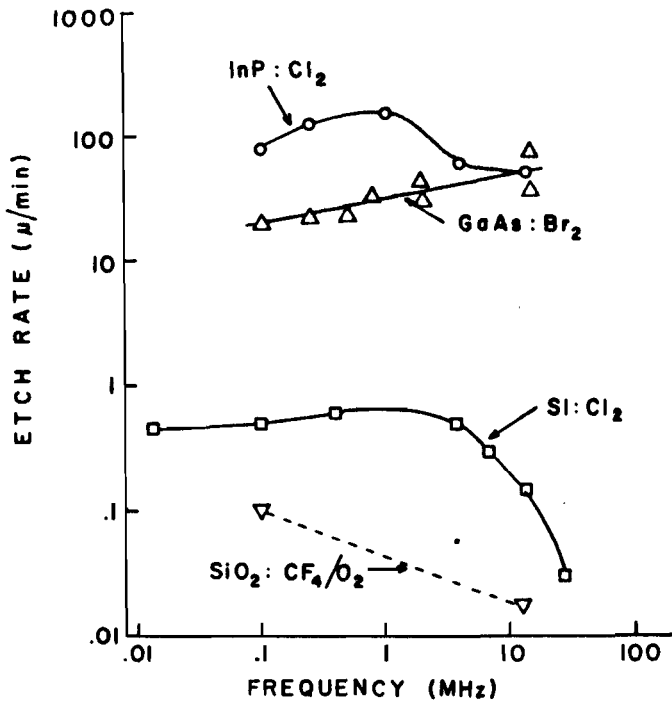


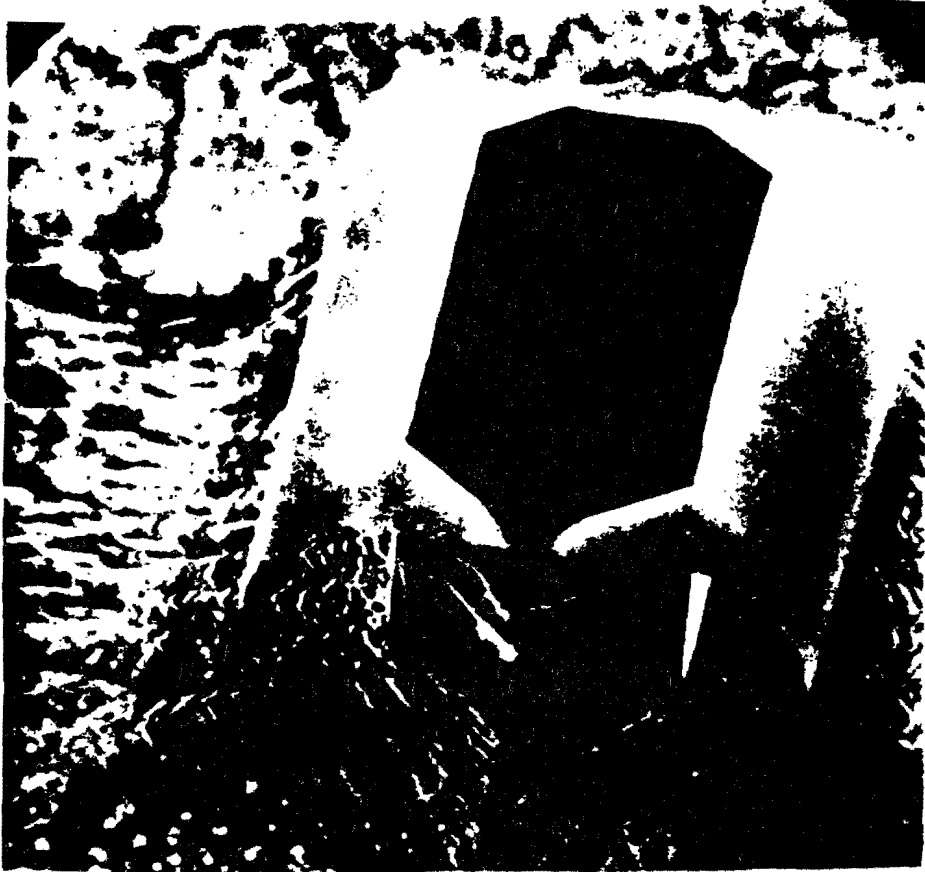


Gas Additives		
Additive	Purpose	Example (Additive-Active Gas: Material)
Oxide etchant	etch through material oxide to initiate etching	$\text{C}_2\text{F}_6\text{-Cl}_2$: SiO_2 ; $\text{BCl}_3\text{-Cl}_2$: Al_2O_3 ; $\text{CCl}_4\text{-Cl}_2$: Al_2O_3
Oxidant	increase etchant concentration or suppress polymer	$\text{O}_2\text{-CF}_4$: Si; $\text{O}_2\text{-CCl}_4$: GaAs, InP
Rare Gas, N_2	stabilize plasma, dilute etchant	Ar-O_2 : organic material; $\text{He-CF}_3\text{Br}$: Ti,
Surface inhibitor	induce anisotropy	$\text{C}_2\text{F}_6\text{-Cl}_2$: Si; $\text{BCl}_3\text{-Cl}_2$: GaAs, Al

III-V COMPOUND ETCHING

- CHLORINE AND BROMINE ETCHANTS
- ION ASSISTED AT VERY LOW PRESSURE
- GAAS ETCHED CHEMICALLY AND CRYSTALLOGRAPHICALLY AT INTERMEDIATE PRESSURE
- LARGE ACTIVATION ENERGIES AT INTERMEDIATE PRESSURE



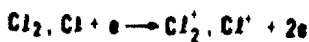


IMPORTANT REACTIONS IN Cl_2 PLASMA ETCHING OF InP

• ETCHANT FORMATION



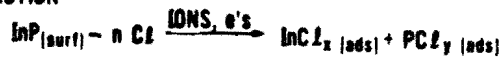
• ION FORMATION



• ETCHANT ADSORPTION



• REACTION

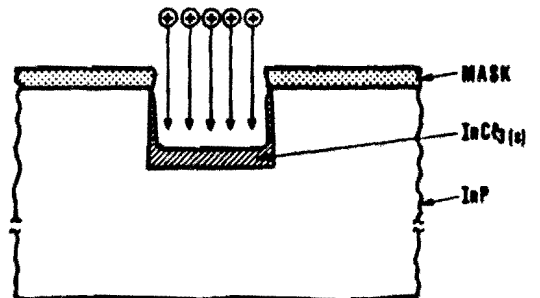


• PRODUCT DESORPTION



ION INDUCED ANISOTROPY

- BREAK BONDS IN UNDERLYING SUBSTRATE.
- ROUGHEN $InCl_3 (s)$ LAYER, INCREASING SURFACE AREA AND HENCE VOLATILITY RATE.
- HEAT $InCl_3 (s)$ LAYER ABOVE AMBIENT SUBSTRATE TEMPERATURE.



4. PLASMA - WALL INTERACTIONS

Dr. Peter C. Zalm works at the Philips Research Laboratories, Eindhoven, The Netherlands. His principal interest is the interaction of high speed particles with solid surfaces.

PLASMA-WALL INTERACTIONS; CONSEQUENCES

P.C. Zalm,
Philips Research Laboratories
5600 JA Eindhoven - The Netherlands

1. Introduction

In these lecture notes we will describe and discuss elementary processes occurring at solid surfaces immersed in low pressure plasmas. Many causes for an observed directionality in etching have been identified - crystal orientation preferentiality, ion-, electron- or foton- bombardment induced decomposition of polymerized adsorbates from the gas phase, etc. There is overwhelming evidence, however, that in the majority of cases where anisotropy was obtained in plasma etching ion bombardment of the surface to be etched played a crucial role. For this reason we will concentrate on the various phenomena accompanying ion bombardment and we try to explain their possible influence on directionality. For an extensive review the reader is referred to ref. [1]. The basic problem, which hampers the understanding of the interaction of a glow discharge with a solid, is the complexity of the whole system. Even in the simple case of a noble gas plasma environment we have to acknowledge the fact that both neutral atoms, a fraction of which may be in an excited state, ions, electrons and photons impinge on the surface simultaneously. Usually their fluxes and energies, if appropriate, are unknown and may vary with time. The use of gas mixtures, containing (fragments of) molecules, further complicates the situation.

An obvious way to circumvent, at least partially, the problems sketched above is to simulate selected process details by letting directed beams of atoms (molecules) and/or ions or electrons of well-controlled composition, flux and energy impinge on a surface in an otherwise UHV environment. Many authors have taken this phenomenological approach and with quite some success

advanced our knowledge, as we will see below. With certainty, however, by far not all aspects of the mechanisms contributing to anisotropic plasma etching have been uncovered. Because of the very nature of such a limited simulation set-up synergistic effects and the influence of trace contaminants cannot simply be accounted for.

2. The interaction of low-energy ions with solid surfaces

When ions emerging from a plasma can reach and bombard the surface to be etched their energy is usually in the range of 30eV to 3keV. Furthermore we may assume that for most practical purposes the ions have their velocity parallel to the surface normal. The latter assumption would only be invalid if dimensions of surface topographical features (masks etc.) become comparable to the plasma sheath thickness.

2.1 NEUTRALIZATION AND SECONDARY ELECTRON EMISSION

For small kinetic energies the ion neutralization probability near a surface is close to unity. The underlying mechanisms are:

- (1) resonance type processes whereby an electron is transferred from the solid into an equivalent energy level in the ion (and back);
- (2) de-excitation via an Auger transition involving two electrons.

Radiative decay processes are negligible because the lifetime for radiation ($\sim 10^{-8}$ s) is long compared to the time spent near ($\sim 5\text{\AA}$) the surface. In Auger neutralization, schematically depicted in fig. 1, one electron tunnels from the solid into the ground state of the ion while a second (valence or conduction) electron is simultaneously excited. The latter acquires the energy released upon neutralization and may escape from the target if it has sufficient momentum perpendicular to the surface. As a consequence the maximum kinetic energy of secondary electrons generated in such an Auger process is predicted to be $E_i - 2\psi$ (ionization energy minus twice the work function of the solid) in excellent agreement with experiment [2] as can be

seen in fig. 2.

At low ion energies ($\leq 1\text{keV}$), the total secondary electron yield is observed to be almost constant (fig. 3 taken from ref. [2]). A fairly accurate ($\sim 25\%$) estimate of the electron yield in this so-called potential electron energy (PEE) regime - i.e. where the potential energy of the incoming ion dominates the secondary electron generation - is given by

$$\gamma_{\text{PEE}} \approx \frac{1}{30} (0.8 E_i - 2\phi). \quad (1)$$

At higher projectile energies, the excitation of weakly bound electrons in the solid through energy transferred from the penetrating particle - governed by the electronic stopping cross section - becomes an additional source for secondary electrons. This kinetic electron emission (KEE) mechanism is usually not dominant below 3keV , as can be inferred from fig. 4. Contrary to PEE, many of the underlying processes in KEE are still not well understood and an adequate theoretical framework has not yet been provided.

Although the secondary electrons are initially ejected with low energy ($< 50\text{eV}$) they may be accelerated over the plasma sheath away from the surface. Then these electrons can ionize atoms or molecules present in the reactor, thereby sustaining the gas discharge. This is especially important in RF plasmas driven with a frequency below the ion plasma frequency $f_i (= \sqrt{n_i^+ e^2 / m_i \cdot \epsilon_0} / 2\pi)$. Only at the lowest gas pressures used in plasma etching ($\sim 10^{-3}$ Torr) the secondary electrons will be able to impinge on the reactor walls, where ternary generations of electrons can be created.

It will be obvious from the above that the secondary electrons play a significant role in the whole plasma scheme.

2.2 PHENOMENA ACCOMPANYING ION PENETRATION

Except for very light ions (e.g. H^+ or He^+), the slowing down mechanism upon penetration is dominated by kinetic energy loss of the ion in a series of binary collisions with target atoms initially at rest, in the energy range discussed here. This is called the elastic or nuclear stopping regime. In this process a number of fast recoils can be created which in turn set other target atoms in motion. A collision cascade develops

and a continuously increasing number of progressively slower particles results until transferable energies become less than the displacement threshold ($\approx 5-10\text{eV}$). The time scale is of the order of 10^{-13}s . The collision cascade is finally damped by energy dissipation through e.g. phonon-assisted processes requiring typically about 10^{-12}s to set in and lasting about $10^{-11}-10^{-10}\text{s}$. Until that time we have a locally "superheated" zone, of the order of the cascade volume around the ion's track, in which all atoms are agitated and move about with energies of the order of electron volts. Although the very concept of temperature is somewhat nebulous in this situation - an estimate would be $T \sim 10^4\text{K}$ -, enhanced diffusion, mixing and segregation of components present in or adsorbed onto the surface will occur.

At the lowest energies ($\lesssim 100\text{eV}$) the projected range, i.e. the penetration depth along the direction of incidence, is of the order of only 10\AA . The energies are too small to generate a collision cascade of displacements and effectively ion bombardment results in deposition. Even at room temperature epitaxial growth may be invoked in this way, because the deposited energy locally results in enhanced surface diffusion to favourable lattice sites. For the highest energies encountered in practical plasmas ($\sim 3\text{keV}$) the projected range of the ions can be some 100\AA , depending on the particular projectile/target combination. Radiation damage, inevitably accompanying ion bombardment, has been observed to extend to depths 3 - 10 times the ion range. As damage may affect electronic properties of the etched surfaces it could be desirable to remove such regions by an additional short plasma effluent or chemical wet etching step even if such a process would be isotropic.

During the collision cascade development chemical bonds between target atoms are continuously broken. These are reestablished later, leading sometimes to the formation of new compounds with mixed-in adsorbed species or with the incident particle itself if it is chemically active. {For example, silicon bombarded with nitrogen ions will form silicon nitride.} Thus, molecules volatile at the substrate temperature could form, a potential source for etching. Also ion-induced desorption may take place.

Finally sputtering, the ejection of target particles during ion

bombardment, occurs. The latter process is considered extremely important in anisotropic plasma etching. Therefore an entire section will be devoted to this subject.

Of course the impinging particles can reflect from the surface back into the plasma. For projectiles with a mass heavier than that of the target atoms and energies in excess of some 100eV the reflection coefficient is usually fairly small. Only for very light ions it may be substantial, as can be inferred from fig. 5. Even if the reflection coefficient is small this does not necessarily imply that the trapping probability in the target is high, because subsequent ion bombardment is very effective in releasing previously implanted inert gas. Only if the implanted species can form strong bonds with the target atoms (either by chemical or dipole Van der Waals-type interactions) its retention may exceed the few percent level.

In the case of molecular projectiles incident on a surface the dissociation probability will be close to unity at energies above ca. 100eV, because the energy transferred in the first collision is generally high compared to the internal binding energy of the molecule. The chemical reactivity of the constituent atoms is often much higher than that of the complete molecule. {For example, Si does not react with Cl₂ at room temperature but does so strongly with Cl atoms.} Thus molecular ion bombardment of surfaces can produce significant quantities of chemically reactive atoms and radicals both through bond-breaking in adsorbed molecules and by fragmentation of the incident projectile itself.

3. The interaction of (excited) neutrals and electrons with solid surfaces

3.1 (EXCITED) NEUTRALS

We can be brief about the role of excited neutral (fragments of) molecules. Contrary to chemical reactions in the gas phase, which are known to be strongly affected by electronic excitation of the interacting species, their role is insignificant in plasma-wall interactions. The reason lies in the highly efficient Auger de-excitation processes "neutralizing" the molecules

internal energy efficiently when it approaches the surface, as discussed in subsection 2.1. All that can possibly be expected is that by ejection of electrons originally bound to target atoms decomposition and finally desorption of molecules present in the surface might take place. Given the relative unimportance of the electronic excitation energy we will from here onward only consider the behaviour of neutral atoms or molecules from the plasma in a general sense, ignoring internal energies of such particles.

Even if the atomic constituents of a molecule are highly reactive, given a certain surface composition, the molecule itself might not interact with the target. Dissociative chemisorption will only occur if the sum of the binding energies of each atomic constituent to the surface exceeds the molecular dissociation energy. For this reason several gases commonly used in plasma etching, as e.g. CF_4 , C_2F_6 , CF_3Cl , CF_2Cl_2 , CF_3H , CCl_4 , are surprisingly inert on almost all surfaces. Their sticking probability is low and consequently the surface residence times of such molecules will be very small ($\sim 10^{-6}\text{s}$). This does not necessarily imply, however, that the steady-state coverage may be neglected. For pressures of the order of 10^{-2} -1 Torr - all but uncommon in plasma reactors - and high electron and ion densities in the plasma bombardment induced dissociation can still be important as we will see in subsection 3.2.

In realistic plasmas not only complete molecules from the parent gas will be present but neutral molecular fragments and radicals abound. In the absence of strong evidence to the contrary, it should be assumed that radicals have reasonably large sticking coefficients and that they will react with the surface. { For example, CF_4 does not stick on Si, but $\text{CF}_{x \leq 3}$ does so with a probability of 0.08-0.75!. } Moreover, charged particle bombardment-induced modification of the surface too may alter the adsorption behaviour of molecules in a plasma environment. It should be noted that for molecular gases not all of the constituent atoms will necessarily always lead to a favourable reaction with the substrate atoms. Part or even all of the effects of the desired component may be counteracted by another.

If a gas as such does react spontaneously with the surface, several options exist. When the reaction leads immediately to

volatile products, which desorb quickly, (rapid) isotropic etching results. Etch selectivity, i.e. the preferential removal of one type of atoms present on the surface to be etched, is likely to be high. Generally an adsorbed gas layer on top of the partly reacted surface will form. The depth to which this altered layer extends depends on the reactive gas flux, the removal rate by desorption and/or volatile product formation and the diffusion through this layer. { For example, Cl_2 only chemisorbs dissociatively on the very surface of Si, whereas for F_2 there is evidence that it not only reacts and etches directly but also that it penetrates to a depth of several monolayers. } Of course reactions may take place leading to stable compound formation (e.g. corrosion effects).

Of course the chemical bonds formed will affect any sputtering action of the ions originating from the plasma. If the "structure" of the reacted surface layer is akin to a "Van der Waals" type solid, of more or less independent molecules, a sputtering yield enhancement results. When it resembles a "glassy" solid, with bond cross-linking, a reduction in sputtering yield may be observed. The former case is expected for monovalent reactive gas atoms, whereby upon reaction a single bond with a target atom replaces an atom-atom bond in the solid. Multivalent atoms from the reactive gas are more likely to form cross-links.

3.2 ELECTRONS IMPINGING ON THE SURFACE

Energetic electrons can excite electrons bound to target atoms. The creation of such so-called core holes may lead to a breaking of the chemical bond between atoms in or on the target surface. Thus, electron-bombardment-induced dissociation of adsorbed molecules might take place. For example, it is known that Si_3N_4 and SiO_2 do not react spontaneously with XeF_2 . { Note: XeF_2 is a white solid with a high vapour pressure. When incident on a solid surface it immediately dissociates in Xe, which desorbs instantaneously, and F_2 . The advantage of using XeF_2 instead of F_2 gas is that less precautions are required during e.g. transport. } Simultaneous exposure to an electron beam, however, results in rapid etching, because of electron induced F_2 dissociation.

tion (see fig. 6).

The possible bond-altering action of ion bombardment can also lead to target decomposition. For example, when SiO_2 is bombarded with electrons it decomposes into silicon and, volatile, oxygen. In contrast, exposure of Si to an electron beam in the presence of oxygen causes the O_2 to dissociate and promotes atomic oxygen into the bulk material thereby creating a surface oxide.

The cross sections for electron stimulated desorption on most surfaces are usually much smaller than for comparable gas phase processes involving electron induced dissociation and dissociative ionization. Nevertheless we believe gas-solid chemical reactions, which happen only in the presence of ion or electron bombardment, are widely occurring phenomena in a plasma environment.

4. Some aspects of sputtering

4.1 THEORY FOR ELEMENTAL TARGETS

Perhaps the best founded, and with certainty the most widely applicable, theory of sputtering of elemental targets by atomic projectiles has been formulated by Sigmund [3]. On the basis of linearized Boltzmann transport equation to describe the collision cascade in a semi-infinite and random medium he arrived at an expression for the backward sputtering yield at an ion energy E given by

$$Y(E) = \Lambda F_D(E, x=0). \quad (2)$$

Here F_D stands for the amount of energy deposited at the topmost atomic layers of the surface ($x \simeq 0$) in the form of target atomic motion. Λ is a material parameter encompassing the angle-, depth- and recoilenergy - averaged escape probability for target atoms set in motion in the cascade. F_D is linearly proportional to the (reduced) nuclear stopping cross section evaluated at the surface and Λ is inversely proportional to a surface escape barrier (usually taken to be equal to the sublimation energy).

The assumption underlying eq. (2) are known to break down for a

number of cases. For a full account of these the interested reader is referred to ref. [3]. In the energy regime discussed in these notes it suffices to know that the results of eq. (2) are invalid for low incident ion energies ($\lesssim 100\text{eV}$) and for light ions, where the energy transferred is insufficient to allow a proper collision cascade development. Several alternative approaches have been proposed to deal with these light ion and so-called threshold energy regimes, none of which are theoretically fully convincing although often satisfactory from a practical point of view.

For numerical evaluation eq. (2), in the case of perpendicular incidence, can be recast into the form

$$Y(E) = C_{pt} S_n(E), \quad (3)$$

where C_{pt} and E_{pt} are characteristic constants depending on projectile and target parameters (viz. atomic number, mass and target atom sublimation energy U_0 in [eV]). These are given by

$$C_{pt} = (Z_p Z_t)^{5/6} / 3U_0 \quad (4)$$

applicable for $1/6 \lesssim Z_t/Z_p \lesssim 5$, which is roughly the region of validity of the theory itself, and the exact expression

$$E_{pt} = \frac{1}{32.5} \left(1 + \frac{M_p}{M_t}\right) Z_p Z_t \left(Z_p^{2/3} + Z_t^{2/3}\right)^{1/2} \text{ [keV]}. \quad (5)$$

The reduced nuclear stopping cross section $S_n(E)$ has been estimated reliably as

$$S_n(E) = \frac{1}{2} \ln(1+E) / \left\{ E + \left(\frac{E}{383}\right)^{3/8} \right\}. \quad (6)$$

For incidence at an angle ϑ with respect to the surface normal theory predicts a rise in yield proportional to $\cos^{-n}\vartheta$, with $1 < n < 2$, because the energy deposited in the outermost atomic layers (F_D in eq. (2)) increases. Experimentally such a dependence on ϑ is observed to hold to about 45° , then the yield flattens off to a maximum at $70^\circ \pm 10^\circ$ (of $Y(\vartheta_{\text{max}})/Y(0^\circ)$ 3-10) and rapidly drops to zero when ϑ approaches 90° (glancing incidence), presumably because of particle reflection. Some examples are given in fig. 7.

Equations (3-6) have proven to be highly successful in pre-

dicting both the functional form of the energy dependence and the scaling with projectile or target parameters of the yield for ion energies exceeding a few hundred electron volts. Also the estimate of the absolute magnitude of the sputtering yield often agrees well with experiment. As an example the experimentally observed yields for noble gas ion bombardment of Mo in the energy range of 0.2-20keV, divided by C_{pt} , are shown in fig. 8 as a function of reduced energy $\mathcal{E} = E/E_{pt}$. Indeed the $S_n(\mathcal{E})$ curve is closely followed. However, for high target-to-projectile mass ratios (e.g. Ne^+ on Mo) and also for heavy ions on heavy mass targets (i.e. $M_p, M_t \gtrsim 60$) the value of C_{pt} required to fit the experimental data has been observed to be lowered, sometimes by as much as 50%, relative to the theoretical value of eq. (4). Consequently the theory should be treated with some caution. A compilation of experimental sputtering yield data for atomic ion bombardment of elemental targets, along with a comparison with theory and some additional information is given in ref. [4].

In order to circumvent the threshold problems in the low energy range ($< 0.5\text{keV}$) discussed previously and to extend the use of eqs. (3-6) to this regime as well, the following empirical rule-of-thumb approach may be taken. Subtract from the yield calculated from eqs. (3-6) the value evaluated at the threshold energy E_{th} , which for practical purposes may be estimated as $E_{th} \approx 8U_0$ for $1/5 \lesssim Z_t/Z_p \lesssim 5$. Strictly formally there is no theoretical foundation for such a forced ad hoc introduction of a threshold but it usually works well. { As $S_n(\mathcal{E})$ can be approximated by $S_n(\mathcal{E}) \approx \frac{5}{3} \sqrt{\mathcal{E}}$ at low energies ($\lesssim 3 \text{ keV}$) a crude but simple estimate for the yield, at perpendicular incidence, including threshold effects can be extracted from eqs. (3-6) as

$$Y(E) \approx \frac{5}{3U_0} \cdot \sqrt{Z_t} (\sqrt{E} - 0.09 \sqrt{U_0})$$

which, with E in [keV] but U_0 in [eV], is valid to within 25% for $0.2 \lesssim Z_t/Z_p \lesssim 5$. This expression shows that the yield is not very dependent on projectile parameters other than incident energy. }

Let us now turn to sputtering of elemental targets by complex molecular ions. As argued before, the molecule will frag-

ment into its constituents upon impact on the surface at almost every energy ($\gtrsim 100\text{eV}$). As a consequence the atoms will individually penetrate and invoke a cascade. The total sputtering yield of the molecular ion may be taken as the sum of the yields of the individual constituents, as non-linear effects will be small in the energy range discussed here. The velocity of the atoms, originally forming the molecule, can be assumed equal to the original ion velocity - i.e. $E_{\text{atom}} = m_{\text{atom}}/m_{\text{molecule}} \cdot E_{\text{ion}}$ - because the energy transferred in the first collision, although high compared to the molecular binding energy, is on average low with respect to the kinetic energy. Atomic sputtering yields may be taken from the compilation of experimental data [4], if available, or from the theoretical estimates, eqs. (3-6). The latter leads to the approximate result

$$Y_{M \rightarrow T}(E) \simeq C_{Mt} S_n(E/E_{Mt}), \quad (7)$$

with

$$(C, E)_{Mt} = \sum_i (C, E)_{p_i t} \quad (8)$$

where M stands for molecule and the sum is over all constituent atoms. Equations (7, 8) imply a "Sigmund"-like behaviour of the molecular ion yield. Thus, the characteristic constants determining magnitude and energy scaling of the sputtering yield for bombardment with a molecule must be taken as the sum of the respective characteristic constants of its constituent atoms. For a simple cluster ion of n identical atoms eqs. (7, 8) reduce to $Y_n(E) = n Y_1(E/n)$, a relation observed to be obeyed experimentally for dimer and trimer sputtering at moderate energies. Of course the same restrictions to the validity and use of eqs. (7, 8) apply as for eqs. (3-6), its theoretical "background". Experimental verification of eqs. (7, 8) is hampered by the fact that in practice molecular ions always contain chemically reactive atoms, for which the simple sputtering theory may not apply as will be discussed in the next subsection.

For compound targets current understanding of sputtering is still very incomplete and a satisfactory theoretical description is largely lacking. The theoretical and experimental situation is reviewed in ref. [5]. The major problems encountered in a description of the processes involved are preferential sputtering of one of the components and ion-induced segregation and

diffusion. As a consequence the dynamics of the sputtering process must be modeled in order to understand the experimental situation. Time-dependent Monte-Carlo computer simulation codes have been developed to deal with this situation. Remarkable successes have been reported but, because of the particulars of a specific projectile/compound target combination, these have had little impact in the uncovering of underlying generalities. In spite of the considerable computational cost and modeling difficulties, related to the weighing of the various potentially competing phenomena, most future progress is expected to come from such simulations. In the mean time sound experimental data must be collected for particular, technologically urgent, cases.

4.2 SPUTTERING WITH REACTIVE IONS

Even in the absence of a possible chemical reaction between target and projectile atoms the trapping of the implanted species can result in a complicated behaviour of the sputtering yield, because of the alteration of the energy deposition, effects on chemical bonds, amorphization or even gas release. { For example, for noble gas ion bombardment of Si the yield is found to increase with fluence to a steady-state maximum attained around 10^{15} ions/cm². } Consequently the predictions of the sputtering theory discussed in the previous subsection do certainly not apply to bombardment with reactive ions, showing a high trapping probability, in an energy and dose regime where the sputtered depth extends to over the projected range of the ions. An increase in the yield, relative to the predictions of eqs. (3-6), may follow from weakening the bonds - lowering of U_0 , the surface escape barrier -, enhancing the deposited energy density - $F_D(E)$, the kinetic energy transferred to target atom motion at the surface - and formation of volatile reaction products. { This situation probably exists in, for example, Si bombarded with F^+ ions which might lead to SiF_4 formation. } In reverse, similar arguments can be put forward to expect a yield decrease for specific projectile/target combinations. { For example, Si bombardment with N^+ or N_2^+ ions results in silicon nitride formation, a material with a higher resistance to sputtering than Si itself. }

The most systematic investigations on Reactive Ion Beam Etching (RIBE) in relation to plasma processing has been carried out by groups at IBM (Coburn, Winters and co-workers, see e.g. refs. [1, 6]) and Hitachi (Miyake, Tachi and Tokuyama et. al., ref. [7]), although many others have also contributed substantially. Almost all of these experiments were centered around ions of halogen - or halogen containing molecules incident on Si or its compounds. Often the sputtering yield obtained with such projectiles is related to the yield of comparable mass noble gas ions to show or deduce "chemical enhancement effects". This procedure has been subjected to critique, however, on the basis of the arguments leading to eqs. (7, 8) and general comments pertaining to the effects accompanying reactive ion implantation, as discussed before. Although the pioneering efforts by the IBM group are recognized, we will briefly summarize the general features observed in RIBE taking data from Hitachi as an example. The latter were obtained with mass-selected and energy-analyzed ion beams thus allowing for an easier interpretation.

In fig. 9 the observed [7] energy dependences of the steady-state sputtering yields, of all possible projectiles resulting from ionization of CF_4 , of Si bombarded at normal incidence are shown. As carbon ions are seen to be deposited onto or incorporated into the Si at all energies, also the curve for F^+ on elemental C is included.

First consider the results for $^{19}\text{F}^+$ or $^{20}\text{Ne}^+$ on Si. The physical sputtering yield of both ions should be roughly equal according to eqs. (3-6).

Thus, the observed yield increment of about 0.15 Si atoms/ion for F^+ relative to Ne^+ was attributed to SiF_4 formation. As stated before, however, other arguments could apply - e.g. an increase in $F_D(E)$ or a decrease in U_0 due to F^+ implantation, to keep in line with the language of eqs. (2-6) - and actually can explain the observations. Similar results were obtained in a comparison of Si sputtering yields for $^{35}\text{Cl}^+$ and $^{40}\text{Ar}^+$ ion bombardment, where also incorporation of Cl in the top atomic layers of the Si was observed. Thus, one must rightfully conclude that the chemical role of the reactive ion bombardment is not merely to stimulate the reaction path leading to volatile product formation.

The trends observed for these and other reactive atomic ion elemental target combinations can be summarized in the following very crude rule-of-thumb estimate for the expected chemically induced yield enhancement or reduction, relative to the comparable mass noble gas ion result or the prediction of eqs. (3-6):

- i) $\Delta Y_{\text{chem}} \lesssim + a/b$, if projectile P and target T can form a volatile compound T_aP_b . {Note: \lesssim to account for particle reflection and sputtering.};
- ii) $\Delta Y_{\text{chem}} \sim - b/(a+b) \cdot Y_{\text{phys}}$, if the product T_aP_b is involatile. {Note: \sim because it is only an order of magnitude estimate of the effect.}

For all molecular (-fragment) ion bombardments studied to date it has been established that the observed sputtering yields lie below the theoretical predictions of eqs. (7, 8), the "fragmentation-into-it's-constituents" sum rule.

In fig. 9 the comparison is made for CF_2^+ on Si (Σ_{the} gives the estimate of eqs. (7, 8). The reason is fairly simple: deposition or incorporation of one of the constituents is not accounted for by the theory! Consequently part of the other molecular constituents (F in this case) are needed to scavenge the deposit. Attempts have been made to account for this by using experimental elemental yield data in approach otherwise somewhat analogous to the one leading to eqs. (7, 8). In the case of CF_n^+ on Si, such an experimental fragmentation sum rule would read

$$Y_{CF_n^+ \rightarrow Si}^{(E)} = \left[\frac{Y_{C^+ \rightarrow Si} \left(\frac{E}{1 + \frac{19}{12}n} \right)}{Y_{F^+ \rightarrow C} \left(\frac{E}{n + \frac{12}{19}} \right)} + n \right] \cdot Y_{F^+ \rightarrow Si} \left(\frac{E}{n + \frac{12}{19}} \right), \quad (9)$$

where experimental yield data at the appropriate energies have to be inserted. {Note that $Y_{C^+ \rightarrow Si}$ has a negative sign!} In fig. 9 the comparison is made for CF^+ on Si (Σ_{exp} gives the estimate of eq. (9)), but similar observations pertain to $CF_{2,3}^+$ on Si. The agreement is especially poor at lower energies. Again the reason is simple: carbon deposited onto or incorporated into silicon differs from elemental C (e.g. through carbide formation)! Thus the experimental values of $Y_{F^+ \rightarrow C}$ are unappli-

cable in this case.

Finally for CF_3^+ on Si the yield curve in fig. 9 is compared with the average of the (mutually almost identical) results for Ar^+ and Kr^+ on Si ($M_{\text{Ar}}=40 < M_{\text{CF}_3}=69 < M_{\text{Kr}}=84$). We have already discussed why such a comparison is in fact quite meaningless.

For compound targets the assessment of possible chemical enhancement effects upon the use of reactive (molecular) ions is further complicated by preferential sputtering, ion-induced segregation and diffusion. Yet another macroscopic problem arises because it has to be established whether or not all constituents in the compound can and/or will form volatile products. { For example, when SiO_2 is bombarded with CF_n^+ , $n \leq 3$ no carbon deposition takes place, presumably because of volatile CO formation. By the way, note that it has been known already for quite some time that for plasma-etching of Si in a CF_4 discharge the results improved considerably if a few percent of O_2 was added to the gas. }

Again, it is impossible to give general rules for the expected sputtering yields of compound targets under reactive molecular ion bombardment. It appears, however, that observed reactive ion etch rate selectivities for an element and its compounds (e.g. $\text{YCF}_3^+ \rightarrow \text{Si} / \text{YCF}_3^+ \rightarrow \text{Si}_3\text{N}_4$ or SiO_2) are roughly of the same order of magnitude as those obtained under "real" plasma conditions with the same type of gas.

A major problem in RIBE simulations of plasma processes is that both for elemental and compound targets the absolute sputtering yield is usually an order of magnitude lower than the corresponding plasma etch rate. Consequently the basic principles underlying plasma etching have to be unraveled by yet another type of experiments, to be discussed in the last section.

5. Synergistic effects (chemically enhanced/reduced sputtering)

It has been known for a long time that the sputtering yield of metals bombarded with noble gas ions is considerably reduced if oxygen is introduced in the vacuum system as a contaminant gas. The reason for this is the formation of metal oxides, with a low sputtering yield, induced by ion beam mixing of adsorbed oxygen into the top atomic layers. Surprisingly, the reverse situation of a yield enhancement by simultaneous exposure to a

reactive gas flux has begun to be explored only in the last decade. Pioneering work in this area was again carried out by the IBM group (Coburn and Winters et al., ref. [8]). They showed that the etch rate of Si bombarded with Ar^+ ions in the presence of XeF_2 gas is enhanced by more than an order of magnitude when compared with the individual actions of either ions or gas separately. Fig. 10, taken from this work, has become a classic in the field. It was immediately recognized that these findings were very important for (anisotropic) plasma etching and that probably one of the fundamental processes had been uncovered. This initial success prompted many other research groups to start investigations along similar lines. Below we try to summarize their results, which allow for a qualitative understanding of synergistic effects of combined exposure of a surface to ions and a reactive gas flux. Some general results can now be given, but a quantitative description of etch rate enhancement or reduction awaits future developments.

Although obviously etch rates attract the direct attention, most of our understanding about the mechanisms in chemically assisted sputtering (or ion beam induced etching) stems from the study of the resultant reaction products. In particular the investigation of the emitted products' compositions and, perhaps even more significant, the kinetic energy distributions of the ejected particles as a function of ion energy and reactive gas-to-ion flux ratio has been foremost important. In fig. 11 the experimental set-up is shown which was used to measure these quantities in the Philips-AMOLF collaboration (see ref. [9]). A target (6), mounted on an oven (5) capable of heating the sample up to 1000K, is flooded with reactive gas from an inlet (7). Mass and energy selected ions from a source (1-4) impinge on the surface at an angle of 60° . Neutrals emitted from the target perpendicularly within a solid angle of 10^{-4}sr pass a charged diaphragm (8) and are ionized (9) just in front of the entrance of a quadrupole mass spectrometer (10). Here the freshly formed ions are mass analysed and detected by an electron multiplier (11). Time-of-flight distributions can be measured by electronically modulating (3) the ion beam pseudo-randomly and coincident detection. Correlation techniques are used to unveil the particles' energy distributions. Only those signals, sufficiently

above background, are detected which stem directly from neutrals ejected during ion bombardment. Corrections for velocity dependent ionization efficiency and flight time from source or to detector are applied in later off-line analysis.

When silicon is exposed to a chlorine beam, no spontaneous reaction takes place. Above a target temperature of 300°C etching starts to become significant, the reaction product being SiCl_4 . At temperatures in excess of 800°C, removal of silicon as SiCl_2 dominates [9]. It has been proven unambiguously, however, that when Si is bombarded with Ar^+ ions in the presence of a Cl_2 gas flux on the target - such systems will be denoted by $\text{Si}(\text{Cl}_2; \text{Ar}^+)$ from here onward - Si, Cl, SiCl , SiCl_2 and (re-emission of previously implanted) Ar as such are ejected from the surface in roughly equal amounts under certain experimental conditions [9]. These particular products themselves already cast serious doubts about the possibility that the role of the ions would be merely to stimulate the thermal reaction path by local heating of the surface upon impact. Observed "sputtering" yields for the $\text{Si}(\text{Cl}_2, \text{Ar}^+)$ system exceed normal Ar^+ yields of Si by a factor of about 5, which constitutes yet another argument against such a process as a "superheated" cascade volume would have to small a surface area ($< 100 \text{Å}^2$) and exist too short ($< 10^{-11} \text{s}$) to explain the observations.

The strongest argument against a mere assisting role of the ions stems from the kinetic energy distributions of the reaction products. For a "thermal" behaviour the energy distribution would have a Maxwell-Boltzmann (MB) like shape, i.e.

$$\Phi_{\text{MB}}(E) \propto E \exp(-E/kT), \quad (10)$$

with T either the substrate temperature, T_s , or the temperature of the superheated zone, T_{LTE} , in a Local Thermal Equilibrium type approximation. In any case T should be the same for all reaction products ejected.

In a normal physical sputtering or collision cascade (C-C) model the kinetic energy distribution, for elements emitted perpendicularly to the surface, is given by

$$\Phi_{\text{C-C}}(E) \propto E/(E+U_0)^3, \quad (11)$$

where U_0 is the surface escape barrier for the particular product emitted, which is usually identified with the particle's

binding energy inside the solid. { Note that for ejected (fragments of) molecules eq. (11) is only valid up to its dissociation energy, E_d . The asymptotic roll-off at high ejection energies ($E \gg E_d$) becomes $\propto E^{k-\frac{k}{n}}$, where n is the number of atomic constituents. }

The experimentally observed kinetic energy distributions of products ejected in the $\text{Si}(\text{Cl}_2; \text{Ar}^+)$ or $\text{Si}(\text{XeF}_2; \text{Ar}^+)$ systems are more complicated than eqs. (10) or (11) suggest. In general, however, the major part of a spectrum follows the predicted collision cascade behaviour of eq. (11). An example is given in fig. 12, which shows both the raw time-of-flight data and the extracted energy spectrum for SiCl from $\text{Si}(\text{Cl}_2, 5 \times 10^{14}/\text{cm}^2\text{s}; \text{Ar}^+, 3\text{keV}, 5 \times 10^{16}/\text{cm}^2\text{s})$. A low energy MB contribution at T_S is sometimes observed (curve 1), which is believed to be due to molecules released from the bulk by desorption out of the void tunnel along the ion track. This contribution, if present at all, is always less than 20% of the total. A high temperature LTE-type MB contribution (2) can at best explain only the medium or the high energy part of only a single individual product's spectrum and certainly not the spectra for all products simultaneously with one T_{LTE} . fitting the kinetic energy distributions with the CC predictions (see e.g. curve 3 in fig. 12 but remember the note following eq. (11)) gives good agreement. The extracted "binding energies" U_0 for all individual products emitted, under the conditions valid for fig. 12, are: $U_0(\text{Si}) \approx 4\text{eV}$, slightly below the sublimation energy of silicon; $U_0(\text{Cl}) \approx 2\text{eV}$, typical for Si-Cl bond energies; $U_0(\text{SiCl}_{1,2}) \approx 0.4\text{eV}$, indicative for the interaction of a highly polarizable molecule with a solid; $U_0(\text{Ar}) \approx 0.05\text{ eV}$, typical for the Van der Waals binding energies of a noble gas atom in a solid.

These observations reveal a very important aspect of the role of the bombarding ions. Obviously mixing of adsorbed species into the topmost atomic layers takes place. { $\text{SiCl}_{1,2}$ molecules with their observed low binding energies of only 0.4 eV could never have resided on the surface: they would simply desorb instantaneously! For the $\text{Si}(\text{Cl}_2; \text{Ar}^+)$ system it has been established independently that Cl exists inside the outermost atomic layers. } The mixed-in reactive species will form bonds

with the target atoms, thereby "weakening" the solid. { This explains the reduction of $U_0(\text{Si})$ in the $\text{Si}(\text{Cl}_2; \text{Ar}^+)$ system relative to the sublimation energy. } In turn this enhances the sputtering yield, cf. eqs. (3-6).

Both mixing efficiency and sputtering yield increase with the deposited energy (as target atom motion) distribution function $F_D(E)$, cf. eq. (2), which in turn increases with energy roughly $\propto \sqrt{E}$ in the range discussed here. Many different regimes exist depending on whether the rate of mixing is faster, slower or comparable to the removal rate. The reactive gas-to-ion flux ratio will largely determine the particular situation one will be in, with the exception of rather special cases where the chemistry is radically different from the usual situation. { For example, in $\text{Si}(\text{F}_2$ or XeF_2 ; noble gas ion) mixing of F into the Si is spontaneous, even on the absence of ions, because of fluorine diffusion. For $\text{Si}(\text{SF}_6$; noble gas ion) at room temperature only normal physical sputtering occurs because the surface coverage with SF_6 is negligible as it will not stick. At -200°C a thick condensed SF_6 layer will form and we have essentially sputtering of frozen CF_6 gas! } Some typical examples are given in figs. 13 and 14.

6. Conclusions

In these lecture notes we have discussed elementary processes occurring at solid surfaces immersed in low pressure plasmas. The importance of charged particle impingement onto targets was stressed. In particular the role of synergistic effects, by simultaneous exposure of a surface to a reactive gas beam and energetic particle bombardment, for plasma etching has been emphasized. Although it is easy to comprehend the physics underlying the observed phenomena, little predictive power emerges from the remarks and conclusions presented in these pages because they are not readily transferable to processes taking place under realistic plasma conditions. Our intention was only to give you some broad views about what might be going on. All we tried to do is make you aware that there are no obvious conclusions which can be drawn in advance, when starting with a novel plasma.

{ Some examples: (i) The presence of ions not necessarily implies

loss of etch selectivity. Si bombarded ions in the presence of F_2 gas etches faster than with only either one, whereas F_2 inhibits Al sputtering by ions. (ii) The presence of ions does enhance directionality, but etch anisotropy may nevertheless be small because of other rapidly etching constituents in the plasma (see e.g. fig. 15). } The influence of plasmas on polymers (resists, masks etc.), although recognized as an important topic, has been carefully avoided in these notes for two reasons. First of all the matter is highly complicated and by far not as well established and investigated as simple elemental or compound solids. Secondly, the author's complete ignorance in this field must be mentioned.

Finally, one remark seems appropriate. It must be acknowledged that no justice has been done to many excellent contributions in the field of plasma-wall interactions. The list of references is far from complete and only intended to give you an entrée in the literature. The urge for brevity necessitated the present approach. To those learned colleagues, who happen to stumble upon these notes, I humbly apologize for my mischiefs.

References

- [1] H.F. Winters, in : Topics in Current Chemistry, Vol. 94
(Springer, Berlin, 1980) p.69.
- [2] H.D. Hagstrum, in: Inelastic Ion-Surface Collisions (Academic Press, New York, 1977)p.1.
- [3] P. Sigmund, in : Sputtering by Particle Bombardment I
(Springer, Berlin, 1981) p.9.
- [4] H.H. Andersen and H.L. Bay, in : ibid p.145.
- [5] G. Betz and G.K. Wehner, in : Sputtering by Particle Bombardment II (Springer, Berlin, 1983) p.1.
- [6] J.W. Coburn and H.F. Winters et.al., J. Appl. Phys. 48
(1977) 3532, 4973, 50 (1979) 3989.
- [7] K. Miyake, S. Tachi and T. Tokuyama,
Jap. J. Appl. Phys. 20 (1981) L411; 21 (1982) 141;
J. Appl. Phys. 53 (1982) 3214.
- [8] J.W. Coburn and H.F. Winters et.al.,
J. Vac. Sci. Technol. 16 (1979) 391;
B1 (1983) 469, 927; Phys. Rev. B23 (1981) 823; Surf. Sci.
103 (1981) 177; 123 (1982) 427; and references therein.
- [9] A.W. Kolfshoten, F.H.M. Sanders, J. Dieleman, P.C. Zalm,
R.A. Haring and A.E. de Vries et.al.,
Appl. Phys. Lett. 41 (1982) 174; J. Appl. Phys. 55 (1984)
3813; J. Vac. Sci. Technol. A2 (1984) 487; Nucl. Instr.
Meth. B7 (1985) 809.

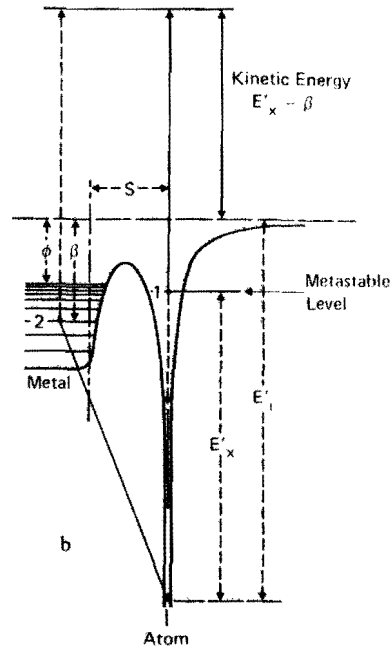
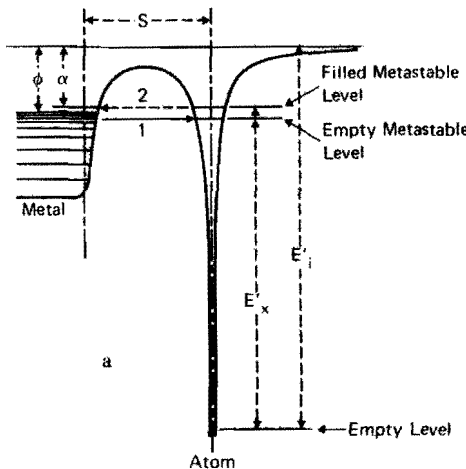
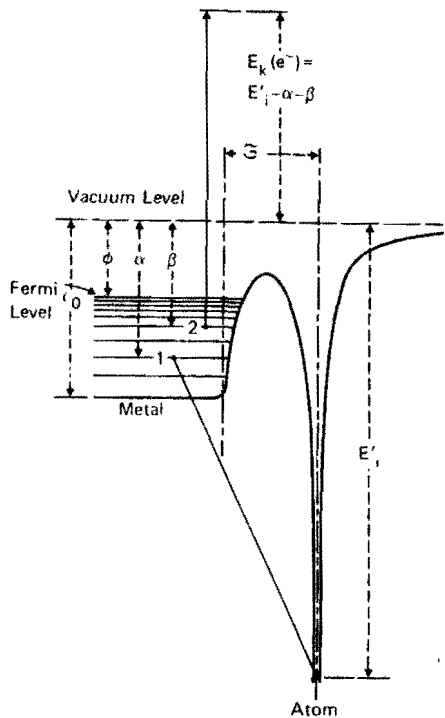


Fig. 1 Auger neutralization of an ion at a metal surface presented schematically. $E_k(e^-)$ is the kinetic energy of an electron observed outside the metal. ϕ is the work function and E_i' the ionization energy. ($E_i' < E_i$ where E_i is the energy needed to ionize an atom in free space.) ξ is the distance of the ion from the surface.

Fig. 1 Schematic diagram illustrating resonance neutralization of an ion (transition 1) or resonance ionization of an excited atom (transition 2) at a metal surface. Transition 1 can occur only at energy levels which are filled inside the metal and transition 2 at levels which are empty. (A similar figure was published in Ref. 5). b. Schematic diagram illustrating Auger de-excitation of an excited atom at a metal surface. The exchange transition is indicated by the full lines, while, the process not involving electron exchange between the metal and the atom is indicated by the dashed lines.

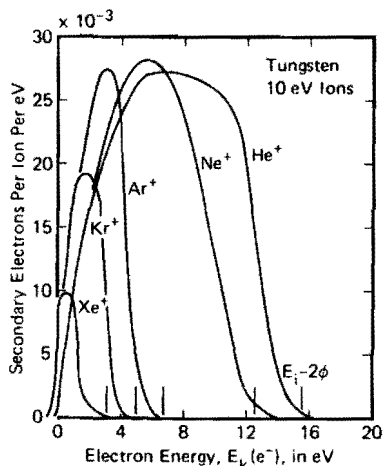


Fig. 2 Energy distribution functions for electrons ejected from tungsten by 10 eV noble gas ions. Vertical lines on the abscissa indicate the energies $E_i - 2\phi$.

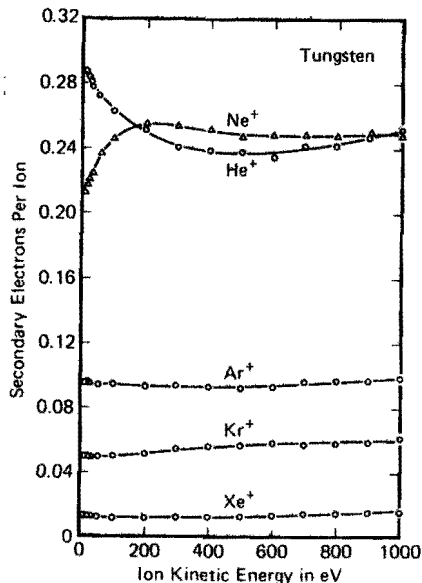


Fig. 3 Total electron yield versus ion kinetic energy for singly charged ions of the noble gases incident on atomically clean tungsten. Ions are all in the ground state.

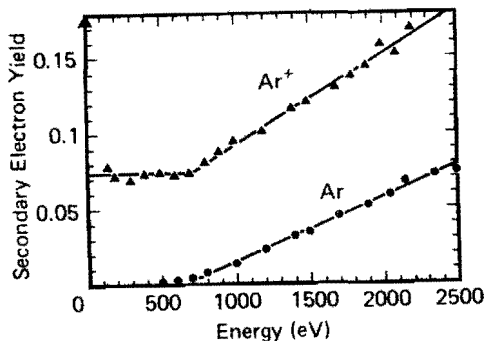


Fig. 4 Secondary-electron yields as a function of kinetic energy for Ar^+ and neutral argon atoms.

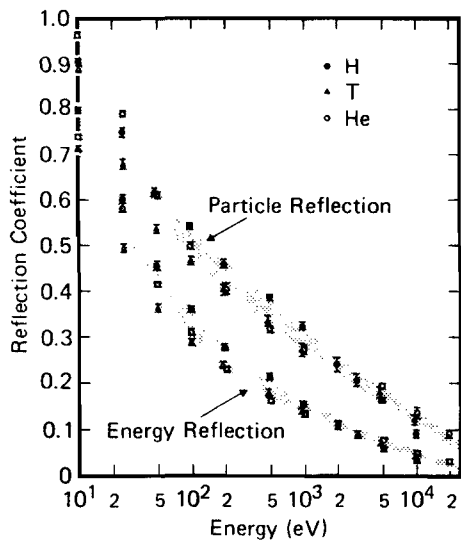


Fig. 5. Theoretical calculations of the reflection of energy and the reflection of particles for H, He, and T from copper. Calculations based on computer simulation. Normal incidence. R_E/R_N is the average fractional energy of a reflected particle.

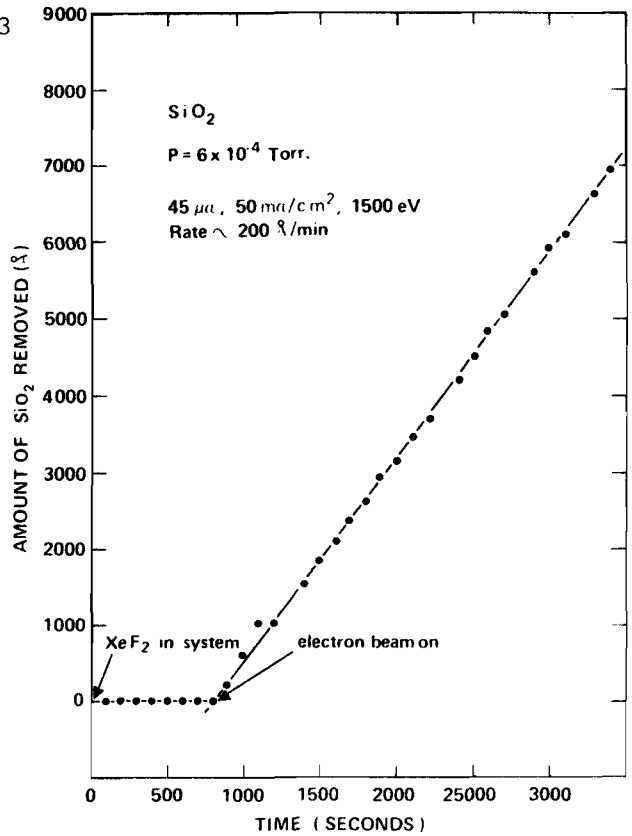


FIG. 6. Electron-assisted gas-surface chemistry using 1500-eV electrons and XeF₂ on SiO₂. P (total) = 6×10^{-4} Torr with most of the ambient gas being xenon. Neither exposure to XeF₂ nor an electron beam produces etching by itself. Simultaneous exposure produces an etch rate of $\sim 200 \text{ \AA}/\text{min}$.

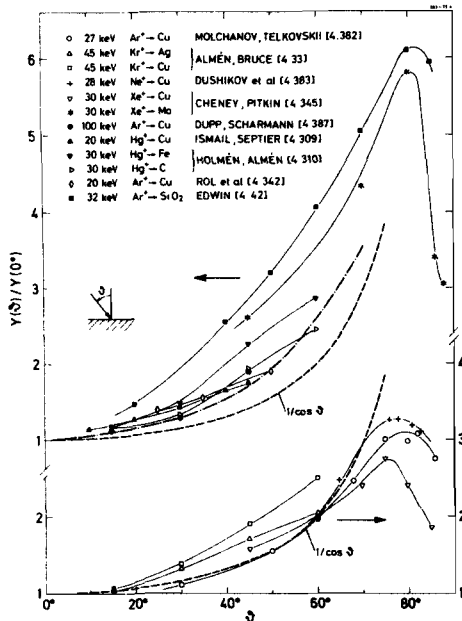
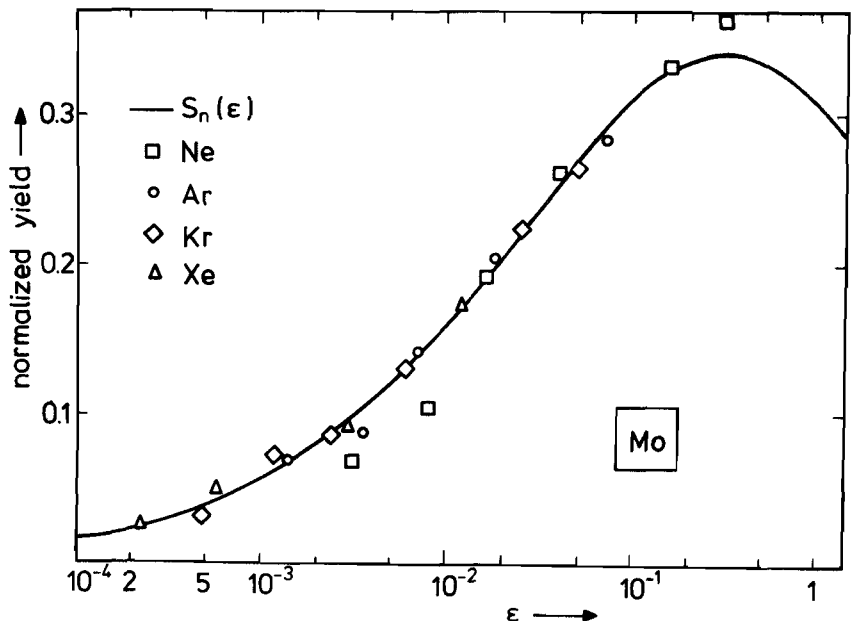


fig. 7

fig. 8



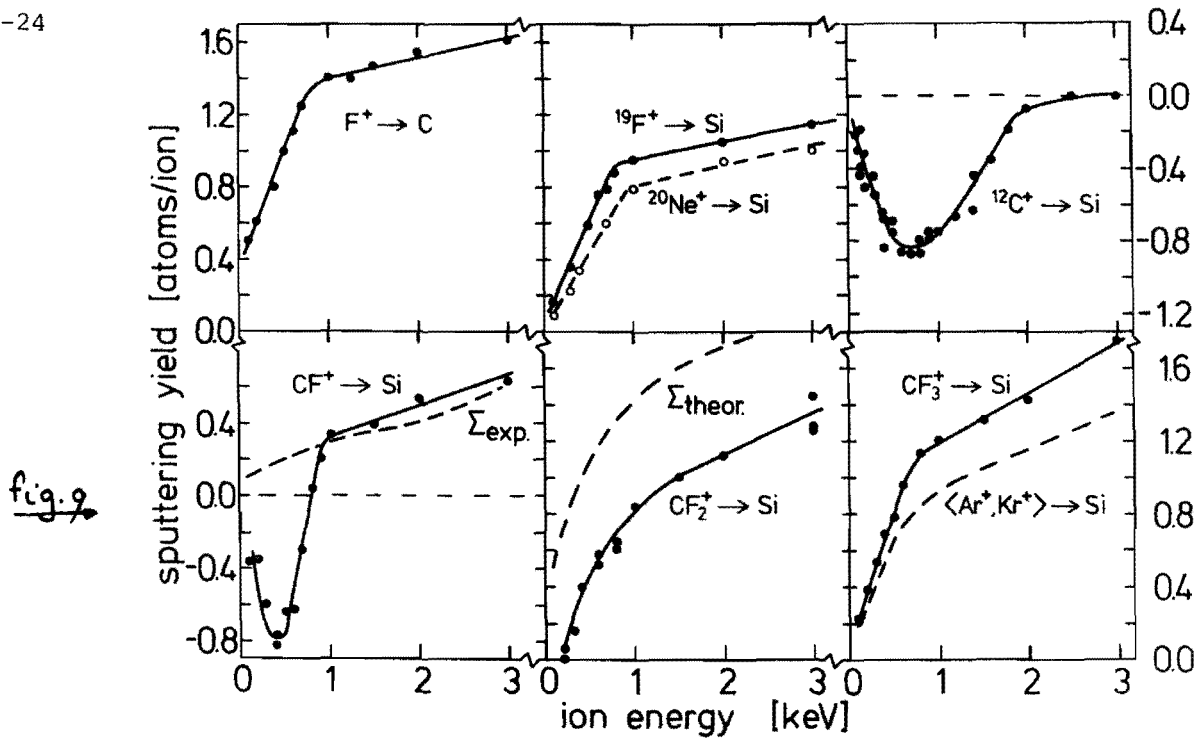


fig. 9

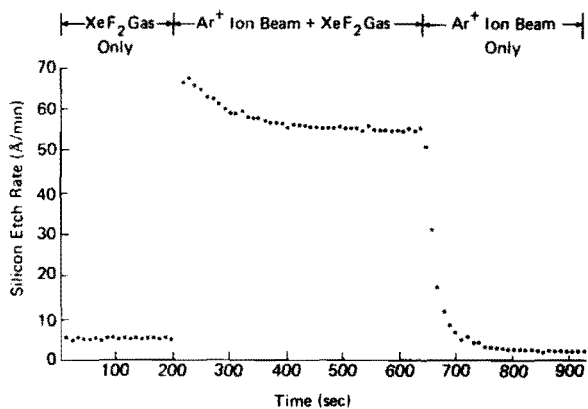


FIG. 10 Ion-assisted gas-surface chemistry using Ar⁺ and XeF₂ on silicon (volatile reaction product). Ar⁺ energy = 450 eV, Ar⁺ current = 0 ($t < 200$ sec), Ar⁺ current = 2.5 μ A ($t > 200$ sec), XeF₂ flow = 2×10^{15} mol/sec ($t < 660$ sec), and XeF₂ flow = 0 ($t > 660$ sec). (The Ar⁺ current density and the XeF₂ flux are not uniform over the Si surface. The effective area for the Ar⁺ current and the XeF₂ flux are estimated at 0.1 and 0.3 cm², respectively.)

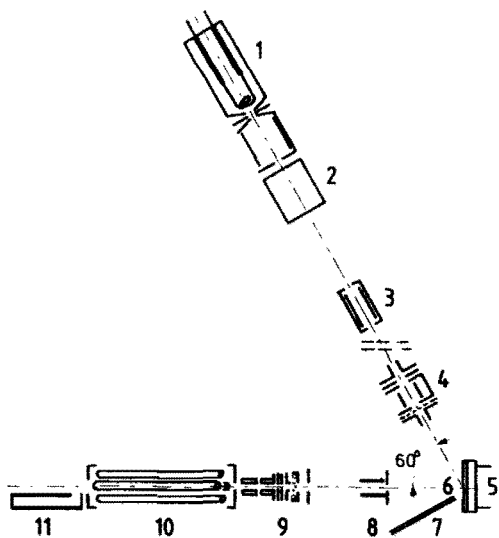


Fig. 11. Schematic, not to scale, view of the TOF apparatus. 1. Ar⁺ ion source; 2. Wien filter; 3. electronic beam modulator; 4. decelerator; 5. oven annex target holder; 6. Si target; 7. Cl₂ gas inlet; 8. diaphragm; 9. ionizer; 10. quadrupole mass spectrometer, 11. magnetic electron multiplier.

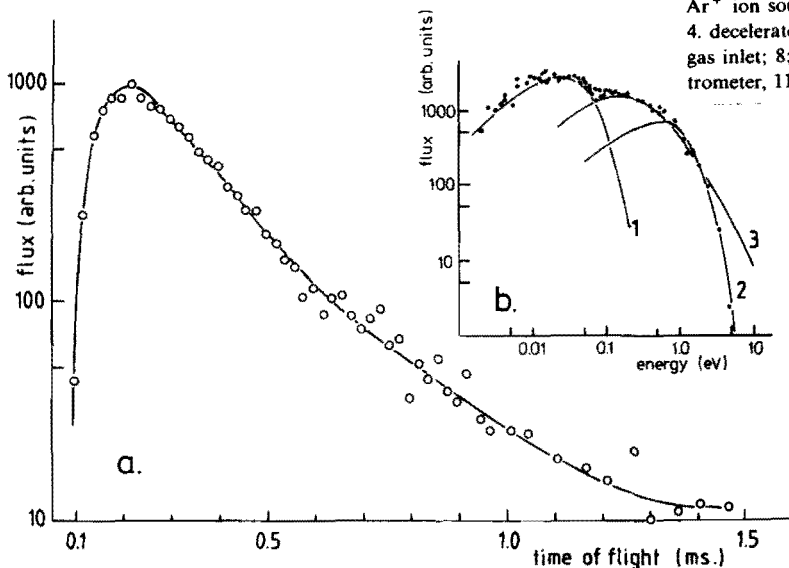


Fig. 12. (a) Time of flight (TOF) spectrum for SiCl obtained by bombarding Si at 300°C with 3 keV Ar⁺ ions (flux approximately 5×10^{14} /cm² s) under simultaneous exposure to a Cl₂ gas flux of about 5×10^{16} /cm² s. (b) Insert. Corresponding energy distribution curve (EDC). The fitted substrate temperature Maxwell-Boltzmann M-B distribution (labeled 1) as well as a local thermal equilibrium contribution (2), fitted to the high energy tail, and a collision cascade (C-C) contribution (3) are indicated.

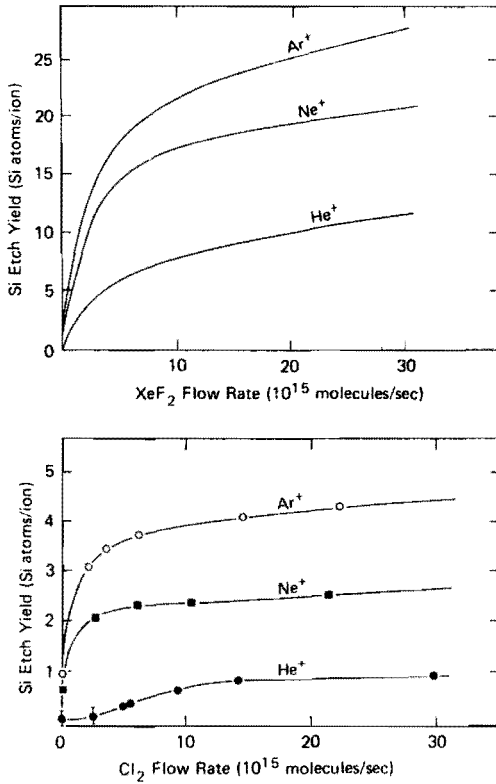


FIG. 13. (Top) Etch yield of Si as a function of the XeF₂ flow rate for bombardment with 1 keV He⁺, Ne⁺, and Ar⁺. (Bottom) Etch yield of Si as a function of Cl₂ flow rate for bombardment with 1 keV He⁺, Ne⁺, and Ar⁺. Both curves were obtained using "molecular beam-ion beam" experiments.

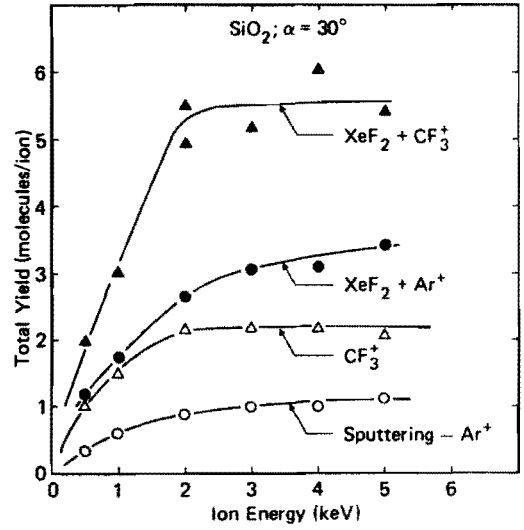


FIG. 13^{*} SiO₂ yields vs ion energy. The bottom two curves were obtained with no flow of XeF₂. Therefore, the bottom curve (argon-ion bombardment) is caused by physical sputtering. The top two curves were obtained with a flow of XeF₂ of ~ 1.5 × 10¹⁶ molecules/sec.

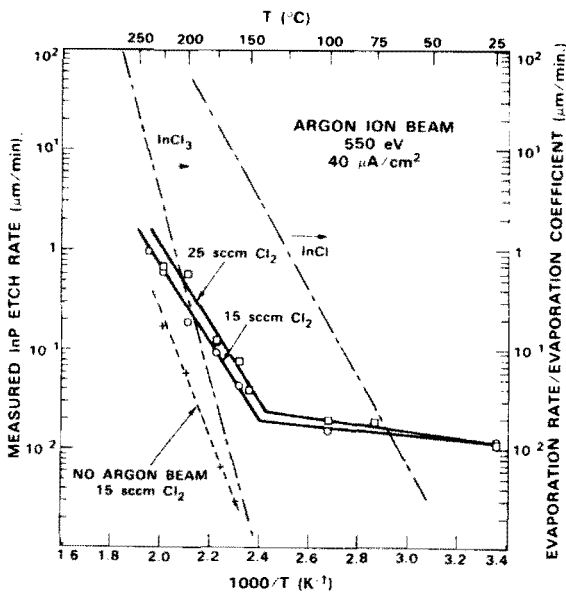


Fig. 14. Etch rate versus 1/T for InP samples etched with a 40 μA/cm² 500 eV argon beam and 15 sccm of Cl₂. Also shown is the spontaneous rate in Cl₂ only and the evaporation rate of InCl and InCl₃ converted to an effective InP etch rate.

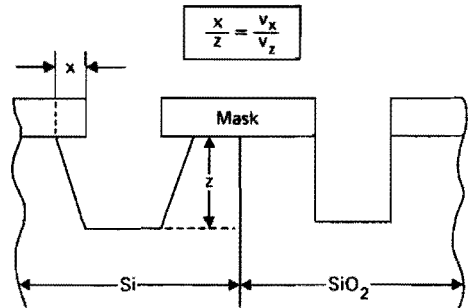
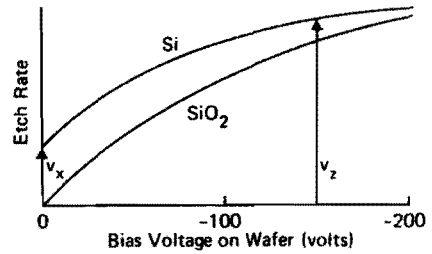


Fig. 15 Illustrative figure to show the relationship between the shape of the etched wall profile and the dependence of the etch rate on the wafer potential (see text for discussion)

5. BASICS OF REACTOR DESIGN

Dr. Alfred J. van Roosmalen and Ir. Carol de Vries work at the Philips Research Laboratories, Eindhoven, The Netherlands. Dr. van Roosmalen is in charge of dry-etching process research and development for silicon VLSI. The research interests of Ir. de Vries are in basic studies of R.F. plasmas for dry etching.

BASICS OF REACTOR DESIGN

C.A.M. de Vries and A.J. van Roosmalen

Philips Research Laboratories Eindhoven, The Netherlands

1. Approaches and concepts

A large variety of reactors is in use for plasma assisted etching and deposition. In order not to complicate things too much the emphasis of this lecture will be mainly on etching, but applications in deposition are mentioned when appropriate. On several places use is made of concepts and equations derived in the introductory talk 'Basics of Gas Discharges'. The terms LF (50 - 500 kHz) and HF (10 - 50 MHz) also stem from that lecture.

The first dry etch reactors were based on the generation of chemically active species in an rf discharge with external electrodes, see Figure 1. No use is made of directed fluxes (ion bombardment) and pattern definition is strictly isotropic, as in wet chemical agents. The operation of such systems is more or less self-evident and will not be discussed here further.

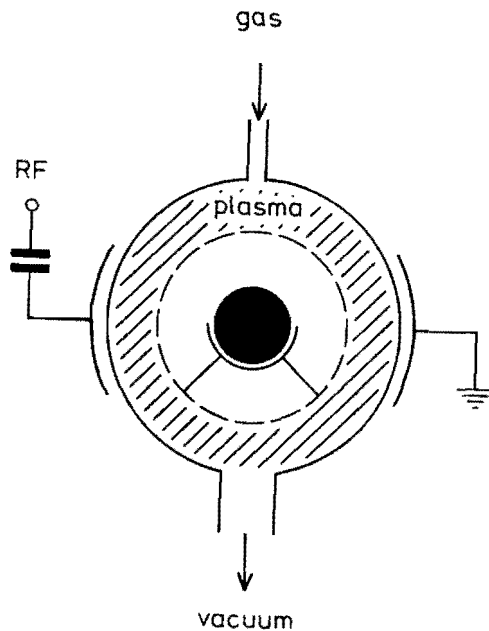


Fig. 1. Barrel reactor for afterglow processing. Typical conditions: $p = 100 \text{ Pa}$; $P = 10 \text{ kW/m}^3$.

In many advanced etch processes a substantial high-energy ion bombardment is required for anisotropic pattern transfer. This can be achieved in reactors with internal electrodes. Geometric and symmetry aspects play an important role in such systems, especially if the excitation frequency is in the HF band.

A commonly used reactor configuration is depicted in Figure 2. Basically it consists of a high-vacuum chamber in which two parallel electrodes are positioned. The top electrode and the chamber walls are electrically grounded; the lower electrode

(and substrate holder) is connected through a dc-blocking capacitor to an rf generator (mostly 13.56 MHz). A system as in Figure 2 is usually referred to as a reactive-ion etch (RIE) or cathode-coupled reactor. Normal gas pressures lie between 1 and 10 Pa. The ion sheaths in a 13.56-MHz discharge are capacitive, and large ac potentials are built up across them when rf power is dissipated in the system. Because the powered electrode in this reactor is small relative to the sum all grounded surfaces in contact with the plasma, the powered electrode capacitance will be less than that at the grounded electrode. Hence, capacitive voltage division takes place,

$$V_1 / V_2 = C_2 / C_1 , \quad (1.1)$$

where V is the sheath rf peak voltage (about equal to the sheath dc self-bias), C the sheath capacitance, and 1 and 2 are for the powered and ground electrode, respectively. Writing the capacitance in terms of sheath thickness d and area A

$$C_2 / C_1 = A_2 / A_1 \cdot d_1 / d_2 . \quad (1.2)$$

The Child-Langmuir equation relates the positive ion current density in the sheath to sheath thickness and voltage. Assuming equal ion current density to all surfaces we get

$$V_1 / V_2 = (d_1 / d_2)^{x/(x-1)} , \quad (1.3)$$

where $x = 4$ for space-charge limited current and $x = 3$ for mobility limited ion current. Combining the above equations, and eliminating C and d ,

$$V_1 / V_2 = (A_2 / A_1)^x , \quad (1.4)$$

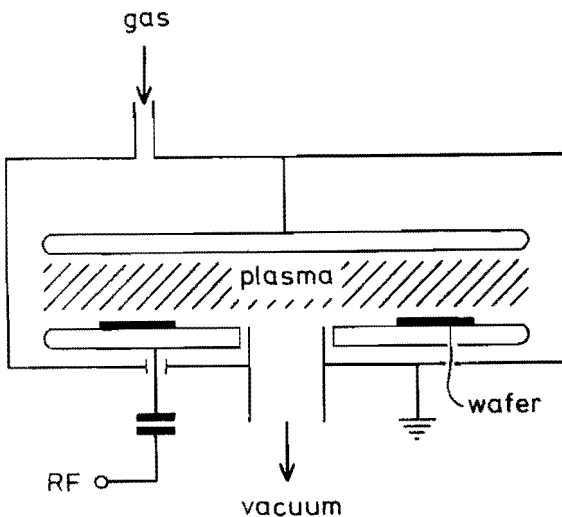


Fig. 2. Batch-type cathode coupled (RIE) reactor. Typical conditions: $p = 5$ Pa; $P = 5$ kW/m².

where x takes the same values as in Eq. 1.3. This expression is known as the area theorem and was derived originally by Koenig and Maissel (1). It indicates that the highest sheath potential is found at the smallest electrode.

According to Eq. 1.4 a slight asymmetry causes a large potential difference. With $x = 4$ and an area ratio of 1.5 we find a voltage ratio of 5, so that the applied rf voltage is found almost completely across the ion sheath at the smaller - here, the powered - electrode. A practical application of the area theorem is the so-called Hex reactor. Here a large area ratio is combined with a uniform field distribution by a concentric configuration of powered and grounded electrode. The name Hex stems from the hexagonal cathode.

Caution should be taken in making quantitative use of Eq. 1.4. Firstly, several of the assumptions underlying the model are open to discussion (2), and secondly it is not easy to decide what surfaces should be assigned to what electrode in calculating the precise area ratio. Nevertheless, the agreement between measured and calculated values can be good for low pressure - below 10 Pa - and low area ratio, say less than 1.5 (3).

When using higher gas pressures in the system from Figure 2 the discharge contracts and the plasma loses contact with the side walls of the reactor (4,5). This immediately influences the voltage distribution since the effective area ratio drops. At a sufficiently high pressure (20 - 200 Pa) the voltages at powered and grounded electrode can be of comparable magnitude, which implies that high energetic ion bombardment is now also encountered on the grounded electrode. This leads us to Figure 3, showing an anode-coupled or 'plasma etch' (PE) reactor. The fact that the substrates are now on a grounded surface has some advantages in handling and loading the system.

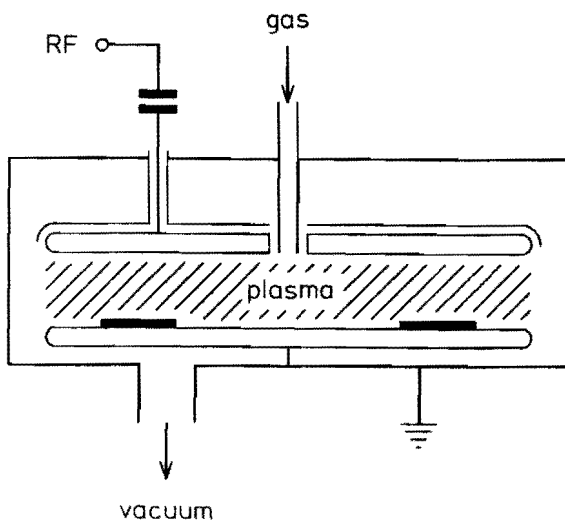


Fig. 3. Batch-type anode-coupled (PE) reactor. Typical conditions: $p = 30$ Pa; $P = 5$ kW/m².

In the systems from Figures 2-4 a dc voltage can usually be measured across the reactor, provided that the electrodes are sufficiently conductive (6). For the RIE system this voltage will be close to the ion sheath dc self-bias at the powered electrode, since the potential drop at the - large - grounded electrode is small. The PE system is almost symmetrical so that the net dc voltage is low. Note that this does not mean that the ion sheath potentials are small.

The conclusion so far is that there is no principal distinction between RIE and PE systems with respect to energetic ion bombardment. Actually, it would be more preferable to speak of low-pressure cathode-coupled, and high-pressure anode-coupled instead.

For reactors operating in the LF band we have to modify our conclusions slightly. Symmetry aspects do play a role, but the effect is much less pronounced since there is no capacitive voltage division. Most systems are of the type in Figure 4, with an operating pressure between 10 and 100 Pa. Generally speaking one can say that these systems are symmetrical. It should be noted that the full rf potential appears on each electrode during its cathodic cycle, this contrary to the high-pressure HF system where the applied voltage is split in half. This adds to the fact that the sheath voltages for an LF discharge are already substantially higher than in a corresponding HF system. Combined with the relatively low degree of dissociation it is now conceivable that high-pressure low-frequency anode-coupled discharges often exhibit a behavior quite similar to low-pressure high-frequency cathode-coupled systems (7,8). Both have a high energy ion bombardment and a low concentration of reactive neutrals.

Etch rates in the reactors discussed so far are between 50 and 100 nm min⁻¹. When used for production a number of samples is loaded to be etched simultaneously, typically 6 - 24. For this reason these systems are called 'batch' reactors. By increasing the power density in the symmetrical, high-pressure system (and lowering the frequency, if necessary), it is possible to increase etch rates up to 1 μm/min. With careful tuning

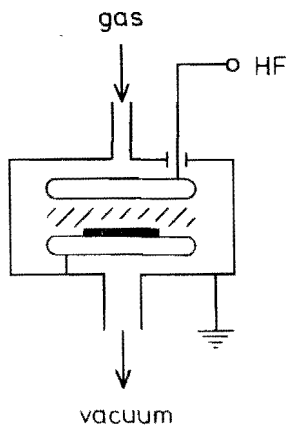


Fig. 4. Single-wafer reactor. Typical conditions: $p = 200$ Pa; $P = 50$ kW/m².

the etching can still be directional. This observation has opened the door to a class of reactors where only one sample is etched at the time, see Figure 4. Individual sample handling and ease of automation are the main advantages of these so-called single wafer etch reactors; the throughput in terms of samples per hour can be the same as in commercial batch-loaded reactors.

There exist more reactor configurations for dry etching than only those treated above. Some of these less-common systems are reviewed in the last section of this lecture.

Many plasma deposition systems are of the same type as the etch reactor in Figure 3; both LF and HF excitation are used. Others are based on standard furnace pipes. The electrodes are brought in through the open end either as parallel plates or as an rf-driven wafer carrier.

2. Matching networks

Most rf generators have a fully resistive output impedance which matches the normal 50 or 75 ohm coaxial transmission lines. With a matching network it is possible to adapt the variable impedance of reactor and discharge to the fixed cable resistance. In unmatched systems large reactive currents can flow that do not contribute to the net power transfer. Another reason to use matching networks is that in high frequency systems standing waves can occur on the transmission line which will cause losses and rf interference and, for severe conditions, arcing in connectors and cables (9-11).

A matching network is a network made of passive components that is put between generator and reactor to optimize power transfer. Assume that a load with an impedance $Z_2 = R_2 + j X_2$ has to be matched to a system with open circuit voltage V and impedance $Z_1 = R_1 + j X_1$. The power absorbed by the load is

$$P = V^2 R_2 / ((R_1 + R_2)^2 + (X_1 + X_2)^2) \quad (2.1)$$

Obviously, maximum power transfer is achieved if $R_1 = R_2$ and $X_2 = - X_1$; the network output impedance has to be the complex conjugate of the load impedance.

We have seen in 'Basics of Gas Discharges' that discharges operating in the HF band (10 - 50 MHz) behave mainly capacitive with a small resistive component, while LF systems (50 - 500 kHz) are mainly resistive with a small capacitive component. Different types of matching networks are used for both frequency regimes.

For systems operating in the HF band, e.g. at 13.56 MHz, the L-type network (Figure 5) and the π -type network (Figure 6) are used mostly. Matching can be achieved by simultaneously adjusting the capacitors C_1 and C_2 . This can be done automatically with servomotors and a circuit that measures the phase angle and magnitude of the matching network input impedance (12). For an L-network it can be derived that to transform a real cable impedance Z_{in} to a complex load impedance $Z_{out} = R + j X$,

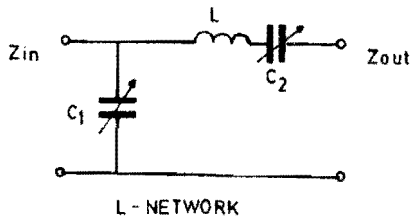


Fig. 5. Diagram of an L-type matching network.

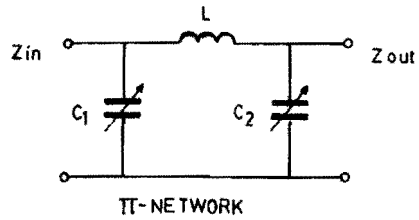


Fig. 6. Diagram of a π -type matching network.

$$R = Z_{in} / (1 + (\omega C_1 Z_{in})^2) , \quad (2.2)$$

$$X = \omega L - 1 / \omega C_2 - R / (Z_{in} / R - 1)^{0.5} , \quad (2.3)$$

where ω is the excitation angular frequency.

The π -type matching network has a wider matching range, the L-type invokes less blind currents because there is no closed loop within the circuit (11). Blind (= reactive) currents can be the source of significant power losses. A current of 50 A and a parasitic resistance of 0.2 ohm will cause 500 W power dissipation. In certain matching networks and network - reactor connectors up to 50 % of the transferred power can be lost (13).

LF systems are often matched with a step-up transformer, see Figure 7. Reactive components are thus neglected and the output resistance is varied in steps. Note that in case no series capacitor is used a net current flow through the discharge is possible, so that no net dc self-bias can be built up across the reactor. Moreover, dc currents are drawn through the substrates to be etched which is generally undesirable. The same holds for π -type networks.

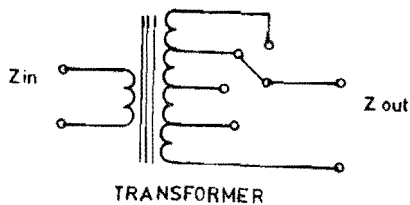


Fig. 7. Diagram of a step-up transformer matching network.

3. Electrode construction

A typical rf-powered electrode system may look like the one shown in Figure 8 (6). At the backside of the electrode a metal shield is fitted which is grounded and suppresses the occurrence of plasmas at the backside of the electrode. The distance between the shield and the electrode must be less than the ion sheath (dark space) thickness for the applied conditions to prevent striking of a discharge between electrode and shield. Therefore the shield is commonly called the dark-space shield. The dark-space thickness is in principle a function of gas type, pressure, power input, and frequency. To be sure one can take a very small gap to prevent all discharge formation but now the reactor parasitic capacitance becomes very high, thereby inducing large blind currents. Moreover, dust particles can cause arcing.

The shape of the electrodes and the dark space shields can have a large influence on discharge behavior. Sharp edges will cause very high electric fields, see Figure 9, which can lead to locally intensified plasmas, instabilities and sputtering of electrode materials. Holes, ports, and bolts in walls and electrodes can cause hollow cathode type of behavior. This means that electrons are caught between the high voltage sheaths on either side of the hole, thereby getting the opportunity to be bounced back and forth and increasing the local degree of ionization. Also gas inlets and pumping ports are suspect.

The materials that are used in the system are also important. Of course the materials of which the reactor is made should withstand the aggressive environment but they must also be compatible with process demands. Aluminum is readily attacked by chlorine and must be protected by a layer of e.g. aluminum oxide deposited by anodization or plasma spraying. Stainless steel can cause problems because metals like iron, nickel, and chromium can be sputtered from it that are known to degrade silicon device performance. The electrode material, especially that of the powered electrode, has a large influence on plasma behavior, both physically and chemically. Due to the large variety of interactions between gas molecules and the wall the electrode material can have a large chemical influence if it reacts with the gas radicals; it can also act as a recombination center (14,15). Physically it can affect the plasma because of variations in the secondary electron emission coefficient with ion bombardment (16). Another important effect is backsputtering of small amounts of metal from the electrode to the substrate to be etched. These trace amounts of metal can act as a local mask and thus produce surface roughness. It is also possible that the metal contaminant acts as a catalytic center and invokes surface polymerization of species from the discharge. This can block further etching, especially in fluorine-based discharges (17).

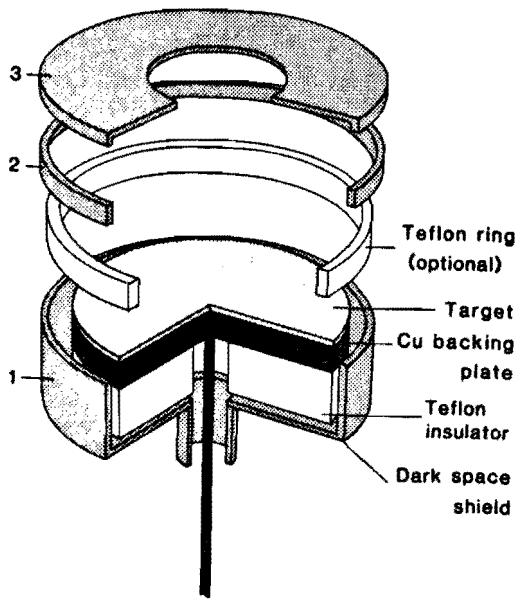


Fig. 8. Schematic drawing of a typical rf-powered electrode assembly.

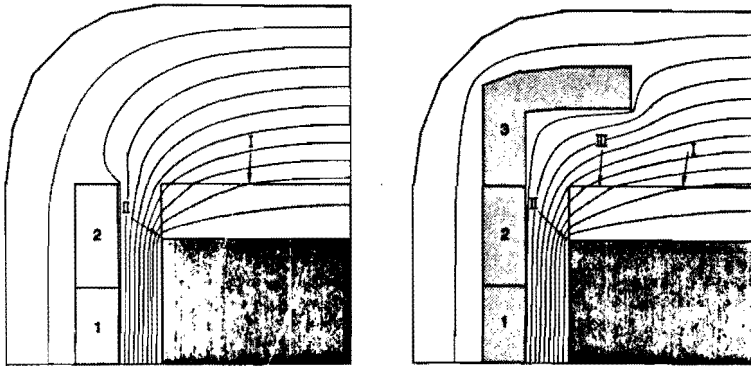


Fig. 9. Plot of equipotential lines (constant voltage difference) from electrostatic simulation of the sheath around the electrode assembly. Dark space shield is assumed to be at ground potential, the electrode at -520 V and the plasma at $+60$ V.

4. Parasitic impedances

It is a bit unfortunate that so many plasma systems operate at 13.56 MHz. Frequencies in the MHz range and higher are rather difficult to handle from a standpoint of electrical engineering. We saw already that the HF discharge is mainly capacitive. The output impedance of the rf generator is, however, in most cases resistive to allow low-loss power transfer using 50 or 75 ohm coaxial lines. A matching network has to transform the generator output impedance to that of the reactor input, see section 2.

That is where the problem begins. The match box and the reactor contain lots of electrical components - resistors, capacitances, inductances - that are not directly visible. In the MHz range and above feedthroughs, shieldings, pipes, bolts and nuts, and even platework form impedances with values that cannot be ignored (9,10). This is caused to a large extent by the skin effect, i.e., the phenomenon that high-frequency electrical currents in conductors are forced to the surface. The nominal penetration depth δ in a plane conductor is given by

$$\delta = (\rho / \pi f \mu)^{0.5} , \quad (4.1)$$

where ρ is the resistivity, f the frequency in Hz, and μ the magnetic permeability. For a copper conductor the value of δ is only 5 μm at 13.56 MHz, which implies that in any practical piece of metal the current path follows contours only.

As an example we will analyze a commercially available parallel-plate reactor (5), see Figure 10. A 13.56-MHz power supply is connected to the top electrode via a matching network; a grounded metal shield is mounted to suppress parasitic discharges at the back of the electrode. The bottom electrode is earthed via a stub and an external connection. For the rf current flow we have to realize that the skin effect allows surface conduction only. The simplified electrical equivalent circuit of the reactor is shown in Figure 11. The inductances and capacitances in this diagram were calculated from the equations for coaxial cables

$$L = \mu l / 2\pi \ln (b / a) , \quad (4.2)$$

$$C = 2\pi \epsilon l / \ln (b / a) , \quad (4.3)$$

and for parallel plates

$$C = \epsilon A / d , \quad (4.4)$$

where ϵ is the dielectric constant, l the cable length, a and b the inner and outer conductor diameter, A the plate area, and d the distance between the plates.

The importance of these calculations becomes evident when we apply rf power (18). Note that the interelectrode capacitance vanishes from the circuit as soon as the discharge strikes. Let us assume a capacitive current of 10 A (rms) in

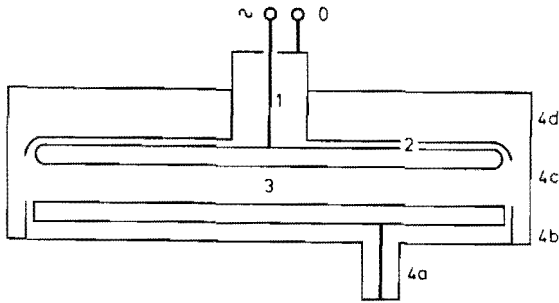
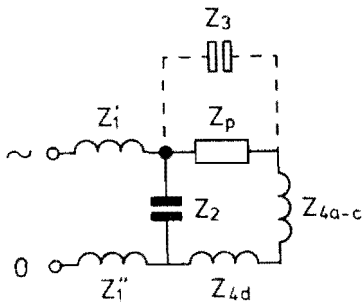


Fig. 10. Schematic drawing of the planar reactor used in the example (Plasma-Therm PK 2440 PE/RIE). Numbers correspond with the stray impedances in Figure 11.



$Z_1 = Z_1''$	20 nH	1.7 j ohm
Z_2	780 pF	-15 j ohm
Z_3	50 pF	-235 j ohm
Z_{4a-c}	32 nH	2.7 j ohm
Z_{4d}	20 nH	1.7 j ohm
Z_p	Discharge	

Fig. 11. Equivalent circuit for the reactor in Figure 10. All values are for 5 cm electrode spacing.

the discharge. For the interelectrode peak voltage we take 500 V, corresponding to 350 V (rms). These values are taken from the discussion on high-frequency sheath formation in 'Basics of Gas Discharges' under assumption that the reactor is fully assymmetrical. Network analysis shows then immediately that the average potential difference between the (earthed) bottom electrode and the (earthed) reactor side wall is 27 V; between the side wall and the edge of the top-electrode shield we find another 17 V. The top-electrode shield as such draws twice as much current as the discharge itself. Combined with the high top stem inductance this gives 200 V and 31 A at the reactor input clamps. It is now directly clear why in a HF system discharges can occur between dc-earthed surfaces. We can also understand

why the measured dc self-bias voltage between powered electrode and ground - in an asymmetric system proportional to the discharge peak potential - can be much higher than the rf peak voltage across the reactor. In this example the dc potential is 500 V since the peak voltage across the discharge was assumed to be 500 V, while the rf potential is 280 V (peak) ($= 1.414 \times 200$ V).

In LF systems parasitic impedances are relatively unimportant although one has to realize that certain protective electrode coatings can act as a series impedance. A major concern in LF reactors is the high electrode potential that develops even under moderate power operation. Not many rf connectors withstand a few kV. Moreover, arcing can occur inside the reactor.

5. Power, voltage and current control

Power, voltage and current measurement may seem to belong to the diagnostics but since one of these parameters is normally used to control the discharge, the reliability and the quality of these controls have a large influence on system behavior.

When attempting to measure rf voltages in high frequency systems the first problem is to avoid unwanted rf interference and capacitive and inductive coupling. An even more severe problem is that it is difficult to find a good reference ground since every piece of wire and every part of the reactor will show some impedance to the 'real' ground. Furthermore, as was shown in Section 4, the reactor construction itself can effectively preclude direct measurement of the rf voltage across the discharge. These problems are much less important at low frequencies.

Measurement of the dc self-bias does not suffer from the above problems but instead two others occur. In the first place the difference between two sheath voltages is measured; the net result can only be translated directly to an ion bombardment energy if the system is asymmetrical, see Section 1. The degree of asymmetry in a given reactor is a function of gas type, pressure, and, to some extent, the rf power. Secondly, if the electrodes are covered with an insulating material measurement of a dc self-bias voltage is not trivial since a conduction channel is necessary. This path can be around the electrode edge or straight through it as a leakage current. In both cases a considerable resistance in series with the voltmeter will occur. The effect is that the measured voltage can be very different from the real voltage at the electrode surface (6).

For generator feedback control some systems use rf current measurement. The current measured with e.g. a current transformer or a series resistor is the vector sum of the resistive and the reactive current flowing through the system. As we have seen above reactive currents are strongly influenced by the reactor stray impedances and do not add to the power dissipation in the plasma. This can make current measurements rather system dependent and not always representative for plasma behavior.

In high-frequency systems rf power is normally measured with a transmission line power meter (10). This system requires a 50 ohm input and output impedance. The basic circuit is given in Figure 12. The mutual inductance M can be sign inverted. The output voltage e is the sum of the voltage resulting from the division of E by R and C and the voltage over the inductance M . If $R \ll 1 / j \omega C$ the result is

$$e = j \omega (R C E + M I) . \quad (5.1)$$

If the components are now chosen such that $R C = M / Z_0$, with Z_0 the input impedance, we find

$$e = j \omega M (E / Z_0 + I) . \quad (5.2)$$

At any one point on the line the net voltage E is the sum of the forward and reflected voltages E_f and E_r and the current I is $E_f / Z_0 - E_r / Z_0$. Thus, depending on the sign of M - the direction of the loop - the output voltage is either

$$e = j \omega M / Z_0 \cdot 2 E_f , \quad (5.3)$$

or

$$e = j \omega M / Z_0 \cdot 2 E_r . \quad (5.4)$$

We now have a directional power meter; by adding an extra circuit the signal can be made frequency independent. The actual output is calibrated to read $E_f^2 / 2 Z_0$ ('forward' power) and $E_r^2 / 2 Z_0$ ('reflected' power). Note that the net power dissipated in the load is not simply the difference of forward and reflected. Similarly, the reflected power is not a real dissipated energy, but only a measure of the standing waves on the cable. Since the in-line meter has to be placed between generator and matching network losses in the network, which can be appreciable, are not taken into account. This can lead to variations from system to system.

In low frequency systems power dissipation can be determined by real-time multiplication of rf current and voltage and

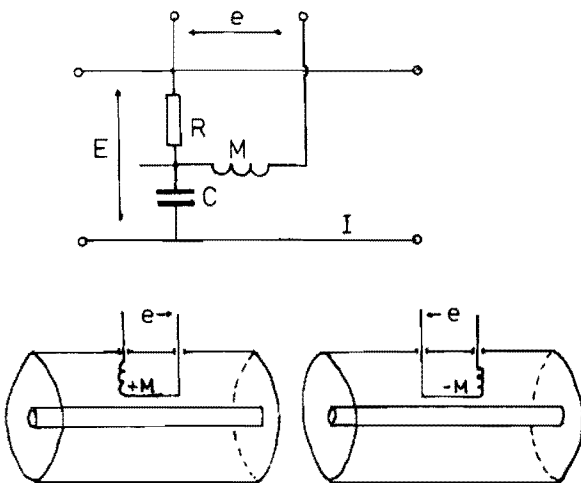


Fig. 12. Basic circuit of a transmission line power meter.

integration of the result,

$$P = 1 / T \cdot \int_0^T E(t) \cdot I(t) dt , \quad (5.5)$$

with E and I the real time voltage and current, respectively, and T the time of one rf cycle. In and output impedance need not be 50 ohm here.

6. Temperature control

In deposition systems temperature is a very important parameter. In 'afterglow' etch systems, where etching relies on chemical reaction only, the wafer temperature also has a strong effect on etch rates. In etch systems with internal electrodes etching is usually dominated by ion bombardment so that the influence of temperature on etch rates is mostly low. The temperature remains important, however, as it influences photoresist mask degradation.

Whereas in deposition systems and chemical dry etch systems the substrates are usually heated it is often necessary to cool it in parallel plate systems to avoid degradation of the photo-mask. In some cases heating of the reactor is necessary to avoid condensation of low-volatile products originating from the discharge.

Heat flow from the substrate to its surroundings can occur via three mechanisms: conduction, convection and radiation.

The heat flux density by conduction is in steady state

$$Q = \Delta T / R_{th} , \quad (6.1)$$

where ΔT is the temperature difference, Q the heat flux, and R_{th} the thermal resistance. The resistance depends on the contact area and on the conductivity of the materials in contact. In the usual plasma etch and deposition systems the mechanical contact between substrate and holder is poor because of intrinsic surface roughness. Therefore, the thermal contact resistance is normally very high (19-21).

Convection in vacuum systems is considerably different from that at atmospheric pressure. The heat capacity of a low-pressure gas is very low, so that the heat transfer to the bulk of the gas phase is negligible. Convection from substrate to holder is of the molecular flow type, however, because they are so closely spaced. This means that gas molecules collide with the surfaces rather than with each other and so heat transfer goes through kinetic and internal energy transfer. Formulas and derivations are complex. Some can be found in ref. (19).

The heat flux density by radiation is for two ideal black bodies given by

$$Q = \epsilon (T_1^4 - T_2^4) , \quad (6.2)$$

where ϵ is a constant, and T_1 and T_2 the absolute temperatures. Practical substrates are not black of course, but in many cases

Practical substrates are not black of course, but in many cases they can be represented as grey. This introduces a coefficient in the equation with a value close to 1. Radiation becomes important at elevated temperatures. It is probably the most important heat transfer channel for substrates in a practical reactor (21).

A possibility to improve the heat transfer from substrate to holder is to clamp the sample mechanically. Because of the surface roughness the thermal resistivity will still be rather high, though. A variation on the clamping principle is to lead a high pressure helium flow to the backside of the wafer, a gas having a very high thermal conductivity. This improves thermal contact by conduction and convection, but gas leaks into the main chamber can have significant influences on the process. In research systems it is not unusual to 'glue' the samples to the electrode with vacuum grease or oil, or photoresist. This is a very effective method for improving conduction but it is hardly useful in a production environment.

In systems operating at high pressures - over 200 Pa - bulk gas phase conduction can become important, especially if a large amount of helium is added.

7. Special systems

Apart from the etch systems we saw in Section 1 several new approaches have appeared in recent years. It has been claimed that these systems have certain advantages over conventional etching with respect to directionality, etch rates, or radiation damage. We will review some of these systems briefly.

7.1 Magnetron etching.

A magnetron etch system is basically a internal-electrode type of reactor where magnets have been placed around or under the electrodes. These systems normally work at low pressures, 0.1 to 1 Pa is typical. A possible configuration is given in Figure 13.

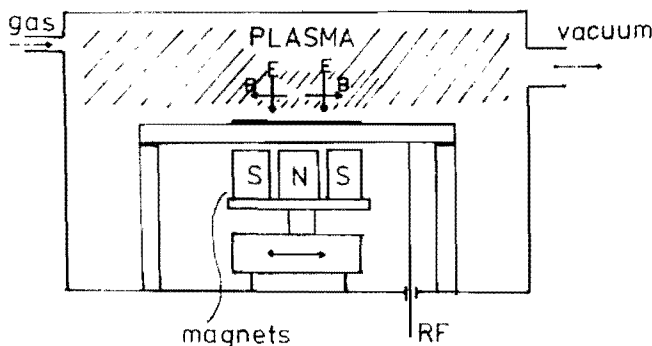


Fig. 13. Planar magnetron reactor. Typical conditions: $p = 1$ Pa; $P = 5$ kW/m² ; $B = 500$ Gauss.

Use is made of the fact that electrons which move in both a magnetic field and an electric field are forced into a helical movement. The same holds for ions but since their mass is much larger the radius of the helix is much larger. An electron which moves in a magnetic field B with a velocity v is subjected to a force

$$F = e \cdot v \times B . \quad (7.1)$$

The direction of the force is perpendicular to both the magnetic field and the velocity (corkscrew rule). In case a particle moves with velocity v at angle θ to the magnetic field it will describe a circular motion around the vector B at a radius

$$r = m v \sin \theta / e B . \quad (7.2)$$

A velocity perpendicular to B of 106 m s^{-1} and a magnetic field of 500 Gauss will result in a radius of about 1 cm. This is smaller than the average system dimensions. The velocity of the electron parallel to B will change the circle into a helix, see Figure 14.

If we have a magnetic field parallel to the substrate electrode electrons emitted from the surface will be trapped in a semicircle. The result of combining the strong electric field in the ion sheath with a perpendicular magnetic field is that the electrons describe a cycloidal path near the surface (2,22).

Trapping the electrons in helical paths near the surface has the effect that high energy electrons stay longer in the plasma, which increases the ionization efficiency. Thus, high charge densities can be obtained at a relative low energy input; charge densities of 10^{17} m^{-3} have been claimed (23,24). Moreover, the discharge can be maintained at very low pressure. The low working pressure and the high charge density of the magnetron discharge makes anisotropic etching possible even if the ion bombardment energy is low. This might eventually lead to a decrease in dry-etch induced damage.

The etch uniformity in a magnetron system depends critically on the homogeneity of the magnetic field. Improved uniformity has been accomplished by using a number of magnets for compensation (24) or by moving the magnets under the substrate continuously (25).

Much work is being done in the field of magnetron etching, but still a lot of research into etch mechanisms and process development has to be done to prove all claims.

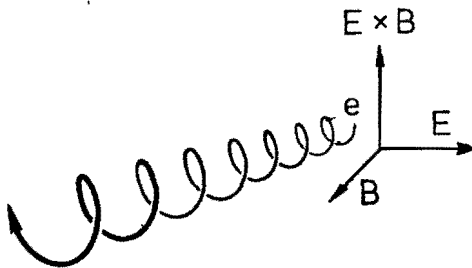


Fig. 14. Electron path in crossed electric and magnetic fields.

7.2 Microwave etching.

In microwave systems the excitation frequency is in the low GHz band (2 - 50 GHz). The corresponding wavelengths are of the order of centimeters. It has already been mentioned in Section 1 that the microwave (MW) discharge has a high degree of ionization and dissociation, but sheath voltages about equal to the floating potential, i.e., 10 - 20 V. Hence, they can produce a lot of ions and radicals but bombardment energies are such that in most cases isotropic etching is achieved.

Microwave discharges must be produced in cavities since in this frequency range impedance matching is otherwise impossible; the frequency is now so high that every piece of metal has a high capacitance or inductance even if a few mm long. The cavity is both reactor and matching network; its dimensions have to be calculated from the wavelength of the radiation it is meant for. A common type is the closed cylinder, see Figure 15 (26).

Because of the discharge and excitation chamber characteristics the microwave plasma is mostly used in afterglow reactors, where wafers are outside the plasma and subjected to the chemically reactive radicals only. Nevertheless, anisotropic etching has been reported at extremely low pressures (0.1 Pa) (27,28).

The principal advantage of microwave etching system is its high efficiency and its low bombardment-induced damage. A disad-

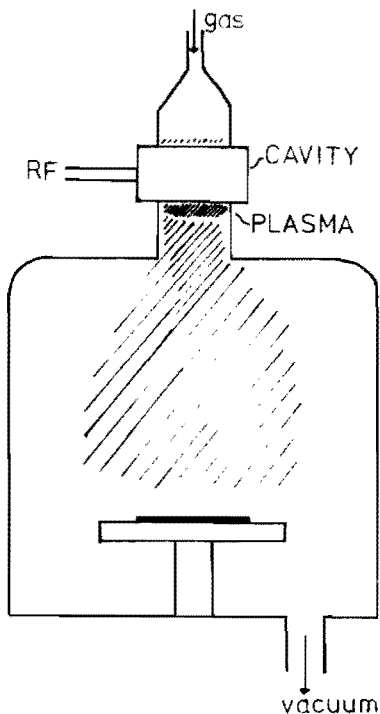


Fig. 15. Microwave afterglow reactor.

vantage is the difficulty to produce a uniform etch over large areas. Since the reactive species have to travel from the place where they are produced to the wafer recombination reactions in the gas and especially at surfaces are very important. Thus far the use of microwave discharges in production systems is limited.

7.3 Plasma Beam

In plasma beam systems the plasma is produced in a chamber separated from the chamber where the substrates to be etched are placed. Ions and neutrals are extracted through an orifice; the ions are accelerated by high-voltage grids before they hit the substrate, see Figure 16. Typical main chamber pressures are in the range 0.01 - 0.1 Pa (29).

The ion source can be a problem. It must be reliable and it also must allow high beam currents. Systems using hot filaments (Kaufmann source) to produce the plasma have a relatively short lifetime with reactive gas plus the risk of contaminating the beam with metal. For these reasons electron-cyclotron resonance sources (ECR) have been introduced recently. Here, a plasma is produced in a magnetically confined microwave discharge (30). The use of grids carries with it the risk of sputtering material that can contaminate the substrate or act as a local mask.

A large variety of plasma beam applications exists. The oldest type is the ion miller. In these systems the substrate is sputter-etched with a beam of noble gas ions. A high accuracy is possible but selectivities and rates are low. In reactive ion beam etching (RIIBE) a reactive gas is used in the ion source. This can help to increase both etch rates and selectivities but the construction of the source is more critical. CAIBE - chemically assisted ion beam etching - combines ion bombardment from a plasma source with an independent supply of reactive gas into the main chamber. It is thus possible to control ion and neutral fluxes and composition independently (31).

Nevertheless, in either case the synergetic effects of ion bombardment and reactive radicals at the surface are not utilized as extensively as in regular plasma etching. Experimental results show relatively low etch rates and selectivities (29-32). Nevertheless, plasma beam etching is indispensable for mechanistic studies. Deposition with beams has the interesting feature of producing layers at relatively low temperatures (33).

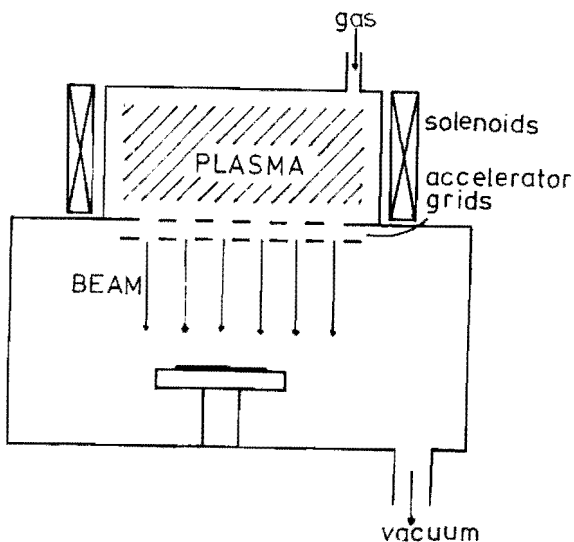


Fig. 16. Plasma beam reactor. Typical conditions: $p = 0.1$ Pa; $J = 5$ A/m²; $V = 500$ V.

7.4 Triode etching.

In triode systems three instead of the usual two electrodes are fitted. This opens the possibility to float an electrode at a certain potential or to use different frequencies at the same time. A schematic drawing is given in Figure 17. The idea behind all this is to decouple the production of radicals from the control of ion bombardment energy to at least some extent.

If one frequency is used there exist several possibilities. Firstly, the non rf-powered electrode can be connected to ground through an adjustable LC network. A rather similar set-up is to divide the rf power from the generator in a special network between the two electrodes (34). Secondly, it is possible to use two generators and two matching networks. The latter system is known as the 'flexible diode' (35). These systems have basically the possibility to adjust the potential distribution between powered and 'grounded' electrode without affecting the dissipated rf power or other parameters.

The use of two frequencies allows efficient production of radicals at high frequency while high-energy ion bombardment is brought about with low frequency. Using more than one frequency in the same system requires special precautions to avoid that one generator influences the other. A concept which can have considerable advantages would be a reactor where a microwave plasma is combined with a low frequency discharge. Such a system has not appeared on the market yet.

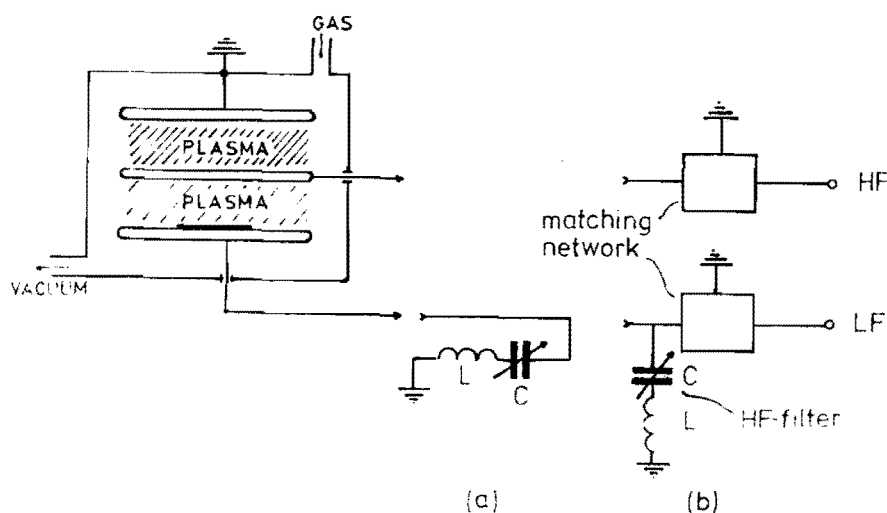


Fig. 17. Planar triode reactor: (a) flexible diode system; (b) dual frequency system.

References

- 1 H.R. Koenig and L.I. Maissel, IBM J. Res. Developm. 14, 168 (1970).
- 2 B.H. Chapman, "Glow Discharge Processes" (Wiley, New York, 1980).
- 3 C.M. Horwitz, J. Vac. Sci. Technol. A 1, 60 (1983).
- 4 F. Martinet, Proc. 3rd Symp. on Plasma Processing, ECS Proc. Vol. 82-6 (1982), p. 379.
- 5 A.J. van Roosmalen, W.G.M. van den Hoek, and H. Kalter, J. Appl. Phys., in press.
- 6 C.A.M. de Vries and W.G.M. van den Hoek, to be published.
- 7 D.L. Flamm, V.M. Donnelly, and D.E. Ibbotson, J. Vac. Sci.
- 9 H. Meinke and F.W. Gundlach, "Taschenbuch der Hochfrequenztechnik" (Springer, Berlin, 1962).
- 10 W.C. Johnson, "Transmission Lines and Networks" (McGraw-Hill, New York, 1950).
- 11 H. Norstrom, Vacuum 29, 341 (1979).
- 12 N.M. Mazza, IBM J. Res. Developm. 15, 192 (1970).
- 13 C.M. Horwitz, J. Vac. Sci. Technol. A 1, 1795 (1983).
- 14 J.W. Coburn and E. Kay, Solid State Technol. 22 (4), 117 (1979).
- 15 H.T. Arends, C.A.M. de Vries, A.J. van Roosmalen and G.C.C. Puylaert, 7th Int. Symp. Plasma Chem. (1985), extended abstract.
- 16 W.G.M. van den Hoek, Proc. 4th Symp. on Plasma Processing, San Francisco, 1983, ECS Proc. Vol. 83-10, 40 (1983).
- 17 A.J. van Roosmalen, Vacuum 34, 429 (1984).
- 18 H. Kalter, 7th Int. Symp. Plasma Chem. (1985), extended abstract.
- 19 A. Roth, "Vacuum Technology" (North Holland Publ., Amsterdam, 1976).
- 20 F. Kreith, "Principles of Heat Transfer" (Harper and Row, New York, 1976).
- 21 G.C. Schwartz and P.M. Schaible, Solid State Technol., November 1980, p. 85.
- 22 F.F. Chen, "Introduction to Plasma Physics", (Plenum, New York, 1974).
- 23 D.C. Hinson, L.I. Walter, H. Chu, and S. Hurwith, Semicond. Internat., October 1983, p. 103.
- 24 I. Lin, D.C. Hinson, W.H. Chu, and R.L. Sandstrom, Appl. Phys. Lett. 44, 185 (1984).
- 25 European Patent Application 821041464 (1982).
- 26 M.A. Heald and C.B. Wharton, "Plasma Diagnostics with Microwaves" (Wiley, New York, 1965).
- 27 K. Ninomiya, K. Suzuki, and S. Nishimatsu, Ext. Abstr. 16th Conf. on Solid State Devices and Materials, Kobe (1984), p. 463.
- 28 K. Suzuki, S. Okudaira, and I. Kanomata, J. Electrochem. Soc. 126, 1025.
- 29 P.J. Revell and G.F. Goldspink, Vacuum 34, 455 (1984).
- 30 S. Takami, Jap. J. Electr. Engineer., September 1983, p. 82.

- 31 E.D. Wolf, I. Adesida, and J.D. Chinn, *J. Vac. Sci. Technol. A* 2, 464 (1984).
- 32 S.J. Fonash, *Solid State Technol.*, January 1985, p. 150.
- 33 T. Tsukada, *Jap. J. Electr. Engineer.*, September 1983, p. 79.
- 34 R. Anglson, D. Gates, K. Monahan, R. Steger, W. Richardson, and J. Wilson, *Proc. 6th Int. Symp. Plasma Chem., Montreal* (1983), p. 651.
- 35 L.M. Ephrath and R.S. Bennett, *Proc. 1rst Int. Symp. VLSI Sci. Technol., ECS Proc. Vol. 82-7* (1982), p.108.

6. DIAGNOSTICS FOR RESEARCH AND APPLICATION

Dr. Peter C. Zalm works at the Philips Research Laboratories, Eindhoven, The Netherlands. His principal interest is the interaction of high speed particles with solid surfaces.

Dr. Guy Turban, Professor at the Université de Nantes, France. His principal areas of research are plasma deposition of Si - N, a - Si:H and a - Si - C:H thin films, plasma modelling, plasma etching of silicon compounds, refractory metals and polymers and plasma diagnostics with mass spectrometry and Langmuir probes.

Dr. Jacques P.M. Schmitt, Director of research appointed by CNRS at the Ecole Polytechnique, Palaiseau, France. His principal areas of research include plasma deposition mechanisms, amorphous silicon and thin film photovoltaic devices.

6.1. Surface and Thin Film Analysis

P.C. Zalm

This article was not submitted in time to the editor in a reproducible form and could therefore not be included in the proceedings.

MASS SPECTROMETRY OF LOW-PRESSURE REACTIVE PLASMAS.

Guy TURBAN

Laboratoire de Physique Corpusculaire - U.A. CNRS 838
 Université de Nantes, 2 rue de la Houssinière - 44072 NANTES Cedex

1. Introduction

Analysis of reaction mechanisms and reaction rates in gas discharges necessitates a detailed knowledge of the various gas constituents and their variation with time. While the optical spectroscopy becomes an ideal diagnostic for the study of excited species, the mass spectrometry remains irreplaceable in the identification and the quantitative determination of ions and neutral molecules. In some cases neutral free radicals have been also detected. In this lecture the mass spectrometric apparatus is described with emphasis on the sampling of species of the discharges. Then a method for the quantitative determination of the neutral composition is given. The detection of neutral free radicals and the application of mass spectrometry to kinetic analysis is also explained. Finally examples of positive and negative ion measurements are given for plasmas used in deposition of thin films and etching.

2. Experimental systems (ref. 1-9)

A schematic representation of a mass spectrometric set-up is given in Figure 1. The basic arrangement may be divided into four parts : the plasma reactor, the sampling system including the orifice and the intermediate chamber with electrostatic lenses, the mass analyzer and the ion detection system. The most powerful apparatus is that, as shown in Fig. 1, in which the particle beam is extracted from the plasma through a sampling aperture of 50 - 200 μm and analyzed by a quadrupole mass filter disposed **in view** of the orifice. With this configuration four kinds of species are detected : neutral molecules, neutral free radicals, positive ions and negative ions.

2.1. Mass spectrometers

Three spectrometers are usually encountered :

- The time - of - flight (T.O.F.) spectrometer. Pulses of ions are formed in the ionization source and then are injected into the drift region of length L with a constant energy qV_0 . The time, in seconds, required for a given ion to drift the length L is given by :

$$t = L \left(\frac{m}{2qV_0} \right)^{1/2}$$

With small injection voltages (e.g. 10 V), ion drift times for 1 m are about 10^{-5} sec. The T.O.F. spectrometer is a useful instrument when fast changing reactions are to be studied.

- The magnetic sector. The magnetic sector employes the well-known physical fact that moving, charged particles, traversing a magnetic field, follow a circular path which radius is given by

$$r = \frac{mv}{qB}$$

Magnetic sector spectrometer normally deflects the ions through either 60°, 90° or 180°. For monoenergetic ions the resolving power is :

$$\frac{m}{\Delta m} \approx \frac{r}{s_1 + s_2}$$

r : radius of ion path
 s_1 : entrance slit width
 s_2 : exit slit width.

Magnetic spectrometers typically have a resolving power of ~ 100 and are sensitive to partial pressures of 10^{-15} torr.

– The quadrupole mass spectrometer (QMS).

The Q.M.S. is, by far, the most popular spectrometer in use today. It was originally developed by W. Paul and co-workers in 1955. A schematic of Q.M.S. is shown in Figure 2. The analyzing region is basically a set of four cylindrical rods with radius r_0 connected to a dc potential U and a rf potential $V \cos \omega t$. Ions formed in the ion source, or coming from the plasma, enter the filter along the z-axis. With proper selection of U and V , ions of a given q/m will oscillate about the z-axis on stable trajectories and ultimately emerge from the opposite end of the mass filter. Masses may be swept by varying the rf and dc voltage level, keeping the ratio $\beta = U/V$ and the frequency ω constant.

The resolving power $\frac{m}{\Delta m}$ depends only on β .

Because the mass sweep is linear, using voltage scanning, it is convenient to have Δm constant. This is obtained by continuously varying β in order to get $\Delta m = \text{cte}$ while sweeping mass. When operating in this mode, the sensitivity decreases with increasing m , thus making detection of more massive ions difficult.

A proper calibration of the apparatus can solve this problem. (See below § 3.2).

Generally the instrument can detect partial pressures of $\sim 10^{-10}$ torr when using a Faraday cup detector, 10^{-14} torr when using a secondary electron multiplier (s.e.m.) disposed on the mass filter axis, and $\leq 10^{-15}$ torr when using a 90° configuration (off axis) in conjunction with an ion counting system behind the s.e.m. instead of a conventional electrometer amplifier.

The Q.M.S. is a true mass analyzer in the sense that it is not very sensitive to ion injection energy. Axial energy of ions can vary in the range 2 to 20 eV (even up to 50 eV). Thus ions travelling towards the detector can undergo collisions with gas phase molecules, lose energy, and still be filtered properly. This means that the Q.M.S. can be operated at pressure as high as $\sim 10^{-4}$ torr (in fact $p \leq 10^{-5}$ torr is usually recommended). Also the ions directly coming from the plasma need not to be mono-energetic. However some peak shape deterioration (peak splitting) is observed depending on the ion injection energy or misalignment in the case of ions coming from the plasma. The Q.M.S. has advantage of rapid scanning (i.e. 10 scans/sec or 1 a.m.u./msec) which is an interesting feature for the control of plasma processing.

2.2. Neutral sampling

The most crucial problem in mass spectrometric probing of plasmas is the extraction of particles out of the plasma region onto the mass analyzer. The discharge must be sampled without disturbance of the plasma and the particles beam needs to be a correct picture of the composition of the discharge.

The orifice diameter $2R$ should be chosen so that molecular flow conditions are applicable. This is approximately the case when, for a zero length orifice, the Knudsen number is :

$$\frac{\lambda}{2R} \geq 5 - 10$$

with λ the neutral-neutral mean free path. In practical conditions, the flow is found 96 % molecular at 1 torr with $2R = 50 \mu\text{m}$.

The neutral flow conductance must be small enough to guarantee sufficiently low working pressure in the mass spectrometer chamber. Although the aperture should be made as small as possible, experience has shown that diameters ranging from $50 \mu\text{m}$ to $300 \mu\text{m}$ appear to be satisfactory. With a single stage of differential pumping the pressure p_C in the chamber behind the orifice is determined by the area of the aperture A_1 and the effective pumping speed S_1 according to :

$$p_C = \frac{C_1}{S_1} (p_r - p_C) = \frac{Q_1}{S_1} \quad \text{with } p_C \ll p_r$$

C_1 is the conductance of the aperture of area A_1 . Then, $C_1 = \frac{1}{4} \bar{v} A_1$ with $\bar{v} = \left(\frac{8kT}{\pi m}\right)^{1/2}$.

Q_1 is the molecular flow rate in the aperture.

If $p_r = 1$ torr, $\bar{v} = 4.10^4$ cm/sec and $2R = 50 \mu\text{m}$

$p_C = 9.810^{-7}$ torr with $S_1 = 200$ l/sec.

A medium size diffusion pump or turbomolecular pump could be used in this case.

In order to obtain more versatility in the choice of the aperture size and the operating pressure range and to ensure a long spectrometer lifetime a dual differentially pumped sampling arrangement is often used (Fig. 1 and 3). The flow through the second orifice of area A_2 is molecular with a flow rate :

$$Q_2 = \frac{1}{4} \bar{v} A_2 (p_C - p_s) = (p_s - p_{s0}) S_2$$

By posing $\Delta p_C = p_C - p_{C0}$ and $\Delta p_s = p_s - p_{s0}$, it follows that $\Delta p_s = \frac{A_2}{S_2} \frac{1}{4} \bar{v} (\Delta p_C - \Delta p_s)$ if $p_{C0} = p_{s0}$ (background pressures),

and on the other hand $\Delta p_C = \frac{Q_1 - Q_2}{S_1}$.

These relationships in conjunction with the expression of the flow rate Q_1 :

$$Q_1 \approx \frac{1}{4} \bar{v} A_1 p_r$$

give an expression :

$$\Delta p_s = K(m) \cdot p_r$$

which indicates the proportionality between Δp_s and p_r .

The ionization of the neutral species reaching the cross-beam ion source is performed by an electron beam perpendicular to the neutral beam and set at energies varying from 20 eV to 70 eV. Low electron energy (20 eV) gives simpler fragmentation patterns than high energy but with smaller ionization efficiency.

In order to avoid interference between ions coming from the discharge and ions produced from neutrals in the ionizer, a magnetic or electrostatic deflexion of the ion beam may be necessary before reaching the mass spectrometer chamber.

2.3. Positive ion sampling

The collisionless extraction of ion through the plasma sheath in front of the aperture is assured if the mean free path of ions λ_i is much larger than the sheath thickness s : $\lambda_i \gg s$ (with $s \approx 3$ to $5 \lambda_D$)

λ_D Debye length = $74 \mu\text{m}$ with $n_e = 10^{10} \text{cm}^{-3}$ and $kT_e = 1 \text{eV}$.

The length of the orifice should be much smaller than its diameter to reduce as far as possible reactions of ions within the orifice channel and the interaction of ions with the inner surface of the tube.

The positive ions are accelerated towards the orifice disc by the electric field existing within the sheath, while electrons and negative ions are repelled.

If the orifice is electrically floating the voltage across the sheath will be :

$$V = \frac{1}{2} \frac{kT_e}{q} \ln \left(\frac{\pi}{2} \frac{m_e}{m_i} \right).$$

For $m_i = 30 \text{ a.m.u.}$ $V \approx 5 \frac{kT_e}{q}$, that means that an accelerating field for positive ions exists without any additional bias of the sampling aperture.

When the extraction is collisionless ($\lambda_i \gg 2R$), the ion current density for an ion of mass m_i is expressed by the Child-Langmuir law

$$j_i = \frac{4\epsilon_0}{9} \left(\frac{2q}{m_i} \right)^{1/2} \frac{V^{3/2}}{s^2}$$

or, in the case of low voltage, by the Bohm current :

$$j_i = 0.6 q n_i \left(\frac{kT_e}{m_i} \right)^{1/2}$$

When the ionic mean free path is smaller than the orifice diameter ($\lambda_i \ll 2R$) the extraction is of diffusion type. That happens when the reactor pressure $p_r > 10 \text{mtorr}$.

The current density j_i at the orifice is given by a mobility-limited law :

$$j_i = \frac{9\epsilon_0}{8} \mu_i \frac{V^2}{s^3}$$

where μ_i is the mobility of positive ions.

Since $\mu_i = \frac{q\lambda_i}{m_i \bar{v}_i}$ with $\bar{v}_i = \left(\frac{8kT_i}{\pi m_i} \right)^{1/2}$,

the ion current ratio of two ionic species of masses m_i and m_k reaching the aperture will be, in all extraction cases, related to their plasma density ratio by :

$$\frac{j_k}{j_i} = \frac{n_k}{n_i} \left(\frac{m_i}{m_k} \right)^{1/2}$$

If the aperture is too large, causing the sheath to collapse, the plasma may penetrate the low pressure region behind the orifice and edge effects could strongly influence the electric fields. The mass spectrum measured in this instance would not necessarily represent the ion concentrations present in the unperturbed plasma.

Electrostatic lenses may be mounted inside the intermediate chamber in order to focus ions onto the second aperture. The ion signal may be substantially increased by the lens system which determines the solid angle of particles collection.

2.4. Negative ion sampling

In usual situations negative ions are confined inside the plasma bulk by the potential barrier of the sheath. In order to extract a negative ion beam from a plasma a positive bias of the aperture higher than the plasma potential itself is needed.

In the case of strongly electronegative plasmas (e.g. SF₆ or CCl₄), the extraction is easier because of the lowering of the plasma potential by the low mobility of negative particles (negative ions instead of electrons). A positive bias on the electrostatic lens behind the orifice can be sufficient to get measurable negative ion beam.

By this way the relative ionic abundance can be obtained. For absolute measurement, another diagnostic, e.g. Langmuir probe, must be employed.

For the detection of negative ions with the Q.M.S. the biasing of the s.e.m. has to be reversed in comparison with that used for positive ion detection. The first dynode is connected to + 3 kV with respect to ground, the last dynode to + 5 kV, for example, instead of - 3 kV and - 0.5 kV respectively for positive ion detection.

2.5. Other refinements

In order to obtain a better sensitivity in the ion detection two methods are sometimes employed :

- a pulse counting at the output of the s.e.m. This is recommended for negative ion measurement.

- a modulation of the extracted beam at the exit of the sampling orifice, in conjunction with a synchronous detection. This is of great interest for free radical studies.

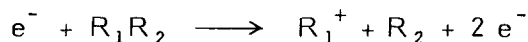
3. **Analysis of neutrals from reactive plasmas** (ref. 5, 11-28).

One of the most useful applications of mass spectrometry in plasma chemistry is the quantitative analysis of the gaseous mixtures produced in the discharge.

The spectrometer must be previously calibrated with pure gases, separately injected, at a controlled pressure. This is a very expensive and unsafety procedure in the case of corrosive and unusual gases such as : Si_nH_{2n+2}, COF₂, F₂, HF, SOF₂, SO₂F₂, SOF₄ etc... A more practical method is to use fragmentation patterns and sensitivity factors of these gases published in litterature and to calibrate the spectrometer, as a function of mass, with a standard gas mixture (He, N₂, Ar, Kr, Xe).

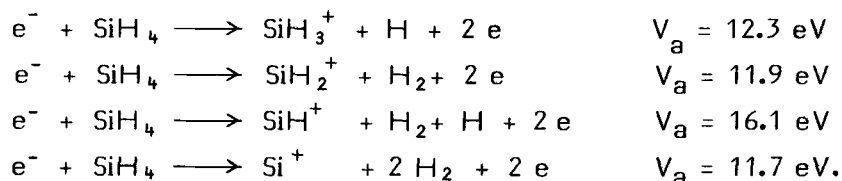
3.1. Mass spectra

The electron impact on a molecule R₁R₂ leads to a dissociative ionization reaction :



if the electron energy is greater than V_a the appearance potential of the molecular ion R₁⁺. Measurements of the ion current resulting from this reaction have been

made for numerous molecules and its plot as a function of the electron energy is called the ionization efficiency curve. In the example of SiH_4 , four ions are detected :



The relative abundance of the various ions issued from the parent molecule at a given electron energy is known as the fragmentation pattern.

For SiH_4 the fragmentation pattern at 70 eV is :

m/e	ion	relative abundance α_j
28	Si^+	28
29	SiH^+	29
30	SiH_2^+	100
31	SiH_3^+	79

This result is, in principle, relatively independent of the apparatus and can be found in the mass spectra indexes. In most of elements the isotopic abundance has to be taken into account for a correct assignment of the ion mass.

For example in Si :

$$^{28}\text{Si} = 92.2 \% \quad ^{29}\text{Si} = 4.7 \% \quad ^{30}\text{Si} = 3.1 \%$$

If p is the partial pressure of the molecular compound in the mass spectrometer, each ion current i is proportional to p provided that this pressure is sufficiently low ($< 10^{-6}$ torr)

$$i \propto p$$

When calculating absolute values, the most abundant peak of a molecule is compared with the peak height of the most abundant peak of nitrogen ($m/e = 28$) or n-butane ($m/e = 43$). These ratios N or B are given in mass spectra tables.

3.2. Calibration of the mass spectrometer

The spectrometer can be calibrated with pure gases and the sensitivity factor used for mixtures.

The sensitivity of the spectrometer is defined by :

$$i(m_j) = S(m_j) \Delta p_s .$$

$S(m_j)$ in A/torr (usually $> 10^3$ A/torr with a s.e.m.)

$\Delta p_s = p_s - p_{s0}$ is the pressure variation produced by the introduction of the compound.

$i(m_j)$ in amperes is the intensity of the most abundant peak due to the electron impact fragmentation of the compound.

The sensitivity factor S depends on the nature of the gas.

It is convenient to define the factor F which is independent of the gas and depends on the physical characteristics of the spectrometer.

$$F(m_j) = \frac{S(m_j)}{\sigma(m_j)}$$

$\sigma(m_j)$ (in cm^2) is the partial ionization cross-section of the molecule m for the ion of mass m_j .

In $F(m_j)$, the s.e.m. gain $G(m_j)$ is taken into account for.

An empirical relationship for $G(m_j)$ is :

$$G(m_j) = \frac{G(o)}{(a + b m_j)^{1/2}}$$

where $G(o)$ ($\sim 10^3 - 10^4$) is the sem gain relative to Faraday cup gain for N_2 or Ar .

With a differentially pumping system it is shown that the pressure variation Δp_s in the spectrometer chamber is related to the reactor pressure p_r according to :

$$\Delta p_s = K(m) \cdot p_r$$

$$\text{with } K(m) = \frac{A_1 \cdot A_2}{S_1 S_2} \left(\frac{kT}{2\pi m} \right) \left[1 + A_2 \left(\frac{1}{S_1} + \frac{1}{S_2} \right) \left(\frac{kT}{2\pi m} \right)^{1/2} \right]^{-1}$$

The partial pressure p_r in the reactor is obtained from the peak intensity $i(m_j)$:

$$p_r = \frac{i(m_j)}{K(m) \cdot F(m_j) \cdot \sigma(m_j)}$$

In the simple case where the ion and the molecule have the same masses ($m = m_j$) a global transmission coefficient of the apparatus can be defined by :

$$T(m_j) = K(m_j) \cdot F(m_j)$$

$T(m_j)$ is the only experimental value of practical use. For example, Figure 4 shows the variation of $T(m_j)$ values measured between masses 4 to 129 in the apparatus represented on Fig. 1 by using a standard gas mixture (He , N_2 , Ar , Xe , Kr).

The cross-sections $\sigma(m_j)$ are taken from the literature. In a more usual case where $m_j \neq m$ the partial pressure will be calculated from the relationship :

$$i(m_j) = \sigma(m_j) \frac{K(m)}{K(m_j)} \cdot T(m_j) \cdot p_r(m).$$

When m and $m_j \geq 20$ a.m.u. it can be verified that :

$$\frac{K(m)}{K(m_j)} \approx \frac{m_j}{m} \quad \text{with an accuracy better than 2 \% .}$$

In the case of molecules for which $\sigma(m_j)$ is unknown either the N or B factors may be used according to :

$$\sigma(m_j) = \sigma(28, N_2) \cdot N(m_j) \cdot \frac{\alpha_j}{100}$$

$$\text{or } \sigma(m_j) = \sigma(43, n C_4 H_{10}) \cdot B(m_j) \cdot \frac{\alpha_j}{100}$$

where α_j is the relative abundance of the peak of mass m_j in the fragmentation pattern (in %). j When the pure gas is available from a commercial cylinder the term $[\sigma(m_j) \cdot \frac{K(m)}{K(m_j)} \cdot T(m_j)]$ can be experimentally determined (direct calibration).

3.3. Mass interferences

Each molecular ion of mass m_j can originate from several parent molecules of the plasma. The mass interference is taken into account by using the correction :

$$[1] \quad p_r(m) = \left[\frac{i(m_j)}{T(m_j) \cdot m_j} - \sum_{m'} p_r(m') \frac{\sigma(m_j, m')}{m'} \right] \cdot \frac{m}{\sigma(m_j, m)}$$

where $p_r(m')$ is the partial pressure of the parent molecule of mass m' which contributes to the intensity of the ion m_j , and $\sigma(m_j, m')$ the partial ionization cross-section for the ion m_j of the molecule of mass m . The neutral composition of plasmas can thus be obtained by resolving the system of linear equation [1]. As an example the mass peaks and their assignments for a C_2F_6 plasma are given in Table 1.

Table 1

Assignments of peaks detected in the C_2F_6 plasma.

m/e (a.m.u.)	ion	parent molecules
62	$C_2F_2^+$	C_2F_2
69	CF_3^+	$CF_4, C_2F_4, C_2F_6, C_3F_6, C_3F_8, C_4F_8, C_4F_{10}$
81	$C_2F_3^+$	C_2F_4
93	$C_3F_3^+$	C_4F_6, C_4F_8
100	$C_2F_4^+$	$C_2F_4, C_2F_6, C_3F_6, C_3F_8, C_4F_8, C_4F_{10}$
119	$C_2F_5^+$	$C_2F_6, C_3F_8, C_4F_{10}$
131	$C_3F_5^+$	$C_3F_6, C_4F_8, C_4F_{10}$
143	$C_4F_5^+$	C_4F_6, C_5F_8
150	$C_3F_6^+$	C_3F_6
169	$C_3F_7^+$	C_3F_8
181	$C_4F_7^+$	C_4F_8

The evolution of the molar fraction of the main neutral molecules as a function of the total pressure p_r is given of Figure 5.

When using a modulated molecular beam mass spectrometer neutral impurities can be detected (~ 1 ppm).

3.4. The detection of neutral free radicals

The direct detection of radicals by mass spectrometry presents some difficulties. The gaseous free radicals are estimated to have low concentration ratio (10^{-5} - 10^{-4} for SiH_n in silane discharges) ; so they must be discriminated from the large concentration of the parent molecule.

For this, two methods can be used : ionization by low energy electrons, or photo-ionization.

In the first method radicals are ionized with electrons the energy of which is lower than the ionization potential V_i of the molecule M but higher than the appearance potential V_a of the radical.

V_i and V_a are reported in Table II for SiH_3 and SF_2 detection :

Table II
Threshold energies (eV) for ions from the neutral parents.

ion	neutral radical	appearance potential V_a	neutral molecule	ionization potential V_i
SiH_3^+	SiH_3	8.4	SiH_4	12.3
CF_2^+	CF_2	11.7	CHF_3	17.5
	—	—	C_2F_4	15.2

Successful detection of SiH_3 radical in silane discharge, CF_2 in CHF_3 and C_2F_4 discharges have been reported. Atoms have also been detected by mass spectroscopy eg : N^4S from N_2 discharge, O^3P from O_2 discharge, F^2P from F_2/Ar or CF_4 discharge, Cl^2P from Cl_2 discharge.

The sensitivity of radical detection by electron impact ionization is unavoidably reduced by the low ionization efficiency of 10 - 15 eV electrons compared to standard 70 eV electrons.

Another method is the use of photoionization mass spectrometry. In this technique the ionization is produced by rare gas resonance lines (Ar 11.6 and 11.8 eV, Kr 10.03 and 10.64 eV) or the Lyman α line (10.2 eV) of hydrogen.

CF and CF_3 have been observed in a $\text{CF}_4 - \text{H}_2$ plasma by this technique.

3.5. Application in plasma kinetics

A kinetic analysis of the discharge can be performed by mass spectrometry. Different approaches have been proposed. In the conventional gas flow method, the discharge tube is a plug-flow reactor. The residence time is used as a kinetic parameter. A more realistic approach for plasma deposition or etching is to describe the discharge as a backmixed reactor controlled by diffusion. For example the injected molecule concentration N_M is governed by a balance equation :

$$Q_M/V - k_1 N_M - N_M/t_R = 0$$

where Q_M is the flow rate of the injected molecules, V the volume of the reactor, k_1 the rate constant for molecule decomposition and t_R the mean residence time of molecules in the plasma.

The concentration N_M can be measured by mass spectrometry and permits the determination of rate constant k_1 . Such a study have been made for silane plasma and CF_4 plasma.

A more sophisticated method is to use the relaxation technique in which the discharge current is modulated and the response of the plasma chemical system measured by mass spectrometry. Information on the rate constants of the elementary processes are deduced from these measurements.

3.6. Isotopic labelling

In order to identify the intermediate radicals and the reactions which occur in reactive plasmas, the isotopic labelling technique can be used. For example the study of $SiH_4 - SiD_4$ plasma bring indirect evidence of SiH_2 and SiH_3 free radicals in the gas phase. The disilane formed in the plasma, $Si_2H_{6-n}D_n$, exhibited all degrees of deuteration $n = 0$ to 6. SiH_2D_2 and $SiHD_3$ have also been detected.

However such a study is rather complex due to the mass interferences in the spectra. Also the interpretation implies the knowledge of the elementary reactions.

3.7. Control of the plasma etching process

Time recording of various peaks can bring information during plasma etching. For example, in Figure 6, the variation of the peak 47 (COF^+ for COF_2 and SiF^+ for SiF_4) illustrates the etching of a sandwich of poly-Si/ SiO_2 /mono Si.

Pollution of the reactor walls or the wafer surface may be detected by recording several key peaks before or during the plasma sequence.

4. Ion spectrometry (ref. 17, 19, 23, 25, 26, 28)

The detection of positive and negative ions is currently done by mass spectrometry. In this section some examples, taken in deposition and etching applications, will be presented as an illustration of the capability of this diagnostic means.

4.1. Positive ion studies

Absolute measurements of ion currents are possible with QMS. However it is sometimes observed some fluctuations of the ion intensity during time or from run to run for the same plasma conditions. The causes are often a modification of the surface state of the electrodes and the walls of the reactor by deposition or etching. This variation affects the electron emission coefficient of surfaces and thus the ionization of the gas. In major situations the ionic abundance $i/\sum i$ is found to be reproducible. The extracted ion currents ratio $i(m_j)/i(m_k)$ is related to the corresponding ion density n_j/n_k in the plasma by the expression :

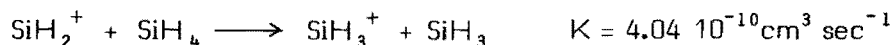
$$\frac{i(m_j)}{i(m_k)} = \left(\frac{m_k}{m_j}\right)^{1/2} \frac{T_i(m_j)}{T_i(m_k)} \cdot \frac{n_j}{n_k}$$

The transmission factor T_i for ion depends on the ion mass and energy. Reported measurements of T_i indicate a constant value in a QMS for m_i varying between 28 up to 84 a.m.u. and a decrease for higher masses (ref. 8).

The primary interest of ion sampling from discharge is to compare the mass spectrum to that expected from the direct electron impact ionization of molecules.

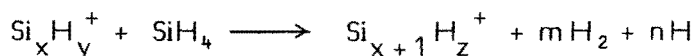
4.1.1. Example of SiH₄ plasma.— Figure 7 shows the evolution of the SiH_n⁺ ions in a SiH₄–He plasma as a function of pressure. The relative abundance of ions differs strongly from that observed in the direct ionization of silane. Except for very low pressures (50 mtorr), SiH₂⁺ is never the most abundant. The same evolution is obtained at given pressure by dilution of SiH₄ in helium.

The predominance of the SiH₃⁺ ion over the SiH₂⁺ ion is explained by the ion-molecule reaction :



This can be guessed by calculating the distribution of the SiH_n⁺ ions by using the silane concentration obtained by mass spectrometry.

Ion clusters Si_xH_y⁺ with x = 2 to 9 and y ≤ 2x + 3 have been observed in silane glow discharges. A chain reaction mechanism leads to these large Si-containing clusters

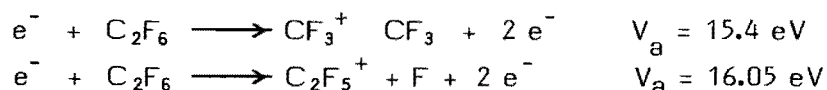


where 4 + y = 2m + n + z.

These ion-molecule reactions may occur both in the plasma bulk and in the sheath across which the ions are extracted. In this sheath the accelerated ions may also participate in charge-exchange and fragmentation reactions. For example ions sampled at the cathode of a dc silane discharge have a distribution pattern very different from that obtained at the anode or at the wall : SiH_n⁺ ions contain less H atoms at the cathode than at the anode.

4.1.2. Example of C₂F₆ plasma.— The evolution of the relative intensities of positive ions extracted from a C₂F₆ plasma as a function of pressure is given in Figure 8. The most abundant ion is always CF₃⁺ as in electron impact ionization of C₂F₆ but the relative abundances of ions are quite different from those expected from direct ionization of C₂F₆.

In particular the rate of production of C₂F₅⁺ from C₂F₆ is of the same order of magnitude than that of CF₃⁺. The two direct ionization reactions which are :

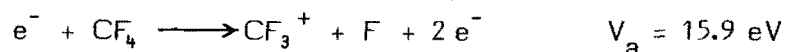


are not sufficient to describe the relative abundance.

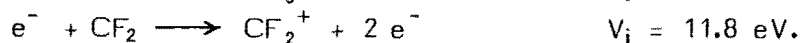
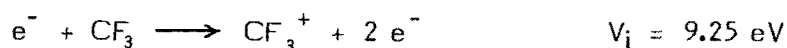
Other ionization processes must be taken into account for to explain these mass spectrometric measurements.

In particular :

- the ionization of other neutral molecules present in the plasma (CF₄ for example):



- the ionization of molecular radicals :



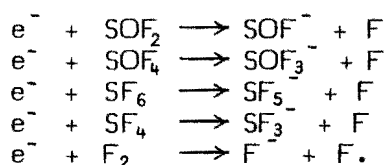
4.2. Negative ion studies

Negative ion currents extracted from a plasma vary with the biasing potential. However it is found that relative ionic abundances are reproducible. In silane plasmas the Si_nH_m^- ions with $n = 1$ to 6 have been detected by QMS.

In electronegative gases, e.g. SF_6 , the negative ion analysis is essential in order to understand the main reaction channels in the discharge. Figure 9 illustrates the variations of the relative ionic abundances $i/\Sigma i$ in a $\text{SF}_6 - \text{O}_2$ plasma with a silicon sample of the r.f. electrode in comparison with a bare r.f. electrode. An increase of the intensities of SF_3^- , SOF_3^- , SOF^- is observed in conjunction with a decrease of the SF_5^- and F^- intensities. This result must be correlated with the mass spectrometric study of neutrals.

In the same conditions SF_6 and F_2 concentrations are decreased whereas SO_2F_2 , SOF_2 , SOF_4 and SF_4 concentrations are increased.

By this way different attachment reactions may be postulated :



4.3. Application to end point detection

The great interest of the ion detection in view of the control of plasma etching processes is that it is a very sensitive method. For example the fluorides and oxyfluorides of refractory metals have a vapor pressure lower than SiF_4 and are thus difficult to detect as neutral effluents. It is easier to observe them by the positive ions issued from the ionization in the plasma of these neutral products. Table III gives the positive ions observed during the etching of refractory metals in $\text{SF}_6 - \text{O}_2$ and $\text{CF}_4 - \text{O}_2$.

Table III

Positive ions detected during the etching of refractory metals

Metal	Ions
W	WF_n^+ ($n = 3-5$), WOF_m^+ ($m = 1-3$)
Mo	MoF_n^+ ($n = 3-5$), MoOF_m^+ ($m = 1-3$)
Ta	TaF_4^+ , TaF_5^+

Figure 10 illustrates the control of etching of WSi_2 in a M.O.S. structure by recording the peak intensities of WF_5^+ and SiF_3^+ during the process. Therefore mass spectrometry can provide an alternative method to the optical emission spectroscopy when emission lines of etching products are unknown or difficult to observe.

References

- (1) P.H. Dawson and N.R. Whetten
Mass spectrometry using RF quadrupole fields.
in Adv. Electron Electron Physics. Vol. 27, p. 59.
Ed. L. Marton, Acad. Press.
- (2) M. Mosharrafa and H.J. Oskam
Application of mass spectrometry to the study of gaseous plasmas
Physica 32, 1966, p. 1759.

- (3) D. Lichtman
Perspectives on residual gas analysis
J. Vac. Sci. Technol. A2 (2), Apr. June 1984, p. 200.
- (4) T.D. Mark and H. Helm
Mass spectrometry as a technique for studying atomic properties of low pressure plasmas.
Acta Physica Austriaca 40, 1974, p. 158.
- (5) G. Turban, B. Grolleau, P. Launay and P. Briaud
A mass spectrometric diagnostic of C_2F_6 and CHF_3 plasmas during etching of SiO_2 and Si.
Rev. Phys. Appliquée. submitted.
- (6) J.B. Hasted
The mass-spectrometric monitoring of ions in plasma
Adv. Mass Spectrom. Vol. 6. Ed. A.R. West, 1974, p. 901.
- (7) A. Picard, G. Turban and B. Grolleau
Plasma diagnostics of a SF_6 radiofrequency discharge used for etching of silicon.
to be published.
- (8) J. Perrin, A. Lloret, G. de Rosny and J.P.M. Schmitt
Positive and negative ions in silane and disilane multipole discharges.
Int. J. Mass Spectrometry and Ion Process. 57, 1984, p. 249.
- (9) H.A. Weakliem
Diagnostics of silane glow discharges using probes and mass spectroscopy
in Semiconductors and semimetals, Vol. 21 - Hydrogenated amorphous silicon -
Part A - Preparation and structure - 1984, Ed. J. Pankove, Academic Press.
- (10) F.H. Field and J.L. Franklin
Electron impact phenomena
Academic Press, 1957.
- (11) A. Cornu and R. Massot
Compilation of mass spectral data, Vol. 1 and 2.
Heyden and Sons, 1975.
- (12) W.H. Beattie
Mass spectral intensities of inorganic fluorine-containing compounds.
Appl. Spectr. 29, 1975, p. 334.
- (13) R.W. Kiser
Introduction to mass spectrometry and its applications
Prentice-Hall, 1965.
- (14) D. Rapp and P. Englander-Golden
Total cross sections for ionization and attachment in gases by electron impact.
J. Chem. Phys. 43, 1965, p. 1464.
- (15) J.A. Beran and L. Kevan
Molecular electron ionization cross sections at 70 eV.
J. Phys. Chem. 73, 1969, p. 3866.
- (16) G. Smolinsky and D.L. Flamm
The plasma oxidation of CF_4 in a tubular-alumina fast-flow reactor.
J. Appl. Phys. 50, 1979, p. 4982.

- (17) J.W. Coburn and E. Kay
Some chemical aspects of the fluorocarbon plasma etching of silicon and its compounds.
IBM J. Res. Develop. 23, 1979, p. 33.
- (18) S.N. Foner
Mass spectrometry of free radicals.
Adv. Atom. Molecular Physics, Vol. 2, 1966, p. 385.
Academic Press.
- (19) M.J. Vasile and G. Smolinsky
Ionic and neutral species detected by mass spectrometry in a rf discharge in C_2F_4 .
J. Phys. Chem. 81, 1977, p. 2605.
- (20) R. Robertson, D. Hills, H. Chatham and A. Gallagher
Radical species in argon - silane discharges.
Appl. Phys. Letters 43, 1983, p. 544.
- (21) T. Hayashi, M. Kikuchi, T. Fujioka and S. Komiya
Observations of radicals and neutral molecules in R.I.E. with photoionization mass spectrometry.
Proc. ISIAI - IPAT, Kyoto 1983, p. 1611.
- (22) G. Nolet
Kinetics of decomposition of silane in a low pressure discharge
J. Electrochem. Soc. 122, 19, p. 1029.
- (23) G. Turban, Y. Catherine and B. Grolleau
Ion and radical reactions in the silane glow discharge deposition of α -SiH films.
Plasma Chem. Plasma Process. 2, 1982, p. 61.
- (24) J.J. Wagner and S. Veprek
Chemical relaxation study of the heterogeneous Si - H system under plasma conditions.
Plasma Chem. Plasma Process. 3, 1983, p. 219.
- (25) G. Turban, Y. Catherine and B. Grolleau
A study of the silane glow discharge deposition by isotopic labelling.
Thin Solid Films 77, 1981, p. 287.
- (26) G. Turban, Y. Catherine and B. Grolleau
Mass spectrometry of a silane glow discharge during plasma deposition of α -SiH films.
Thin Solid Films 67, 1980, p. 309.
- (27) H.W. Lehmann, E. Heeb and K. Frick
Plasma diagnosis by time resolved mass spectrometry.
Solid State Technology, oct. 1981, p. 69.
- (28) Y. Catherine, G. Turban and B. Grolleau
Neutral and ion chemistry in a C_2H_4 - SiH_4 discharge
Plasma Chem. Plasma Process. 2, 1982, p. 81.

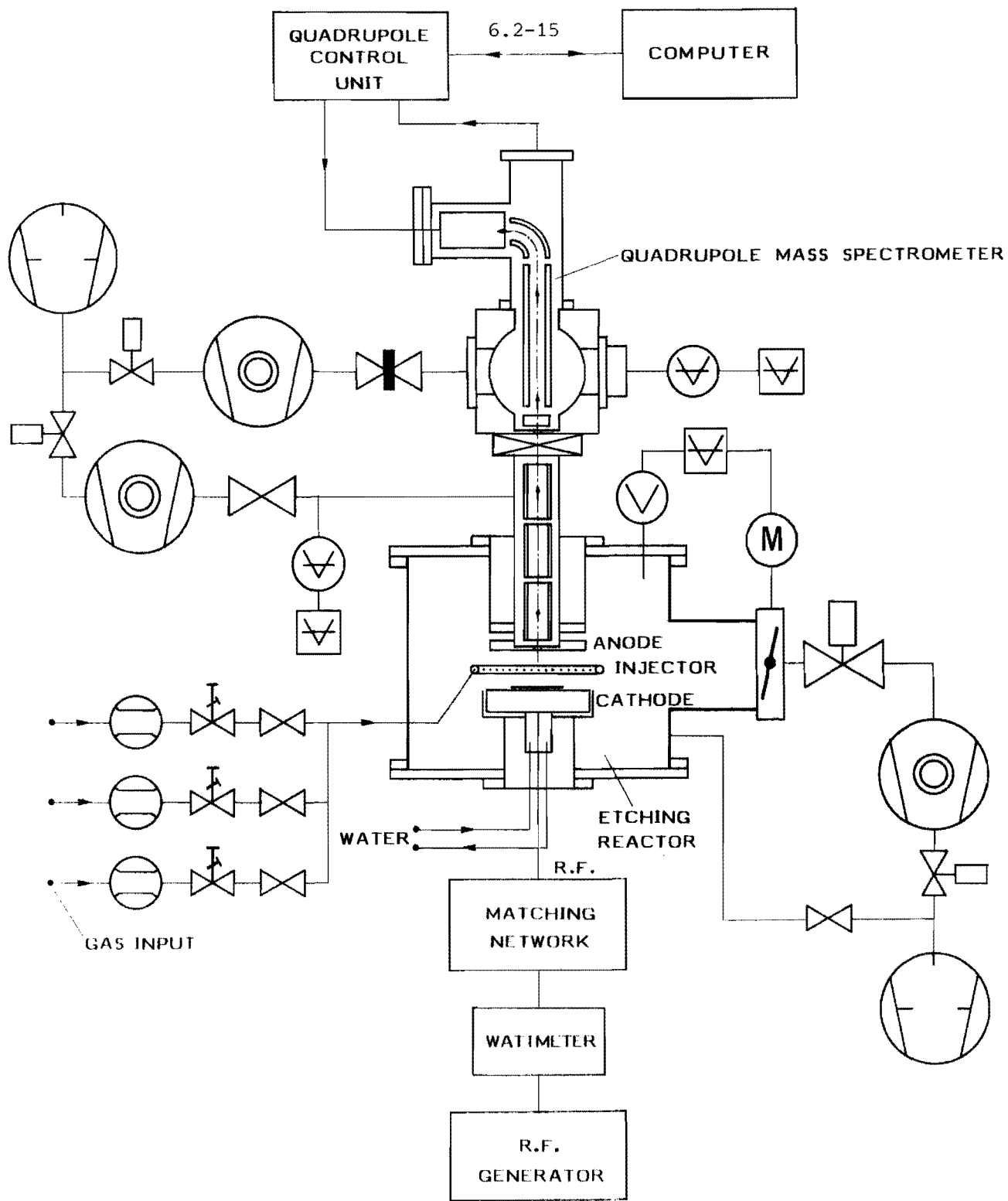


Fig. 1. Schematic representation of the mass spectrometer with the sampling system and the dual differentially pumped chamber.

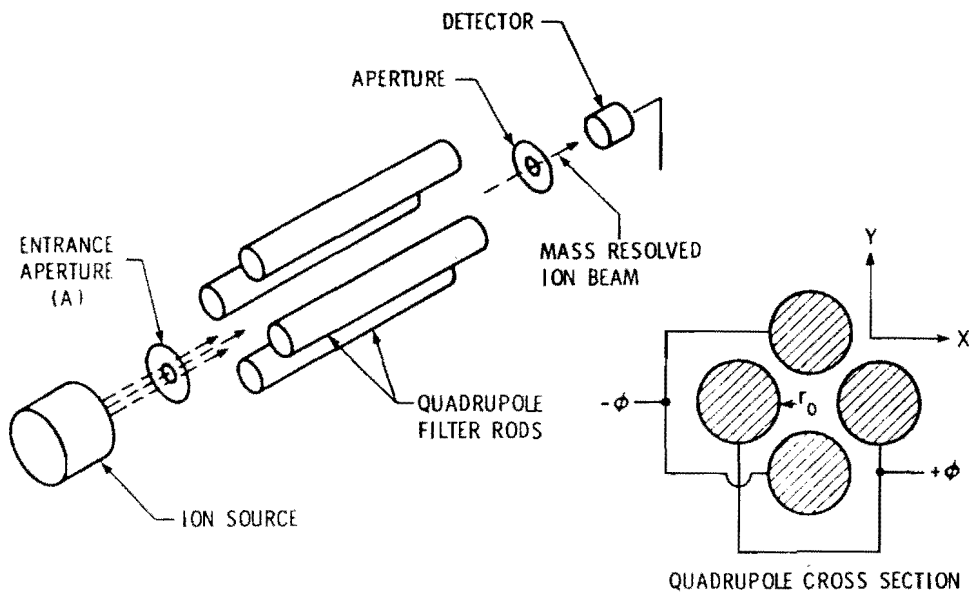


Fig. 2. Quadrupole mass filter.

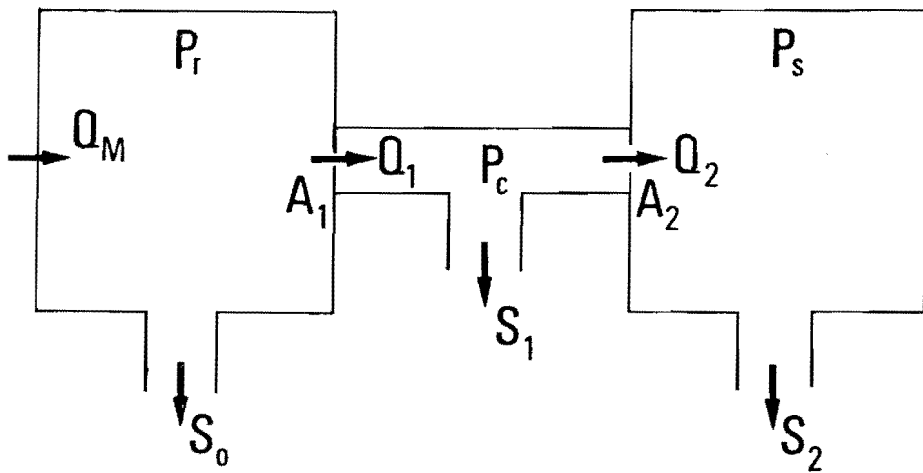


Fig. 3. Gas flow diagram.

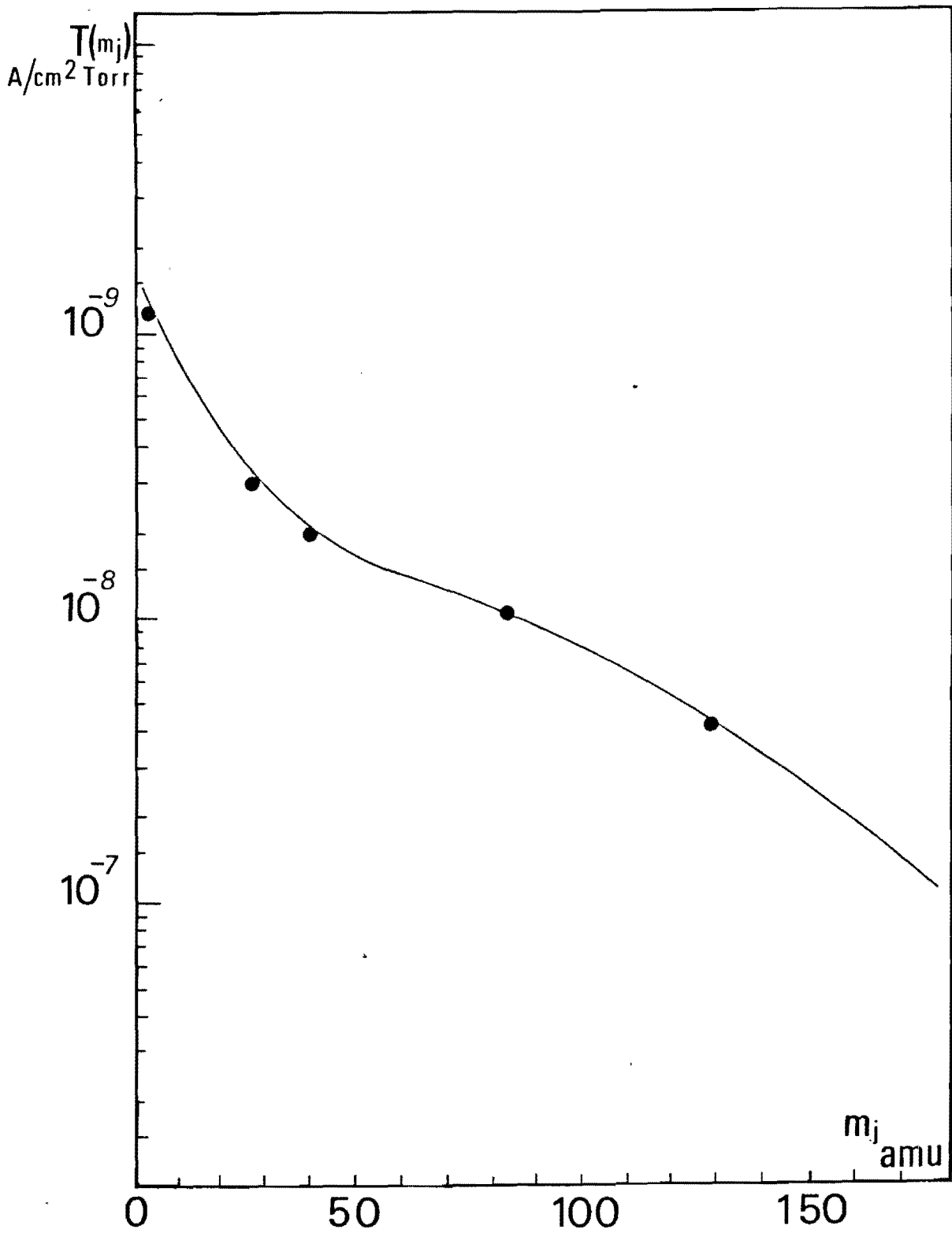


Fig. 4. Global transmission coefficient $T(m_j)$ for neutral molecules.

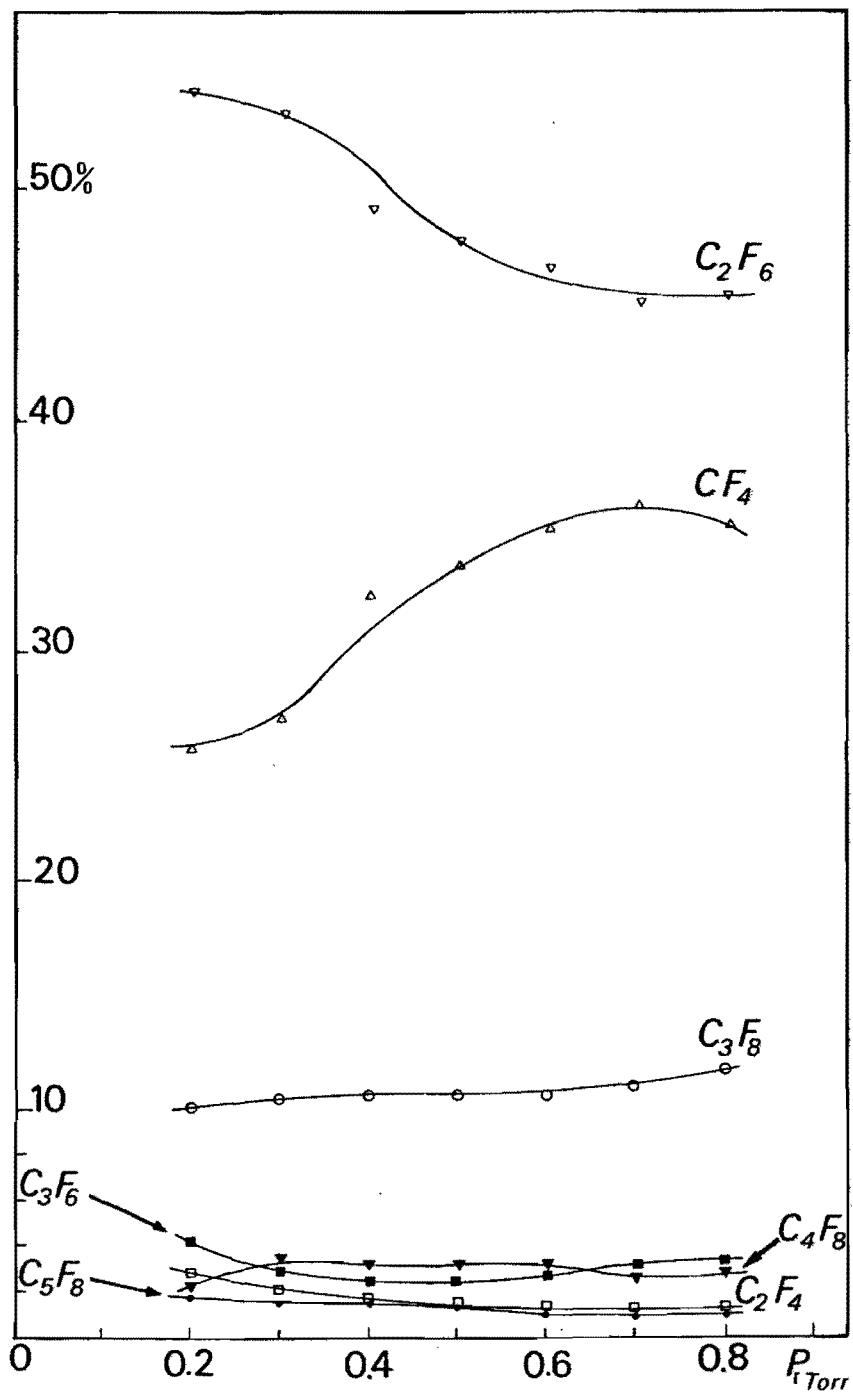


Fig. 5. Molar fractions in the C_2F_6 plasma.

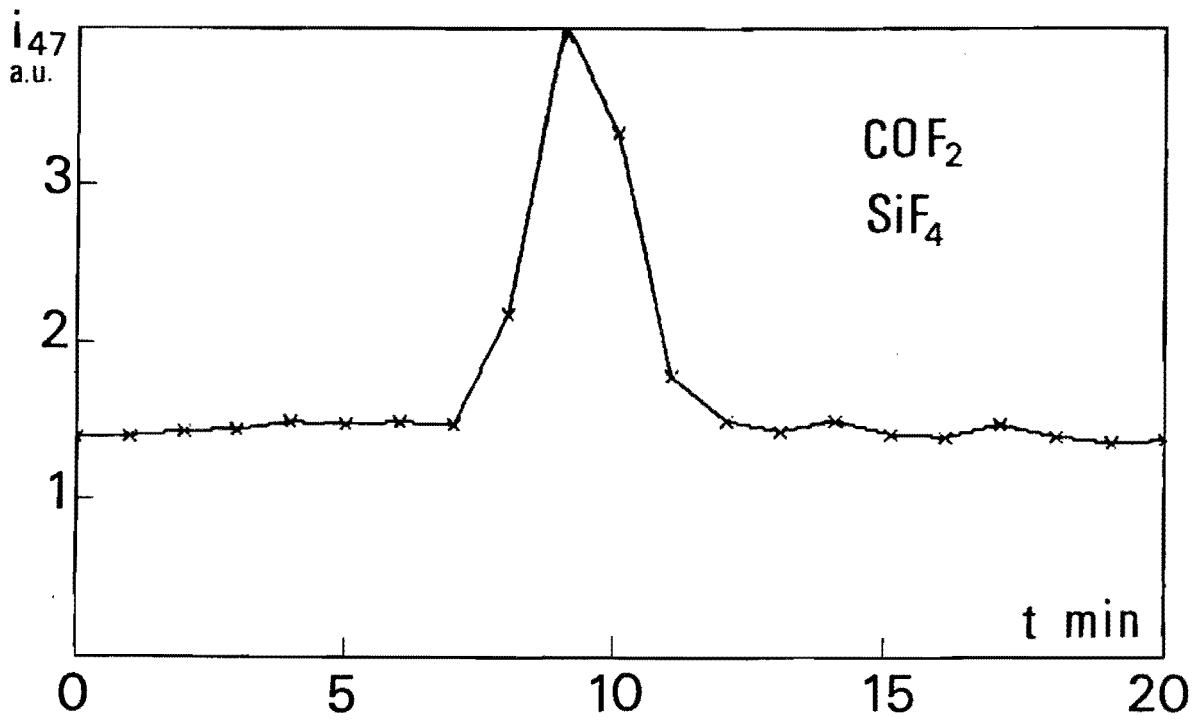


Fig. 6. Time evolution of peak 47 during plasma etching of a sandwich Si - SiO₂ - Si.

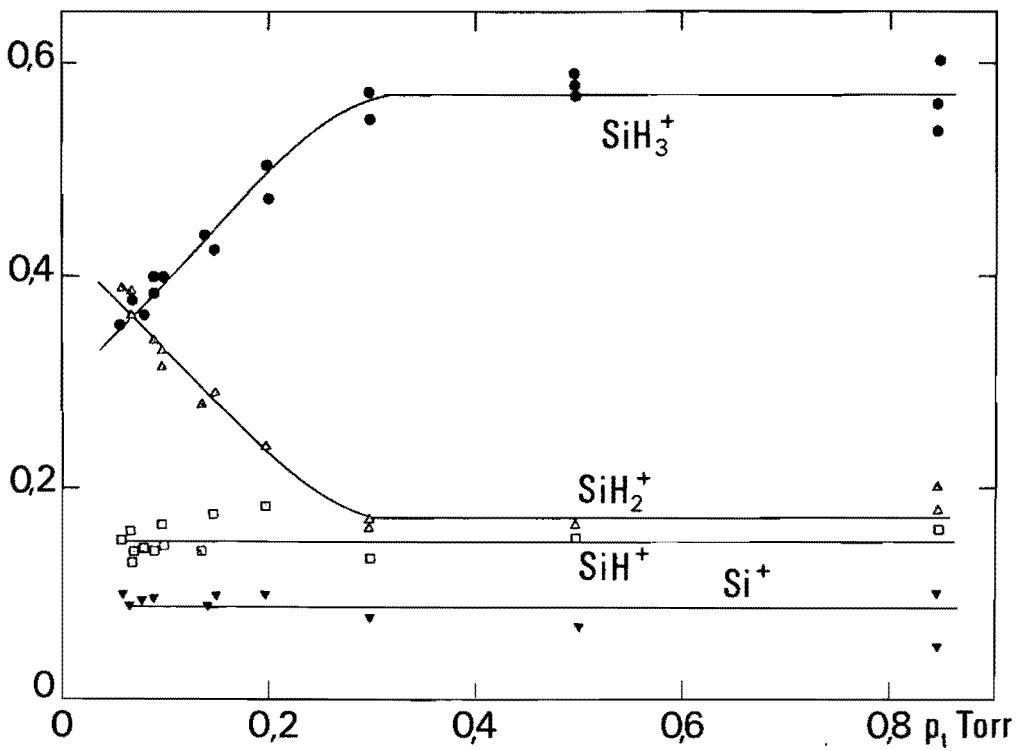


Fig. 7. Relative SiH_n^+ ion intensities in a SiH_4 -He discharge.

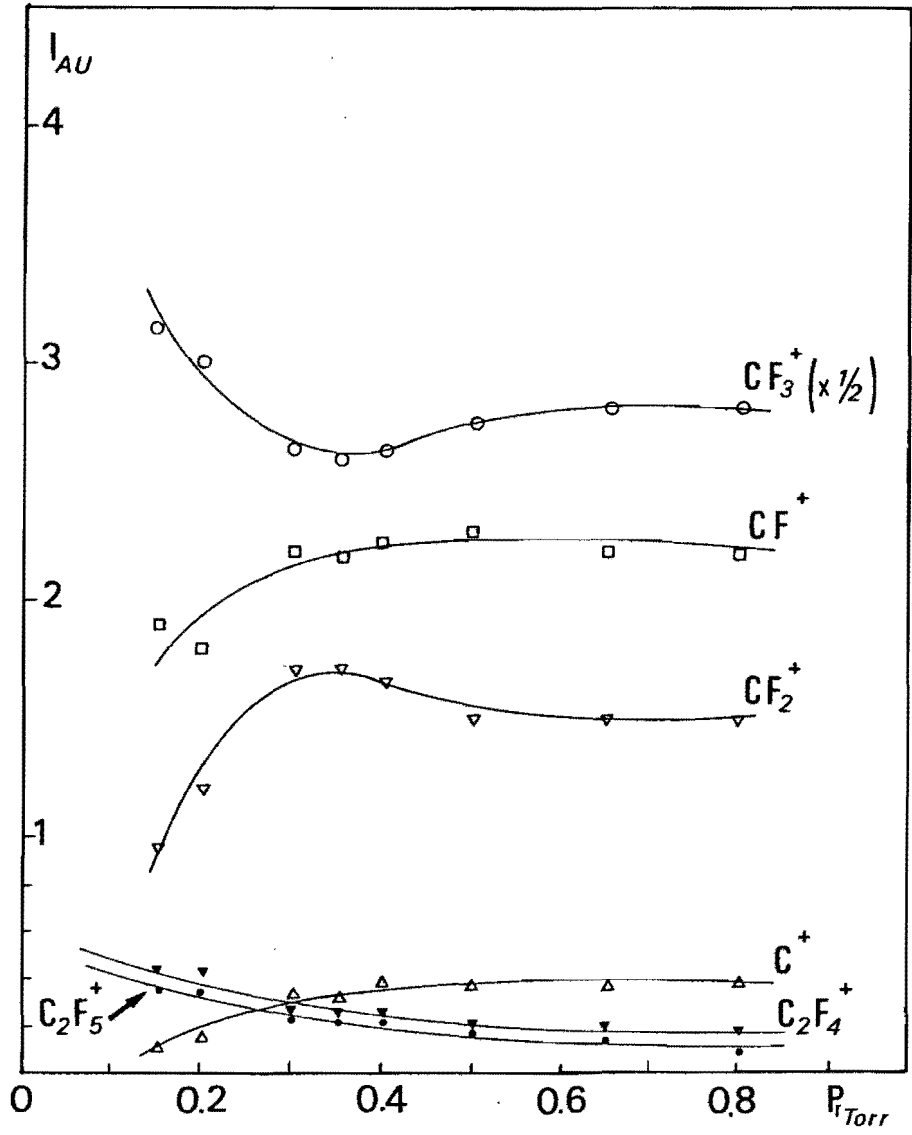


Fig. 8. Relative ionic intensities in the C_2F_6 plasma.

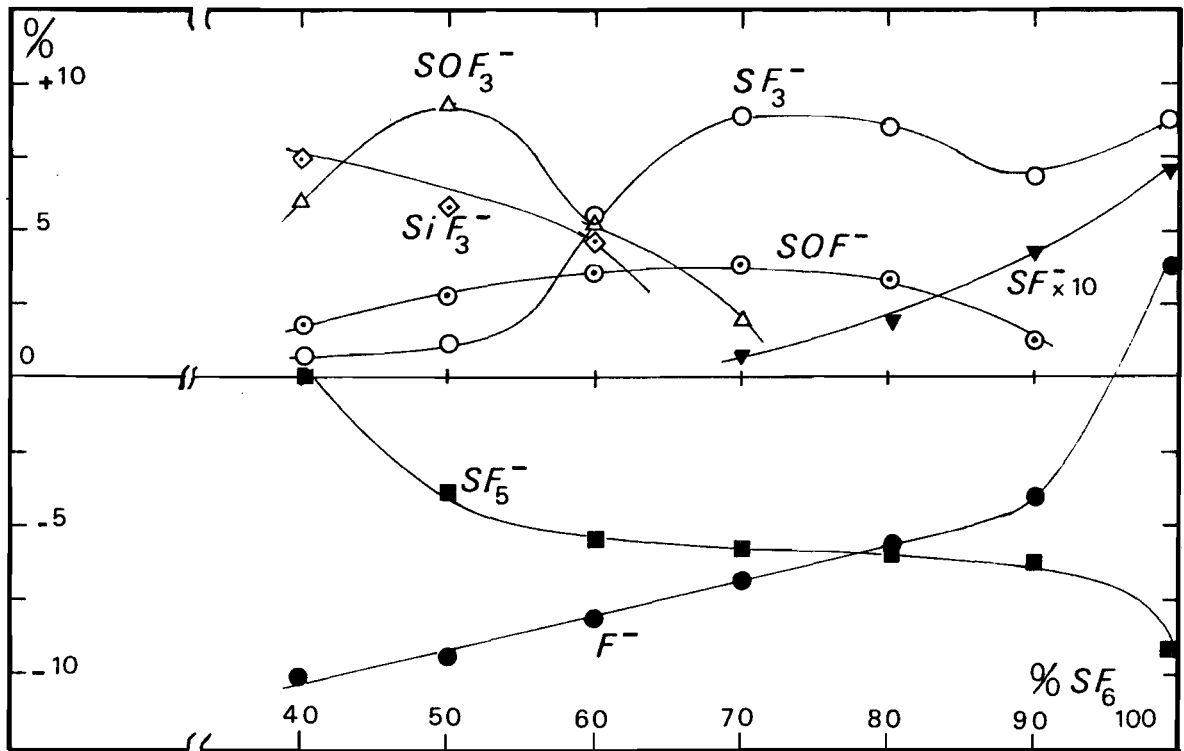


Fig. 9. Variations in the negative ion abundance in SF₆ - O₂ plasma between the presence and the absence of silicon.

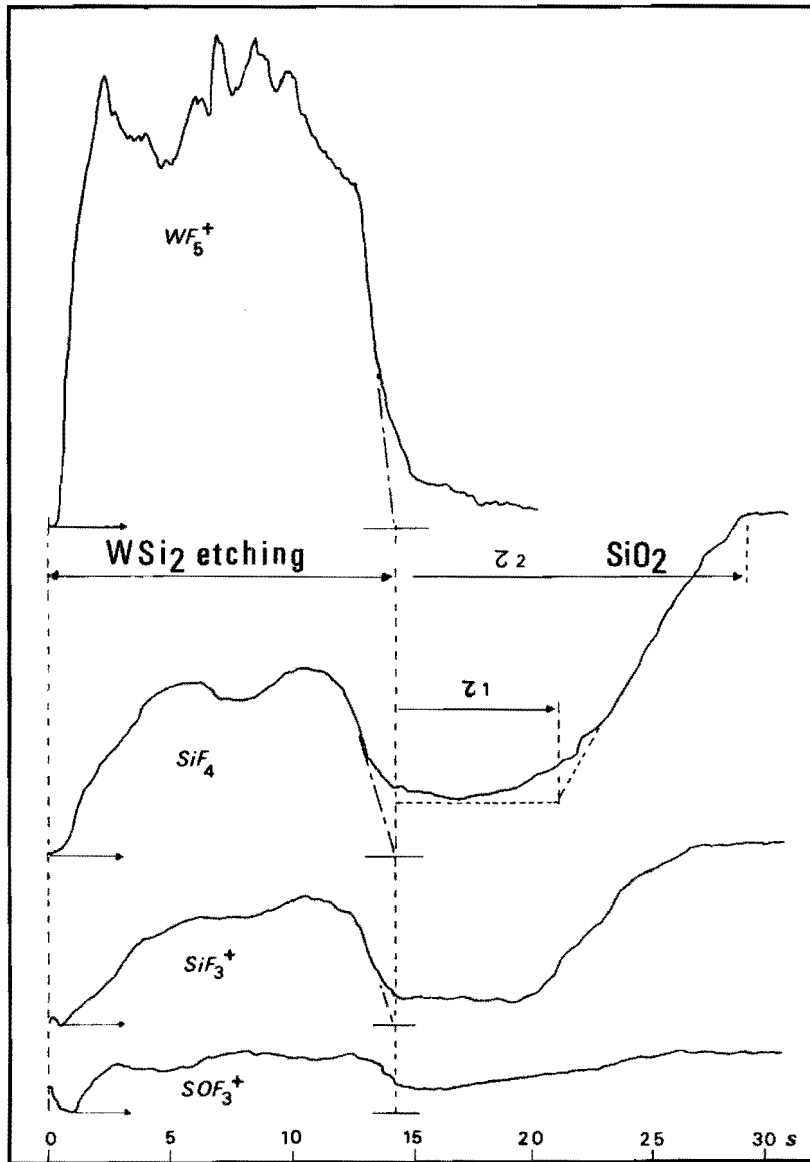


Fig. 10. Time dependence of WF_5^+ and SiF_3^+ during plasma etching of $\text{WSi}_2\text{-SiO}_2\text{-Si}$ in $\text{SF}_6\text{-O}_2$.

6.3. Optical Spectroscopy

J.P.M. Schmitt

This article was not submitted in time to the editor in a reproducible form and could therefore not be included in the proceedings.

7. SURVEY OF APPLICATIONS IN PLASMA ETCHING AND PLASMA DEPOSITION; PLASMA-SAFETY CONSIDERATIONS

Dr. G. Kenneth Herb is distinguished member of technical staff at AT & T Bell Laboratories, Allentown, Penn., USA. His expertise is in VLSI process technology, particularly plasma technology, metallization and reliability analysis for VLSI circuits.

This article was not submitted in time to the editor in a reproducible form and could therefore not be included in the proceedings.

8. SURFACE TREATMENTS AND PLASMA POLYMERIZATION

Dr. Jaques Amouroux, Professor at the Ecole Nationale Supérieure de Chimie de Paris - Université Pierre et Marie Curie, France and Director of the Plasma Chemical Reactor Laboratory (E.N.S.C.P.). His principal areas of research include thermal plasma and non equilibrium plasma for surface treatment, pilot plant and metallurgy like production of Photovoltaic Silicon.

SURFACE TREATMENTS AND PLASMA POLYMERIZATION

J. AMOUROUX Professeur,
 Dr A. GICQUEL, Dr. F. AREFI, Dr S. CAVVADIAS, Dr J.L. BRISSET

Plasma chemical reactor laboratory - ENSCP -
 Université Pierre et Marie Curie 11 rue Pierre et Marie Curie
 75231 Paris Cedex 05. Tel.: (1) 633 42 83 FRANCE

The main developments of the plasma surface interactions are largely correlated with the degree of freedom of the molecules in the boundary layer. In this way we propose to present the control of the non equilibrium level of a low pressure plasma with its consequences on the chemical reactivity. The second developed aspect deals with the excitation process of a complex molecule during its interactions with electrons. Taking into account this preliminary aspect we can analyse some chemical mechanisms occurring during surface treatments.

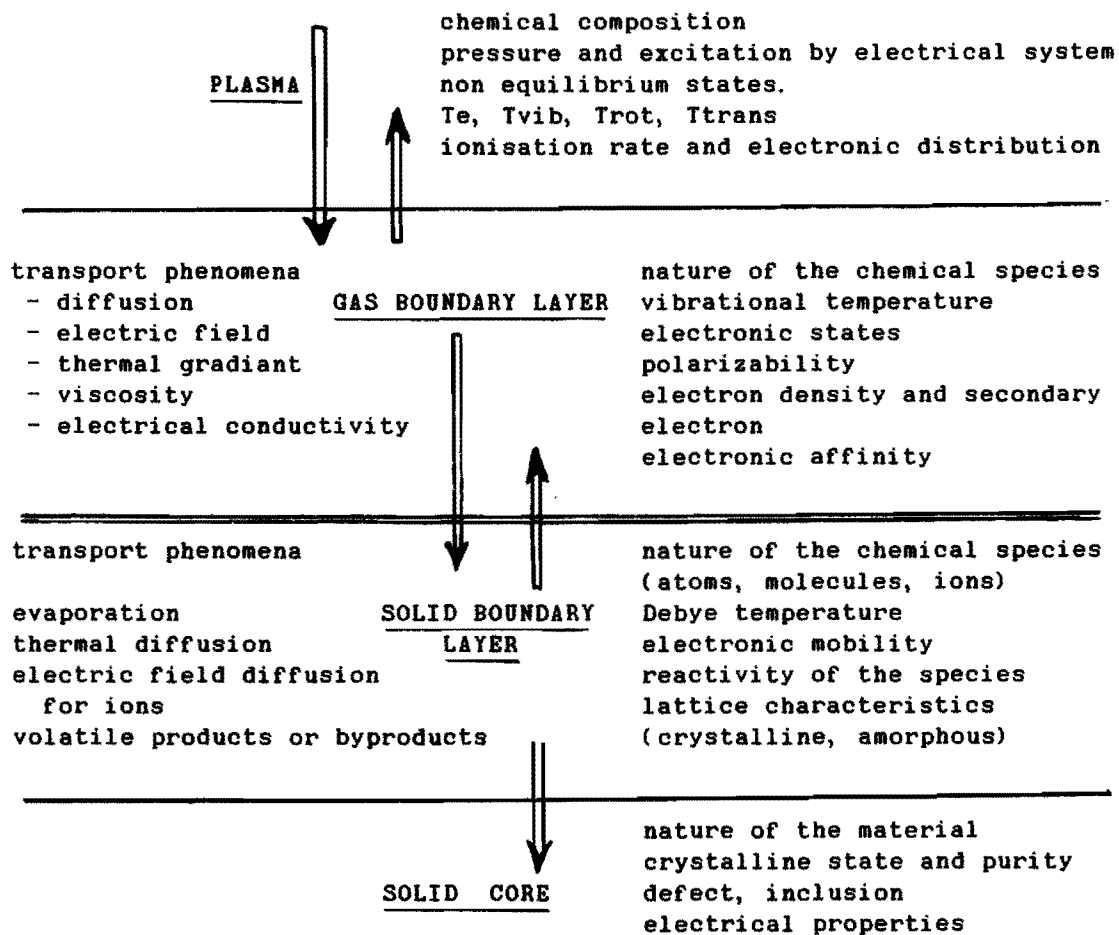
1. role of the vibrational excitation, application to the nitriding process
2. chemical properties of the excited molecules and radicals according to Lewis acid base properties, application to etching.
3. role of the nature of the substrat during a surface treatment; comparison between polymer, glass, silicon during a treatment by a fluorocarbon plasma.
4. role of oxygen in a fluorocarbon plasma; competitive mechanisms

1. GENERALITIES

Looking over the recent industrial applications (fig.1) we observe the large developpments of plasma techniques using a great number of electrical excitation sources such as RF, Microwave, Corona, Laser, Glow discharge... For the industrial applications the reproductibility, the control and the efficiency imply large fundamental studies and new diagnostic methods. In that way in situ diagnostic methods of the boundary layers (gas and solid) are today developed in order to provide a better understanding of the main chemical zone of the plasma reactor. Boundary layers depend on the gas mixtures, on the material, and on the electrical characteristics of the plasma source. We have summarized (fig.2) the main phenomena in these layers which indicate the role of excitation mechanisms in the vicinity of the surface material (16).

SURFACE TREATMENT APPLICATIONS (fig.1)

Properties needed	treated materials	Main mechanisms of the treatment	industries
wettability, adhesive surface roughness, cleaning	polymer paper metal glass carbon fiber	polar groups in the matrix on the surface trapped radicals in the matrix P	packing industry textil and paper photoghraphic sound and video automobile/aero- nautic medical membrane and material tyre industry sticking
dielectric properties	polymer glass silicon	trapped radicals in the matrix metal inclu- ded or deposited trans- fer of electrical charges grafting and reticulation organometallic function	microelectronic semiconductor piezoelectric material insulation and electric indus- tries photovoltaic industries
waterproof encapsulation anticorrosion	polymer metal silicon	grafting of fluorocarbon groups polymerization fluorocarbon inclusions	textil industry electronic, paper, storage of energy
hardness friction coefficient	metal material silicon	nitriding, carburation carbon layer such as diamond, ceramic depo- sition	metallurgical treatment mecanical indus- tries jewelry industries electronic
optical properties optoelectronic	metal glass quartz fiber silicon	antireflecting layer of organometallic PCVD of controlled refractive index, transparent electrodes, semiconductor deposition (Si ₃ N ₄ , SiGe, III V...)	photovoltaic industries electronic industries doping optical fiber industries textil industry
thermal properties	metal glass silicon	nitride ceramic (Si ₃ N ₄ , TiN) oxyde SiO ₂ TiO ₂ , SnO ₂ carbide SiC, WC,	metallurgical and mecanical industry textil fiber medical appli- cation, jewelry nuclear
electronic properties	silicon, III V polymer, glass	PCVD, diffusion phenomena of B, As, P. amorphous layers compositions Pinhole and defects etching from fluoro- carbon plasma	photovoltaic industries electronic industries new detectors
specific absorption	polymer or silicon	modifications of surface grafting and support adsorption	support for analysis by gas chromatography and HPLC

Fig. (2): Plasma surface interaction

2. NON EQUILIBRIUM PLASMA SYSTEM AND CORRELATION WITH THE MOLECULAR EXCITATION

It is usual to distinguish between electron and heavy particles in order to characterize the energy transfer from the electrical power to the gas. In this manner two distinct temperatures T_g and T_e may exist. The difference between these two temperatures can be derived from an energy balance (1):

$$\frac{T_e - T_g}{T_e} = \frac{\pi m_g (\lambda_e e E)^2}{24 m_e (K T_e)^2}$$

where m_g is the mass of heavy particles

λ_e is the mean free path length of the electrons

E electric field strength

$\pi m_g / 24 m_e$ mass ratio between heavy particles and electrons

$\lambda_e e E$ amount of electron energy along one mean free path length

$K T_e$ average thermal energy of the electrons

Figure 3 shows in a semischematic diagram how the electron and the gas temperatures separate from another (case of an electrical arc) when decreasing the pressure.

However the energy of the electrons depends on different parameters such as diameter of the reactor, pressure, and on the gas mixture. Von Engel

(1) propose a semiempiric equation to determine the order of magnitude of the electronic temperature:

$$\left[\frac{eV_i}{KTe} \right]^{-1/2} \times e \left[\frac{eV_i}{KTe} \right] = 1.16 \times 10^7 [CPr]^2$$

e electron charge (coulomb) V_i ionization potential Ar = 13.12 volts
 T_e electron temperature (K) Ne = 15.6 volts
r radius of the discharge reactor (cm) C: gas Cte He 4.10^{-3} H2 10^{-2}
P pressure (mm Hg) Ne 6.10^{-3}
K Boltzmann Cte A 4.10^{-2}

examples for nitrogen

P torrs	C	r	CPr	T_e	EeV
20	4.10^{-2}	5	4	18.000 K	2.3
5	4.10^{-2}	1.25	0.25	28.000 K	3.6

From these results, it can be noticed that the average energy of the electrons can be modified by changing the working parameters such as pressure or the radius of the reactor.

At last a modification of the gaseous mixture, in particular by introduction of electrophile atoms or molecules such as fluorocarbon gases decreases the energy distribution.

The maxwell or Druyvestein distribution of the energy of the electron

$$f(\epsilon) = C \epsilon^{1/2} \text{EXP} \left(-0.55 \left(\frac{\epsilon^2}{\bar{\epsilon}} \right) \right)$$

where ϵ energy of the electrons

$\bar{\epsilon}$ average energy

$f(\epsilon)$ function distribution of the electrons

provides the population of the electrons with a given energy. The intersection of the energy distribution function and of the excitation cross section for a molecule gives us the population of an excited state. (fig.6).

However the energy transfer by electronic collision in a nitrogen discharge (fig.7) provoking electronic excitation of the molecule only begins for an average energy of the electron superior than 1 ev.

Taking now into account the potential diagram for N2 (fig.8), the cross section of these species (fig.9) and the electronic average energy we can determine the main excitation states in the discharges. These states (vibrational and electronics) are responsible of the energy transfer and the new chemical reactivity. (5).

By this method we are now allowed to indicate, for a complex molecule the evolution of its chemical properties:

- new electronic states
- increase of electronic density on antibonding orbital \rightarrow weak chemical bonds and increase of reactivity
- orbitals reactivity
- triplet states i.e. radical productions
- vacancy orbitals and free pair of electrons (Lewis acid-base properties)
- ions formation
- negative ions (reduction properties)
- positive ions (oxydation properties)
- modification of the molecular shape
- modification of the symmetry, bond angle, hybridation, loss of atom and radical formation
- vibrational excitation

That is to say that the chemical properties of the plasma phase depend

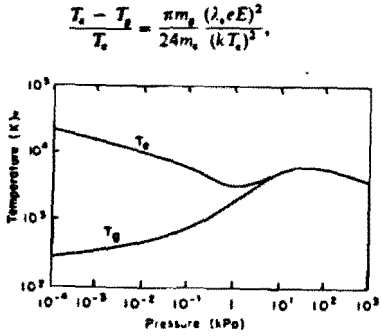


Fig3: Electron and heavy particle temperatures as a function of pressure.

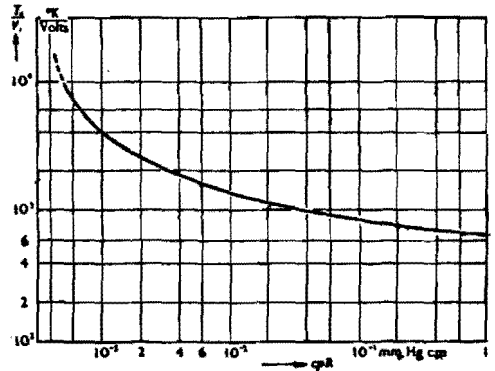


Fig4: Electronic temperature in function of the working parameters. (After (1))

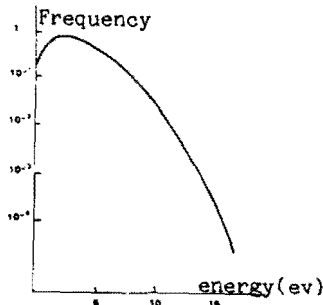


Fig5: Free electron energy distribution with electronic temperature of 28000 K.

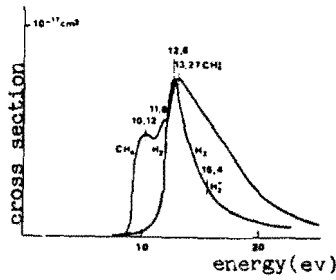


Fig6: Excitation cross section as a function of the electron energy.

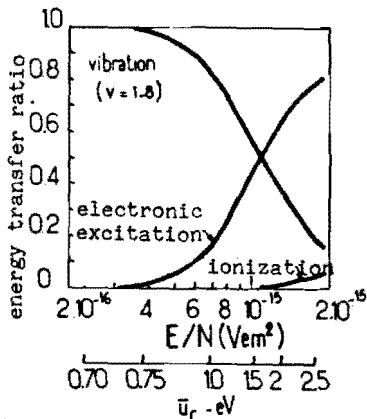


Fig 7: Energy transfer to the molecules by electronic collisions in an N₂ discharge (After (2)).

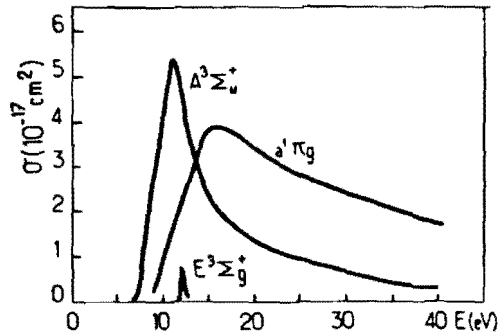


Fig9: Excitation cross section of the N₂ metastables from the fundamental (3).

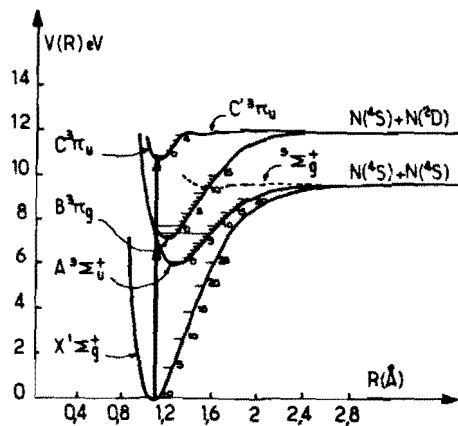


Fig8: Potential energy curves and vibrational levels after Gilmore (4)

mainly on the pressure and on the chemical composition of the gas feeding the plasma reactor and electrical parameters.

However, the boundary layer produces large modifications of these properties due to the heat and mass transfer between the gas layer and the target. Consequently the understanding of the plasma gas properties is no more sufficient to characterize the boundary layer. For example the viscosity phenomena modified the mass transfer through the boundary layer; but these properties

$$\eta = \frac{m \bar{c}}{3\pi d^2 \sqrt{2}}$$

\bar{c} average quadratic speed
 d particule diameter
 m mass

depend essentially on the average quadratic speed, i. e. on the molecular mobility of the specie due to the polarizability by the electric field strength, which is specific near the solid surface.

At last we have to take into account the modification of the reactivity due to the target effect, its electronic excitation by plasma impact, produced electronic diffusion, sputtering by ion bombardement, evaporation phenomena of atom or volatile species. In other words the direct study by emission spectroscopy of this layer and of the surface of the target allows the control of the surface treatment.

3. MODIFICATIONS OF PLASMA REACTIVITY BY VIBRATIONAL EXCITATION

A large part of the plasma energy is stored on the vibrational level of molecules and radicals. The chemical reactivity of vibrational energy had been studied by Polanyi (4,5) for a non equilibrium system, e. g. in the following endothermic reaction $H + HF \longrightarrow H_2 + F$ $\Delta H = 1.37$ eV (fig. 2) the evolution of the reaction rate depends on the energy distribution between the vibrational, rotational and the translational levels. So, for the same energy content in the chemical system, we can increase the reaction rate by a factor of 10000 with a specific vibrational excitation. In the general case given below:



Polanyi presents an interpretation in function of the enthalpy of the reaction. On the next diagram (fig. 11) we can notice that the exothermic systems are controlled by the energy barrier in the entrance valley which is crossed over by the translational energy of BC molecule, while the endothermic system are controlled by an energy barrier in the exit valley i. e. by the vibrational energy of the chemical specie BC.

These results point out that the reaction rate coefficient will be written as:

$$k = \int_{0}^{\infty} V_r \sigma (V, J, V' J', E_r) f (V_r T) dV_r$$

where $f(V_r)$ is the fraction of the collisions in which V_r lies between V_r and $V_r + dV_r$. E_r is the relative kinetic energy and the transformation depends on the vibrational and rotational energies of the reagents molecules.

4. DYNAMIC OF THE SURFACE REACTION MECHANISMS

The three main steps of a surface reaction are adsorption, chemical reaction, and recombination-desorption. Nevertheless the surface reaction can be controlled by a Langmuir Hinshelwood or a Rideal mechanism. In both cases the adsorption mechanism depends on the nature of the excited molecules of the plasma and on the excited atoms of the lattice.

Volken had calculated and demonstrated that for heterogeneous catalysis

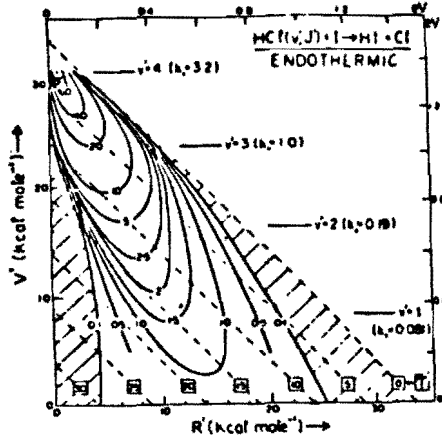


Fig 10: Role of vibrational energy on the rate constant for endothermic reactions.

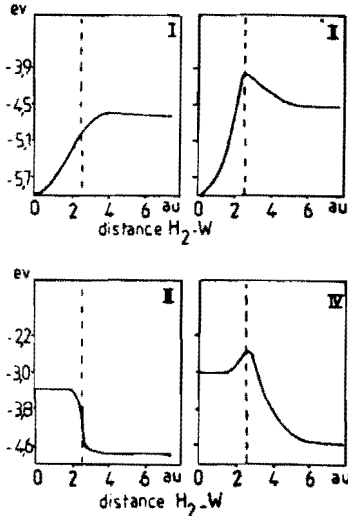


Fig 12: Energy profiles of recombination reactions along the reaction paths for different potential surface after Wolken (9). I, II repulsive surfaces; III, IV attractive surfaces.

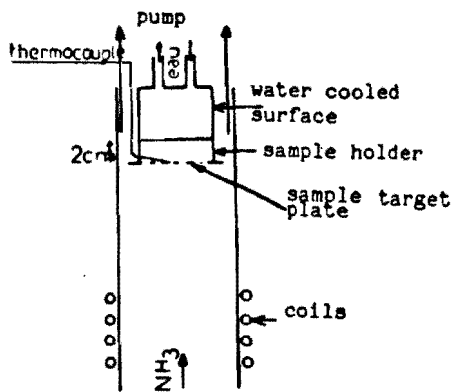


Fig 16: Reactor scheme

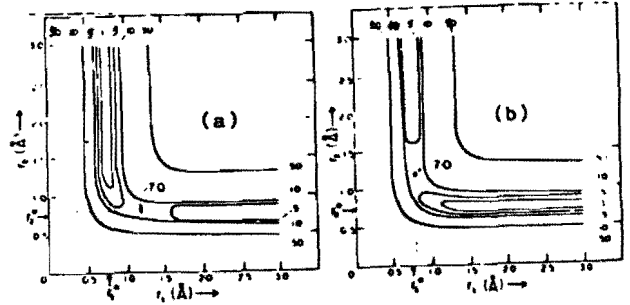


Fig 11: Position of the activation barrier according to the exothermic (a) or endothermic (b) character of the reaction.

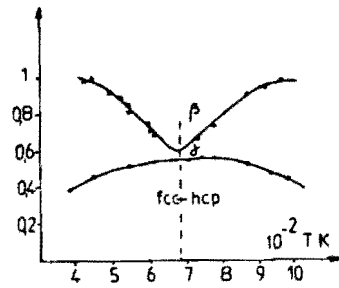


Fig 14: Temperature dependence of the chemical energy accommodation coefficient and atom recombination probability for the N atom/Co syst. (10)

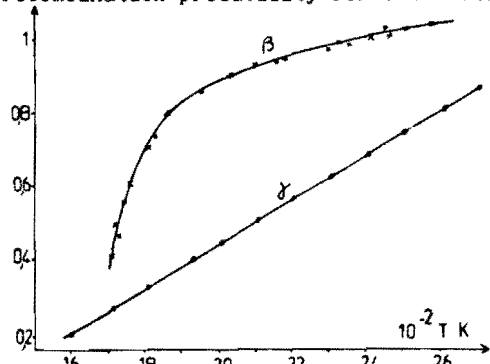


Fig 13: Temperature dependence of β and γ for the N atom/tungsten system after Halpern and Rosner (10).

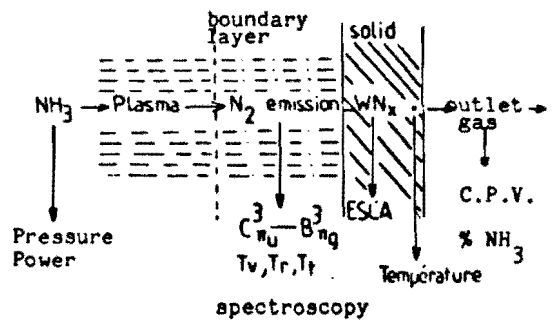


Fig 15: Technics of characterisation of the plasma and of the treated solid surface.

both of the steps: adsorption and recombination-desorption must be exothermic. Therefore the desorbed molecules are vibrationally excited (fig. 12)(6).

Moreover the energy transfer between the gas boundary layer and the solid during the recombination-desorption step was demonstrated by Halpern and Rosner (10) to be shared between the gas and the solid. The energetic fraction taken by the metal is $\beta \cdot \gamma$, where β is defined such as $\beta = Q / \Delta n(D/2)$ and γ is the recombination probability of the N atoms sorbed at the surface. They have demonstrated that the $\beta \cdot \gamma$ product depends on the nature of the metal. (fig: 13, 14).

Generally, during a chemical nitrogen surface treatment, β increases with the temperature, by contrast it decreases in the absence of surface reactivity.

5. ROLE OF THE VIBRATIONAL EXCITATION DURING THE NITRIDING SURFACE

TREATMENT BY NH₃: Role of the boundary layer

The study of the nitriding of metallic targets is developed in a plug flow reactor with energy powered by a radiofrequency source (40 MHz). The plasma process is created between the coil and the metallic sheet fixed (perpendicular to the flow) by a rod. The dynamic plasma flow of NH₃ at low pressure (5-20 torrs) is observed by emission spectroscopy while the metal surface is analysed by ESCA and Vickers microhardness. (fig. 15, 16) (12, 13, 14).

5.1. EXCITATION LEVEL OF N₂ MOLECULE IN A NH₃ PLASMA Role of the target

During the pyrolysis of the NH₃ molecules we obtain the formation of N₂ by an endothermic reaction $2\text{NH}_3 \rightleftharpoons \text{N}_2 + 3\text{H}_2$ $\Delta H = 1\text{eV}$. The spectroscopic observations of N₂ through the radiative transition $C^3 \pi u \rightarrow B^3 \pi g$ ($\lambda = 3804 \text{ \AA}$) permit to characterize the vibrational and rotational level of the system, in agreement with Ricard's calculations (15).

However the measure of the vibrational state and the rotational state demonstrate, similarly to the theoretical study of the second part, the deviation between the vibrational temperature and the rotational temperature (fig. 17). However the characterization of the plasma-metal boundary layer demonstrates an increase of the vibrational excitation from 3400 K to 4200 K with transition metals while a Si target (100) decreases the vibrational temperature from 3400 K to 2900 K (fig. 18, 19).

Finally the energy exchange in the boundary layer and the electronic excitation level are correlated with the nature of the substrat.

5.2. HEAT TRANSFER TO THE TARGET (fig. 20)

The measurements of the temperature of the target by a thermocouple confirm the difference of heat transfer to the silicon and to the transition metals. Under the NH₃ plasma impact at 5 mbars, the silicon reaches a temperature 200°C higher than tungsten.

5.3. REACTION RATE OF NH₃ DECOMPOSITION (fig. 21)

The NH₃ decomposition rate in the plug flow reactor is measured by a gas chromatography analysis of the outlet gas. The data are in agreement with the theoretical studies of the reactivity in function of the vibrational level (Polanyi and Wolken theories). In fine a large vibrational excitation of the molecules near the target leads to an increase of the pyrolysis while a decrease of the vibrational level inhibits the chemical decomposition.

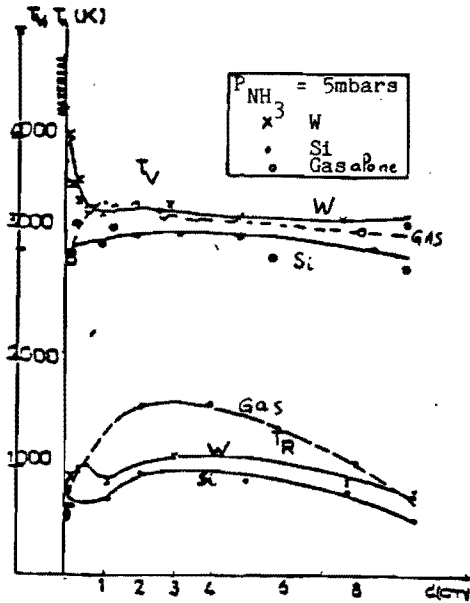


Fig17: Vibrational and rotational temperatures in an NH_3 plasma. Influence of various metals on these temperatures.

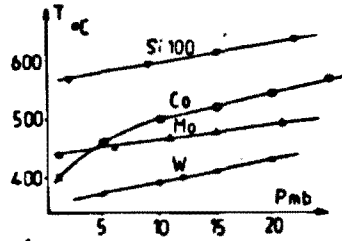


Fig20: Solid temperature versus pressure according to the nature of the metals.

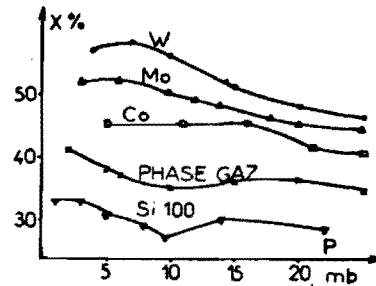


Fig21: NH_3 decomposition rate as a function of pressure in gas phase and heterogeneous phase. ($PI = 1 \text{ KW}$, $D^0 = 0,6 \text{ l/min}$)

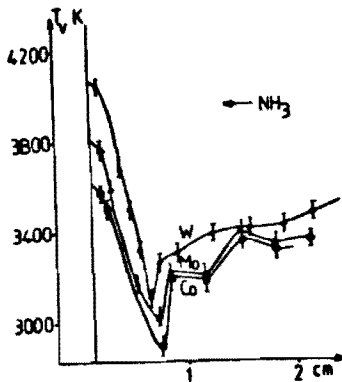


Fig18: Vibrational temperature according to the nature of the transition metal.

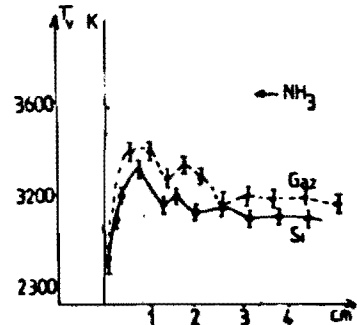


Fig19: Vibrational temperature in presence of silicon.

	standard samples			treated W samples $P = 5 \text{ mbars}$, $P I = 1 \text{ KW}$, $D^0 = 0,3 \text{ l/min}$, $D_{arriv} = 1 \text{ MN}$			
	W	WN	W_2N	NH_3	$N_2 - H_2$ 80% - 20%	$N_2 - H_2$ 50% - 50%	N_2
$W_{4DS/2}$	242,6 eV	244,5 eV	247,5 eV	244,3 eV 247,8 eV	247,8 eV	247,3 eV	246,7 eV
N_{1a}	—	397 eV	397 eV	396,7 eV	396,2 eV	396,5 eV	396,6 eV
% W	100 %	—	—	—	—	—	10 %
% WN	—	100 %	—	80 %	—	—	—
% W_2N	—	—	100 %	20 %	100 %	100 %	90 %
$N_{1a} / W_{4DS/2}$ (N fixation rate)				2,3	1,0	0,8	0,3

Fig 22: ESCA results .Identification of the new bonds created on tungsten by various plasmas.

5.4. SURFACE MODIFICATIONS (ESCA ANALYSIS AND VICKERS MICRONARDNESS)

The surface nitriding of the target depends on the chemical reactivity of the plasma species in the boundary layer i.e. on the species NH_3 , NH , and N_2 . Therefore an increase of the vibrational level of the gas boundary layer produces an increase of the N/metal ratio i.e. the nitrogen fixed onto the target. The ESCA analysis indicates the nature of the chemical bond between nitrogen and the metal, the relative concentration of nitride and its evolution in function of the residence time (fig. 22). These results are in agreement with the Vickers microhardness and demonstrate that the mechanisms of nitriding are controlled by the diffusion phenomena in the metal. (fig. 23).

5.5. ROLE OF NH SPECIES AND SURFACE NITRIDING PREDICTION

The decomposition of NH_3 involves radicals and atoms formation such as NH species (6,11). The measurements by the spectroscopy emission of the transition $\text{NH} (A^3\Pi \rightarrow X^3\Sigma)$ (fig. 24) ($\lambda = 3360 \text{ \AA}$) allow to demonstrate the role of the boundary layer and the adsorption phenomena during the pyrolysis of the NH_3 molecule.

Nevertheless these results demonstrate that an increase of the vibrational excitation of NH or N_2 is correlated with an increase of nitrogen chemisorption and consequently with an increase of nitriding of the target. Therefore we have demonstrated that the reactivity of the plasma in the boundary layer with respect to the surface can be controlled by the vibrational excitation of the species such as NH or N_2 . The chemisorption mechanisms are the key step of the surface treatment, i.e. that the sticking probability depends on the vibrational state. According to Wolken theories, the dynamics adsorption proceed through an attractive surface potential with an energy barrier controlled by the vibrational energy of the species such as NH , NH_3 or N_2 . Any modification of the chemical composition, of the pressure, and of the nature of the target provokes a modification of the nature of the excited species in the boundary layer and their vibrational energy. Consequently the nitriding process is controlled by all these parameters.

5.6. ROLE OF THE IMPURITIES OF THE LATTICE OF THE TARGET (fig. 25)

A plasma treatment of a pure and a doped silicon target allows to compare the role of the impurities included inside the lattice. The ESCA analysis of the untreated doped silicon indicates the presence of chemical bonds such as Si-B, B-O, B-H, metallic B. By treating these two materials (Si and Si doped) by different plasma gases (N_2 , N_2H_2 , NH_3 and H_2) the specific reactivity of the excited species with the lattice is illustrated by figure 25. For instance the nitrogen plasma transforms specifically the Boron metal atoms incorporated in the lattice, in B-N compounds while NH_3 plasma produces B-N and B-Si-H compounds. At last an H_2 plasma treatment increases the B-Si-H and the photovoltaic efficiency of the material by an elimination of the electronic defects.

In conclusion of this first part, the characterization of the boundary layers (plasma gas and material) allows us to control the process. Nevertheless, for this aim, high resolution emission spectroscopy, ESCA analysis of the treated surface and of the raw material, and a good knowledge of the chemical reactions between the gaseous excited species and the target are necessary.

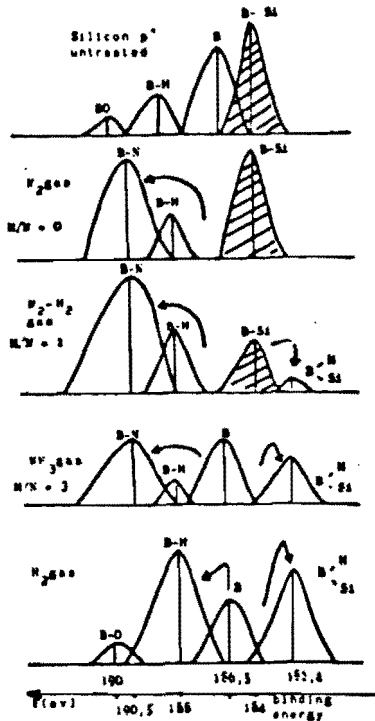


Fig 25 :Modification of the silicon surface according to the nature of the plasma.

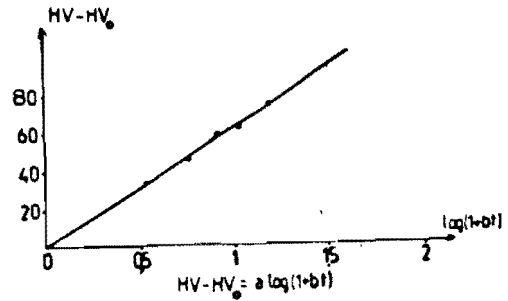


Fig23 :Law of microhardness variation into the metal after treatment.

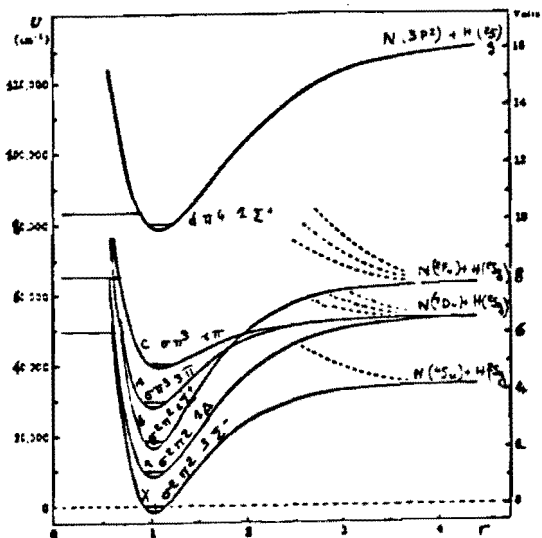


Fig24:NH potential energy curves.

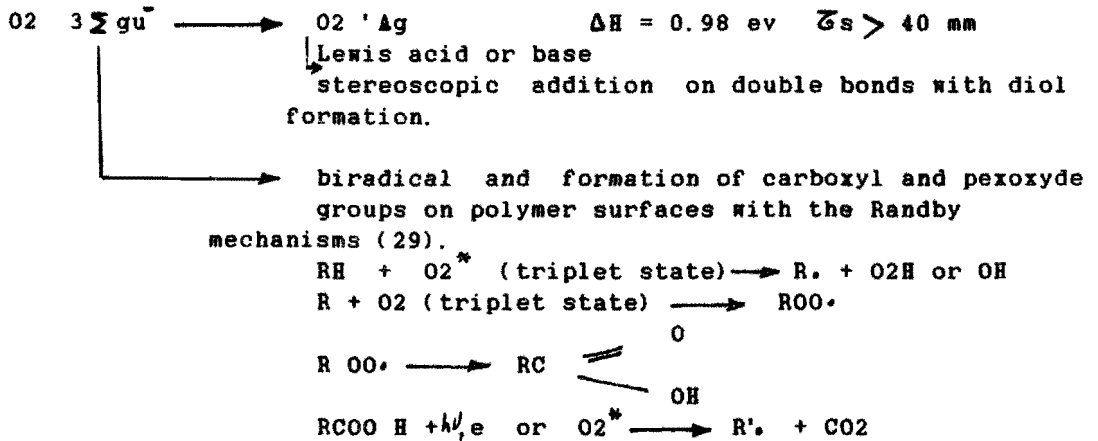
Excited States	Excitation threshold from $NH(X^3\Sigma^-)$	Excitation threshold from NH_3
$NH(a^1\Delta)$	1 ev	$\rightarrow NH(a^1\Delta) + H_2(\frac{1}{2}\Sigma_g^+)$ 5.5 ev
$NH(b^1\Sigma^+)$	2.1 ev	
$NH(A^3\Pi_1)$	3.8 ev	$\rightarrow NH(A^3\Pi) + 2 H(1s)$ 12.1 ev
$NH(C^1\Pi)$	5 ev	$\rightarrow NH(C^1\Pi) + H_2(\frac{1}{2}\Sigma_g^+)$ 9.2 ev
$NH(d^1\Sigma^+)$	9.8 ev	$\rightarrow NH(d^1\Sigma^+) + H_2(\frac{1}{2}\Sigma_g^+)$ 14.1 ev

Fig24 bis:Excitation threshold of NH (17)

6. CHEMICAL REACTIVITY OF RADICALS AND IONS. Applications to polymerization and etching

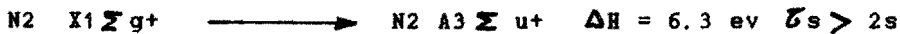
During the electronic excitation we observe large modification of the molecular orbitals with odd electrons, vacancy orbitals, thus the chemical properties and the polarizability of the molecules or radicals depend on these new electronic states. For further clarifications we can choose some examples:

6.1. TRANSITION BETWEEN TRIPLET STATE TO SINGLET STATE OF O₂ MOLECULE



These mechanisms are largely employed for the corona treatment of polymer surfaces such as PET or PE films or fibers to explain the wettability increase (fig. 26, 27, 28) (34).

6.2. TRANSITION BETWEEN SINGLET TO TRIPLET STATE (biradical production) (application to nitriding of titanium)

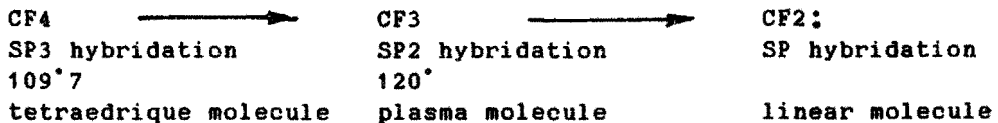


The odd electrons of the antibonding orbital are responsible for the high reactivity of N₂ biradical chemisorption and nitride formation.

6.3. MOLECULAR SHAPE AND HYBRID ORBITAL (30)

Application to etching or polymerization

The molecular orbital implies the molecular shape, thus an electron or atom loss leads to a modification of bond angle i.e. a modification of the shape and the reactivity.



an increase of the reactivity from CF₄ to CF₂ results from the modification of the electronic density, the shape of the molecule and its Lewis acid/base properties.

6.4. POLARIZABILITY

The electrical field strength in the boundary layer induces dipole dipole formation, and large modifications of the electronic density i.e. polarizability of the heavy molecules. The surface reactivity increases with the polar molecules, specially in the case of the transition metals with d orbital properties (Lewis acids).

Large applications such as surface polymerization, encapsulation, and



nonpretreated PE fiber



x 2000

Fig 26: SEM micrographs of a nonpretreated PE fiber and a corona discharge pretreated one ($I = -150 \mu A$, $d = 8mm$, $t = 1h$)

$\phi = 0,25 \text{ mm}$

Atm. : air

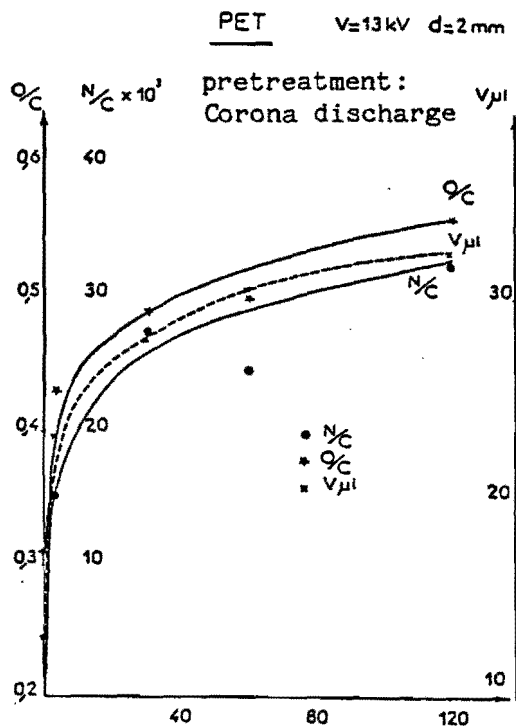


Fig 28: Variations of the ratios O/C, N/C and the volume of the drop in function of the pretreatment time.

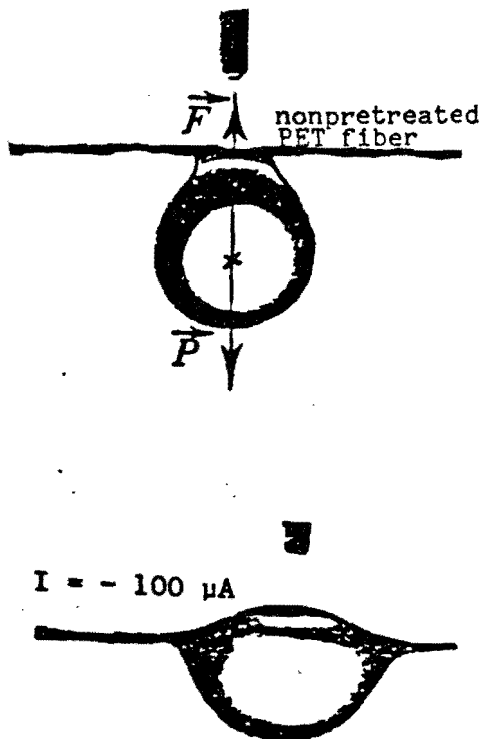


Fig 27: Determination of the wettability of a PET yarn ($\phi = 0.25mm$) by measuring the volume of a drop of water (pretreatment: corona discharge, $t = 5mn$, $d = 2mm$)

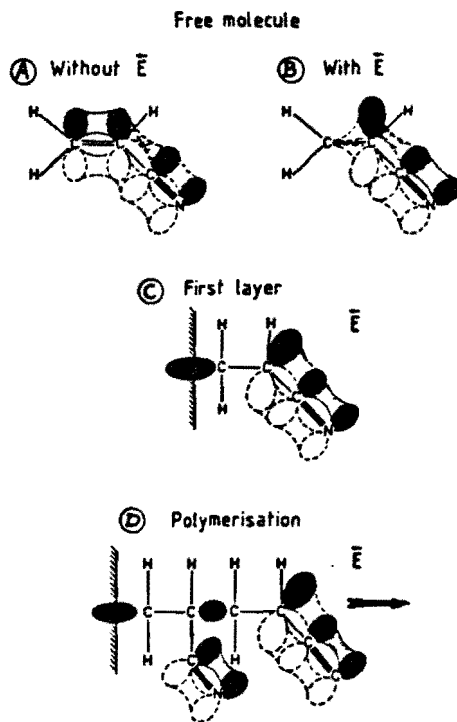
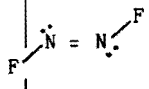

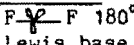

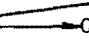
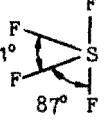


Fig 29: Mechanisms of acrylonitrile molecule grafting on a cathode surface.

Fig. 31 Radicals - shapes and properties

Tetraedrique shape		Planar molecule		Planar molecule
Bond angle 109°		bond angle 120°		Bond angle 120°/180°
Hybridation SP3		hybridation SP2		hybridation SP2/SP
molecule	negative ions or molecule Lewis base	positive ions Lewis acid	radical	biradical or Lewis acid
CH4 109°	CH3-	CH3+	.CH3	:CH2 (carbene) fond state singlet excited state singlet 1Σ triplet 3
CF4 109°	CF3-	CF3+	.CF3	:CF2 singlet state 105° Lewis acid triplet state 150° biradical time life 1 s at P205
CCl4	CCl3-	CCl3+	.CCl3	.CCl2
CHF3				:CF2 + HF
CHCl3				:CF2+ + HF-
CBrF3	CF3-	CF3+	.CF3	:CCl2 + HCl :CF2
SiF4 weak Lewis acid	SiF3-	SiF3+	.SiF3	:SiF2 lifetime 150 s
SiH4	SiH3-	SiH3+	.SiH3	:SiH2
NF3 102°	NF2- 		.NF2	.NF
NH3	NH2- strong Lewis base (110°)		odd electron in π orbital Lewis base	:NH biradical π fond state triplet state XΣ - excited state singlet state Lewis acid Δ, Σ, +
ClF3	 etching rate 5000Å/mn		.ClF2 (F--F) SP Lewis base	BF3 120° Lewis acid
BrF3	Lewis base etching rate 50.000 Å/mn			
complex molecules				
XeF2	 F--F 180° Lewis base etching rate 45 000Å/mn			
IF5	 Lewis base			
SF6	 O2		 SF4 101° Lewis base	
			SOF2	

6.6. POLYMERIZATION PROCESS (26, 27, 28)

Large applications of plasma polymerization are controlled by different activations mechanisms such as ionic, radical or photonic activation. However in a plasma reactor the mechanisms which occur are much more complex due to the composition with other phenomena such as excitation of some of radicals trapped in the lattice, diffusion of ionic species, etching of oligomers, inclusion of metallic species of the support in the final product, or at last reactivity between gas monomer and contamination molecules such as oxygen in the plasma reactor.

6.6.1. GENERAL MECHANISMS OF PLASMA POLYMERIZATION (26)

The study of different teams working on plasma polymerization is summarized in the next figure which explains the reason of the complexity of the chemical plasma polymerization and the crosslinking phenomena (fig. 32).

The kinetic simulation of these reactions explains the evolution of the polymerization rate in function of the kinetic constantes such as etching, decomposition or deposition steps (fig. 33).

From these interpretation we can try to measure the role of different parameters during a surface treatment and the role of the substrate.

1. Interaction between the substrate and the radicals without any oxygen contamination
 - non volatile species production = grafting
 - volatile species formation = etching or evaporation by pyrolysis
2. no interaction between the substrate and the radicals without oxygen contamination
 - plasma deposition phenomena
 - plasma polymerization
3. Interaction between the radicals and the molecules of the substrate
 - diffusion or doping
4. Interaction between the substrate and the radicals with oxygen contamination
 - competition between ashing, or oxydation mechanisms and polymerization phenomena, formation of organometallic layers with metallic oxydes such as semiconductor organic layer of SnO₂C_x or TiO₂C_x...
5. Interaction between the lattice of the substrate and the radicals
 - diffusion or doping
 - etching and chemical deposition with metal inclusion in the form of clusters inside the polymer deposited.

6.6.2. FLUOROCARBON POLYMERIZATION ON DIFFERENT TARGETS WITHOUT OXYGEN CONTAMINATION (31, 32)

Fluorocarbon polymerization of monomer (e.g. C₂ H₂ F₂) on different raw materials (silicon, glass, PET or PP) can be developed by corona discharge or glow discharge plasma.

By using a tubular glow discharge reactor with an inductive RF plasma, the plasma deposition on a silicon target depends on the pressure and the power of the plasma. ESCA analysis of the polymer film shows the main chemical bonds and radicals present through a thickness of 100 Å of the layer. The presence of CF, CF₂, C₂F, and SiF or F- bonds depend on the plasma condition whereas the carbon species found are in agreement with

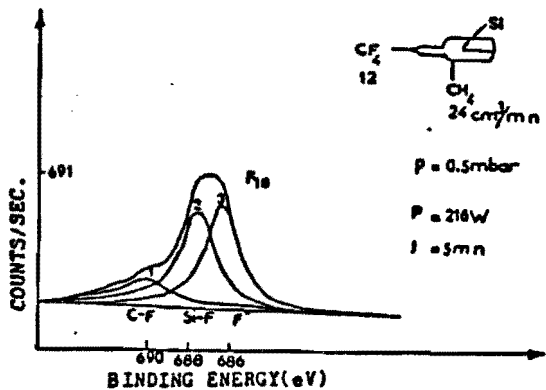


Fig 36: Decomposed F1s peak (ESCA analysis) for the pretreated silicon.

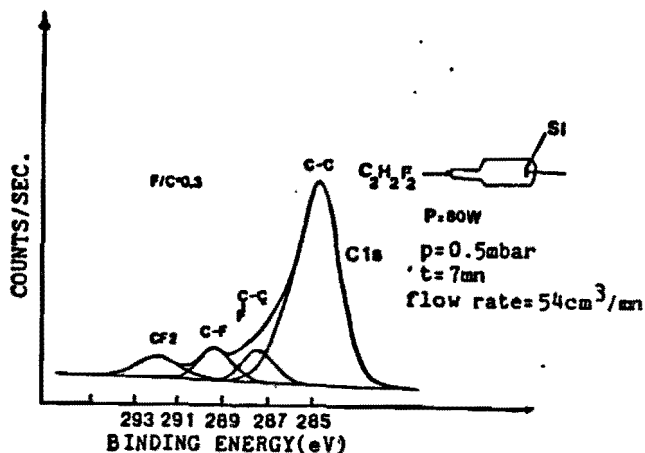
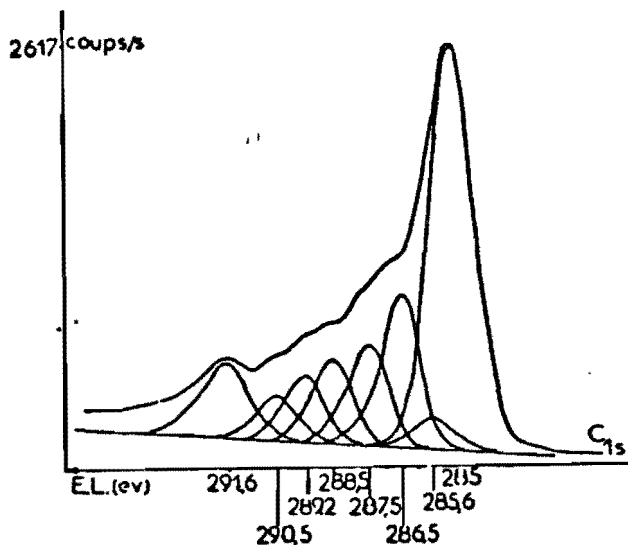


Fig 37: Decomposed carbon peak of ESCA analysis for the pretreated silicon in an atmosphere of $C_2H_2F_2$.



E_b	Chemical Environment
285	CH_2-CH_2
285.6 ± 0.1	$CH_2=CF_2$
286.5 ± 0.1	$-CF_2-CF_2-$, C-O
287.4 ± 0.2	$C=O$, C-F bonding in position
288.6 ± 0.2	$-CFH-CFH-$, C=O
289.3 ± 0.2	$-CFH-CF_2-$, C=O-H
290.2 ± 0.2	$-CF_2-CH_2-$
291.6	$-CF_2-CFH$

Fig 38: Decomposed carbon peak of ESCA analysis for the pretreated PET film.

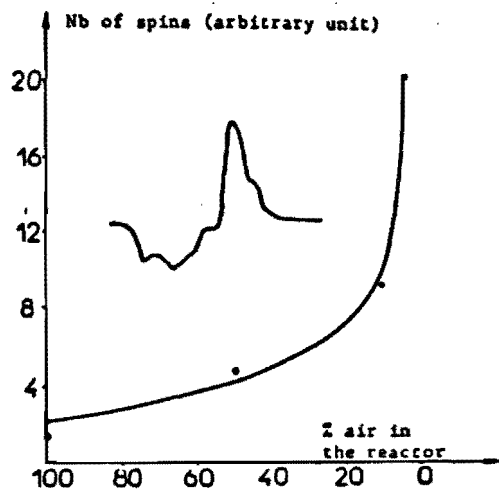


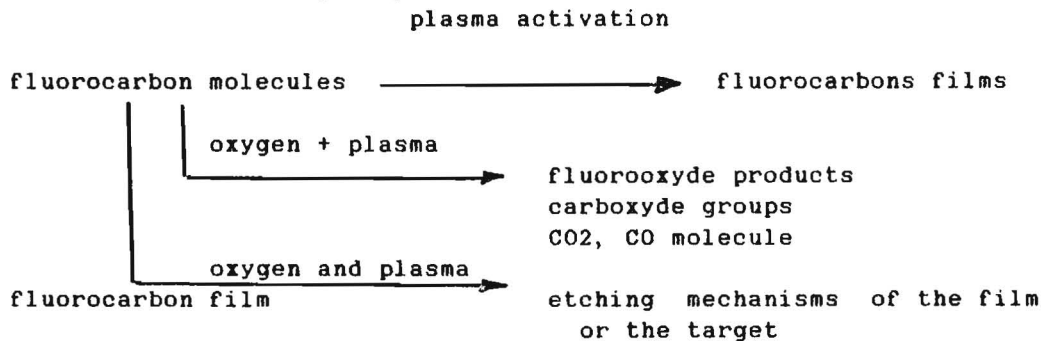
Fig 39: Variation of the free radical concentration in function of the residual air in the reactor. Experimental conditions: $t=2.8$ sec., Ar flow-rate= $280 \text{ cm}^3/\text{mn}$, $p=1 \text{ atm}$, PP thickness= $18 \mu\text{m}$

thermodynamic calculations (fig. 34,35,36,37). A decrease of the H/F and the C/F ratios of the gas mixture induces etching mechanisms of the target while an increase of these ratios allows a polymerization layer formation.

Taking the same monomer but employing another mode of electrical (fig. 38) excitation (HT corona discharge) provides polymeric film grafted to the surface of a substrate such as PET film. These mechanisms emphasize the need to control the total elimination of oxygen impurities inside the reactor.

6.6.3. ROLE OF THE OXYGEN CONTAMINATION DURING A FLUOROCARBON PLASMA POLYMERIZATION PROCESS

By introducing oxygen molecule or air with the fluorocarbon gas the plasma polymerization would depend on competitive reaction consisting mainly of the three following steps:



By using ESCA and ESR analysis (fig. 39,40,41) we have clearly demonstrated the competitive phenomena occurring during the deposition: that is the grafting rate of the fluorine groups increases (F/C ratio) when the oxygen concentration decreases (demonstrated by ESCA analysis). With an argon C2F2H2 (85% 15%) mixture, that is when excluding the oxygen the high stability of the layer obtained is measured by only a slight decrease of F/C ratio when washed with acetone; while the oxygen/Argon/C2H2F2 mixture produces fluorocarbon oxide groups which were rapidly eliminated upon water or acetone washing. These techniques could be developed for encapsulation of paper, PET or PP films and allows multilayers deposition phenomena (fig. 42,43,44).

6.6.4. ROLE OF THE TARGET: glass or metal target

By using glass or metallic targets plasma polymerization would depend on the reactivity of fluorocarbon radicals with the atoms of the lattice for example in the case of the substrate glass, large diffusion of fluor atom in the lattice through a depth of 0.2 to 0.3 μm indicate the chemical affinity of the fluor atoms for a calcosodic glass. Therefore a large part of the fluor proceeding from the plasma polymerization of the fluorocarbon diffuse in the lattice of the target (fig. 45,46,47,48,49) (42). When the target is a metallic one the system is much more complex and allows organometallic polymerization formation with interesting semiconductive properties.

6.6.5. COMPLEX ORGANOMETALLIC FILMS

Large new applications such as transparent electrodes, photovoltaic antireflective layers, electronic or semiconductivelayers... require an inclusion of the metal in the polymeric film (34,36,37,38).

In the next diagram we can suggest the chemical reactions which allow

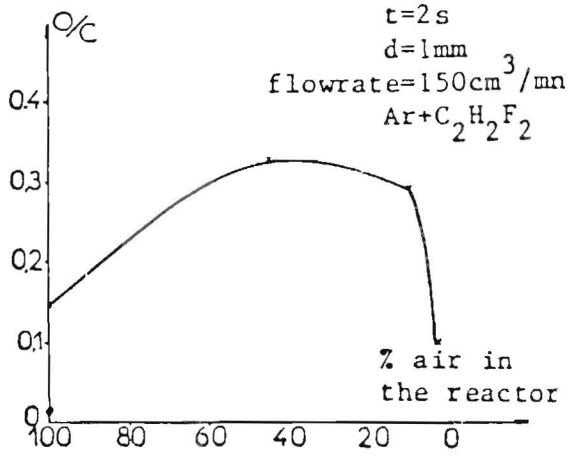


Fig 40: O/C ratios obtained by ESCA analysis in function of the residual air in the reactor.

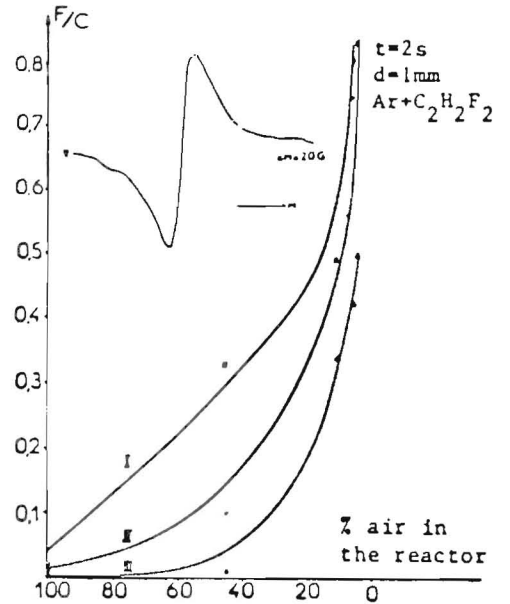


Fig 41: F/C ratios obtained by ESCA analysis in function of the residual air in the reactor. PP pretreated: I-after treatment II- washed 1h in H₂O, III- washed 1h in H₂O and 1h in acetone.

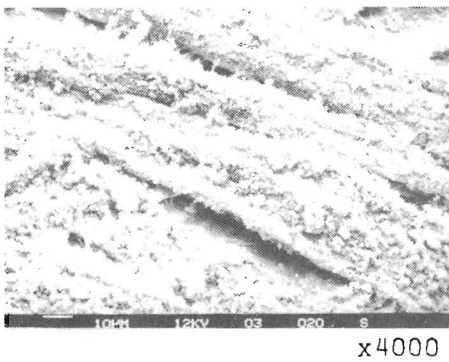
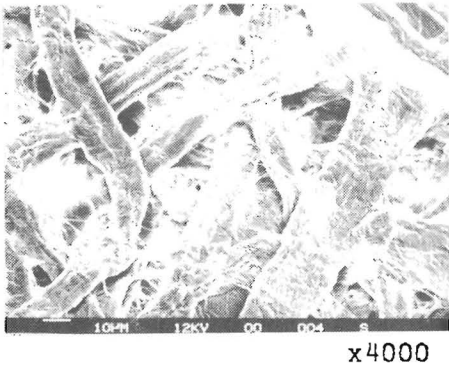


Fig 42: Polymeric aspect observed by SEM on paper ;
 a-nonpretreated
 b-pretreated ($t=30mn$, $d=3mm$, $I=200 \mu A$, $V=14.3$).

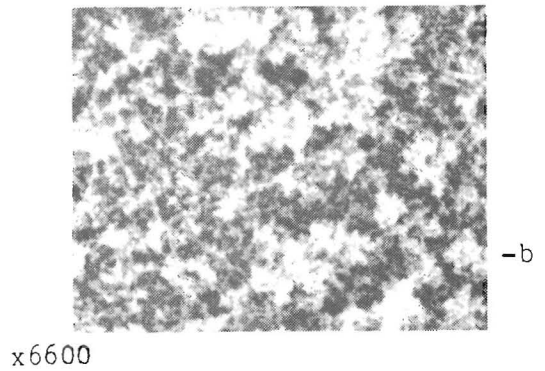
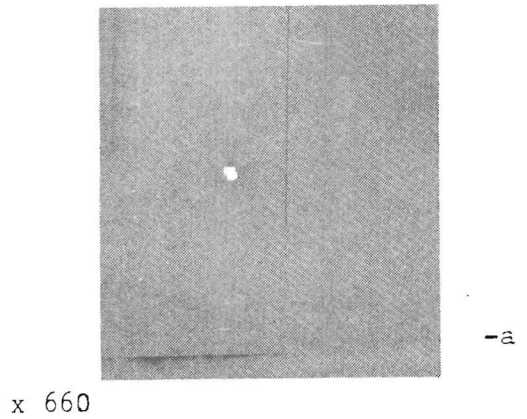


Fig 43: Polymeric aspect observed by SEM on PET film ;
 a-nonpretreated
 b-pretreated ($t=15mn$, $d=3mm$, $I=130 \mu A$).

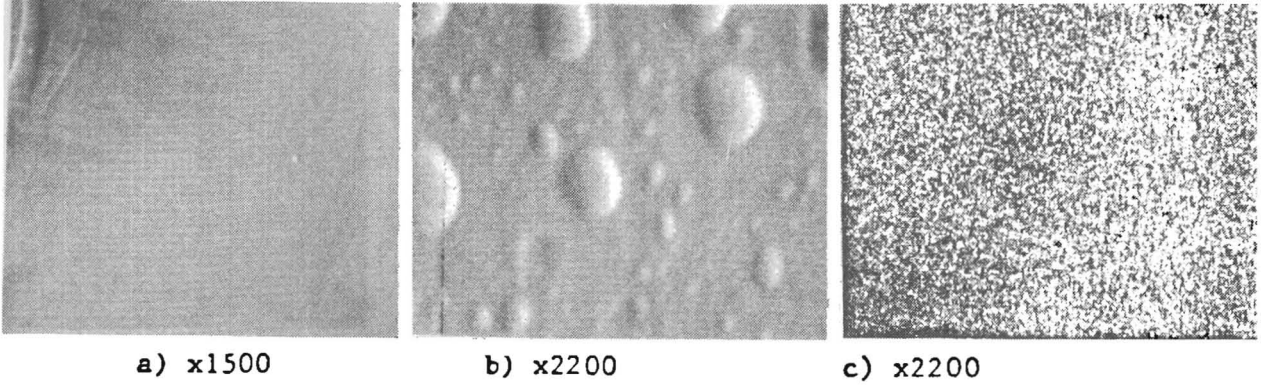


Fig 44: Pretreated pp films in a mixture of $C_2H_2F_2 + Ar$ observed by SEM.
 a) nonpretreated
 b) pretreated in presence of 100 % air
 c) pretreated in presence of 4,5 % air

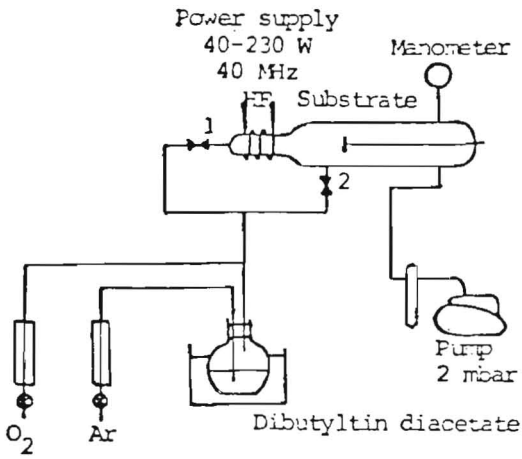


Fig 45 : Schematic diagram of the glow discharge apparatus

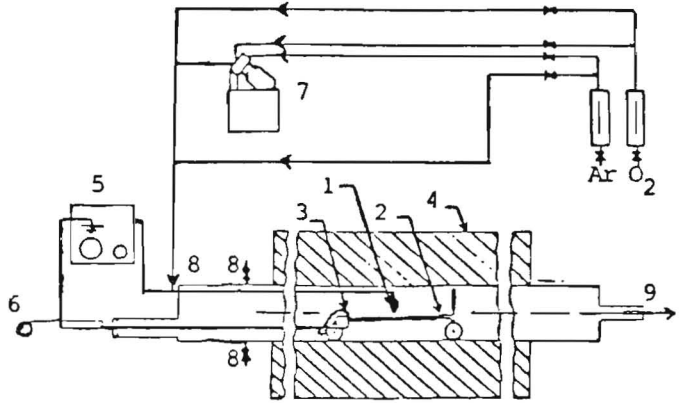


Fig 46 : Corona discharge installation
 1: active electrode
 2: glass slide on the plane mass electrode
 3: thermocouple
 4: tubular furnace (20-600°C)
 5: high tension generator (20kV max, 60kHz)
 6: substrate traction electrical supply
 7: ultrasonic nebulization system
 8: gas inlet
 9: gas exit

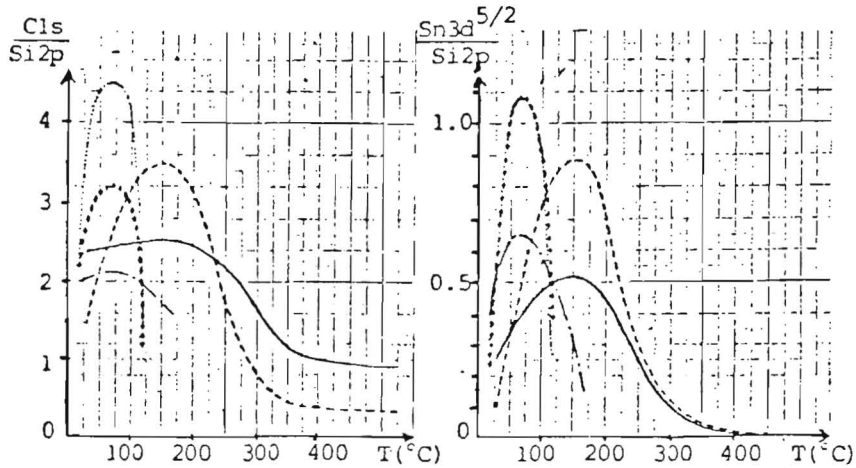


Fig 47 & 48: Effect of the treatment temperature on resp. carbon and tin signals in ESCA ($V_{appl} = 10kV, d_{Ar} = 1.31/h, discharge\ gap: 0.5mm$) (41)

- 4mm thick glass ($O_2: 10l/h$)
- 4mm thick silica ($O_2: 10l/h$)
- + + + 2mm thick glass ($O_2: 5l/h$)
- - - 2mm thick glass ($O_2: 10l/h$)
- 2mm thick glass ($O_2: 15l/h$)

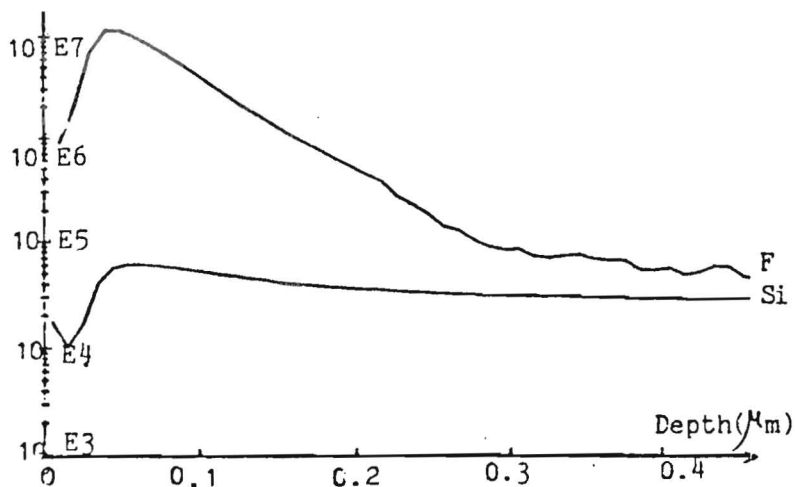


Fig 49: SIMS depth profiles of silicon and fluor. Discharge conditions: $T=200^{\circ}\text{C}$, $V=8\text{kV}$, $d=0.5\text{ mm}$, CF_4 flow-rate: 0.45 l/h .

	E_b (eV)	X/Si_{2p}
C_{1s}	285 288.8 291	6.2
O_{1s}	532.5	2.3
F_{1s}	685.2	2.4
Na_{1s}	1072.5	0.65
$\text{Ca}_{2p\ 3/2}$	347.6	0.7
Si_{2p}	103.2	1

Fig 50: ESCA ratios. Discharge conditions: $T=200^{\circ}\text{C}$, $V=8\text{ kV}$, $d=0.5\text{mm}$, CF_4 flow-rate: 0.45 l/h .

Figure 51
PACVD Process

Material Deposited	Chemical Reaction	Temperature of Substrate ($^{\circ}\text{C}$)	Application
Al_2O_3	$\text{AlCl}_3 + \text{O}_2$	250-350	passive encapsulating layer for electronics
SiO_2	$\text{SiCl}_4 + \text{O}_2$	1000	optical films
TiO_2	$\text{TiCl}_4 + \text{CO}_2$	O_2	dielectric in MOS
BN	$\text{B}_2\text{H}_6 + \text{NH}_3$	400-700	Diffusion doping of Si
Si_3N_4	$\text{SiH}_4 + \text{N}_2/\text{NH}_3$	350	Encapsulation of III - V semiconductors
TiN	$\text{TiCl}_4 + \text{N}_2 + \text{H}_2$	400-600	Hard layer for wear resistance
SiC	$\text{SiH}_4 + \text{C}_2\text{H}_4/\text{CH}_4$		electrochemical machining tools Thermal printer heads
TiC	$\text{TiCl}_4 + \text{CH}_4$	500-700	hard layer for wear resistance
As	AsH_3		III-V semiconductors
Mo	$\text{Mo}(\text{CO})_5$		Antireflectance coating
Ni	$\text{Ni}(\text{CO})_4$		
Si	SiH_4	300	Semiconductors

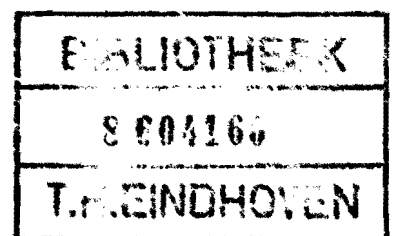
BIBLIOGRAPHY.

1. A. Von Engel Ionized gases Clarendon: Oxford (1955).
2. Nighan Phys. Rev. A, 2, 1989, (1970).
3. Borst Phys. Rev. n°5, 648, (1972).
4. F.R. Gilmore J. Quant Spectr Rad. Tranf. 5, 369, (1965).
5. M. Capitelli and E. Molinari Topics and Current Chemistry Vol 90, pp.60 (1980).
6. F. Cramarossa, G. Ferraro, E. Molinari J. Quant. Spectr. Rad. Transf. 14, 419-436, (1973).
7. J.C. Polanyi J Chem. Soc. Farad. Trans. , 389-409, (1973).
8. J.C. Polanyi and M.H. Wong, J. Chem. Phys. 51(4), 1439-1450, (1969).
9. J.H. Mc Creery and G. Wolken, J. Chem. Phys., 66(6), 2316-2321, (1977).
10. B. Halpern and D.E. Rosner, J. Chem. Soc. Farad. Trans., 60, 1883-1912, (1977).
11. R. D'Agostino, F. Cramarossa, S. De Benedictis, G. Ferraro, Plasmachemistry and plasma Processing, 1, 1, 19-35, (1981).
12. D. Rapakoulias, J. Amouroux, M.P. Bergougnan, A. Gicquel, Rev. Phys. Appl., 17, 95-101, (1982).
13. M.P. Bergougnan, A. Gicquel, J. Amouroux, Rev. Phys. Appl. 18, 335-346, (1983).
14. A. Gicquel, M.P. Bergougnan, J. Amouroux, Proceed of the 4th Symposium on Plasma processing Electrochemical Society, 83, 10, 169-174, (1983).
15. A. Ricard, Ann. Chim., 8, 303,312, (1983).
16. A. Goldman and J. Amouroux, Chap. "Plasma Chemistry", 293-345, (1983), Electrical Breakdown and Discharges gases- Part B., Macroscopic processes and discharges. Ed. by E.E Kunhardt, L.H. Luessen, Plenum Publisching Corp.
17. K. Fulani, I. Fuzika and K. Kuwata, J. Phys. Chem. Vol. 81, 13, 1252-1257, (1977).
18. G. Lecayon, Y. Bouizem, C. Le Gressus, C. Reynaud, C. Boiziau, C. Jurel, Chem. Phys. Letters, 91, 6, 506-510, (1982).
19. P.J. Arpino, Actualite Chimique, 4, 19-28, (1982).
20. R. Walder, J.F. Franklin, Int. Mass Spectrom. Ion Phys., 36, 85-91, (1980).
21. K.N. Hartman, S.Lias, P. Ausloos, A.M. Rosenstock, S.S. Schroger, C. Schmidt, D. Martinsen, G.W.A. Milne, Compendium of gas phase basicity and proton affinity mesurements U.S. N.B.S. Washington DC. (1979).
22. C.R. Moylan, J.I. Brauman, Ann.Rev. Phys. Chem., 34, 187-215, (1983).
23. M. Berthelot, J.F. Gal, Act. Chimique, 2, 19-23, (1984).
24. M. Fusio, R.T. Mc Iver, R.W. Taft, J. Amer. Chem. Soc., 103, 4017-4029, (1981).
25. P. Chang, San Diego, Plasma etching and plasma Technology, 2d Int. Conf. Nov. 1984.
26. H. Yasuda, J. Polymer Sc. Macromol. Rev. 16, 199-293, (1981).
27. A.T. Bell, Topics in Current Chemistry, 94, 43-68, (1980).
28. F. Arefi, J. Amouroux, M. Goldman, Ann. Chim. 2, 19-25, (1984).
29. B. Ranby and J.F. Rabek Singulet oxygen, Reactions with organic compounds and Polymers, Wiley- Interscience. Chichester (1978).
30. L. Gillepsie, The electronic repulsion theory of chemical bond, W.L. Luder ed., Dunod, Paris, (1967).
31. J. Amouroux, M. Goldman, F. Arefi, F. Rouzbehi, French Patent No 83125 (1983), U.S Patent No 634.741 (1984), Japon Patent No 158533 (1984), Eur. Patent 401592.5/1984.
32. F. Arefi, Doctorat Ing. Docteur Thesis, Universite P. et M. Curie, (1984).
33. E. Kny, L.L. Levenson, W.J. James, K.A. Averbach., J. Phys. Chem., 84, 1635-1638, (1980)

34. O. Demuth, r.Cuelho, J. Amouroux, M. Goldman, IEEE proceedings, Toulouse, 1983.
35. R.K.Sadhir, W.J. James, R.A. Averbach, Thin Solar Films, 17-29, (1982).
36. D.R. Secrist, J.D. Mackenzie, Bul. Am. Ceram. Soc., 45, 784-770, (1966).
37. N. Inagaki, T. Nischio, K. Katsunta, J. of Polym. Sci. Lett. Ed, 18, 765-770, (1980).
38. A.R. Reinberg, Ann. Rev. Mater. Sci., 9, 341-373, (1979).
39. B.R. Loy, J. of Polym. Sci. Part A., 1, 2251-2259, (1979).
40. H. Fischer, K.H. Hellwage, J. of Polym. Sci., 56, 33-45, (1962).
41. S. Thomas, J. Amouroux, ISPC-7 Eindhoven, 1985.

**ADVANCED COURSE ON
LOW-PRESSURE PLASMAS
TECHNOLOGY AND APPLICATIONS**

**EINDHOVEN UNIVERSITY OF TECHNOLOGY
EINDHOVEN, THE NETHERLANDS
JUNE 26-28, 1985**



LECTURE NOTES

VOLUME 2

EDITED BY P. MASSEE and W.F.H. MERCK

Address of the editors:

Massee/Merck
Department of Electrical Engineering
Division EG
Eindhoven University of Technology
P.O. Box 513
5600 MB Eindhoven, The Netherlands.

© EINDHOVEN UNIVERSITY OF TECHNOLOGY

All right reserved. No part of this publication may be reproduced or used in any form or by any means - graphic, electronic or mechanical, including photocopying, recording, taping or information storage and retrieval systems - without the prior, written permission of the editor.

CIP-GEGEVENS KONINKLIJKE BIBLIOTHEEK, DEN HAAG

Advanced

Advanced course on low-pressure plasmas: technology and applications. Eindhoven, the Netherlands, June 26-28, 1985. Lecture notes. Vol. 1. / ed. by P. Massee and W.F.H. Merck. - Eindhoven: University of Technology. - Fig., tab
Met lit. opg., reg.
ISBN 90-6144-998-7
SISO 655.7 UDC 533.9:621.794 UGI 650
Trefw.: plasmatechnologie.

This volume contains three papers that were not available in time to include in volume 1.

The titles of the papers are:

6.1. Surface and thin film analysis (P.C. Zalm)

6.3. Optical spectroscopy (J.P.M. Schmitt)

7 Survey of applications in plasma etching and plasma deposition
(G.K. Herb).

6.1. Surface and Thin Film Analysis

P.C. Zalm

Dr. Peter C. Zalm works at the Philips Research Laboratories, Eindhoven, The Netherlands. His principal interest is the interaction of high speed particles with solid surfaces.

SOME REMARKS ABOUT SURFACE AND THIN FILM ANALYSIS

P.C. Zalm, Philips Research Laboratories, 5600 JA Eindhoven - The Netherlands

1. INTRODUCTION

After a surface has been subjected to a plasma treatment it is often desirable to investigate it by analytical techniques in order to establish what alterations (modifications, residu deposition or compositional changes) have been caused. In general this will require some kind of surface sensitive measurement technique. Charged particle beams impinging on the target are often used for information gathering, because of their ability to be focussed which in turn enables localized sample inspection. An obvious problem, which exists for almost all surface analytical techniques, is that the measurement itself may affect or change the target. Moreover, the more surface sensitive a technique is the easier contamination from atmosphere or rest gas in a vacuum system will influence the observations. In these lecture notes we will very briefly present and discuss the basic principles and operating characteristics of some commonly used surface analytical techniques.

1.1 SIMPLE KINETIC GAS THEORY

For a gas with N molecules per unit volume the number of particles $n(\vec{v})$ with velocity between \vec{v} and $\vec{v}+d_3\vec{v}$ follows Maxwell's distribution

$$n(\vec{v}) d_3\vec{v} = N \left(\frac{m}{2\pi kT} \right)^{3/2} \exp \left\{ -\frac{m}{2kT} (v_x^2 + v_y^2 + v_z^2) \right\} d_3\vec{v}, \quad (1)$$

where m is their mass and T the temperature of the gas. The absolute velocity distribution $n(v)$ is given by

$$n(v) = \frac{4}{\sqrt{\pi}} v^2 \left(\frac{m}{2kT} \right)^{3/2} \exp \left(-\frac{v}{v_0} \right)^2, \quad (2)$$

where the most probable velocity $v_0 = \sqrt{2kT/m} = 129 \sqrt{T/M}$ m/s, with T in [K] and M in [atomic units]. The average velocity $\bar{v} = 2v_0/\sqrt{\pi}$ and the root-mean square velocity $\sqrt{v^2} = v_0 \sqrt{3/2}$, all indicate particle velocities of the order of the velocity of sound in the gas!

From eq. (1) the pressure P exerted on the walls follows as

$$P = NkT. \quad (3)$$

{ Pressure units 1 atm (\approx 1 Barr) corresponds to the pressure of a 76 cm mercury column on earth at 0°C , i.e. $\leftrightarrow 1.0 \times 10^5$ [Newton/m² \equiv Pa(scal)]. 1 mm Hg \leftrightarrow 1 Torr = 400/3 Pa. } From eq. (3) we learn that 1 atm corresponds to a density of 2.5×10^{19} particles/cm³. For comparison : in an elemental solid the density is about 10^{22} - 10^{23} particles/cm³. This implies that one monolayer of solid or condensed material is 3 \AA thick and contains $\sim 10^{15}$ atoms/cm²!

From eq. (1) the number of particles, ν , that hit a surface per unit area and time follows as

$$\nu = N \sqrt{\frac{kT}{2\pi m}} = \frac{N\bar{v}}{4} = \frac{P}{2mkT} = 2.6 \times 10^{20} \frac{P [\text{Pa}]}{\sqrt{MT}} / \text{cm}^2\text{s}. \quad (4)$$

The mean free path, \bar{l} (distance traveled between two collisions), is found to be

$$\bar{l} = (\pi\sqrt{2}Nd^2)^{-1}, \quad (5)$$

where d is the diameter of the particle (assumed to be spherical). { For different types of molecules replace diameter d by the sum of the radii (r_1+r_2); for a multicomponent gas $\bar{l}_j^{-1} = \sqrt{2} \pi \sum_i N_i (r_i+r_j)^2$; for electrons $\bar{l}_e = (\pi\sqrt{2}Nr^2)^{-1}$. }

Formulas (1-5) are only approximately valid and breakdown if the "eigen-volume" of the gas becomes significant (i.e. for N atoms/cm³ if $N \cdot 4/3\pi r^3 \gtrsim \text{mm}^3$ or $N \gtrsim 10^{19}$ - 10^{20}).

When a particle approaches a surface it may collide elastically and reflect back into the system or it can interact (exchange energy) and "stick" to the "wall" atoms : it adsorbes. After some time it may desorb again.

Physisorption: $\Delta E_{\text{ad}} \lesssim 0.4$ eV/atom or molecule (≈ 40 kJ/Mole or 10 kcal/Mol)

Chemisorption: $\Delta E_{\text{ad}} \gtrsim 1$ eV/atom or molecule

{ Physisorption is common for non-polar molecules or atoms (e.g. CF₄, noble gases. Physisorption often precedes chemisorption. Chemisorption of molecules often results in dissociation. } The average surface residence time, $\bar{\tau}$, is given by $\bar{\tau} = \tau_0 \exp(\Delta E_{\text{ad}}/kT)$, where τ_0 is of the order of 10^{-12} s.

1.2. THE INTERACTION OF ELECTRONS WITH SOLIDS

When an electron penetrates a solid it may loose kinetic energy in a variety of ways.

i) By excitation of lattice vibrations ("phonons", $\Delta E_{\text{ph}} \sim 0.01$ - 0.1 eV).

- ii) By causing collective density fluctuations of the target's electron gas ("plasmons", $\Delta E_{pl} \sim 10$ eV).
- iii) By energy exchange in violent binary conditions with target electrons, but not with atoms because of the huge mass difference.

In the latter case electrons originally (strongly) bound to an atom may be excited or even released, leaving a "hole" in the electron shells. Such a hole may be "filled" by less bound electrons and the transition energy gained in this manner can result in either photon emission or ejection of a third, the "Auger", electron (see section 2). In general process iii) leads to fast recoils which in turn may liberate subsequent generations of progressively slower electrons until finally their energy is too low to excite electrons anymore.

The penetration depth of energetic electrons in a solid is roughly given by

$$R(E_{e1}) \simeq 10 E_{e1}^{4/3} [\mu\text{g}/\text{cm}^2], \quad (6)$$

where E_{e1} has to be inserted in [keV] and R can be converted to regular depth units through division by the gravimetric density, ρ in [$\mu\text{g}/\text{cm}^3$], of the solid.

Another interesting quantity is the inelastic mean free path of an electron of energy E, λ i.e. the average distance it may travel in a solid before it suffers some kind of energy loss (see fig. 1). Although not expected a priori, λ is surprisingly material independent and given by

$$\lambda \simeq A/E^2 + B\sqrt{E}, \quad (7)$$

where for elemental targets $A=143/B=0.054$ and for inorganic compounds $A=641/B=0.096$, together with E in [eV] have to be inserted to obtain λ in [nm].

Equation (7) implies a minimum of $\lambda \simeq 5 \text{ \AA}$ around 50 eV, very small indeed! Even between 10 eV and 2 keV always $\lambda < 60 \text{ \AA}$. We will later see that good use can be made of this feature in surface sensitive analytical techniques. The singularity at $E=0$ in eq. (7) is not unrealistic. The mean free paths of very low energy electrons can indeed be of the order of 1 μm , owing to the Pauli exclusion principle. We will not go into this in detail here.

Energetic (E_0) electrons penetrating the electron cloud surrounding a target atom experience the strong Coulomb field of the unscreened nucleus and will be deflected. The Rutherford scattering formula for this process is given by (see also fig. 2)

$$\frac{d\sigma_R}{d\Omega} = \frac{e^4 Z^2}{64\pi^2 \epsilon_0^2 E^2} \frac{1}{\sin^4 \theta/2} \frac{1}{(m_0 c^2 + E_0)^2} \quad (8)$$

($m_0 c^2 = 511$ keV = electron rest energy). Equation (8) is invalid at small angles $\theta \lesssim 1^\circ$, because of the screening, and at high θ ($\sim 180^\circ$) because then the electron spin has to be taken into account. The energy lost by the electron during deflection as photons accounts for the well-known phenomenon of "Brehmsstrahlung".

The total spectrum of electrons emitted from a surface upon exposure to a beam of energetic electrons is given schematically in fig. 3.

1.3. IONS; MISCELLANEOUS REMARKS

Most of the features of ion-solid interaction will be covered in the lecture on "Plasma-wall interactions; consequences" and need not be repeated here. Just remember that ions can be used for sputter-etching (also called "ion milling") and that this phenomenon can be applied for "peeling off" surfaces to study compositional changes as a function of depth (although ion beam mixing, preferential sputtering and non-constant erosion rate will influence the reliability of such a "thin film" or "depth profiling" analysis).

For isolating targets, bombardment with charged particles may charge-up the surface thereby preventing subsequent particles from reaching the surface. Positive biasing of the target can be prevented by spraying it with low-energy electrons from a filament. Deliberate target biasing on conducting surfaces is sometimes useful to prevent secondary electron liberation, thereby allowing for more accurate current determination.

Both electron and ion bombardment may lead to the ejection of electrons from bound levels in target atoms. As a result chemical bonds may be broken and sometimes electron (ion) stimulated desorption may take place. Beams of energetic particles (electrons, ions or photons) will heat up a surface. As a rough order-of-magnitude estimate for a beam with input power Φ Watt, diameter d and penetration depth R , incident on a semi-infinite solid with a heat-of-conduction coefficient C_w [Watt/m.s.K], the temperature difference between irradiated area and infinity is (see also fig. 4)

$$T_0 - T_\infty \approx \frac{\Phi}{4 \cdot C_w \cdot \max(R, d)} \quad (9)$$

2. Characteristics of some surface sensitive analytical techniques

2.1. ELECTRON MICROSCOPY; THE SCANNING PRINCIPLE

The basic idea behind Scanning Electron Microscopy (SEM) is a rather old and conceptually simple one, but with a high versatility. A narrow focussed electron beam ($10-100 \text{ keV}$, $\phi \sim 0.1 \mu\text{m}$ but can be as low as 100 \AA !) is rastered (swept) over the surface to be investigated by magnetic deflection, see fig. 5. Detection of the electrons ejected from the target (their spectrum has been given in fig. 3) in coincidence with the motion of the incoming beam gives highly localized information on the emission behaviour. In principle the contributions of the "true" secondary electrons (with energies $\lesssim 50 \text{ eV}$) and the backscattered primaries (with $E_{\text{prim}} - 50 \text{ eV} \lesssim E_{\text{back}} \lesssim E_{\text{prim}}$) can be separated. E.g. by positioning an electron detector outside the direct line of sight, at a positive bias of some $+100 \text{ V}$ the former group will still be "sucked-in"; a detector in direct line of sight to the sample at a -100 V bias, which stops the slow ones, still registers the latter, reflected, electrons. Of course also the current on the target can be used as an information source. Using the detector signal as input to a video amplifier of a TV-set, of which the line frequency is synchronized with the microscope scanning, an enormously magnified image of the local emission behaviour is obtained. {Magnification depends on area scanned, but may be up to 5×10^4 with resolution limits on the target of the order of 200 \AA !} Because the electron beam is in focus over considerable depth, owing to the electron optics quality, the depth-of-field is large when compared to a conventional light microscope. {LM: d-o-f $300 \mu\text{m}$ at $10 \mu\text{m}$ resolution, down to $3 \mu\text{m}$ at $1 \mu\text{m}$; SEM still has a d-o-f of $100 \mu\text{m}$ at resolved details of less than $0.1 \mu\text{m}$!}

There are several important causes for contrast in SEM images. These will be discussed below. The effects may differ for the secondary electron (SE) signal or the reflected electron (RE) detector output as information carrier.

i) angular contrast

If the beam hits the target at an angle ϑ with respect to the surface normal more secondary electrons will be liberated near the surface with a possibility to escape. Simple geometrical arguments lead to a yield increment $S_{\text{Se}} \propto 1/\cos\vartheta$, a rule obeyed experimentally (for targets with $Z \sim 30$ for $Z \lesssim 10$ the angular dependence is slightly steeper, for $Z \gtrsim 60$ noticeable more gentle). The reflected electron signal S_{RE} also increases with ϑ , but levels off to a maximum at angles $\vartheta \approx 70^\circ \pm 10^\circ$ and becomes very low for

grazing incidence ($\theta \uparrow 90^\circ$) because of specular reflection.

ii) shadow contrast

Elevated details on a surface may block electrons from reaching the detector (fig. 6). The SE signal is affected least because of the attractive potential on the detector.

iii) (w)edge contrast

If the object is partly transparent for the primary beam, locally extra reflected and secondary electrons can escape (fig. 7). Small edges [thickness $d \ll R$ eq. (6)] cannot be seen in the RE mode, only in the SE mode.

iv) material contrast

As the cross-section for scattering off an atom increases with Z (eq. 8) the RE signal is generally higher for heavier elements. No simple rules can be given for the SE signal.

v) potential contrast

The relatively slow SE ($\lesssim 50$ eV) are very sensitive to charge up of certain areas of a target surface a negative (positive) bias enhances (reduces) SE emission. The swift RE are not significantly affected.

The low-energy SE stem from close to the surface ($\lesssim 20-50 \text{ \AA}$, see sect. 1.2 eq. 7), whereas the RE come from much deeper ($t \simeq R$ (eq. 6)/2-3, because they also have to escape!). The RE on average suffered multiple scattering and therefore stem from a laterally less confined region. So both resolution and surface sensitivity of SE is better.

With (good) isolators target charge-up may pose a problem. Coating with a thin conductive layer ($\lesssim 100 \text{ \AA}$) by evaporation or sputter deposition (often of Au) this can be circumvented. The advantage is that in the RE mode material contrast is retained and with SE topographic information can be obtained even better.

Literature : L. Reimer and G. Pfefferkorn -Raster Elektronenmikroskopie
(Springer, Berlin, 1977).

2.2. ELECTRON MICRO PROBE

An energetic electron striking an atom may excite electrons that were originally strongly bound. Thus a deep lying "hole" is created. This may be filled by a less bound, outer shell, electron. The energy regained in this transition, $\Delta E_{\text{trans}} = E_{\text{core electron}} - E_{\text{outer shell}}$, can be emitted in the form of a Röntgen-quant (a photon) of energy $h\nu = \Delta E_{\text{trans}}$, or by ejection of an-

other weakly bound electron (the "Auger" electron, which gets a kinetic energy $E_{\text{kin}} \approx E_{\text{trans}} - E_{\text{weakly bound}}$; see subsect. 2.3.). This photon energy is highly characteristic for the particular element hit. In EMP use is made of this phenomenon. Energy resolved detection of photons emitted from a target upon energetic (10-100 keV) electron bombardment proceeds by diffraction on a crystal or grid and a photomultiplier. [Remember Bragg's law: $2d \sin \theta = n\lambda$.

A problem is that the photon wavelength λ must be of the order of the crystal lattice spacing d (i.e. $\lambda \lesssim 20\text{\AA}$) and that the photon emission probability must be non-zero. Both demands make it impossible to detect very light elements ($Z < 6$).

A second problem is that the electrons create photons over their total penetration depth (eq. 6) i.e. over 0.1-1 μm , which is also approximately the photon extinction length or escape depth. This limits lateral and depth resolution.

Finally photons of heavier atoms can be adsorbed by lighter ones (creating new generations of excitation) on their way out and also electron back-scattering enhances surface sensitivity. Background continuum X-rays originate from "Bremstrahlung" (radiation emitted when an electron penetrates the electron cloud surrounding an atom and is deflected in the field of the atomic nucleus). All of this greatly complicates quantification. Nevertheless EMP analysis can be done and is often combined with SEM to provide elemental information. Detection limits are 0.1 %, for low Z elements, down to 1 ppm.

2.3. AUGER & PHOTO-ELECTRON SPECTROSCOPY

The basic principles are depicted in fig. 8. Electrons are ejected from bound states in the target either by photon absorption or by electron (1-5 keV) bombardment. Elemental information is obtained by energy dependent electron detection. In the former case we may use the electron emitted itself. In the latter case we need to detect the second electron emitted in the Auger process, because the first one does not have a well-defined energy.

With ultraviolet light (UPS, $h\nu \sim 10-40$ eV) only weakly bound (valence) electrons can be ejected. With X-rays deeply bound core electrons can be excited. {These Röntgen photons are created by electron bombardment of a metal (mostly K_{α} radiation of Mg or Al with $h\nu = 1.25$ or 1.49 keV, respectively, is used) as discussed for the EMP in subsect. 2.2; this type of source is not very intense. }

Ejected electron energies in UPS are a few eV. The spectrum is continuous with a lot of fine details. { It's even sensitive to unoccupied electron states in the target! } UPS is not extremely surface sensitive (see also eq.7). In XPS and AES the electrons kinetic energies range from 10-2000 eV, so surface sensitivity is high. The spectra are in principle discrete. For AES the background due to secondary electrons is prohibitively high (see fig. 3). Therefore the AES $N(E)$ vs E curve is usually differentiated. Total $N(E)$ spectra for XPS and dN/dE spectra for AES for all elements exists in the literature.

Auger linewidths are of the order of 5-10 eV, XPS linewidths only around 1 eV, because in the former three levels are involved, one of which is often a broad band. As a consequence energy level shifts due to chemical binding differences between elements and compounds, which are 1-2 eV in magnitude, can only be detected with XPS. { A notable exception: the AES spectra of Si in elemental Si, Si_3N_4 and SiO_2 are clearly distinguishable. } This special feature of XPS necessitates the use of analysers with a much better electron energy resolving power ($\rho = E/\Delta E$) than those commonly applied in AES. Some examples/principles are shown in fig. 9.

For XPS and AES, the detection limit for impurities is rather low, 0.1-1 % of a monolayer i.e. still too high for e.g. doping levels in SiO_2 . Quantification is very complicated for AES and difficult with XPS. Based on gauge factors from elemental spectra concentration estimates from AES and XPS may differ by as much as a factor of 2 and 30 %, respectively, from reality.

Ultraviolet light and Röntgen sources cannot conveniently be focussed, whereas electrons can. Therefore it is only feasible to use AES as an imaging technique (like the SEM, sect. 2.1). Combining XPS and AES with depth profiling through ion beam sputter etching converts these techniques to a thin film analysis tool.

Literature : D. Briggs and M.P. Seah-Practical Surface Analysis (Wiley, New York, 1983).

2.4. SECONDARY ION MASS SPECTROMETRY

Ion bombardment of a target results in the sputtering (ejection) of surface atoms (usually stemming from a depth of $\sim 5 \text{ \AA}$ only!). A small fraction of the emitted particles may be ionized (~ 0.1 %). These ions reflect the composition of the target, which makes their detection useful. Mass analysis of

the sputtered ionic species proceeds by postacceleration and electromagnetic deflection to final detection in a photomultiplier.

Problems with SIMS are that the probability to be ejected and survive as an ion strongly depends on the composition of the target surface. A few percent oxygen coverage may enhance the positive ion emission by orders of magnitude. This so-called matrix effect -i.e. the detection probability of a certain type of atom is included by the atoms surrounding it- makes it very difficult to quantify SIMS results if contamination levels exceed $\sim 1\%$. Carefully prepared gauge samples have been used successfully for calibration purposes.

Also the ejection of clusters besides single atoms complicate a SIMS analysis. For example, 5 keV Ar^+ ion bombardment of Si_3N_4 not only yields N and Si but also e.g. N_2 or Si_2 and SiN_2 which have the same nominal mass. This necessitates a high mass resolving power of the analyser, which is intimately connected to a loss of statistics i.e. a higher contamination level detectability limit.

The biggest advantage of SIMS is that trace amounts of impurities can be detected (~ 1 ppm, i.e. concentrations of less than $10^{17}/\text{cm}^3$, sometimes even down to $10^{14}/\text{cm}^3$!), which is ideal for Si IC-technology.

As the primary ion beam can in principle be focussed, rastering and consequently SIMS imaging are possible. Since sputtering is a natural part of SIMS the extension from static SIMS (spot diameter ~ 1 mm; low ion fluence; only very surface probed) to dynamic SIMS (narrow beam, $\varnothing \sim 10$ μm) in order to do depth profiling for thin film analysis, is a logical one. Ultimately, as in all other sputter-profiling assisted techniques, the depth resolution is limited by such factors as ion beam mixing, preferential sputtering and "peel-off" rate variation, crater wall effects (as e.g. sputter redeposition); see fig. 10.

Literature : H.W. Werner, in : Electron and Ion Spectroscopy of Solids
(Plenum, New York, 1978) pp. 324-441.

2.5. ION SCATTERING SPECTROSCOPIES

An ion has a specific energy and is scattered off an atom, initially at rest, in a specific direction has suffered an energy loss typical for the target-to-projectile mass ratio (see fig. 11)

$$E_{\text{after}}/E_{\text{before}} = \left[\frac{\cos\theta + \sqrt{(M_t/M_p)^2 - \sin^2\theta}}{1 + M_t/M_p} \right]^2, \quad (10)$$

in the hard sphere approximation. This feature is used in Low Energy Ion Scattering (LEIS) spectroscopy where backscattered ions (usually 1-3 keV He^+) are energy-analysed in an electrostatic deflection system at a detection angle θ . Because the neutralization probability is extremely high only particles reflected from surface atoms in a single collision survive as ions. Multiple scattering and penetration of the topmost atomic layers inevitably results in neutralization (except for H^+ ions, therefore these are useless as consequently E_{before} will be ill-defined). The energy spectrum of the backscattered ions immediately reflects the mass composition of the surface.

The sensitivity is good (≈ 0.1 % of a monolayer), the destructivity fair because He^+ ions do not sputter efficiently. All masses with $Z > 2$ can be detected. Quantification is excellent once the yield (ion fraction out/ion in) has been measured for all elements in a specific apparatus. No chemical (binding) information is obtained and matrix effects are virtually absent. In Rutherford Backscattering Spectroscopy (RBS) another, but related approach is followed. Here a high energy (1-2 MeV) light ion (usually He^{++}) beam ($\theta \sim 0.1$ mm) is directed onto the target. Neutralization of the ion does not occur at these velocities, it remains essentially a point particle (dimensions $\approx 10^{-14}$ m!) which only loses energy by electronic excitation of target atoms (the so-called electronic stopping power regime). On the rare occasion that it passes on atomic nucleus, after penetrating to some depth d in the solid, so closely that it will interact (scatter) it does so violently. The chances are small that it undergoes multiple scattering on its way out after this collision. Thus energy dependent detection of He^{++} ions (α -alpha-particles) backscattered over an angle θ provides compositional, depth dependent information (see fig. 12).

The resolution of the solid-state detectors used for α particles is fairly low ($\Delta E \approx 10$ keV). Electrostatic analysers can, unfortunately not be used at such high energies. Therefore, depth resolution is limited to some 50-100 Å. The probe depth may be 1 μm . Detection limits for impurities may be as low as 1 ppm.

In the case of a single crystal target the ion beam may be aligned with any major crystal axis, by placing it in a goniometer annex sample holder stage. If the beam is parallel to an axis the outermost atoms in a row screen the deeper lying ones from the beam in a so-called shadow cone (fig. 13). Thus scattering will be either off the topmost atomic layer or not at all (approximately), the ions "channel". The $N(E)$ vs. E spectrum of reflected ions shows a peak at maximum energy and almost no contribution from scattered,

penetrated, ions that lost some energy by electronic excitation. Surface peak (SP) and channeling minimum also contribute information about reconstruction/relaxation of the outer layer(s) and crystal quality (imperfections, impurities etc.); fig. 14.

Literature : W.K. Chu, J.W. Mayer and M.A. Nicolet-Backscattering Spectrometry (Academic Press, New York, 1978).

2.6. ELLIPSOMETRY

In ellipsometry, a 50 year old technique, polarized light reflection is employed to determine bulk and thin film optical properties (index of reflection n , extinction coefficient k and film thickness), even for submono-layer coverages. The big advantages of this method are its non-destructiveness, no specimen charge-up and applicability in a non-vacuum environment (so it could be used inside a plasma reactor in operation!).

The basic instrument is given schematically in fig. 15, which is largely self explanatory. The total electric vector of the incident light wave can be decomposed in a parallel (p) and perpendicular(s) component to the surface,

$$E_{p,s} = A_{p,s} \exp(i\omega t + \delta_{p,s}), \quad (11)$$

where ω is the angular frequency ($2\pi\nu$) of the light. In general reflection will result in a change of both amplitudes A_p, A_s and phases δ_p, δ_s . These changes are described by two parameters Δ and Ψ , according to

$$\Delta = (\delta_p - \delta_s)^{(r)} - (\delta_p - \delta_s)^{(i)}, \quad \tan \Psi = \frac{A_p^{(r)}}{A_s^{(r)}} / \frac{A_p^{(i)}}{A_s^{(i)}},$$

where the superscript (r) and (i) stand for reflected and incident beams, respectively. The connection to the reflection coefficients $R_{p,s}$ is given by

$$R_p/R_s = \frac{E_p^{(r)}}{E_p^{(i)}} / \frac{E_s^{(r)}}{E_s^{(i)}} = \tan \Psi \exp(i\Delta) \quad (12)$$

For the instrument of fig. 15, the settings (p) of polarizer and (a) of analyser which given minimum intensity on the photocell are related to and as $\Delta = 90^\circ + 2p, \Psi = a$.

The functional dependence for a thin layer l of material on a bulk substrate b

$$\tan \Psi \exp(i\Delta) = f(\lambda_0, n_0, \varphi_0, n_1, k_1, d_1, n_b, k_b), \quad (13)$$

where $\lambda_0, \varphi_0, n_0, n_b$ and k_b are either known, adjustable or measurable in the absence of the thin film, gives a (sometimes extremely) complex equation with

three unknown variables (n_1, k_1, d_1) and two measurable quantities (Δ, Ψ). By calibration with well-characterized gauge samples or angle- and wavelength variation combined with computer-simulation-based educated guessing satisfactory results are obtainable.

From the complex index of refraction $\tilde{n} = n - ik$ the complex dielectric function $\tilde{\epsilon} = \tilde{n}^2 = n^2 - k^2 - i2nk = \epsilon' - i\epsilon''$ can be obtained as a function of photon energy by varying the wavelength. As $\tilde{\epsilon}$ is among others determined by energy loss of the incident wave to single particle and collective excitations of the electrons it is intimately connected to the plasmon dispersion relations and thus to the charge distributions and band structure in the layer.

Normally the third derivatives of ϵ' and ϵ'' are plotted against photon energy $h\nu$ to boost the element-specific features.

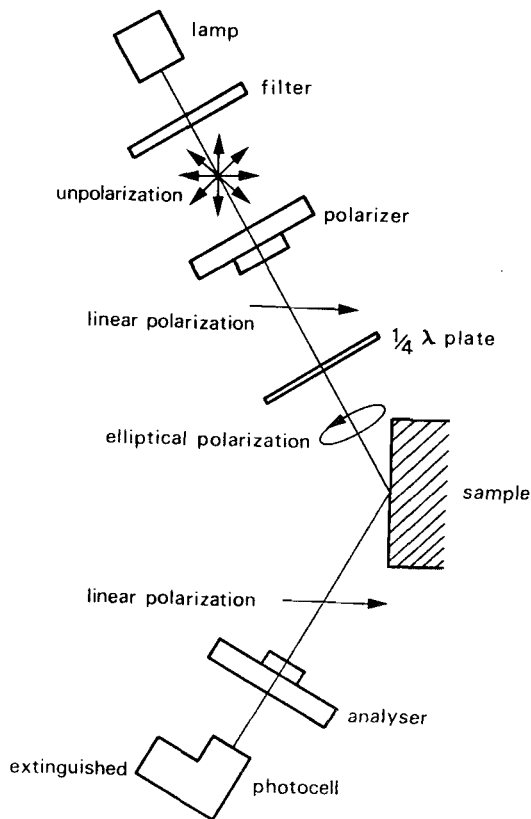


Fig. 15^a Schematic view of the ellipsometer.

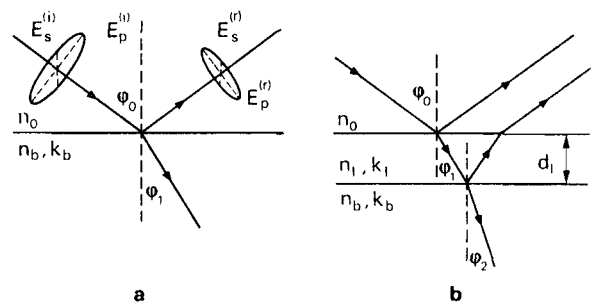


Fig. 15^b Schematic representation of the reflection of polarized light.

- a clean surface (one interface),
- b surface covered by a layer (two interfaces).

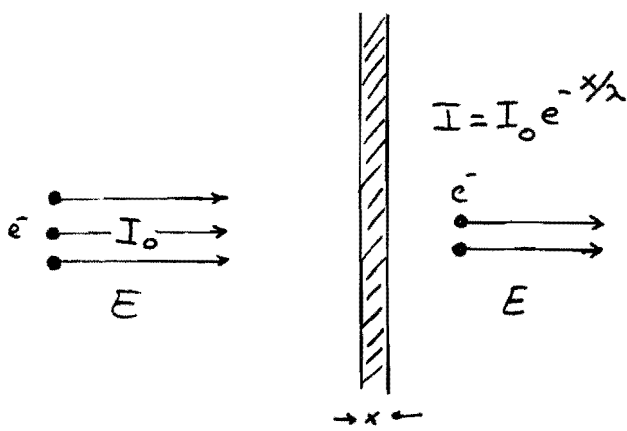


fig.1

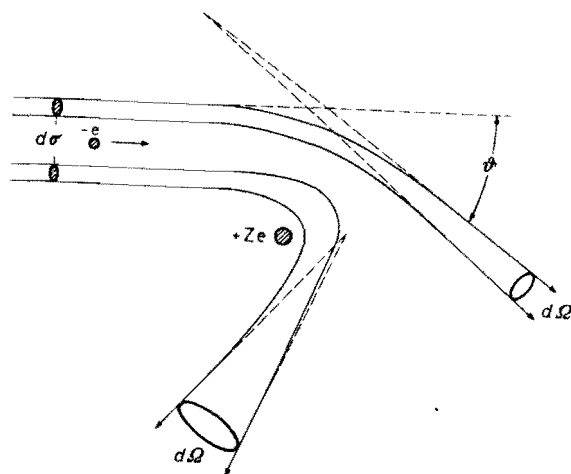


fig.2

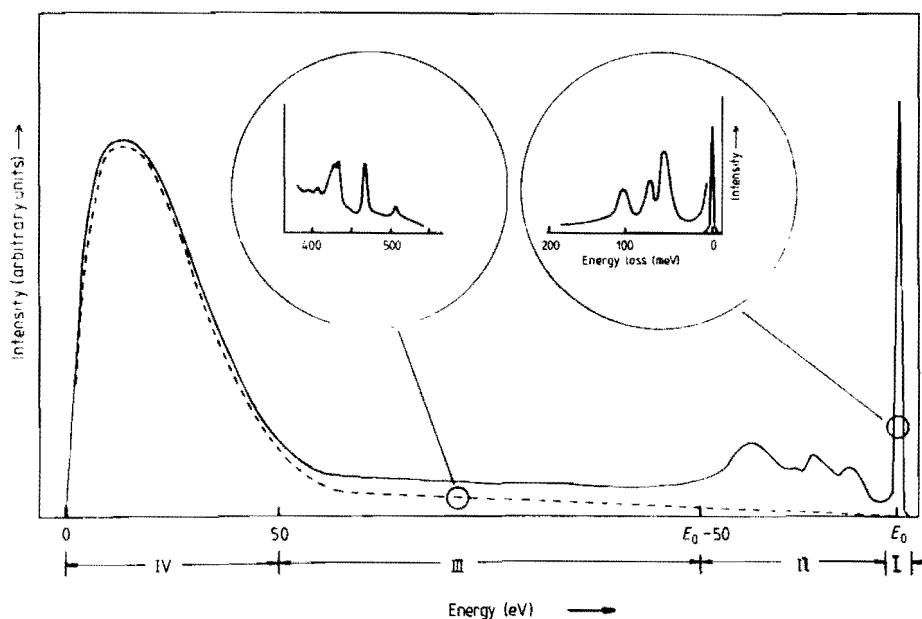


Figure 3. Spectrum of inelastic electrons. I, elastic peak of diffracted electrons; II, primary electrons having suffered from characteristic energy losses due to ionisation and electronic excitation; III, multiple-scattered primaries and secondaries including characteristic Auger electrons; IV, true secondary electrons (broken curve) from cascade processes. The inserts show Auger transitions and phonon losses, respectively. The angular distribution of the various contributions is quite different. The relative intensities therefore depend on the acceptance angle (from Ibach 1977).

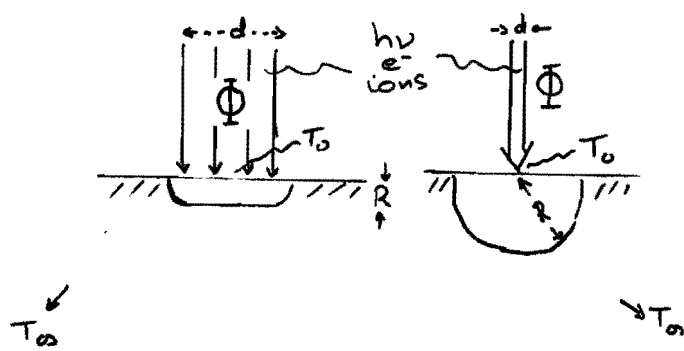


fig.4

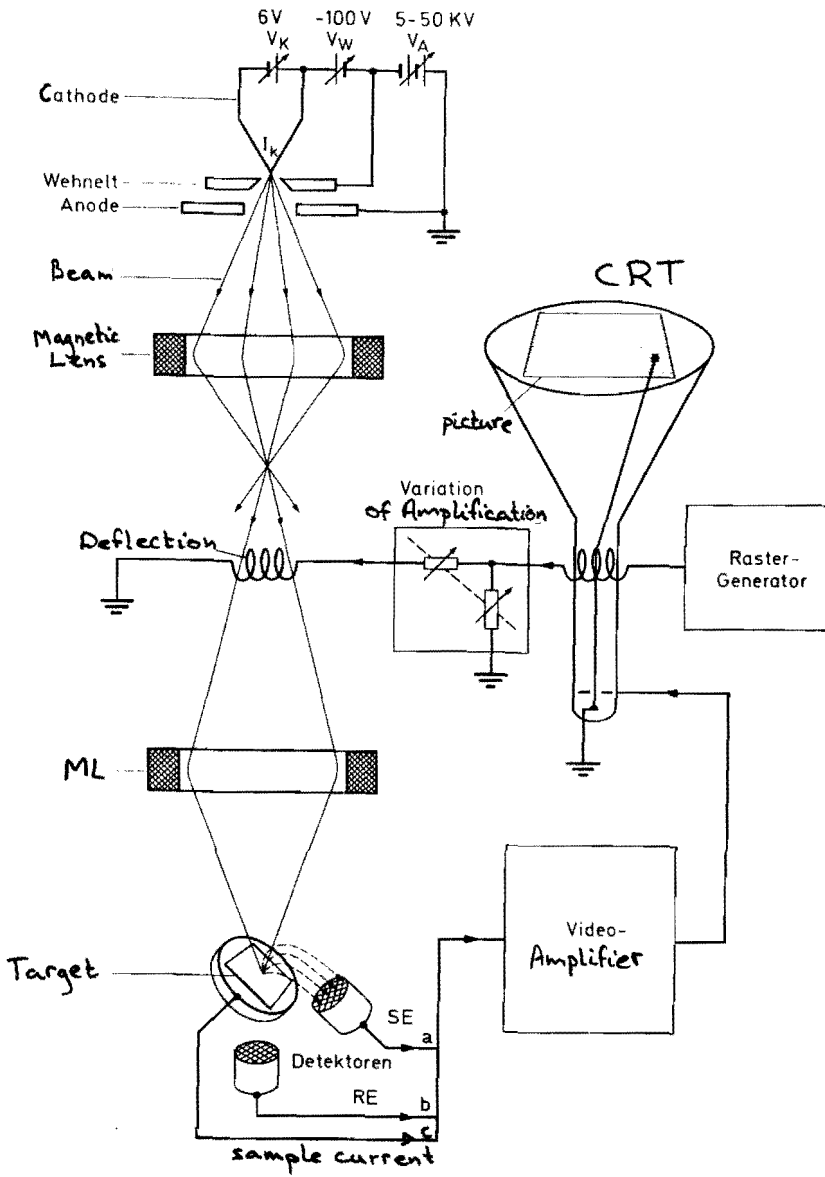


fig. 5

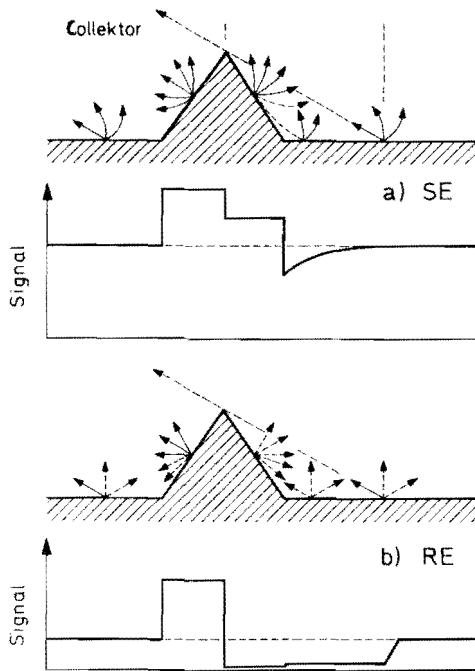


fig. 6

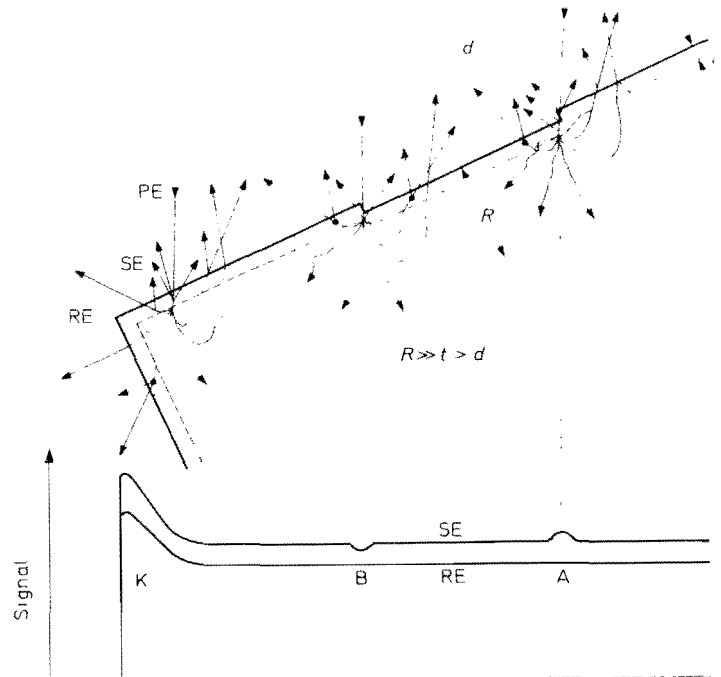


fig. 7

FIG. 8 Three kinds of electron spectroscopy. The one-electron energy-level diagrams at the top are for a mythical ideal free-electron metal. They are *not* drawn to scale. At the extreme left are the electronic configurations in which the letters s, p, d, f, ... signify electrons having orbital (angular momentum) quantum numbers 0, 1, 2, 3, ...; the numbers to the left of the letter denotes the principal quantum number of one orbit; the superscript to the right of the letter denotes the number of electrons in the orbit. At the extreme right are the labels for the orbitals used in X-ray spectroscopy.

The levels E_K , etc. correspond to the binding energies of the electrons measured from the vacuum level.

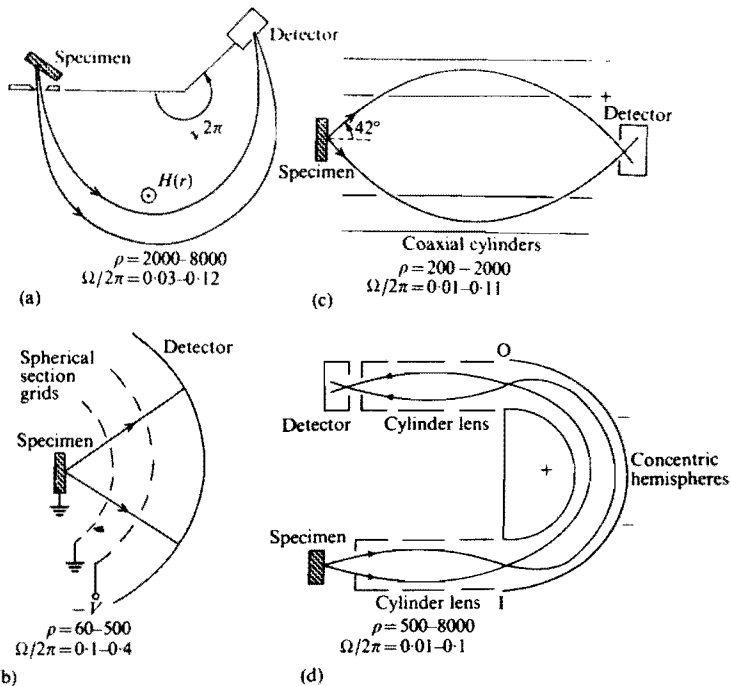
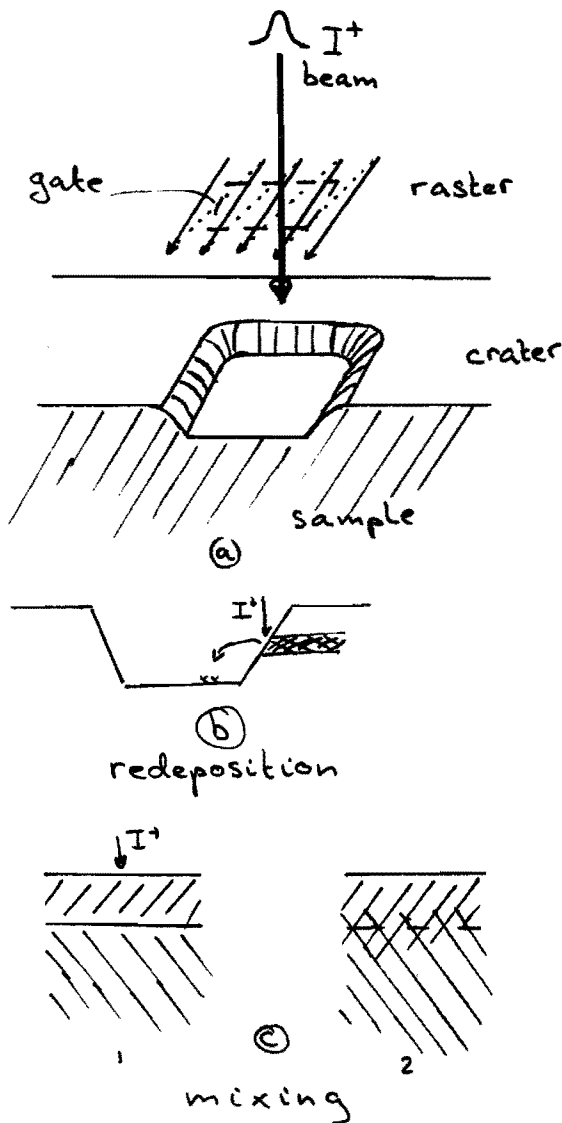
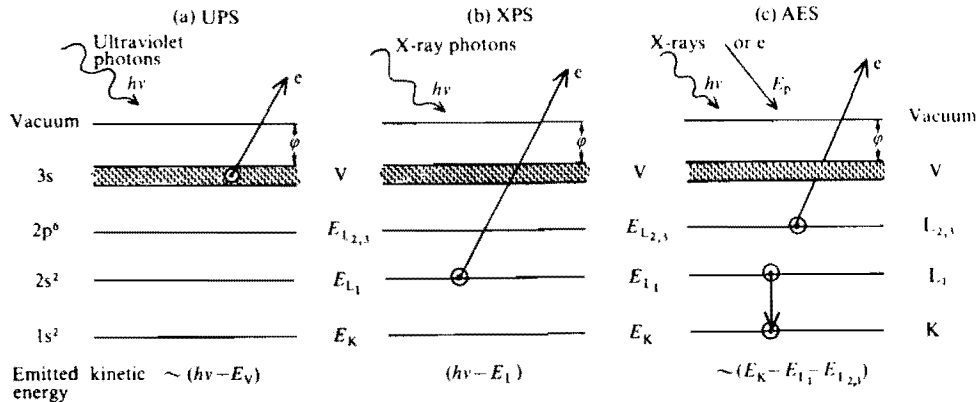


FIG. 9 Four methods of electron-energy analysis after photoemission or an Auger process. Typically accessible ranges of ρ and $\Omega/2\pi$ are indicated for each method. (a) The magnetic double-focusing spectrometer. Here the field H is made to be proportional to $r^{-1/2}$ for an electron trajectory of radius r . (b) The electrostatic retarding potential analyser. The potential $-V$ on the second grid results in electrons with kinetic energies greater than eV reaching the detector. The grids and detector are concentric spherical sections with their centre on the sampling surface and at the centre of the region of electron emission. (c) The electrostatic cylindrical mirror analyser (CMA). Appropriate potentials on the outer and inner cylinders result in electrons with a particular kinetic energy being focused at the detector aperture. (d) The electrostatic concentric hemispherical analyser (CHA). The electron source on the sample surface is focused onto the entrance aperture I of the analyser. With appropriate potentials on the inner and outer hemispheres electrons with a particular kinetic energy are focused on the output aperture O. The three-element output lens then focuses this image onto the (real) aperture of the detector.

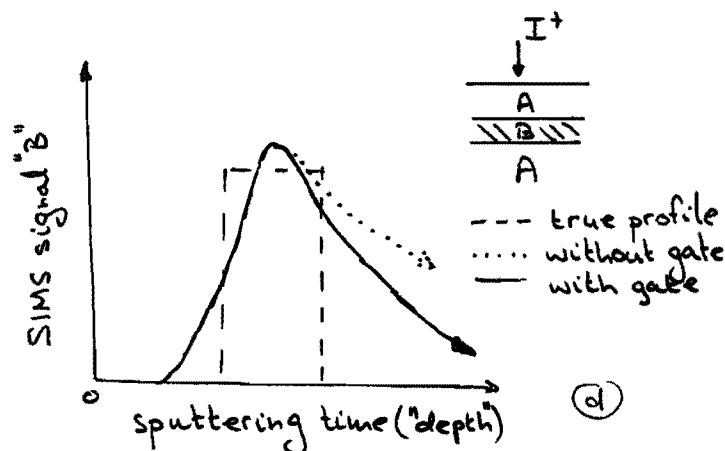


fig.10

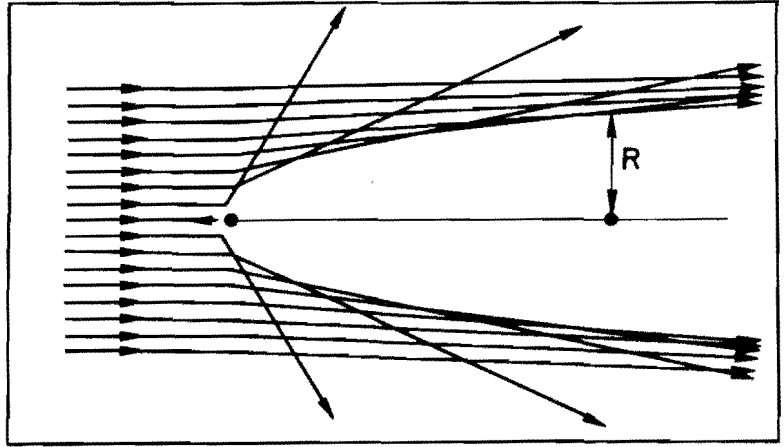
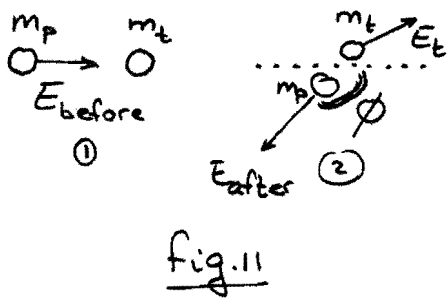


FIGURE 13 Formation of a shadow cone at the second of a pair of atoms aligned with an incident ion beam. The shadow cone radius at the second atom is denoted R.

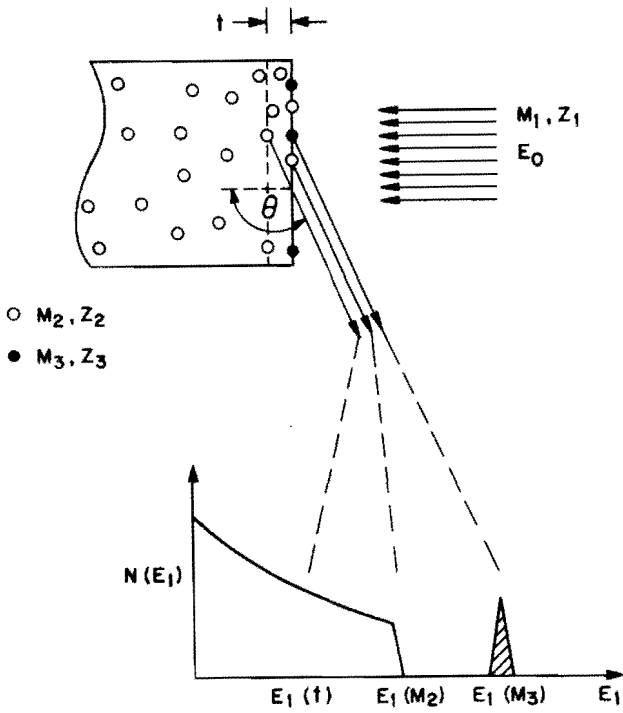


FIGURE 12 (a) Geometry for particles of incident energy E_0 , mass M_1 , and atomic number Z_1 scattering from a surface atom and an atom at depth t of a solid of mass M_2 , atomic number Z_2 , and a surface impurity of mass M_3 ($M_3 > M_2$) and atomic number Z_3 . (b) Energy spectrum of scattered particles with a peak of area Y , corresponding to the areal density of the species M_1 , and a continuum corresponding to scattering from various depths of the substrate.

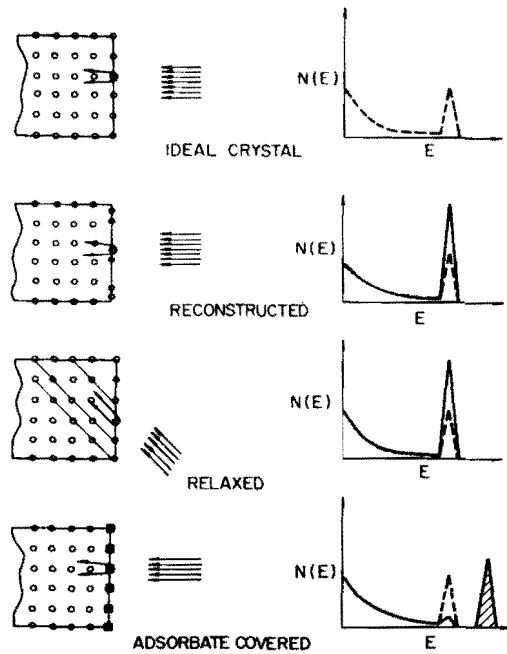


Fig. 14. Schematic of the dependence of the intensity of the SP on different crystal surface structures: (a) The ideal crystal SP from "bulk-like" surface; (b) enhanced SP observed in normal incidence for a reconstructed surface; (c) enhanced SP observed in non-normal incidence for a relaxed surface; (d) reduced SP observed in normal incidence for a registered overlayer.

6.3. Optical Spectroscopy

J.P.M. Schmitt

Dr. Jacques P.M. Schmitt, Director of research appointed by CNRS at the Ecole Polytechnique, Palaiseau, France. His principal areas of research include plasma deposition mechanisms, amorphous silicon and thin film photovoltaic devices.

OPTICAL SPECTROSCOPY IN REACTIVE PLASMAS**J.P.M. SCHMITT****Equipe de Synthèse des Couches Minces pour l'Energétique
LPNHE, Ecole Polytechnique - 91128 PALAISEAU Cedex, FRANCE.****I. INTRODUCTION**

Understanding plasmas is a challenging problem shared by many fields of research like astrophysic, nuclear fusion, gas lasers, spacial telecommunications, arc and lamp technology and fairly new but very active incomers : plasma chemistry and thin film technology. For him who has ever "seen" a plasma, light emission is the most obvious manifestation of the discharge and it already carries a very relevant information: whether the plasma is "on" or "off". Most scientists working at the improvement of any kind of process involving a plasma feel that a tremendous flow of information must be contained in this conspicuous light emission and that they should use it for the sake of understanding the rather impredecible behaviour of their plasmas.

Understanding and interpreting light emission from the plasma is all what the present paper is about. We will find that if indeed very relevant data are contained in plasma spontaneous emission it will not give an obvious answer to all of your problems, it will instead arise a new string of very arduous problems. The mere analysis of spontaneous light emission has indeed several intrinsic limitations which can be overcome with the help of new techniques where the interaction of the plasma with an external light source will provide new informations. This is the field of active spectroscopy which has become extremely successful with the availability of lasers.

All these spectroscopic techniques have two points in common, they need only one or two window ports in the plasma reactor walls and they are practically non perturbing for the discharge. Except for the most sophisticated active spectroscopy set up, these diagnostic tools require, in general, a limited amount of investment in hardware, however, since interpretation of the data can be very touchy, they are rather demanding in terms of human brain.

II - THE BASICS THAT YOU SHOULD KNOW.

There is no hope of doing anything serious in spectroscopy in general and plasma spectroscopy in particular unless you know your basics in quantum electronics. The following lines are not a substitute to the many text books where you can find the relevant knowledge, it is just a list of key words. You should make sure that these key words mean something clear to you before struggling with a plasma spectrum.

II-A - ATOMIC SPECTRA

Electronic states. Energy levels. Quantum number. Ground state. Ionization energy. Rydberg states. Fine and Hyperfine structure. Statistical weight. Stark and Zeeman effects.

II-B - MOLECULAR SPECTRA

Group theory. Rotator quantification. Harmonic oscillator quantification. Statistical weight. Molecular potential. Adiabatic dissociation energy. Molecular energy levels.

II-C SELECTION RULES

Coupling of an atom with radiation. Matrix element and oscillator strength. Selection rules. Vertical transition for molecules. Rotation and vibration selection rules. Metastable states.

II-D - THERMODYNAMICS AND RADIATION TRANSPORT

Spontaneous emission. Life time. Absorption and stimulated emission. Black body radiation. Einstein coefficients. Optical thickness. Boltzman law for rotation and vibration. Optical pumping.

II-E - LINE WIDTH

Natural width. Doppler, Stark and collisional broadening. Resonant trapping and broadening. Gaussian, Lorentz and Voigt profiles.

III - SPONTANEOUS EMISSIONIII-A - TECHNIQUES IN SPECTROSCOPYa - Window

The first step toward spectroscopy is to implement a window in the plasma system. One should be careful to

- keep a dark background or use an adapted reflecting system (not really recommended)
- use a window transparent in all the spectral range you are able to study with your detection system.
- adapt the optical aperture of your observation port to your monochromator.
- use one or two lenses to go toward your monochromator. One lens can be the vacuum window.

Problems can arise from plasma depositing non transparent films on the window. Possible solution are : i) place the window at the remote end of a long tubing, ii) protect the window by a disposable transparent film (possibly on a roller), iii) protect the window by a blanket of neutral gaz.

Monochromators can be very bulky and difficult to place near a reactor. A convenient way consists in using fiber optics as a long and flexible connexion (but UV is likely to be absorbed on the way).

b - Monochromators

The grating monochromator is today in the visible and near UV

range the best compromise for luminosity and resolution. One should make sure that the grating is well covered by the incident light. Practical resolution of a grating monochromator varies with the actual size of the apparatus. For most standard experiments a 50-70cm focal length monochromator will be appropriate. More ambitious experiments on molecular species or line width can require much larger systems.

Prism monochromator can still be of interest for system having a difficult optical access, hence a small geometrical aperture. Fourier transform spectrometers are interesting but available only for the infra red. Finally, interference filters cannot be used for scanning a spectrum but they are usefull for monitoring an interesting emission line during a process.

III-B - SPECTRA IDENTIFICATION

The analysis of the radiation emitted by a discharge will generate a spectrum. In a typical spectrum three types of components can be identified. Isolated strong lines (or multiplets) generally originate from single atoms (neutral or positively charged). Clusters of regularly distributed lines are band emission from molecular species. One band is associated to a given electronic and vibrational transition, the many lines correspond to the various rotational levels. Sometimes the string of lines in a given band turns back generating a peak of overlaying lines called a band head. Broad featureless spectrum can be a continuum emission or a molecular band spectrum where the individual lines are too close to be resolved. Continuum emission can have various origins: free electron collisions (brehmstrahlung), ion recombination (free bound) and molecular radiation involving a repulsive state.

Identifying the features of a given spectrum requires reference to spectroscopic data books [1] or shape recognition from an experienced spectroscopist. If you do not have this kind of books (or man) in your library you will find them in the nearest lab dealing with astronomy, molecular physics, gas lasers, quantum electronics, chemical analysis etc.... You will

first look for emission candidate made of a combination of the atomic elements which are introduced in the plasma : reactants, carrier gas, walls. If your spectrometer is sensitive you may have to identify also unexpected impurities.

III-C - MECHANISM FOR SPONTANEOUS EMISSION

The following pages will emphasize only the mechanisms of interest for low pressure plasma. In high pressure systems excitation and emission are often dominated by collisions and reabsorption effects that we will not consider here.

a - Typical orders of magnitude.

In low pressure plasmas the background neutral density ranges from $3 \cdot 10^{13}$ to $3 \cdot 10^{16} \text{ cm}^{-3}$. The density of charge depends on the volumic power dissipated in the system, it can vary from 10^8 to 10^{11} cm^{-3} . Hence the degree of ionization, except for a few extreme cases, remains below 10^{-3} . Similarly the degree of dissociation (concentration of chemically unstable radicals/concentration of stable background molecules) also remains below 10^{-2} .

In an electric discharge the energy is fed mostly to the free electrons. Fast electrons are then dissipating their kinetic energy by sustaining the ionization, exciting the background gas to various levels, and creating the expected chemical reactivity in the system.

b - Electron impact excitation

Except for some continuum emission, all plasma emissions originate from excited atoms and molecules decaying down to a lower state and emitting a photon. The basic excitation mechanism is the impact of a fast electron on a ground state stable species.



The cross section for this process is a function of the impact energy of the electron. If σ is the cross section, $f_e(v)$ the electron distribution function, the number of excitation events per unit time and unit volume is given by:

$$(2) \quad dN/dt = [\text{Ar}] [e] \langle \sigma |v| \rangle, \quad \text{with}$$

$$(3) \quad \langle \sigma |v| \rangle = \int f_e(v) \sigma(v) |v| d^3v / \int f_e(v) d^3v.$$

Electron can also excite non stable species. Most of the time there will be for a given emission several competing mechanisms leading to identical emission. For ionized argon emission for example



where Ar^M is for the metastable state of argon. The relative importance of the 3 channels will depend on the 3 cross sections and the 3 concentrations, $[\text{Ar}]$, $[\text{Ar}^M]$ and $[\text{Ar}^+]$. Common sense tells that in mild discharges $[\text{Ar}^M]$ and $[\text{Ar}^+]$ will remain relatively small and that channel (4) will dominate. For stronger plasmas one should look into the problem in details. Hopefully for rare gas, at least the cross sections for excitation are known. Unfortunately for most reactive plasma, only a very few cross sections are known.

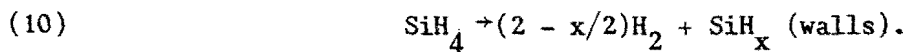
For molecules, electron impact can lead to simple excitation



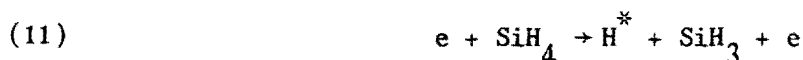
Above an energy threshold it can result in dissociative photoexcitation



It appears that in a molecular plasma a given emission can also have many possible origins. We give here the example of silane discharge depositing hydrogenated amorphous silicon with the overall reaction



The atomic hydrogen Balmer lines are observed in emission, they may originate from



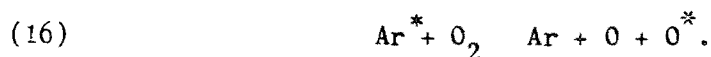
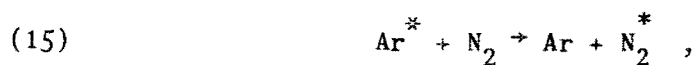
Depending on which process dominates, Balmer lines will tell something about the reactant SiH_4 , the by-product H_2 , or a reactive intermediate H . It takes sometime and careful experiments before a given channel can be demonstrated to be dominant. In the silane case, channel (11) is the most important except for systems at relatively low pumping rate where molecular hydrogen accumulates.

c - Other excitation mechanisms

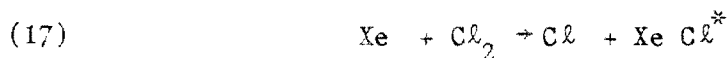
There are many excitation mechanisms beside electron impact. They tend to remain second order effects in low pressure plasmas but they are many exceptions

- Cascading. A given level can be populated directly by electron impact or indirectly by excitation of upper states and subsequent radiative cascading down to the level of interest. This effect is in general already included in the excitation cross sections in so far as they are measured via emission intensities.

- Excitation transfer. A long lived excited species (metastable) can collide with a second body and transfer its excitation



In general the cross section for such process is large when the transfer is "resonant", i.e. when energies are rather equal for both excited states. In the same family are reactive excitation transfers where a chemical reaction takes place along with the transfer. This mechanism is the most important step in excimer lasers



- Chemiluminescence. In some case the stored energy providing emission is not initially on an electronic state (metastable) but merely chemical energy delivered during an exothermic reaction



- Optical pumping. An atom or a molecule can also experience the reverse process of emission



In low pressure plasma the probability for a photon emitted in the plasma to be reabsorbed is very low except, possibly, for resonance lines. Therefore optical pumping will be a relevant mechanism only when the photons are provided by a tunable laser for an active spectroscopy experiment.

d - Spontaneous emission and quenching

Except for metastable states, atoms and molecules after excitation will radiatively decay down to lower levels. The probability for one particle on state u (upper) to decay toward state ℓ (lower) is expressed in terms of a frequency $A_{u\ell}$, which is inversely proportional to the transition oscillator strength and matrix element. If at time $t = 0$, a number N_0 of particles are placed on state u , and if the medium is optically thin (no photon reabsorption) and non collisional then the average number of state u will vary as

$$N_u = N_0 \exp -(\sum A_{u\ell})t \quad ,$$

where the sum is for all states below u .

Collisions with a background gas may shorten the u state life time, via non radiative deexcitation or excitation transfer. This effect is named quenching and can be described by a frequency proportional to the background gas pressure. Quenching becomes in general important for pressure of the order of one Torr.

e - Coronal equilibrium

In low pressure plasma chemistry, excitation transfer and quenching can often be ignored. Emission is then described by the coronal equilibrium (from the sun corona) =

- 1 The majority of the species are at the ground state.
- 2 The only excitation mechanism is electron impact.
- 3 The only deexcitation channel is spontaneous emission.

This model is far to be universal but should be the first try in an attempt to model a low pressure plasma.

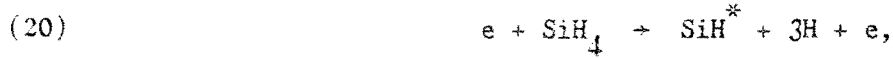
III - D WHAT CAN BE KNOWN FROM EMISSION SPECTROSCOPY ?

a - Qualitative informations.

If a given impurity is identified in an emission spectrum, this represents in itself a valuable information [2] . Turning this into a quantitative data can become a challenging problem. However if the impurity is really a minority component and does not influence any of the plasma parameters, the amplitude of the impurity related emission will vary proportionally to the impurity concentration if the rest of the plasma conditions are kept constant. This will allow, for example, comparaison of process gases of different origin

b - Silane discharge

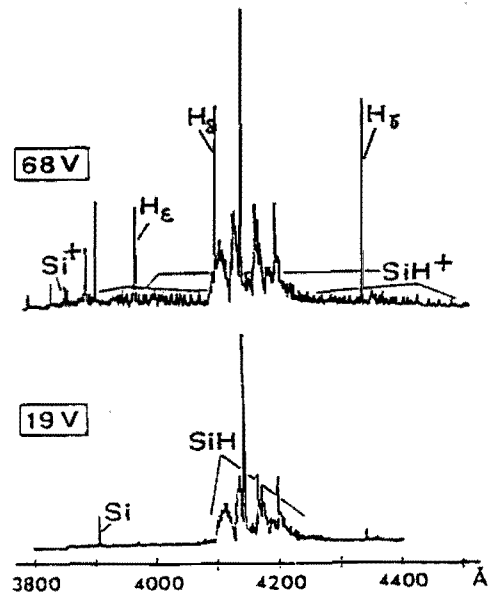
In a low pressure silane DC glow discharge, the only emission mechanism was demonstrated to be [3]



The relative amplitude of the 5 channels depends on the electron energy according to the detailed cross section. Two spectra are shown for two different electron energy and it appears clearly in Fig. 1 that Balmer lines and Si lines become visible above the SiH band system only for high energy electron impact [3] . Here the relative amplitude of the lines will provide informations on the electron energy distribution. This is a quite general

observation that emission from highly excited species (ion lines) is the indication of the presence in the discharge of energetic electrons.

Figure 1. These two spontaneous emission spectra were recorded from the same silane plasma except for the energy of the active electrons which here varies from 68 to 19 eV. The drastic variation of the spectrum arises from the fast variations of the dissociative excitation cross section with electron energy.



It was demonstrated that H₂ emission cannot arise from direct electron impact on SiH₄. Then the detection of H₂ triplet band in a silane plasma emission spectrum is the signature of a background pressure of hydrogen (a by-product of silane decomposition). Then the emission of the Balmer lines could arise from reactions 11-12 and possibly 13. A relative concentration for H₂ and SiH₄ could be deduced from the spectrum analysis but it relies on the knowledge of the excitation cross sections and the electron energy distribution.

c - Actinometry

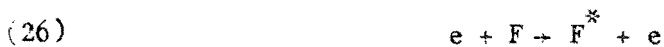
We will give here an example of this popular technique based on

coronal equilibrium. The problem was to monitor the atomic fluorine concentration in a CF_4 based etching system. The technique consists in seeding the discharge with a small amount of non perturbing gas such as Argon. One fluorine and one Argon atomic lines are carefully selected. The emission intensities $I(\text{F})$ and $I(\text{Ar})$ are measured. Finally the atomic fluorine concentration is assumed to be proportional to

$$(25) \quad F \sim [\text{Ar}] * I(\text{F})/I(\text{Ar})$$

They are several touchy points to be checked before actinometry can be trusted.

1. The emission from F should be dominated by the sole channel



excluding competing mechanisms such as



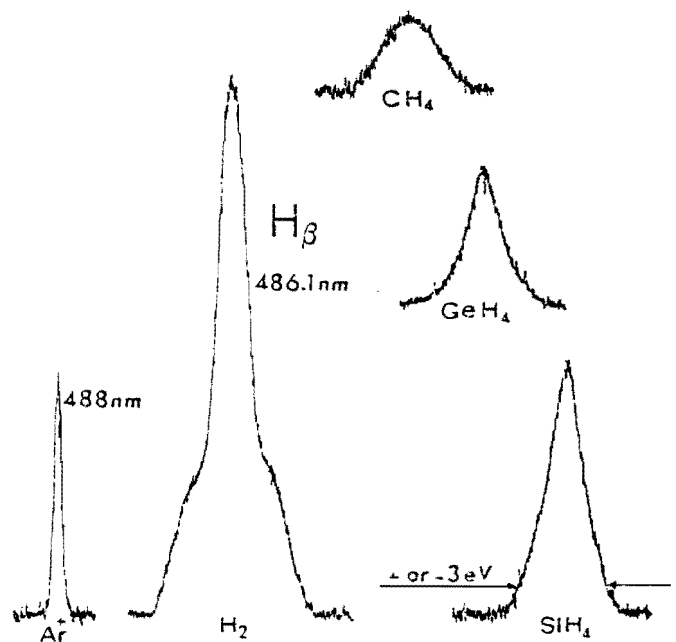
2. Argon emission should be dominated by the sole channel (1) excluding excitation transfer or metastable excitation.
3. The two lines should be selected to origin from levels with very similar excitation cross sections. Since, very often, cross sections are unknown the selection has to be based on theoretical considerations.
4. If experiments at different pressures are to be compared, quenching should be excluded or assumed to be similar for both levels.

Despite this rather discouraging list they are several convincing examples [4, 5] , where actinometry was successfully used in plasma chemistry.

d - Line shape

Measuring the line width and profile of an emission line is, in general, beyond reach of a non specialized laboratory. Only very long monochromator or Perot-Fabry can achieve a sufficient resolution. In principle, in low pressure plasma chemistry, emission line width is dominated by Doppler broadening, hence it gives access to the gas kinetic temperature. However if the radiative species origin from a molecular dissociation as in (8, 11, 12, 27) it will have a large excess kinetic energy related to the molecule repulsive electronic state [6] .

Figure 2. Profile of the atomic hydrogen Balmer line H_{β} as measured from Hydrogen, Methane, Germane and silane plasmas. A narrow Argon line is shown to give the resolution. The broadening in this case is due to large kinetic energy of the excited hydrogen atoms originating from a molecule dissociation.



Finally, for very strong plasmas ($[e] \sim 10^{12} \text{ cm}^{-3}$), the Stark broadening may become very effective for some species (atomic hydrogen) and allows a measurement of the electron density .

IV - ACTIVE SPECTROSCOPY.

IV-A WHY ACTIVE SPECTROSCOPY ?

The main limitation of passive spectroscopy is that only excited species are observed in emission while the majority of the particles are actually on their ground state. The relation between ground state and the electronically excited levels is very often quite obscure and finally through spontaneous emission spectroscopy very little is known about the major constituents of the discharge. Active spectroscopy will use an external source which will give access to the ground state level. Then either the absorption of the light source, the fluorescence induced by absorption or the Raman scattering will provide information on the ground state species. Active spectroscopy in general requires equipment by far more expensive than simple emission spectroscopy but in many cases the possibilities are worth the investment.

IV-B ABSORPTION SPECTROSCOPY

A monochromatic source illuminates the plasma. If the source wave length corresponds to an allowed transition between the ground state and an excited level of a given species part of the light will be absorbed. A measurement on the absorption will give access to the species density averaged along the optical path. For the external source two techniques are possible using either a tunable laser when possible or an auxiliary discharge where the same species emit the appropriate resonant line. Three points make absorption spectroscopy not as easy or universal as it would seem at first.

1. For many species the lowest energy resonant transition is in the far UV. Then tunable lasers are not available and the experimental technique becomes difficult : special window, evacuated system.
2. In the quantitative evaluation of the target species density enters the transition oscillator strength (not always tabulated) and the exact line shape of both the source and the plasma absorption which should be measured (difficult) or estimated.
3. The major drawback is that absorption is not very sensitive. It depends on the oscillator strength but detecting a target species at a density level of the order of 10^{12} cm^{-3} in a 20cm thick plasma already requires quite sensitive techniques. In most low pressure process plasma the ion density is in the $10^9 - 10^{11} \text{ cm}^{-3}$ and the unstable radical typical density is of the same order.

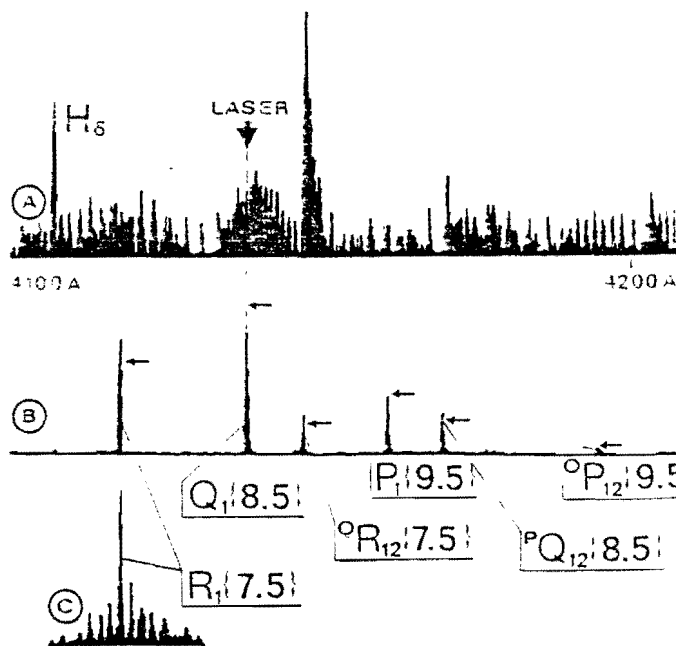
As a consequence of the three above mentioned points the absorption techniques have a very limited field of application in low pressure plasma diagnostic. Some spectacular progress were made recently by increasing the absorption detection sensitivity, one consists in frequency modulating a narrow line tunable laser and detecting the second harmonic by look in technique while slowly sweeping across the absorption line [7]. The second uses two non linear crystals for generating side bands of a laser lines and by remixing of the bands detects any disymmetry arising from absorption [8]. Another consists in introducing the absorbing medium within the cavity of a laser [9]. All these techniques are very promising but so far they require sophisticated equipment and know how.

IV-C LASER INDUCED FLUORESCENCE

The basic scheme of LIF is quite simple. A light beam of the appropriate wave length is absorbed by a target species and pumps up a resonant transition. Then the excited species will decay via the various possible radiative channels. A LIF experiment consists in detecting the fluorescent light resulting from these deexcitation transitions. Achieving sensitivity will require:

1. Isolate well the observation lines from any stray light from the laser. This implies good optical alignment and use of diaphragms and light dumps. If necessary the rejection can be achieved by a monochromator or an interference filter.
2. Discriminate the plasma spontaneous emission from LIF either by chopping a DC laser and lock in detection or better by using a pulsed laser and detecting the temporal decay of fluorescence. A good part of the plasma spontaneous emission can also be separated by using a monochromator in order to restrict the detection to the sole transitions likely to be fluorescent.
3. If possible increase the laser intensity. however, here exists a limit, indeed optical pumping saturates when it becomes compensated by stimulated emission induced by the laser pump itself.

Figure 3. Example of laser induced fluorescence on the free radical SiH. Spectrum A is the spontaneous emission of the excited state of SiH in the plasma. The laser is tuned to overlap one line. Spectrum B is the fluorescence light emitted during 200ns after the laser pulse. B is measured at low pressure (0.3 Torr) C shows the collisional rotation transfer.



In general, LIF can achieve rather outstanding detection level, the observation of a single ion in a multipole trap was recently achieved; practical sensitivity for plasma is in the range 10^6 - 10^9 cm^{-3} . The major drawback for LIF is its limitation to species only accessible to tunable laser, hence excluding all atoms, ions or radicals having all their resonant lines in the far UV. Two other difficulties can alter the sensitivity and the feasibility of LIF : i) collisional quenching becomes important when the pressure reaches the Torr range, LIF is then damped due to competing collisional mechanisms, ii) for molecules or radicals, the excited electronic levels are sometimes unstable due to coupling with repulsive states. In that case LIF is damped due to competing dissociative channels.

When the appropriate laser exists LIF is a very good diagnostic tool for detecting reactive species in low pressure plasmas. It is a local measurement allowing spatial scanning of a reactor. When using a pulsed laser it is also a time resolved measurement allowing the analysis of a post discharge [10]. Relative density measurements are fairly easy, turning the data into absolute measurements is feasible but generally implies enough work to justify a PHD.

Extending the possibilities of LIF by all sorts of sophisticated means is a constant drive for research. Multiphoton optical pumping gives access to far UV resonant transitions, but it requires very powerful pulsed laser. This technique allows identification of fairly large molecule which, after multiphoton photodissociation, can be detected by the fluorescence of some of the resulting excited molecular fragments. The target species resonant absorption can also be detected by other techniques. In opticalgalvanic spectroscopy a variation of the discharge electric parameter is detected as a signature of the transfer of optical pumping energy toward ionisation and electron temperature. In photoacoustic spectroscopy the signature is detected by a microphone or a probe laser deflection, as a consequence of the energy transfer to the gas kinetic temperature. So far, all these advanced techniques are mostly contributing to research in gaseous electronics, but it is only in specific cases that they can be used in low pressure plasma processing.

IV-D RAMAN SPECTROSCOPY

This technique is restricted to molecules. In this case the external source is monochromatic but is not in resonance with an electronic transition of the molecule. The interaction of the incident beam with the molecule can give in first place the classical Rayleigh scattering where the polarisability of the target induces scattering of photons with similar energy as the incident beam. Raman scattering is an other possible process where the scattered photon energy is modified by plus or minus rovibrational quanta, and the scattering center is left with the corresponding modification of its rovibrational excitation. The selection rules for Raman scattering are different from those for direct radiative coupling of the rovibrations with infra-red. The scattered light from a medium appears as a Rayleigh line with red and blue shifted Raman side bands. The red shifted band, the Stokes lines, have a much larger intensity than the blue shifted or anti-Stokes lines. The major problem with Raman scattering is that the cross section is very small. Due to its sensitivity, Raman scattering is well adapted to liquid, but is by far not sufficient for low pressure plasma diagnostic.

The sensitivity greatly improves with CARS or coherent anti-Stokes Raman Spectroscopy. In this technique a tunable laser is added to the main laser. The two beams are focussed and overlapped in the plasma. The tunable laser is tuned to pump a Stokes line, due to non linearity in the molecule polarisability the corresponding anti-Stokes line is coherently pumped. The signal amplitude is proportionnal to the square of the main laser intensity and the target density and directly proportional to the tunable laser intensity. CARS is capable of detecting target density of the order of 10^{11} cm⁻³.

Such a sensitivity makes CARS of marginal interest in low pressure plasma (considering the equipment involved) but CARS becomes extremely attractive in plasma chemistry of flames in the atmospheric range of pressure because; it is a local measurement allowing the identification and the mapping of fairly complex molecules and their temperature [11].

REFERENCES

- [1] HERZBERG G. Spectra of diatomic molecules (Van Nostrand, New-York 1950).
MSU D.K. et Smith W.H. Spectroscopy Letters 10 (1977) 181.
Pearse. Gordon. The identification of molecular spectra (Chapman and Hall,
New-York 1965). Moore C.E. Atomic energy levels. Vol. 1.2.3. (N.B.S.
Washington 1949).
- [2] KAMPAS F.J., GRIFFITH R.W., Solar cells 2 (1980) 384. GRIFFITH R.W., KAMPAS
F.J., VAMIER F.E. and HIRSH M.D., J. Non Cryst. Solids 35-36 (1980) 391
- [3] KAMPAS F.J. and GRIFFITH R.W., J. Appl. Phys. 52 (1981) 1285. DE ROSNY G.
MOSBURG E.R., ABELSON J.R., DEVAUD G. and KERNS R.C., J. Appl. phys. 54
(1983) 2272. PERRIN J. and SCHMITT J.P.M., Chem. phys. 67 (1982) 167.
- [4] MOGAB C.J., ADAMS A.C. and FLAMM D.L., J. Appl. Phys. 49 (1978) 3796.
- [5] GOTTSCHO R.A. and DONNELLY V.M., J. Appl. Phys. 56 (1984) 245. D'AGOSTINO
R. CRAMAROSSA F., COLAPRICOV and D'ETTOLE R. , J. Appl. Phys. 54 (1983)
1284. COBURN J.W. and CHEN M., J. Appl. Phys. 51 (1980) 3134.
- [6] PERRIN J. and SCHMITT J.P.M., Chem. Phys. Letters 112 (1984) 69.
- [7] REID J., SCHERCHUN J., GARSIDE B.K., and BLIK E.A., Appl. Opt. 17 (1978)
300. DEJOSEPH C.A., GARSCADDEN A. , and POND D.R., Proceedings of the
Int. Conf. on lasers "82". Dec. 13-17 (1982).
- [8] BJORKLUND, Opt. lett. 5 (1980) 15. JASINSKI J.M., WHITTAKER E.A.,
BJORKLUND G.C., DREYFUS R.W., ESTES A.D. and WALKUP R.E., Appl. Phys.
Lett. 45 (1984) 372.
- [9] SCHMITT J.P.M., GRESSIER P., KRISHNAN M., DE ROSNY G. and PERRIN J., Chem.
Phys. 84 (1984) 281. ROTH R.M. , SPEARS K.G. and WONG G., Appl. Phys. lett.
45 (1984) 28. DONNELLY V.M., FLAMM D.L., COLLINS G. J. Vac. Science Techn.
21 (1982) 817.
- [10] HATA N., MATSUDA A., TANAKA K., KAJIYAMA K.? MORO N. and SAJIKI N., Jpn, J.
Appl. Phys. Lett. 22 (1983) 1.

7. SURVEY OF APPLICATIONS IN PLASMA ETCHING AND PLASMA DEPOSITION;
PLASMA-SAFETY CONSIDERATIONS

Dr. G. Kenneth Herb is distinguished member of technical staff at AT & T Bell Laboratories, Allentown, Penn., USA. His expertise is in VLSI process technology, particularly plasma technology, metallization and reliability analysis for VLSI circuits.

APPLICATION OF PLASMA ETCHING AND DEPOSITION TO MICROELECTRONIC DEVICES

COPYRIGHT © 1985

BY

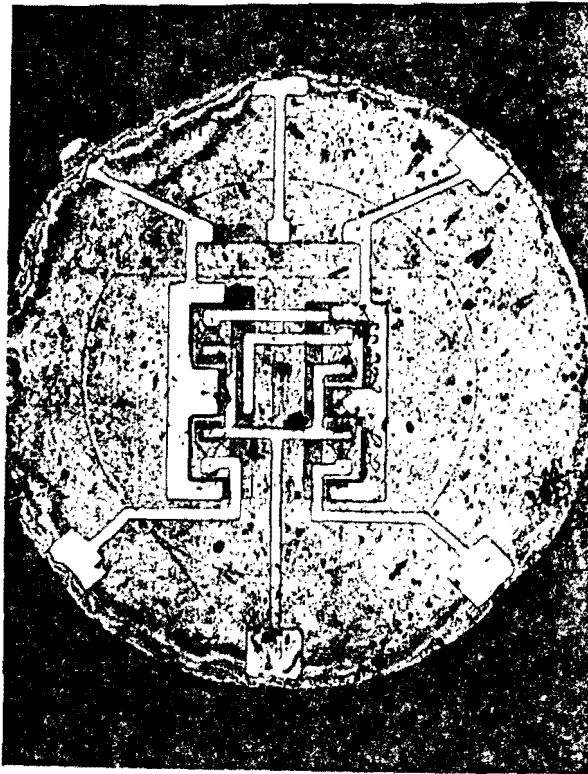
**G.K. HERB
AT&T BELL LABORATORIES
555 UNION BLVD.
ALLENTOWN, PA. 18103
(215) 439-7844**

OUTLINE

- A. HISTORY
INTEGRATION SCALE
WET PATTERN LIMITATIONS**
- B. DRY PATTERN CHARACTERISTICS
TYPICAL VLSI TECHNOLOGY**
- C. DRY PROCESS DEVICE DAMAGE**
- D. PLASMA DEPOSITION**
- E. PLASMA PROCESS EQUIPMENT**
- F. CONCLUSIONS - CAVEATAE de PLASMUS**

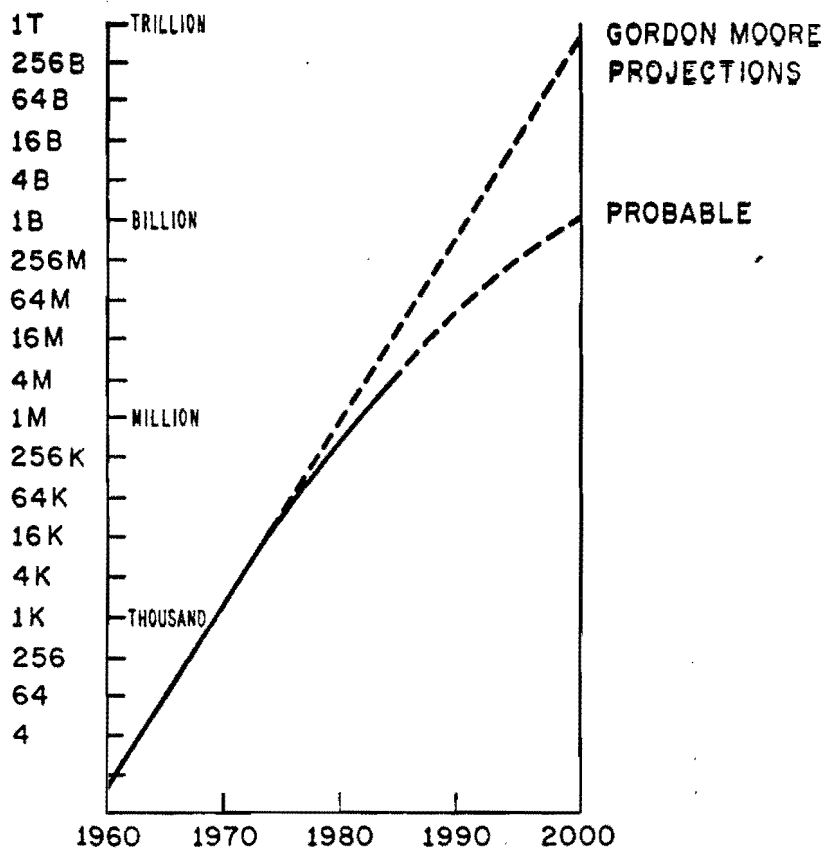


Bell Labs' first transistor, 1947, magnified two times

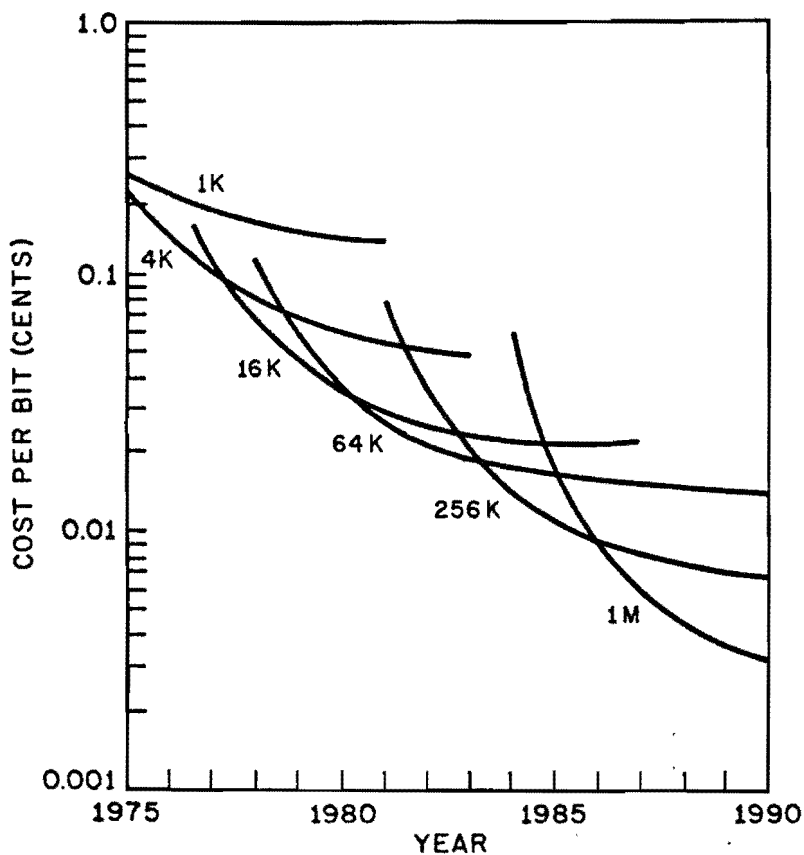


Fairchild Camera's First "IC", 1961, Magnified 1,000 Times

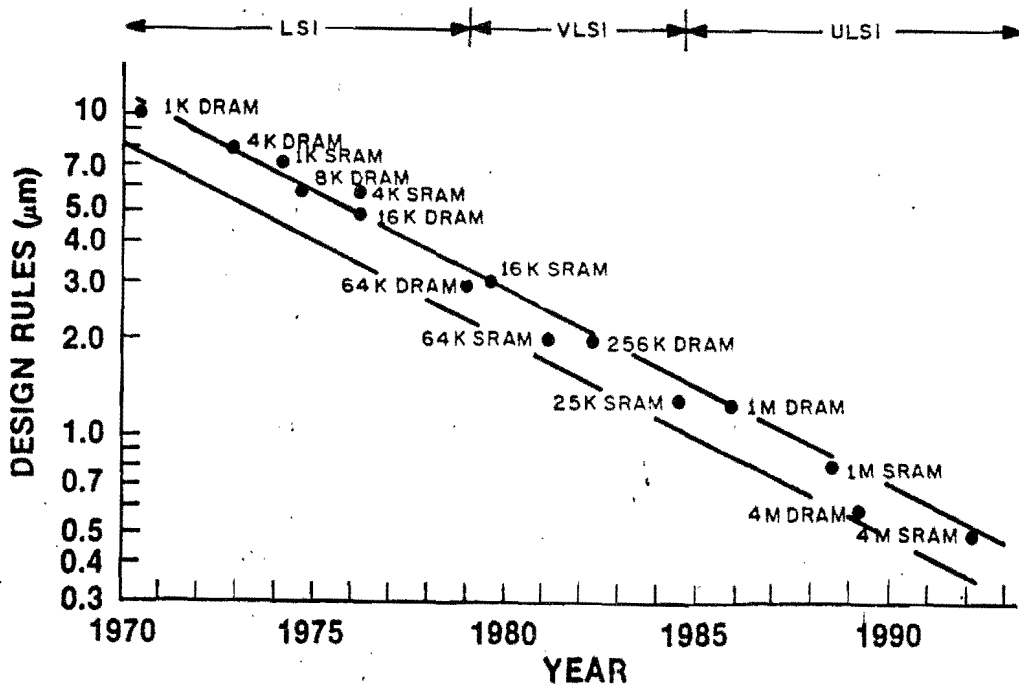
NUMBER OF COMPONENTS PER CIRCUIT



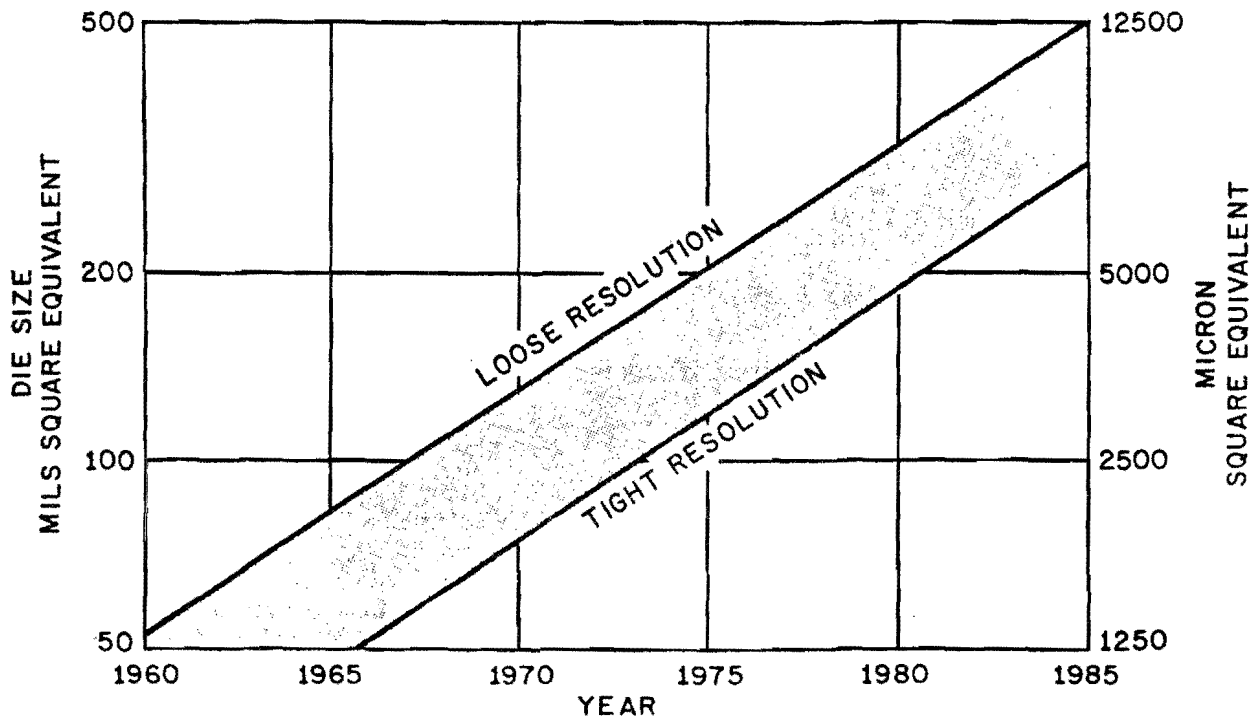
MEMORY IC LEARNING CURVES



PREDICTION OF CMOS STATIC (RED) AND DYNAMIC (BLUE) RAM DESIGN RULES THROUGH THE 1980's (TOBEY, MMT 1985)



MOS DIE SIZE vs TIME



HIGH DENSITY PROCESS WAFER FABRICATION TRENDS (NEW FACILITY AT START-UP)

CHARACTERISTIC	1980	1981	1982	1983	1984	1985
FEATURE SIZE (LOOSEST-MICRONS)	5.0	4.0	3.5	3.0	3.0	2.5
FEATURE SIZE (TIGHTEST-MICRONS)	2.0	2.0	1.5	1.5	1.0	0.7
ALIGNMENT (TIGHTEST OVERALL FIT-MICRONS)	1.0	1.0	0.7	0.5	0.3	0.2
WAFER SIZE (% 100mm/% 125mm)	99	97	95	90	80	60
MASKING STEPS (MINIMUM)	5 + 1	5 + 1	6 + 1	6 + 1	6 + 1	6 + 1
MASKING STEPS (MAXIMUM)	10 + 1	10 + 1	11 + 1	11 + 1	12 + 1	12 + 1
DIELECTRIC THICKNESS (MINIMUM-Å)	400	400	350	300	200	150
JUNCTION DEPTH (MINIMUM-MICRONS)	0.4	0.4	0.3	0.3	0.2	0.2
DEFECT/cm ² (MINIMUM)	3	2	1.5	1.5	1	1
DIE SIZE (MAXIMUM-MILS SQUARE)	300	350	400	430	460	500

HYPOTHETICAL HMOS PROCESS (SIMPLIFIED)

EQUIPMENT USED

PROCESS STEP	EQUIPMENT USED							
	FURNACE HIPOX	FURNACE LPCVD	FURNACE	ION IMPLANT	PHOTORESIST	DRY PLASMA	WET CHEMISTRY SPUTTERING	
GROW THIN OXIDE	X							
DEPOSIT NITRIDE		X						
CONDITION NITRIDE	X							
MASK #1-DEFINE FIELD				X				
PATTERN NITRIDE					X			
IMPLANT FIELD-BORON			X					
REMOVE RESIST						X		
OXIDIZE FIELD	X							
REMOVE NITRIDE					X			
REMOVE OXIDE						X		
MASK #2-DEPLETION DEVICES				X				
IMPLANT ARSENIC			X					
REMOVE RESIST						X		
GROW GATE OXIDE	X							
MASK #3-BURIED CONTACTS				X				
ETCH OXIDE						X		
DEPOSIT POLYSILICON			X					
MASK #4-POLY/GATE				X				
ETCH POLY					X			
ETCH OXIDE						X		
OXIDIZE POLY	X							
IMPLANT ARSENIC SOURCE/DRAIN			X					
DEPOSIT SILOX			X					
MASK #5-CONTACTS				X				
ETCH CONTACT HOLES						X		
REFLOW/DIFFUSE POCL.	X							
ETCH TO CLEAR CONTACTS						X		
DEPOSIT ALUMINUM							X	
MASK #6-METAL				X				
ETCH METAL						X		
ANNEAL (H ₂)	X							
DEPOSIT GLASSIVATION		X						
MASK #7-PADS				X				
ETCH PADS						X		
SUMMARY TOTALS	1	6	4	3	7	3	9	1

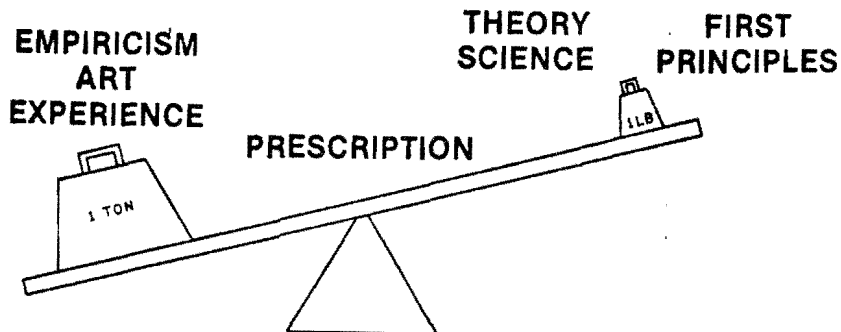
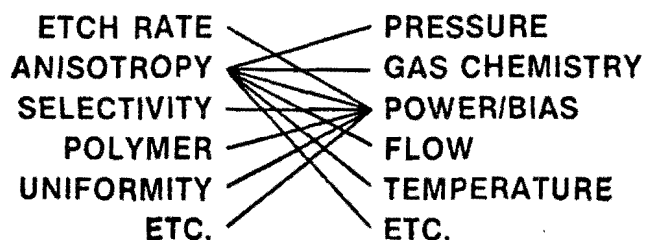
PATTERN TRANSFER PROCESS

	<u>WET</u>	<u>DRY</u>
• RESIST LIFTING - CAPILARITY	YES	NO
• ISOTROPIC ETCH	SEVERE	MODERATE TO NONE
• OVER-ETCH ALLOWED	NO	YES
• SURFACE TENSION - NO ETCH	YES	NO
• QUANTITY OF HAZARDOUS MATERIAL	LARGE	SMALL TO NONE
• AUTOMATED PROCESS	?	YES
• FEATURE ASPECT RATIO	$\geq 5:1$	$< 4:1$

DRY PATTERN PROCESSING

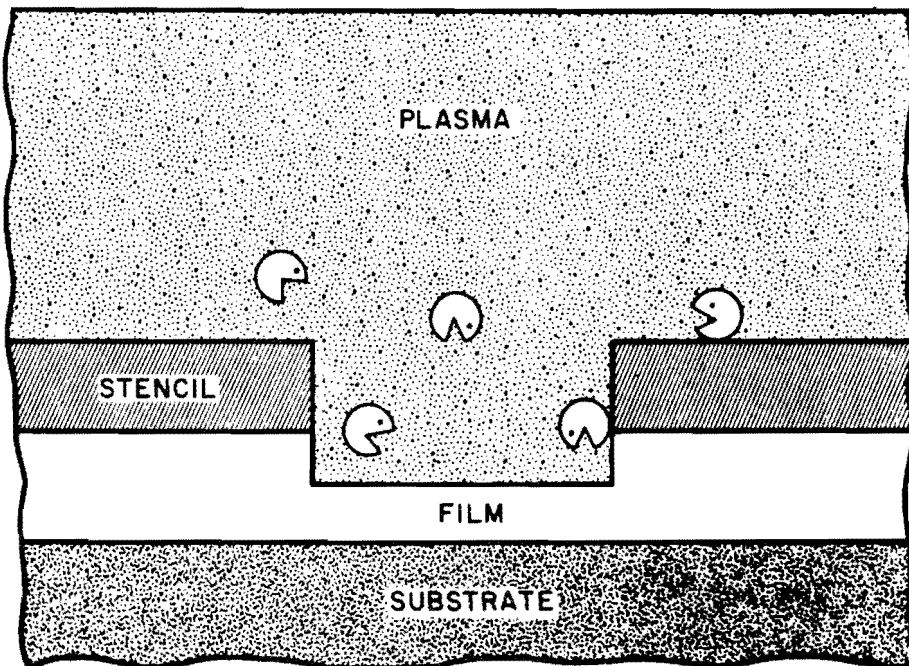
FUNDAMENTALLY FINEST ENGRAVING
TOOL IMAGINABLE BECAUSE OF
ATOMIC-SCALE ETCHANT SPECIES

PROCESS PARAMETERS SYNERGISTICALLY
RELATED TO SYSTEM CONTROLS.

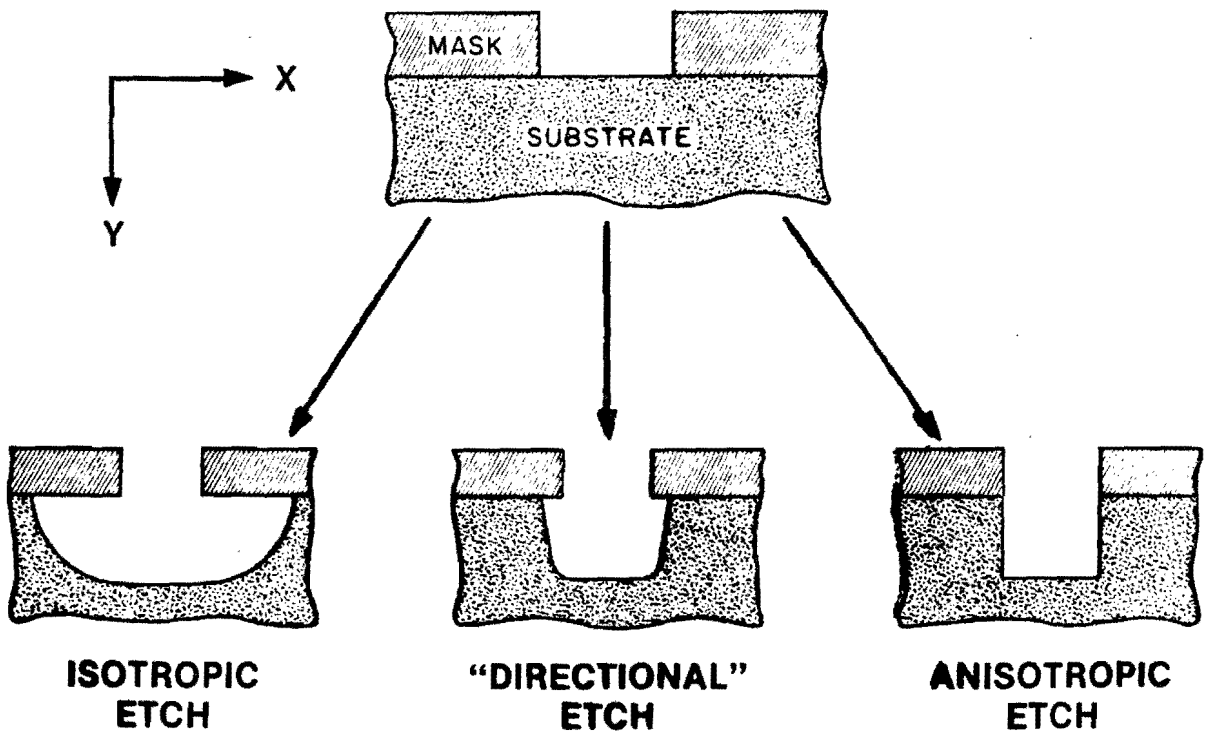
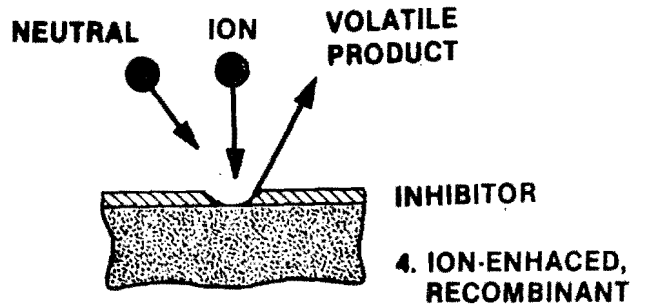
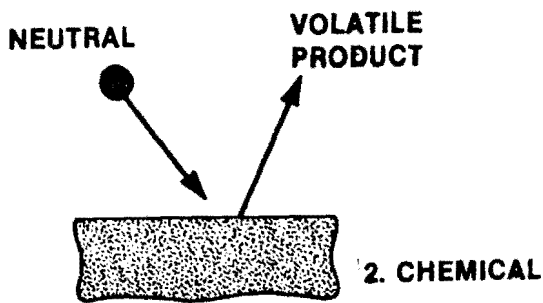
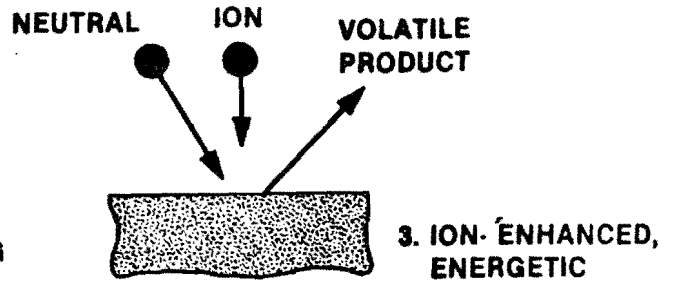
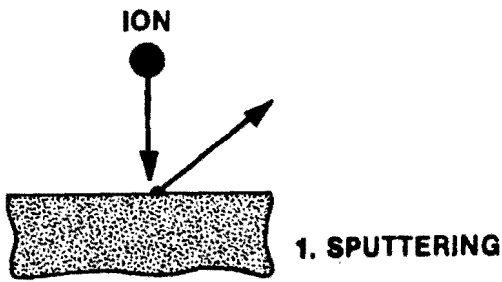


PLASMA PROCESS CONTROL

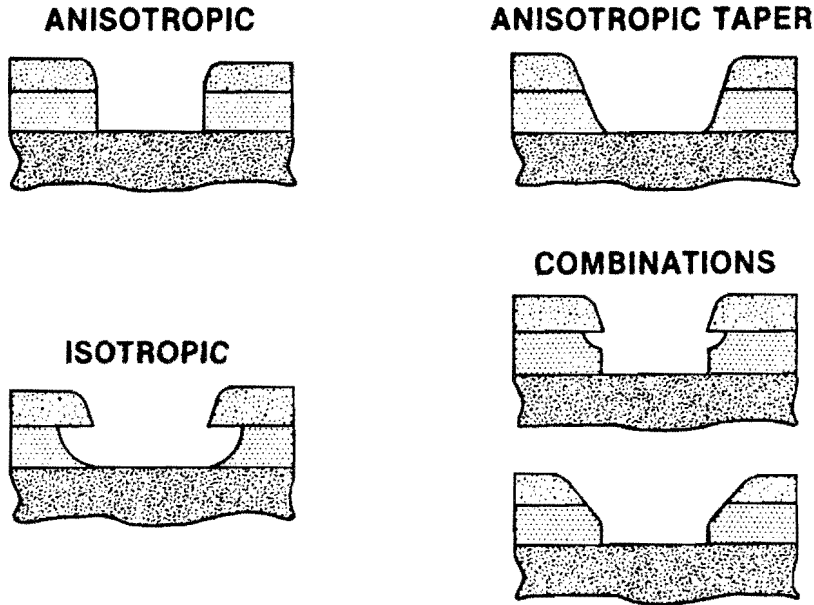
1. ANISOTROPY · FAITHFUL PATTERN TRANSFER ($\Delta \longrightarrow 0$)
2. SELECTIVITY · ETCH RATE RATIO BETWEEN FILM OF INTEREST AND MASK OR SUBSTRATE ($S > 10$)
3. ETCH RATE · HIGH FOR ADEQUATE THROUGHPUT ($N > 25$)
4. LOADING EFFECT · ETCH RATE $\approx \frac{1}{\text{MATERIAL AREA}}$ (N, Δ)
5. UNIFORMITY \rightleftharpoons SELECTIVITY \rightleftharpoons ANISOTROPY
6. SAFETY · FIRST CONSIDERATION



HOW DOES PLASMA ETCHING TAKE PLACE



ETCH PROFILES POSSIBLE IN LOW PRESSURE PLASMA ETCH



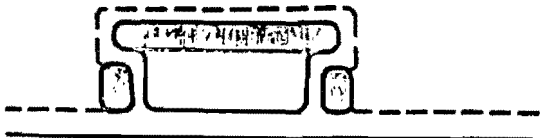
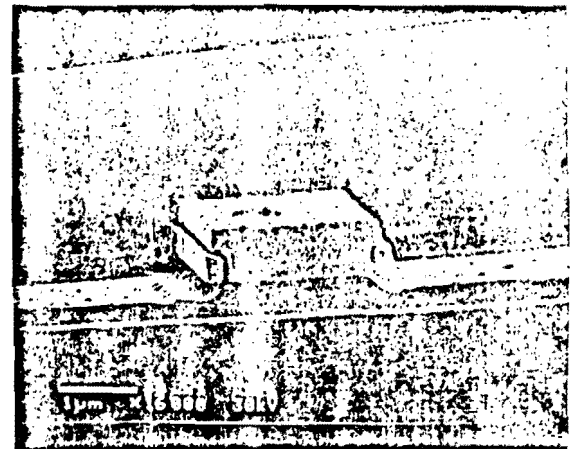
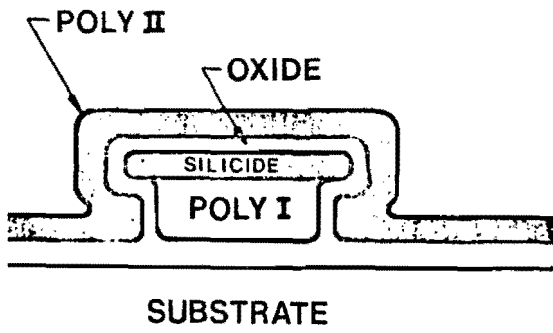
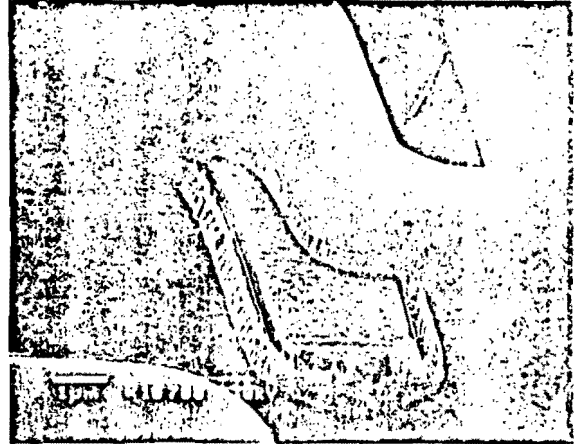
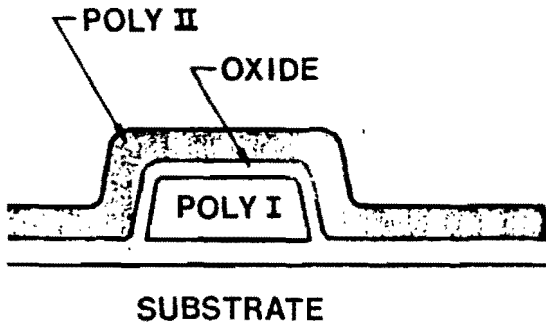
PLASMA NITRIDE CONTACT WINDOW ETCH ON PLATINUM SUBSTRATE



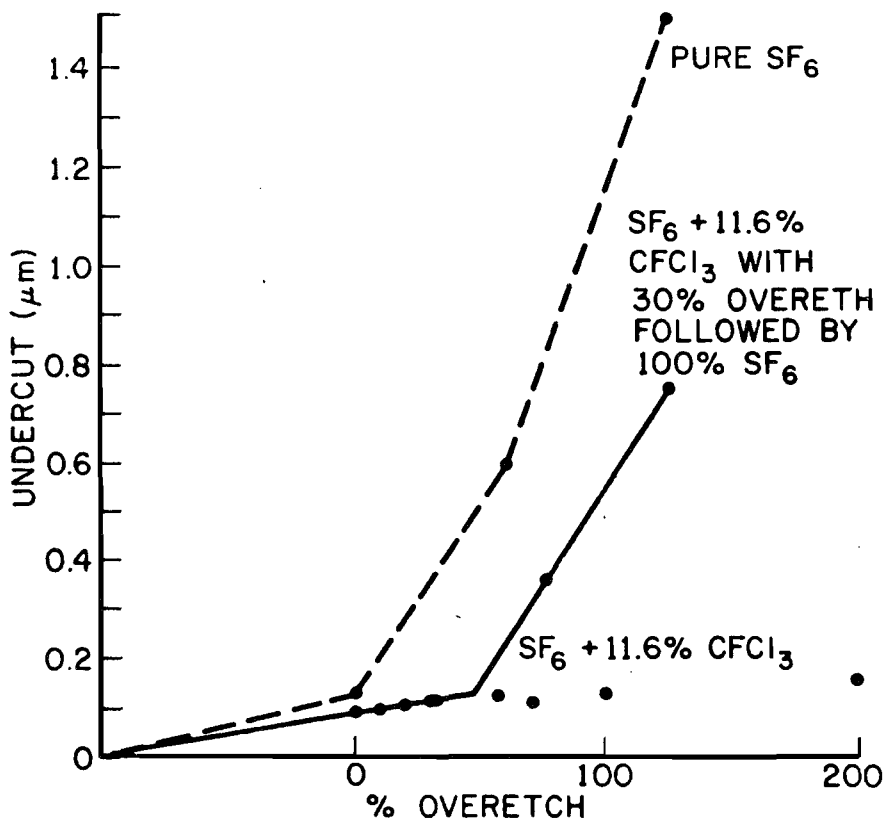
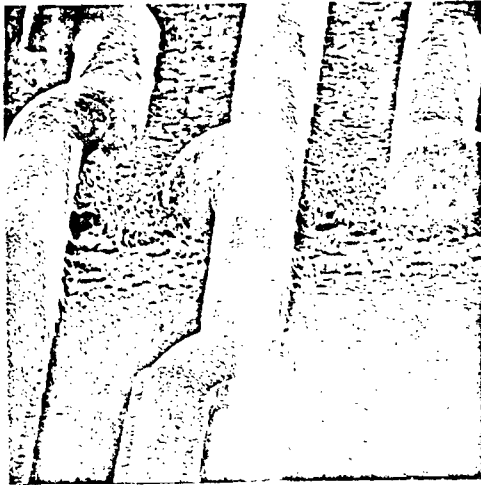
Anisotropic Vertical

Anisotropic Taper

Isotropic-Anisotropic
Taper



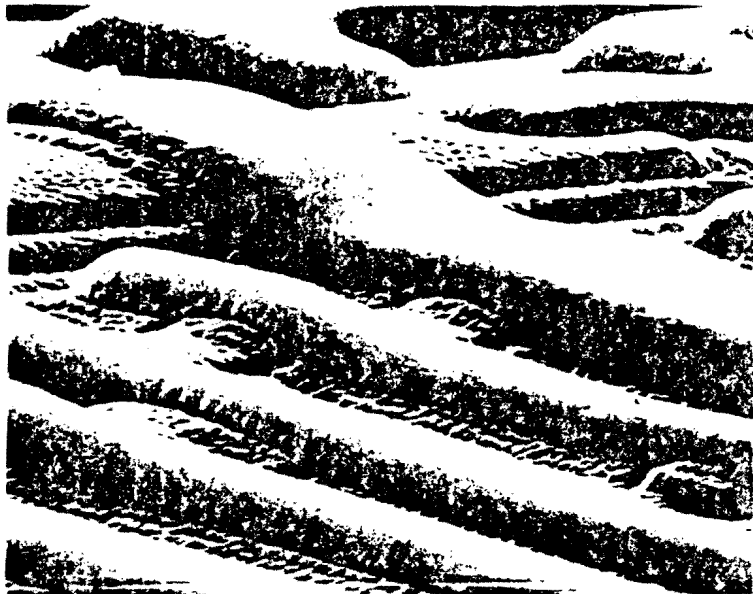
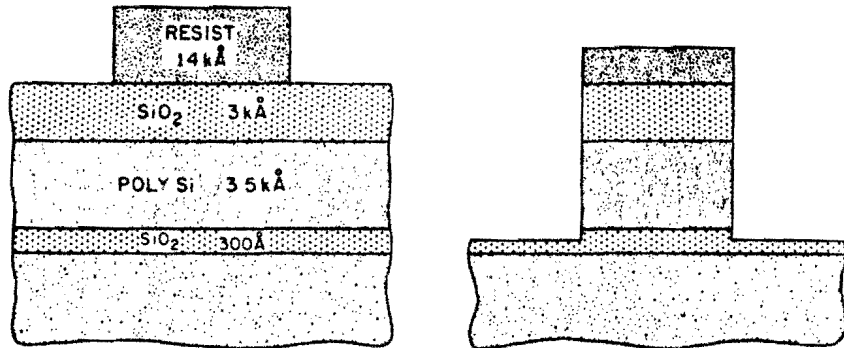
LINEWIDTH CONTROL



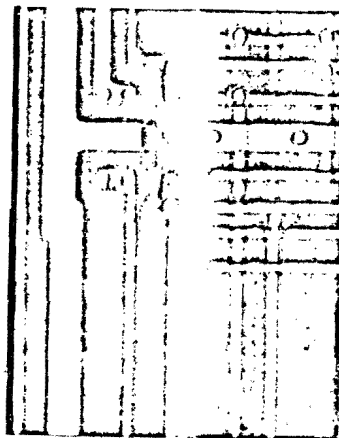
SELECTIVITY REQUIREMENTS

FILM: MASK > 4:1

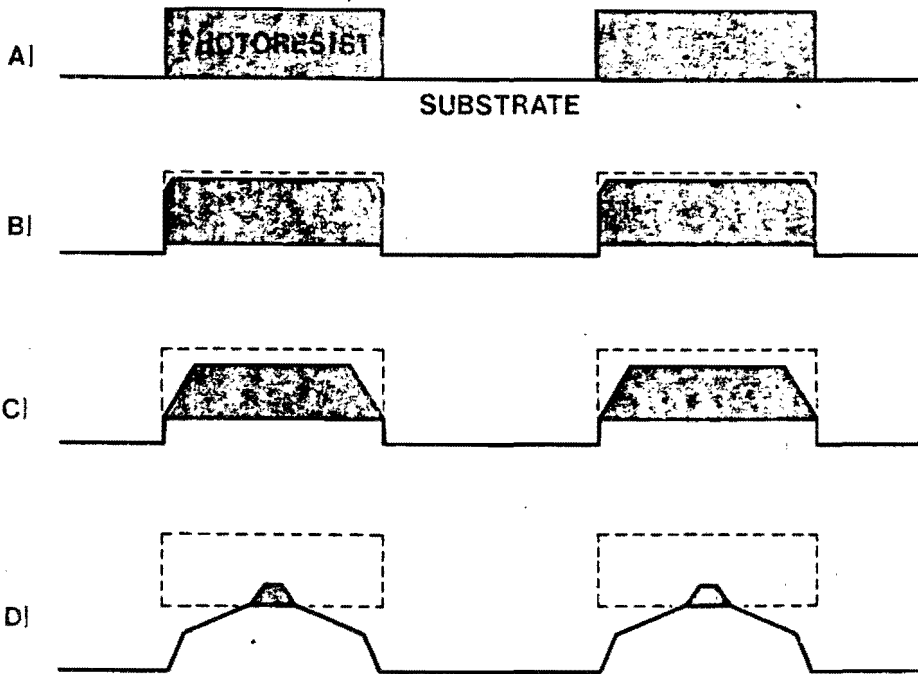
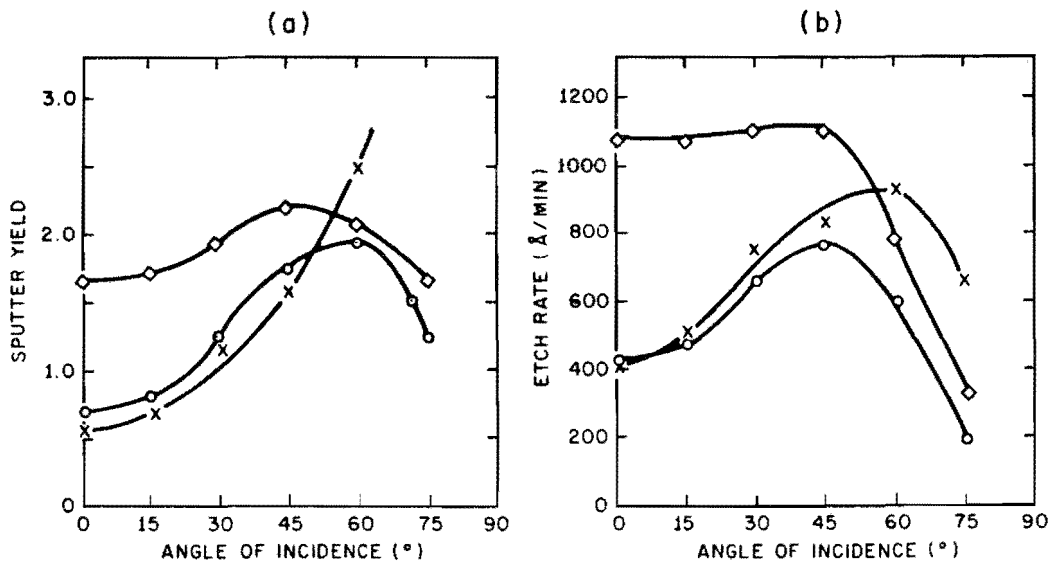
FILM: SUBSTRATE > 20:1



CCl₄ PLASMA ETCH
OPENED ALUMINUM LINE

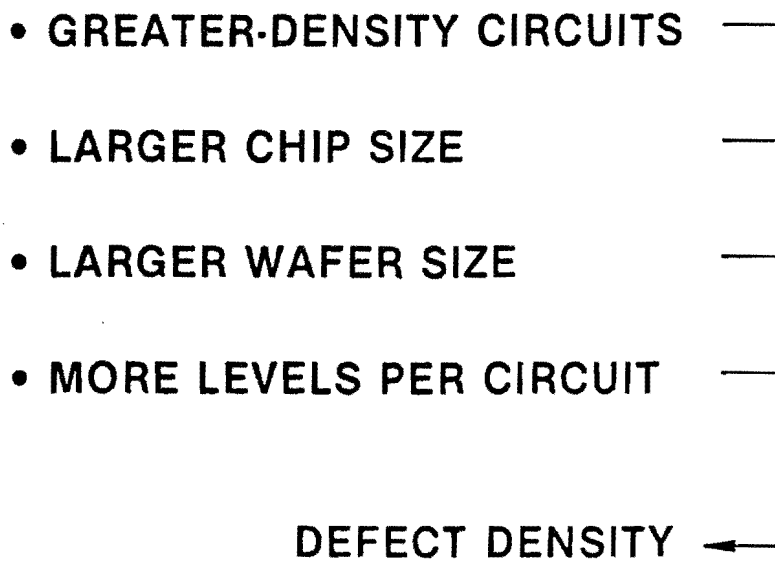


EFFECT OF ANGLE OF INCIDENCE ON (a) SPUTTERING YIELD AND (b) ION ETCHING FOR \diamond , GOLD: O, ALUMINUM: AND X, PHOTORESIST (AZ 1350)

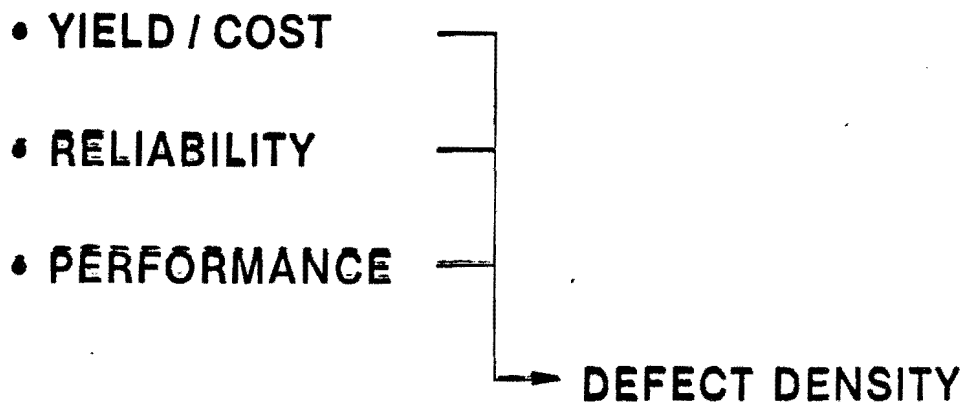


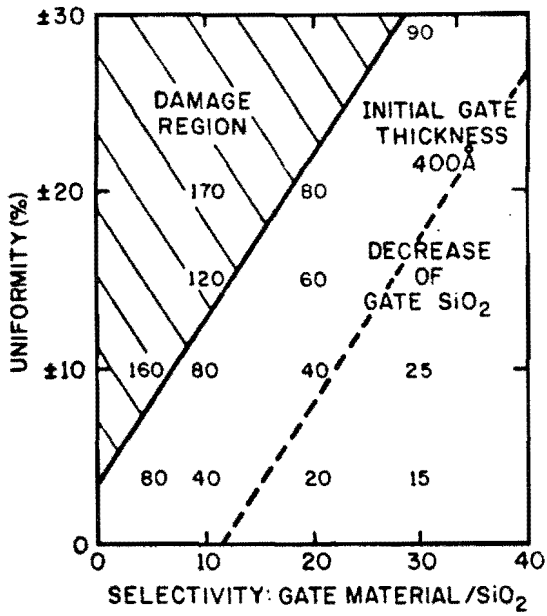
INTEGRATION SCALE

MOORE'S "LAW"

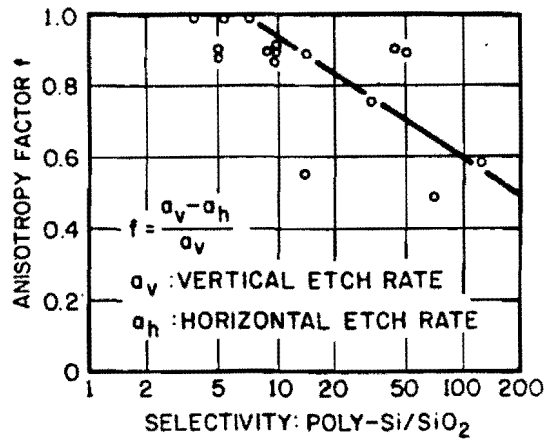


SIC RATIONALE



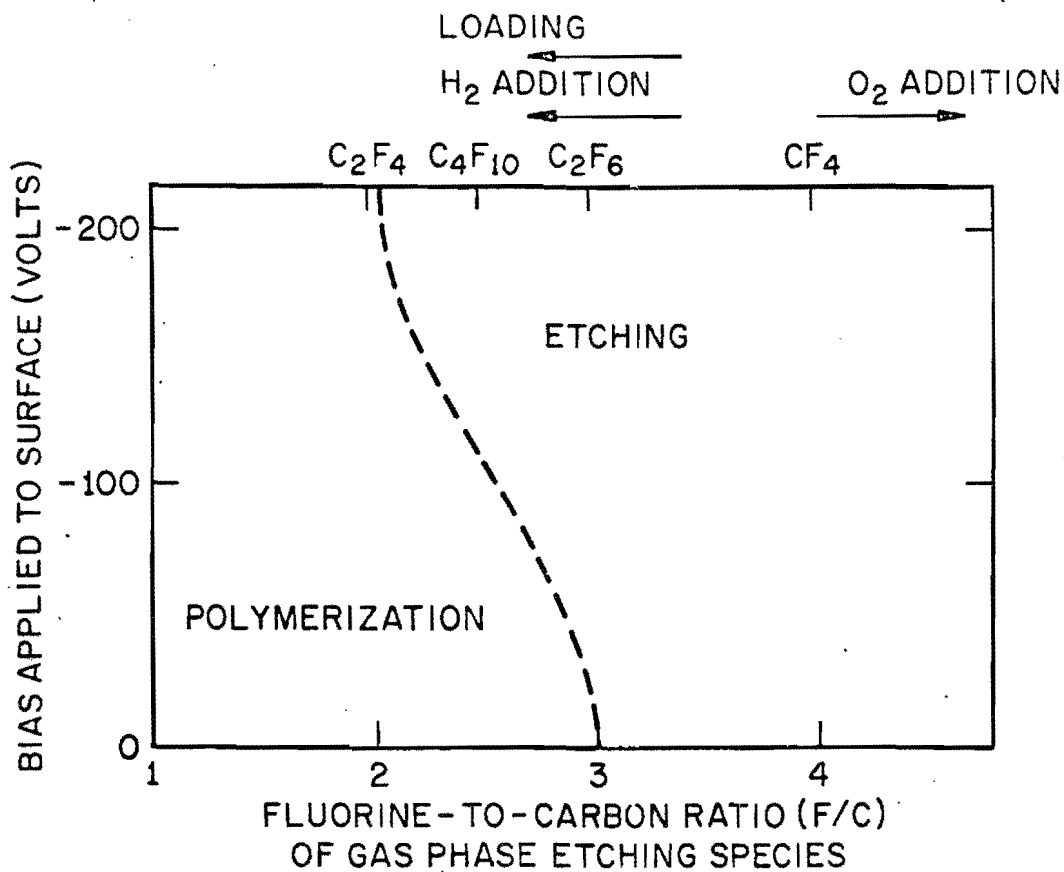


Watanabe, *Jap. J. Appl. Phys.* (1983)



Beinvogl, *Siemens Forsh.* (1982)

CONDITIONS FOR POLYMERIZATION VS ETCHING

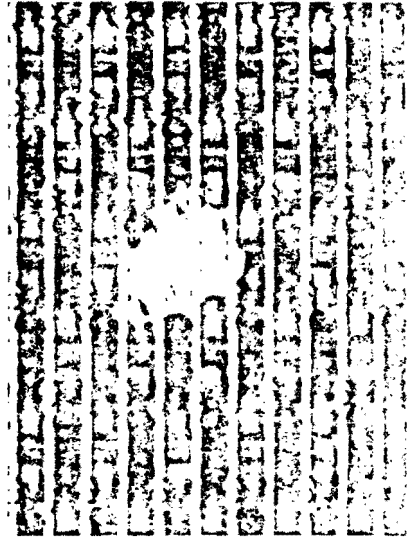


Harshbarger, *Electro Chem. Soc.* (1978)

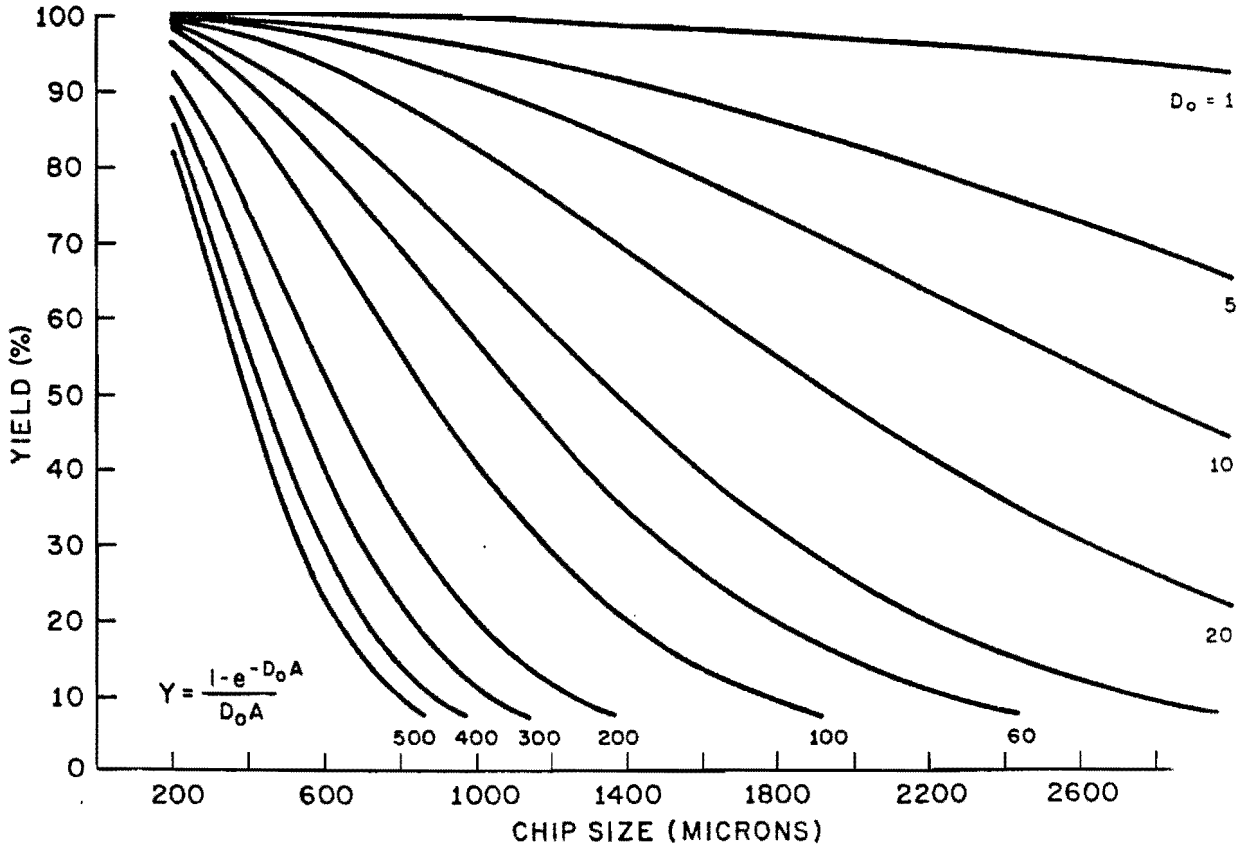
CCl₄ PLASMA ETCH



PLASMA FLAKE



ETCH DEFECT CAUSED BY PLASMA FLAKE



BASIC CHARACTERISTIC OF DRY PLASMA PROCESS FOR VLSI

- **ANISOTROPY FOR FAITHFUL PATTERN REPLICATION**

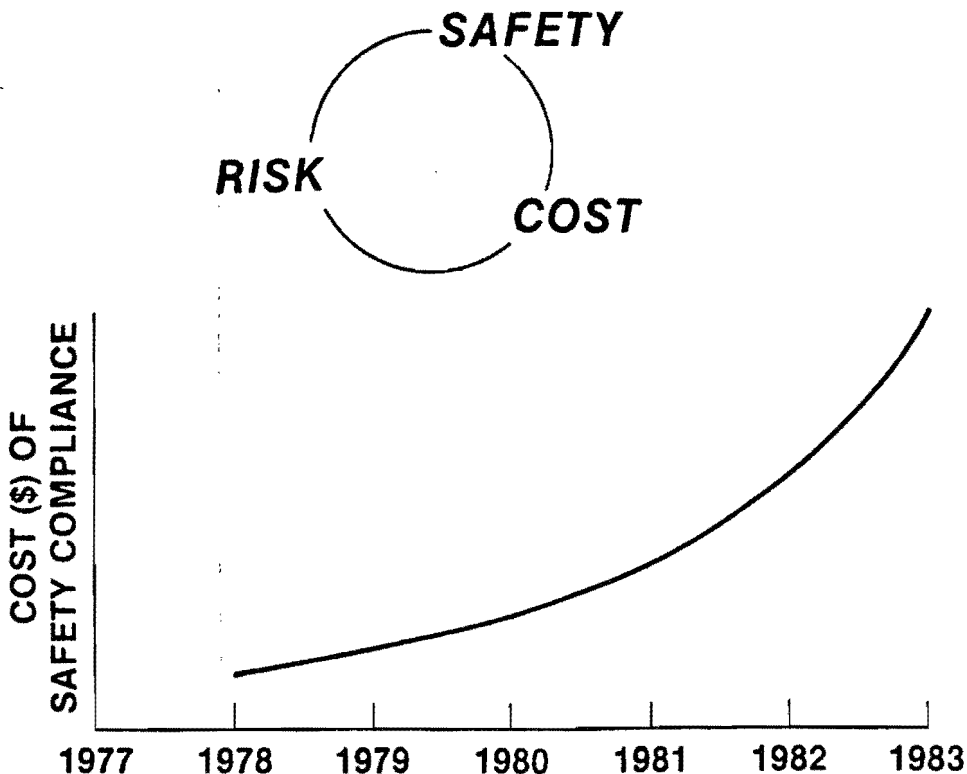
**PLASMA PROCESS MAY DEMAND CONSIDERATION
OF HAZARDOUS AND / OR TOXIC MATERIAL**

**IN ORDER TO PERFORM OUR WORK SAFELY;
WE MUST BE ADEQUATELY INFORMED!**

LIABILITY

Be Familiar With Legislated Obligations.

***Consult Local Safety Representative
For Guidelines.***



CYLINDER GAS CHARACTERISTICS THAT IMPACT SAFETY CONSIDERATIONS

CYLINDER PRESSURE	REGULATOR TYPE
SPECIFIC VOLUME	CYLINDER SIZE
BOILING / FREEZING POINTS	CYLINDER LOCATION
GAS / LIQUID	CYLINDER LOCATION
CORROSIVENESS / FLAMMABILITY	GAS CABINET
TOXICITY	SPECIAL HANDLING
IMPURITIES	SPECIAL HANDLING
<u>AMMONIA</u>	<u>PHOSGENE</u>

COLORLESS GAS WITH A SHARP IRRITATING ODOR. SOLUBLE IN WATER AND MANY SOLVENTS.

PHYSICAL PROPERTIES

COLORLESS GAS WHICH HYDROLYZES IN WATER TO FORM HCl AND CO₂, SOLUBLE IN SOME SOLVENTS.

NONFLAMMABLE ACCORDING TO DOT, BUT CAN BURN VIOLENTLY UNDER THE RIGHT CONDITIONS.

FLAMMABILITY

NONFLAMMABLE ACCORDING TO DOT TESTS, BUT IT WILL BU

25 ppm

TLV

0.1 ppm

500 ppm

IDLH

2 ppm

4837 ppm / 1 hr

LC₅₀ (rat)

110 ppm / 0.5 hr

20 ppm

NOSE IRRITATION

10 ppm

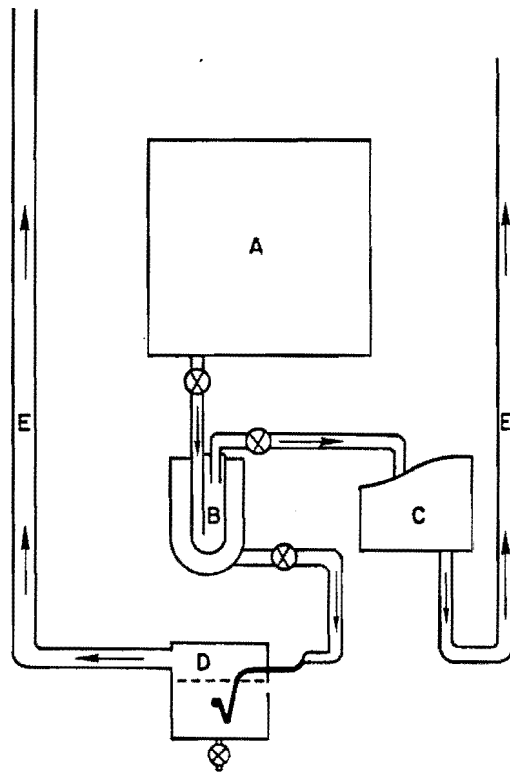
IMMEDIATE BURNING, RESPIRATORY EDEMA.

EFFECTS

DELAYED RESPIRATORY EDEMA

HAZARDOUS GAS MONITORING INSTRUMENTS

- SIMPLE AND FAST
- STABLE
- SPECIFIC
- PERIODIC CALIBRATION
- PROPERLY SITED
- SENSITIVITY BELOW PEL FOR PERSONNEL, AT IDLH FOR EQUIPMENT
- OBEYED
- HAZARDOUS MATERIALS WORKSHOP AND EXPOSITION



CCl₄ RESIDUE ANALYSIS

CHAMBER : C₂Cl₆, CCl₄, C₂Cl₂, C₂Cl₄, CCl₂F₂, C₂Cl₂F₄,
C₂ClF₅, C₂Cl₃F₃, CClF₃, C₂Cl₅, C₂F₄, CF₄, CO₂

POWDER : AlCl₃, AlCl₃•6H₂O, SiO₂

COLD TRAP : C₂Cl₆, CCl₄, Cl₂, HCl, CF₃, CF₄, C₂ClF₅, CClF₃,
C₂Cl₂, C₂Cl₄

PUMP EXHAUST : CCl₄, CF₄

**C₂Cl₆ EVOLVED WHEN WIPING REACTOR SURFACES TO
CLEAN POLYMER**

CARBON TETRACHLORIDE— CCl_4

COLORLESS, NONFLAMABLE LIQUID WITH A CHARACTERISTIC ODOR. OXIDATIVE DECOMPOSITION BY FLAME CAUSES PHOSGENE AND HCl TO FORM.

**CARCINOGEN (POSITIVE IARC) WITH
PERCUTANEOUS ABSORPTION**

TLV	5 ppm
PEL	10 ppm
IDLH	300 ppm

EXCESSIVE EXPOSURE RESULTS IN CENTRAL NERVOUS SYSTEM DEPRESSION. ACUTE EXPOSURE MAY LEAD TO LIVER AND KIDNEY DAMAGE. RESULTS GREATLY INCREASED IF EXPOSED IN CONJUNCTION WITH INGESTED ALCOHOL.

HEXACHLOROETHANE— C_2Cl_6

COLORLESS SOLID WITH CAMPHORLIKE ODOR. IT SUBLIMES AT 189° C.

CARCINOGEN (POSITIVE—NCI)

TLV	1 ppm (10 mg/m ³)
PEL	1 ppm
IDLH	300 ppm

ACTS PRIMARILY AS A CENTRAL NERVOUS SYSTEM DEPRESSANT—NARCOSIS IN HIGH CONCENTRATION

CONSIDERATIONS FOR PUMPING HAZARDOUS GASES

1. UNDERSTAND PROCESS CHEMISTRY AND REACTION EFFLUENTS.

“DO NOT THWART MOTHER NATURE”

- **LARGE BORE/TOLERANCE PUMPS FOR PARTICULATES**
- **INERT PUMP OIL FOR CORROSIVE/REACTIVE GASES**
- **HIGH TEMPERATURE OPERATION FOR HIGH GAS PURGE**
- **NITROGEN BALLAST FOR GAS PURGE**
- **FILTRATION FOR PARTICULATE REMOVAL**
- **DEMISTER FOR OIL CONSERVATION/FIRE PROTECTION**
- **SCRUBBER REACTION BEFORE EXHAUST TO ENVIRONMENT**
- **MONITOR OIL/SCRUBBER/EXHAUST QUALITY**
- **SPENT FILTERS TREATED AS HAZARDOUS WASTE**
- **OVERSIZE PUMP CAPACITY**
- **FAILURE ALARMS INTERLOCKED TO SYSTEM**

RECOMMENDATIONS

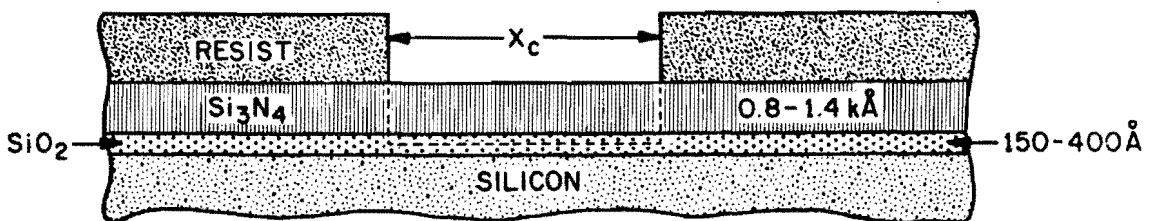
- 1. KNOWLEDGE OF REGULATIONS AND CHEMISTRY.**
SUBSTITUTE RESPECT FOR FEAR.
COMMUNICATE TO WORKERS TO MINIMIZE PSYCHOSOMATIC REACTION.
- 2. SELECT SYSTEM MATERIALS ACCORDING TO APPLICATION.**
CYLINDER SIZE IMPORTANT.
- 3. SAFETY TRAINING UPDATE. CONTINUOUS WORK AREA-PROCESS MONITOR.**
- 4. PROPER SAFETY EQUIPMENT IN VISIBLE AREA.**
BUDDY SYSTEM WITH SCBA FOR CYLINDER CHANGE.
- 5. DESIGN FOR NO-FAIL, HOWEVER, REDUNDANCY FOR EMERGENCY.**
MONITORS ARE VITAL.
- 6. CONSULT FOR STATE-OF-ART FOR EQUIPMENT OR PRACTICES.**
SSA.
CAL-DIR/DOSH REPORT.
LOCAL SAFETY/HEALTH ORGANIZATION.
- 7. GOLDEN OPPORTUNITY TO INFLUENCE LEGISLATION ON SEMICONDUCTOR SAFETY AND VENDOR DESIGN.**

TYPICAL VLSI DRY PATTERN PROCESS TECHNOLOGY

- APPLICATIONS
- STRUCTURE
- CHEMISTRY
- RECIPE
- PROBLEMS

$Si_3N_4 / SiO_2 / Si$

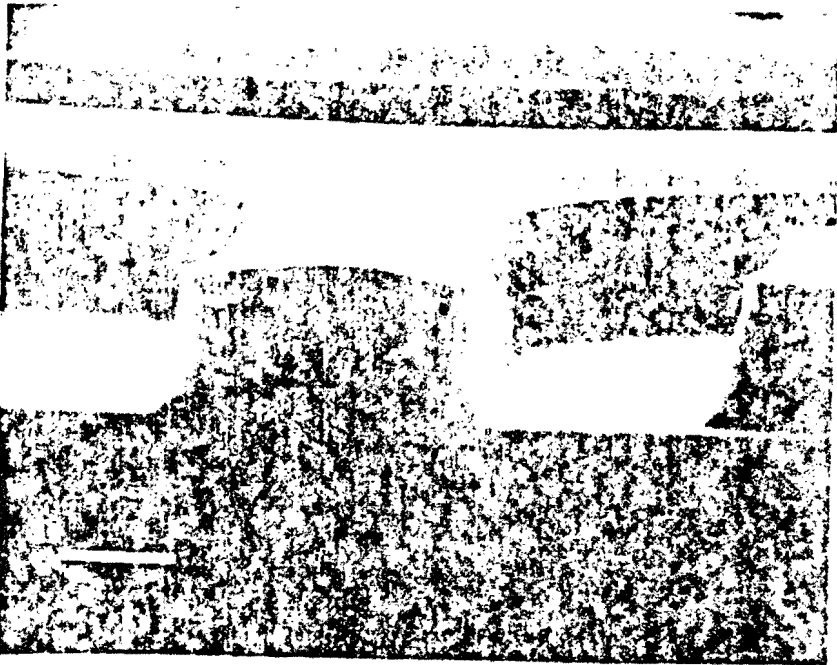
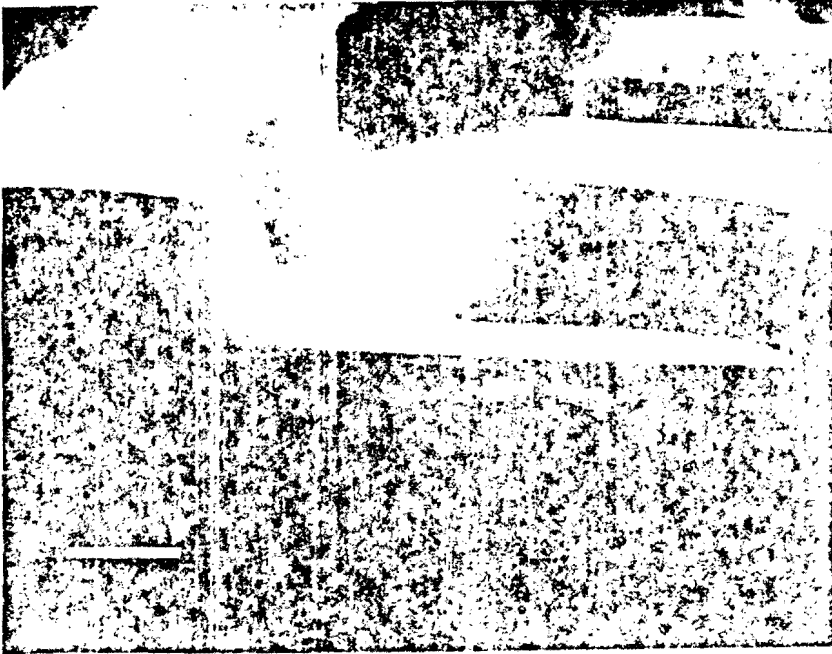
- APPLICATIONS - GASAD, SORT, THINOX, FOX, CAPS



- CF₄, CF₄+O₂, SiF₄+O₂, CBrF₃, CHF₃, C₃F₈, SF₆, NF₃, CH₂F₂, CH₃F

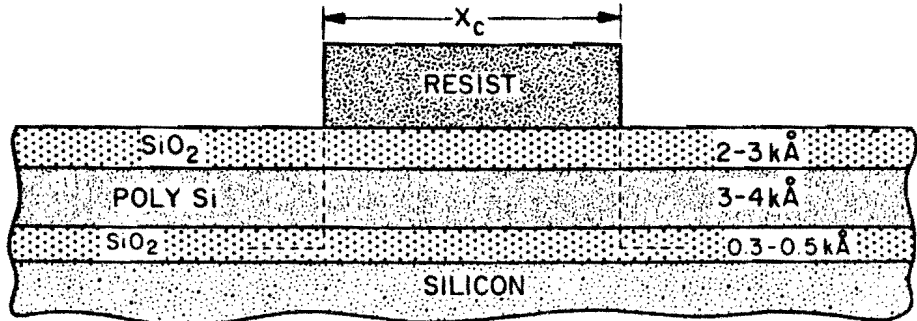
- CF₄ - 100 sccm pressure: 200 mT Diode, plasma
- CBrF₃ - 40 sccm Power: 800 W
- SF₆ - 20 sccm
- O₂ - 8 sccm E.R. (Si₃N₄) ~ 700 Å/min Selectivity ~ 6:1
- ΔX_c < 0.1 micron

- LOW SELECTIVITY (4-8:1) OVER OXIDE
- LOW UNIFORMITY DEMANDS OVER-ETCH
- PLASMA EXPOSURE TO SILICON → OSF



SiO₂ / POLY Si / SiO₂

• APPLICATIONS - CONDUCTOR PATTERN

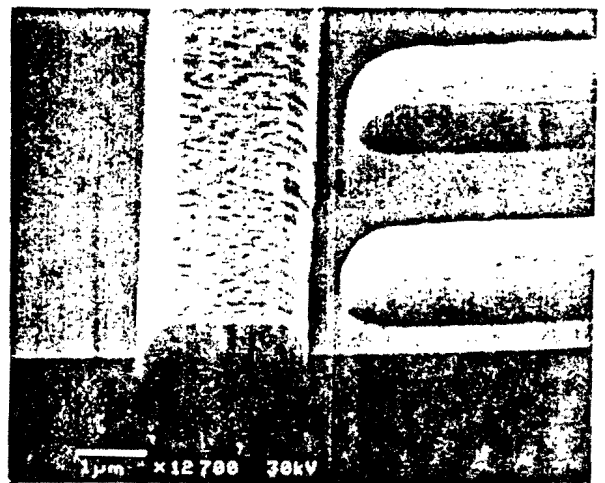
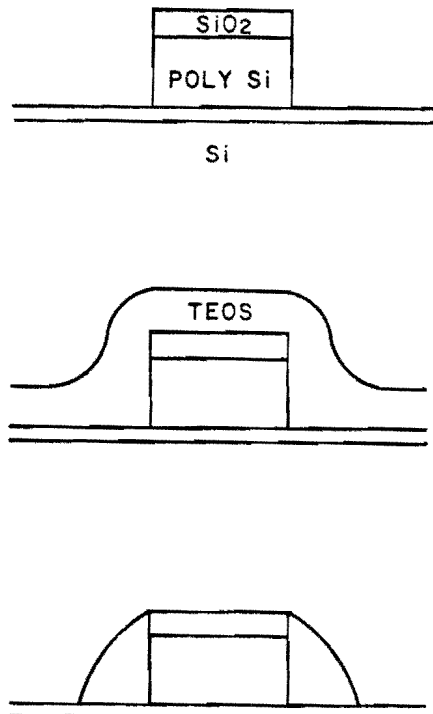


• CF₄, CF₄+O₂, SF₆, SF₆+O₂, NF₃, Cl₂, CCl₄, SiCl₄, CCl₃F, CCl₂F₂, CClF₃

• SF₆ - 50 sccm pressure - 200 mT Diode, plasma
C₂F₄ - 50 sccm Power - 500 W

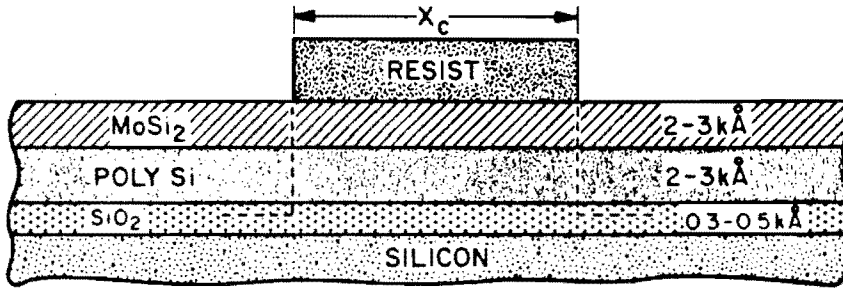
E.R. ~ 2000 Å / min Selectivity ~ 20:1
ΔX_c ~ 0.1 - 0.3 micron

• REQUIRES 2-STEP PROCESS (PERHAPS 3-STEP)
POOR UNIFORMITY (> ± 15%)



SILICIDE/POLY Si/SiO₂

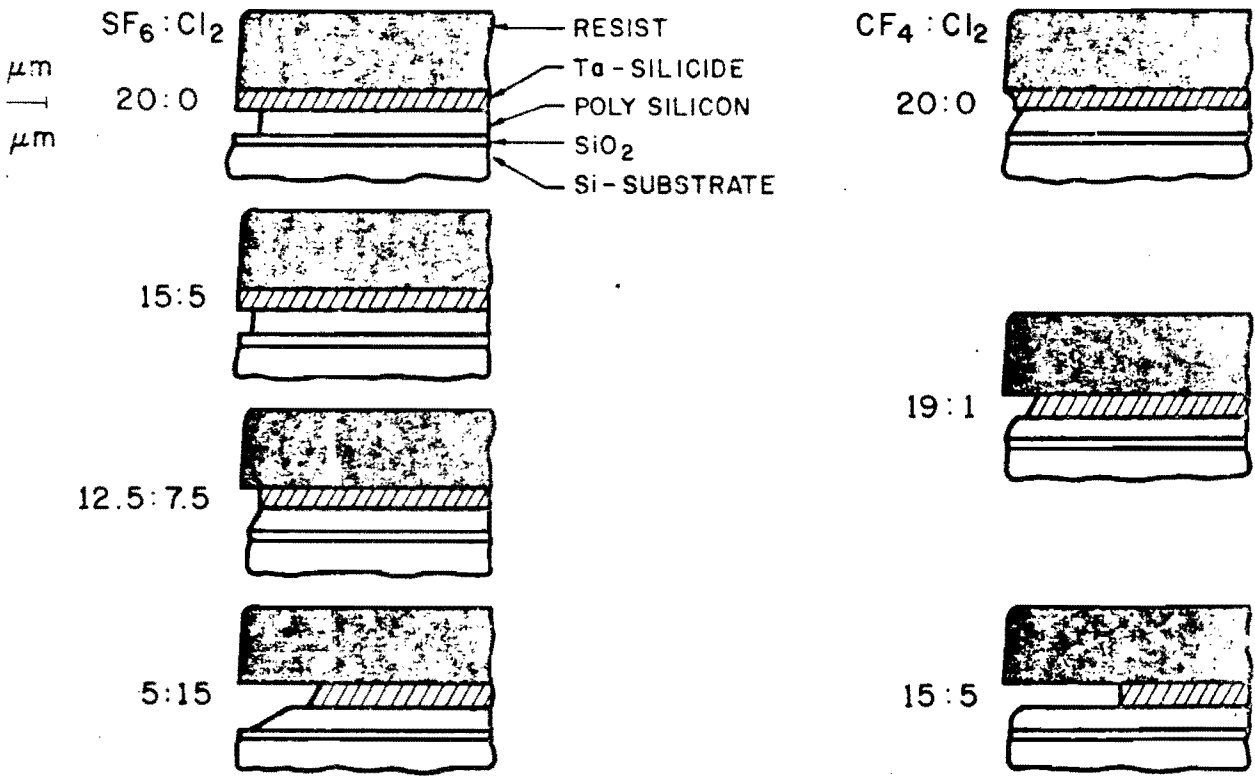
• APPLICATION: CONDUCTOR PATTERN

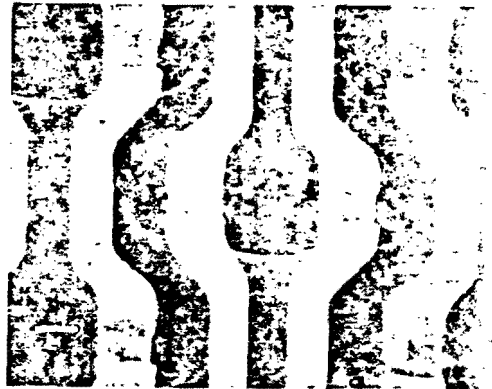
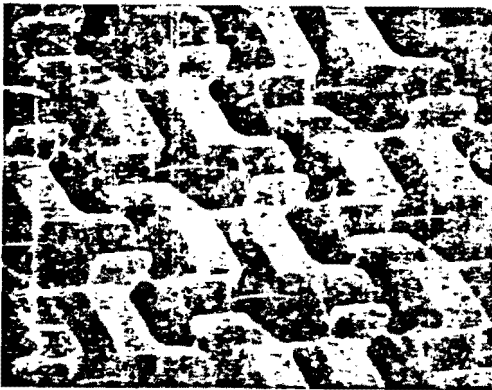
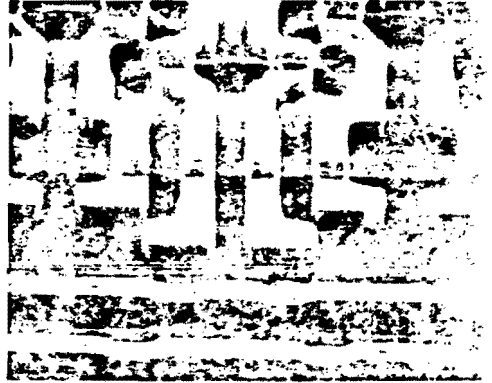


• CCl_3F , $\text{Cl}_2 + \text{BCl}_3$, $\text{CF}_4 + \text{O}_2$, SF_6 , $\text{CCl}_2\text{F}_2 + \text{C}_2\text{F}_6$, $\text{CF}_4 + \text{C}_2\text{F}_6$, $\text{SF}_6 + \text{Cl}_2$, $\text{CF}_4 + \text{Cl}_2$

STEP 1	STEP 2	Diode RSE
CF_4 · 50sccm	CCl_2F_2 · 50sccm	
C_2F_6 · 15 sccm	C_2F_6 · 5 sccm	
pressure · 120 mT	pressure · 60 mT	
Power · 300 W	Power · 100 W	
E.R. (silicide) ~ 1200 A / min	E.R. (poly) ~ 2000 A / min	
MoSi_2 / poly ~ 0.6	poly / oxide ~ 20:1	
$\Delta X_c < 0.1$ micron		

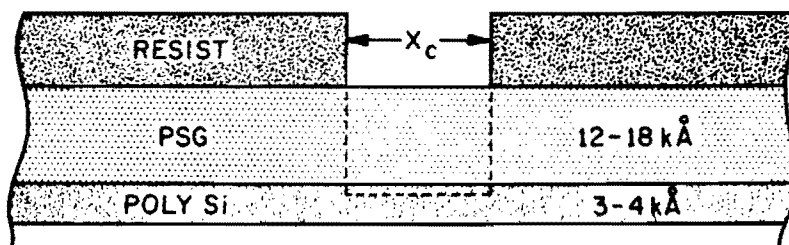
• POLY FEATURE UNDERCUT
POOR OXIDE SELECTIVITY
2-STEP PROCESS REQUIRED





SiO₂ / CONDUCTOR

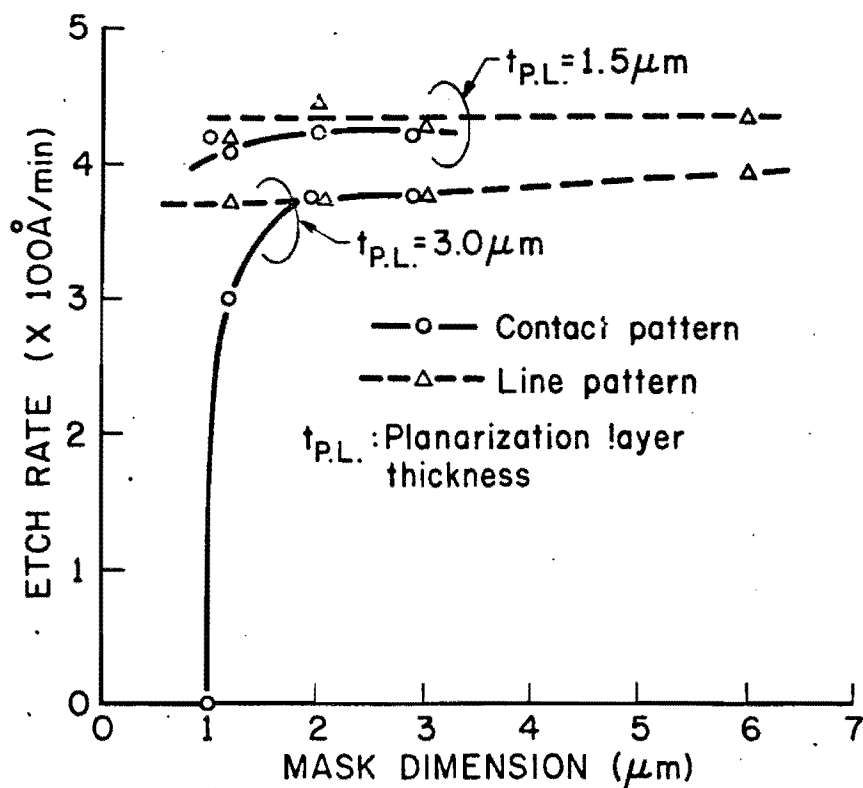
- APPLICATIONS - WINDOWS, VIAS, CAPS



- CF₄, CF₄+O₂, C₂F₆, CHF₃, CHF₃+C₂F₆, CF₄+H₂, C₃F₈, CHF₃+O₂

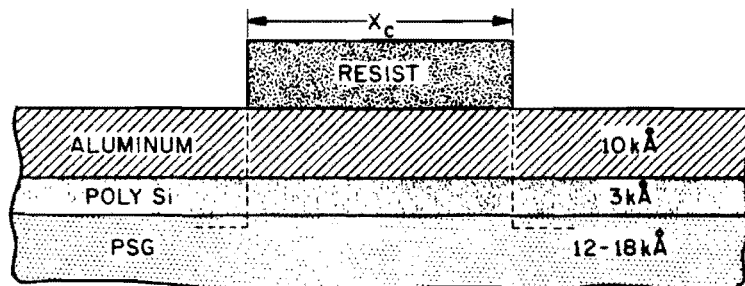
- C₂F₆ · 360 sccm E.R. (PSG) ~ 800 Å / min
- CHF₃ · 240 sccm E.R. (Poly Si) ~ 100 Å / min
- pressure · 750 mT ΔX_c < 0.1 micron
- Power · 1000 W DIODE PLASMA SYSTEM

- POLYMER FORMATION
SELECTIVITY VS OVER-ETCH FOR LOW R_c



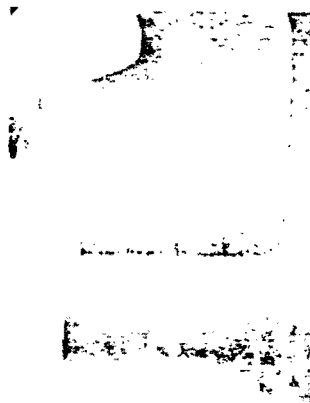
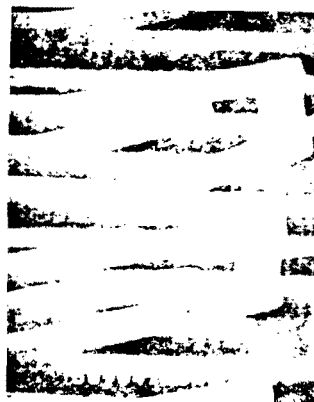
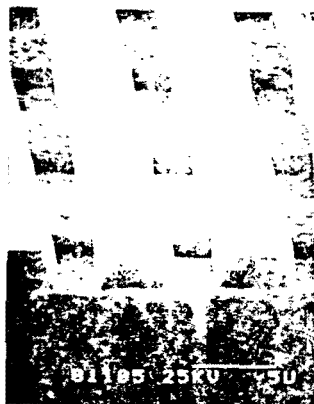
ALUMINUM / POLY Si / SiO₂

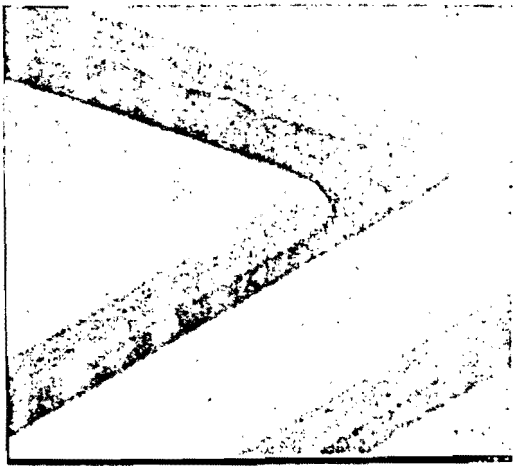
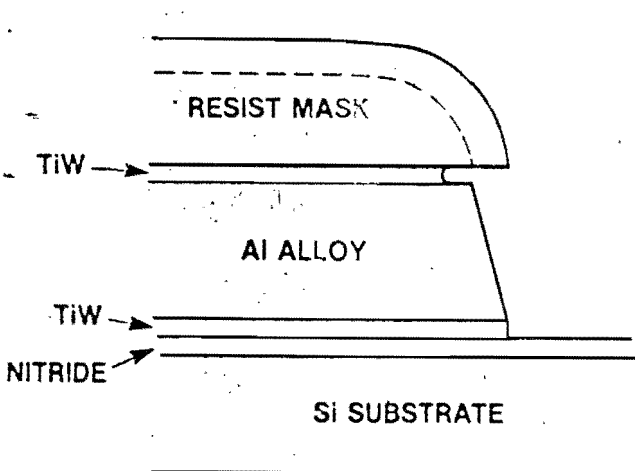
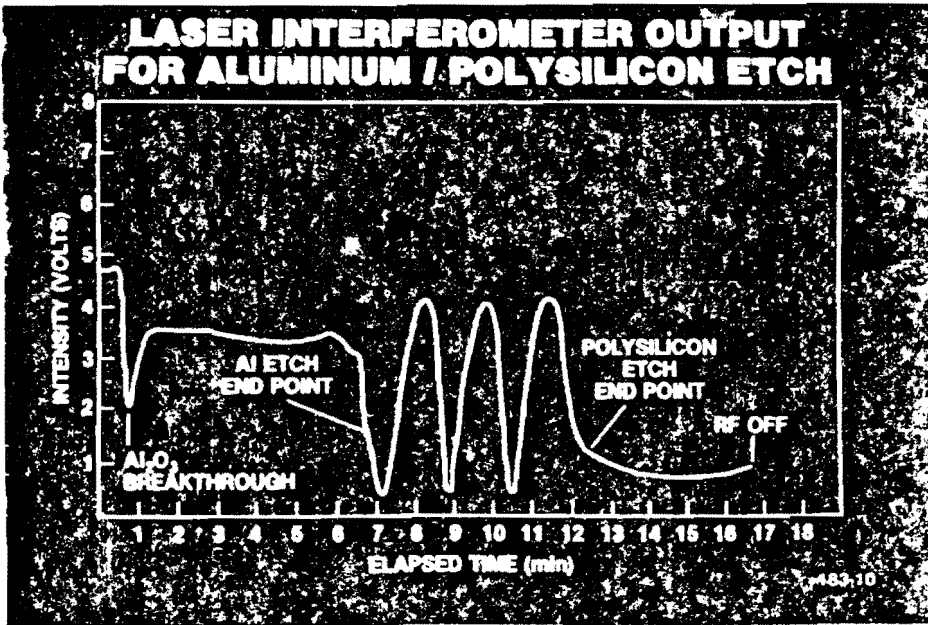
• APPLICATION - CONDUCTOR PATTERN



- CCl₄, SiCl₄, Cl₂ + BCl₃, CCl₄ + Cl₂
- BCl₃ - 70 sccm
Cl₂ - 10 sccm
pressure - 30 mT
Power - 600 W (-200 Vdc)
- E.R. (Al) ~ 750 Å / m
E.R. (poly) ~ 225 Å / m
E.R. (PSG) ~ 50-60 Å / m
 $\Delta X_c < 0.1$ micron
RSE HEX system

- Al₂O₃ PASSIVATION
- RESIST DEGRADATION
- ALUMINUM ALLOYS (Si, Cu)
- SAFETY
- POST-ETCH CORROSION

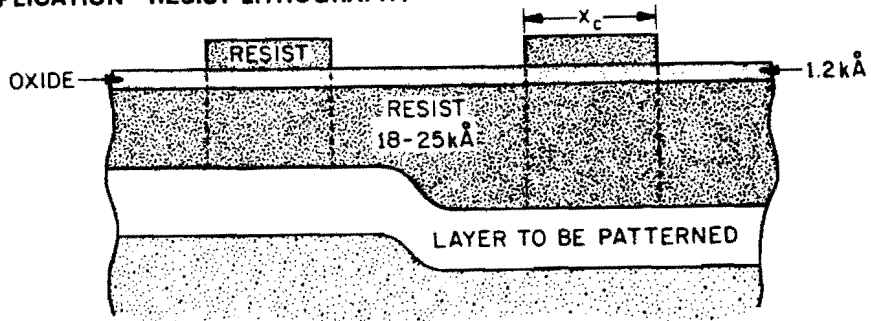




PROFILE CONTROL FOR STEP COVERAGE

TRI-LEVEL RESIST

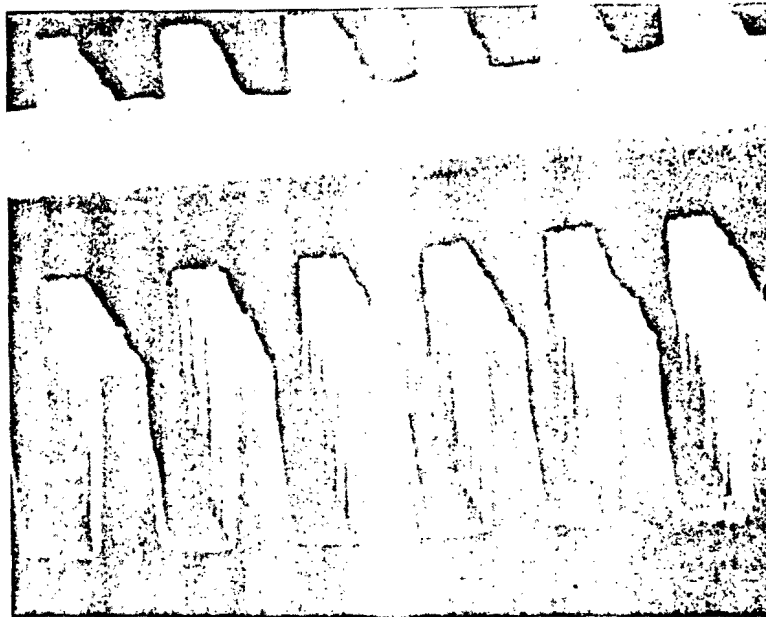
• APPLICATION - RESIST LITHOGRAPHY



- O_2 , $O_2 + N_2$, $O_2 + \text{air}$, CHF_3

STEP 1 (OXIDE)	STEP 2 (RESIST)	Diode RSE
CHF_3 - 60 sccm	O_2 - 80 sccm	
pressure - 15 mT	pressure - 4 mT	
Power - 450 W	Power - 500 W	
E.R. (oxide) - 300 Å / min	E.R. (resist) - 1250 Å / min	
E.R. (resist) - 20 Å / min	E.R. (oxide) - 20 Å / min	
$\Delta X_c < 0.1$ micron		

- DESCUM PRE-STEP MAY BE NECESSARY
- SLOW THROUGHPUT PROCESS
- CLEANLINESS EXTREMELY IMPORTANT

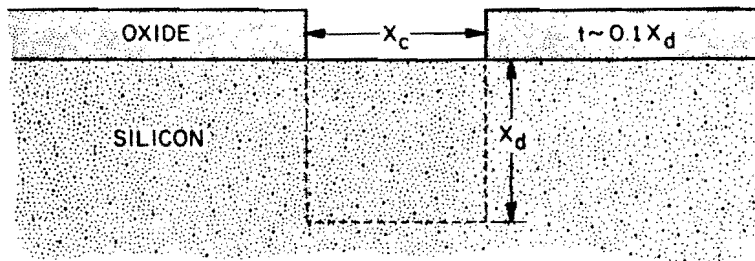


BENEFITS OF PLANARIZATION

- IMPROVED LINEWIDTH CONTROL
- THICK ORGANIC IS MORE EFFECTIVE ETCHING MASK
- ALLOWS REDUCED MINIMUM FEATURE SIZE
- REDUCED INTERFERENCE EFFECTS IN RESIST
- THINNER RESISTS PERMIT HIGHER ALIGNER THROUGHPUT

SILICON TRENCH

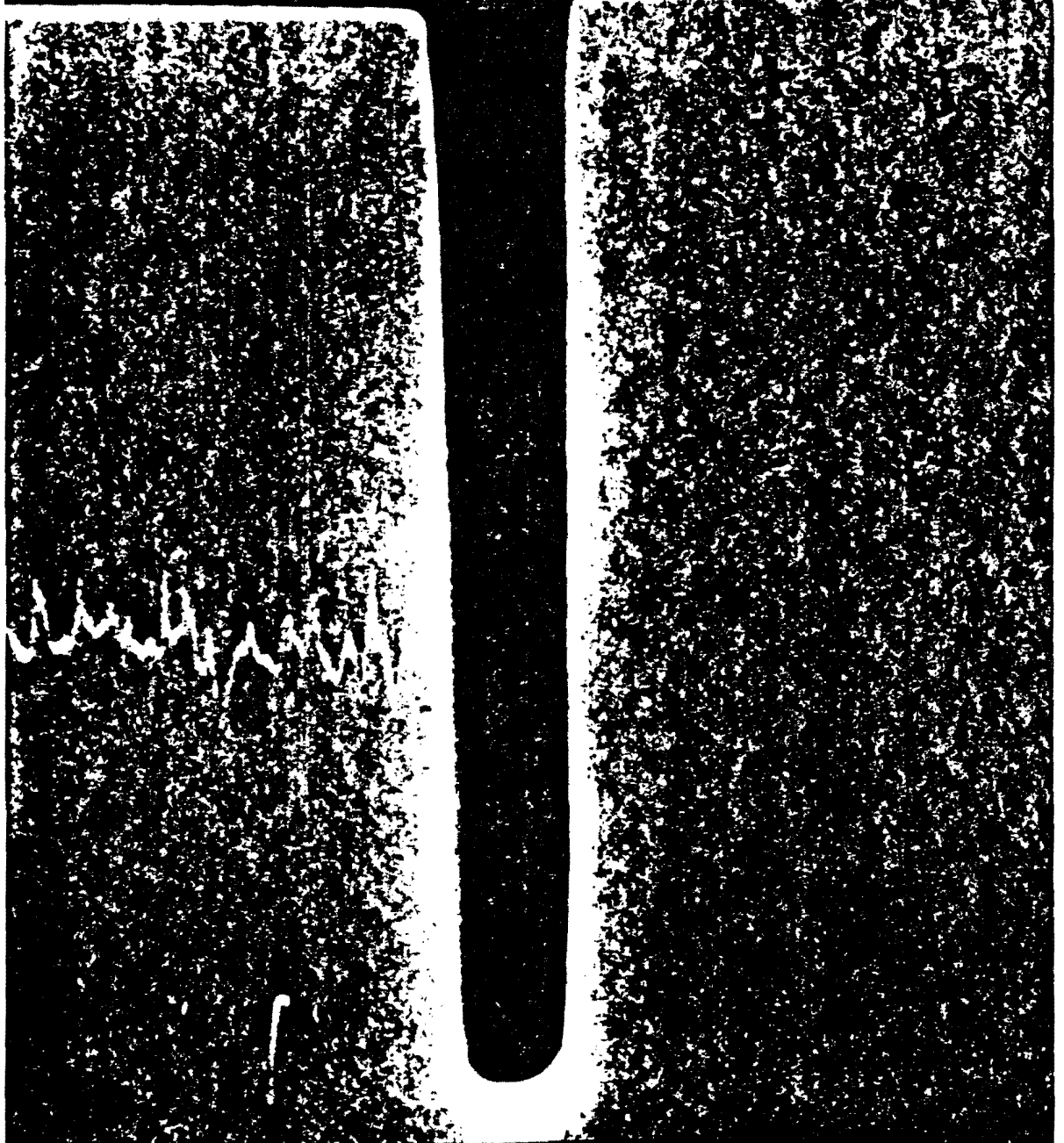
- APPLICATION - DIELECTRIC ISOLATION, BURIED CAPACITOR



- SF_6 , NF_3 , $CF_4 + O_2$, Cl_2 , $BCl_3 + Cl_2$, CCl_4 , $C_2ClF_6 + SF_6$, $CBrF_3$, CCl_3F
- $CBrF_3$ - 25 sccm
 SF_6 - 25 sccm
 pressure - 150 mT
 Power - 150 W
- E.R. (silicon) - 3000 A / min
 Selectivity - Si : oxide = 20:1
 $\Delta X_c < 0.1$ micron
 SWE, plasma mode
- ASPECT RATIO DEPENDS ON SILICON / MASK SELECTIVITY
 CAPACITOR DEMANDS TIGHT CONTROL ON TRENCH PROFILE
 FILLING OF TRENCH
 PLANARIZATION



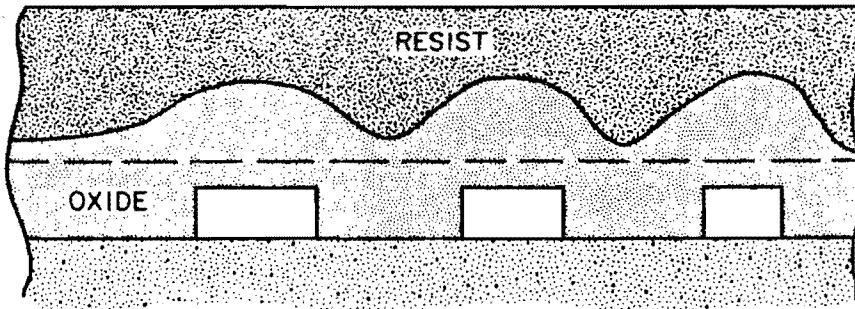
MSC SXTL P-267 <CLD>



77710 20KV X4.00K 7.5um

PLANARIZATION

- APPLICATION - REDUCTION OF TOPOGRAPHY



- $CF_4 + O_2$, $C_2F_6 + CF_3Cl$

- CF_4 - 92 sccm pressure - 400 mT

- O_2 - 8 sccm Power - 500 W

- E.R. (resist) ~ 300 Å / min

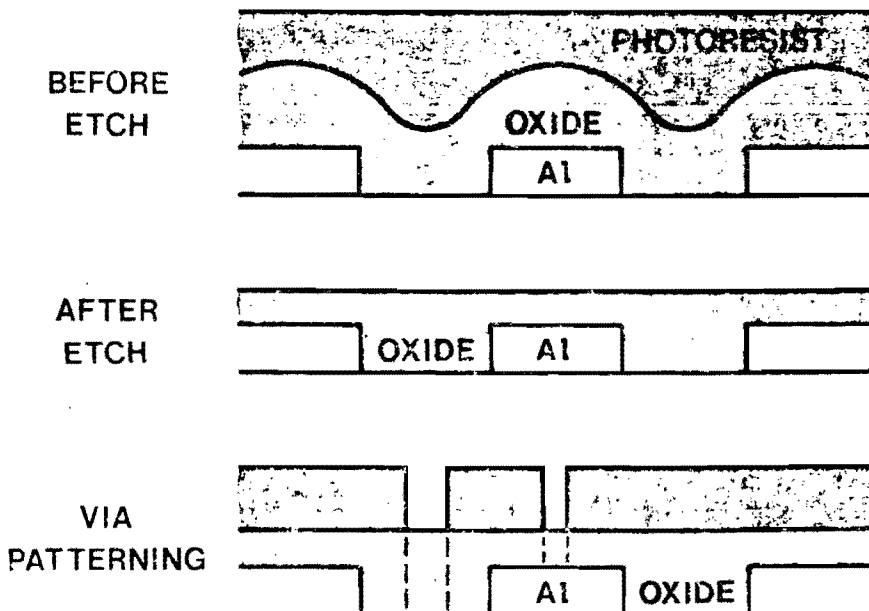
- E.R. (oxide) ~ 275 Å / min

- DIODE PLASMA SYSTEM

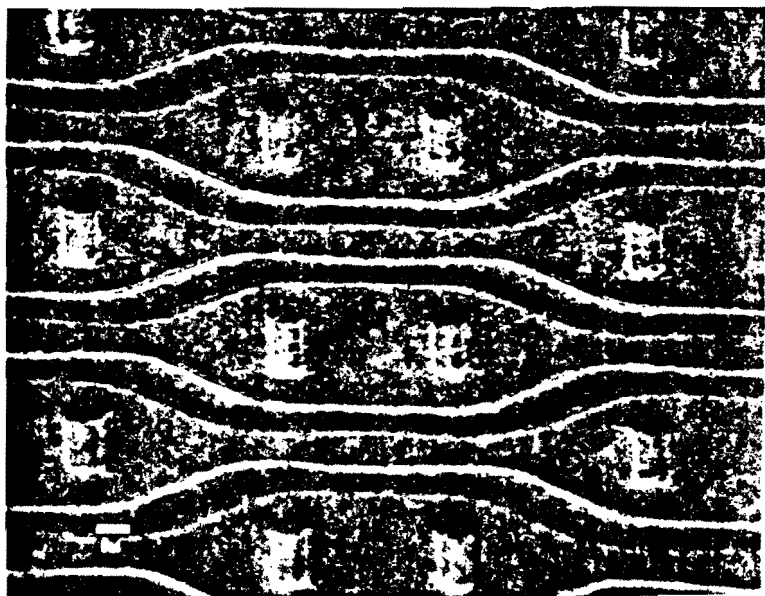
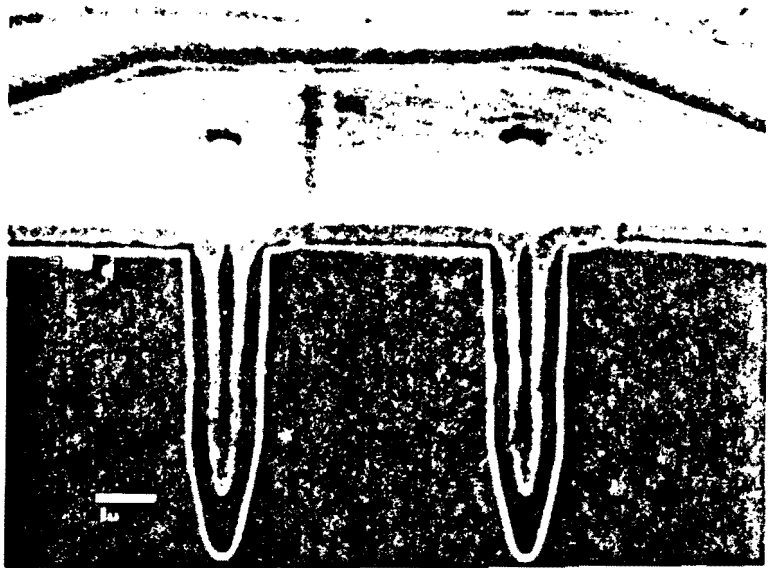
- LOW THROUGHPUT PROCESS

- ETCHED OXIDE SURFACE MUST BE SMOOTH AND FREE FROM BLEMISH

PLANARIZATION OF SURFACE



PLANARIZATION OF DEEP TRENCH CAPACITORS



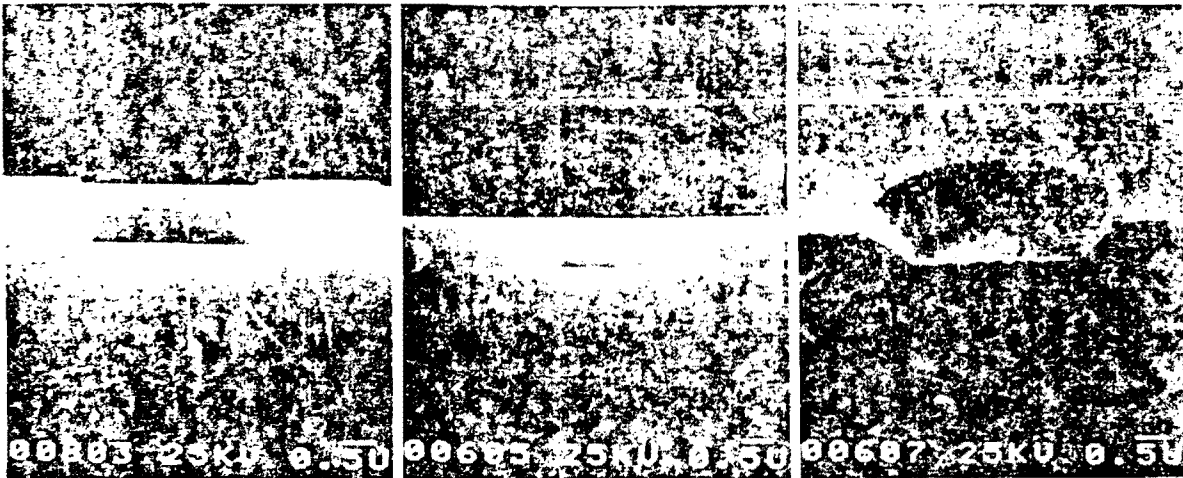
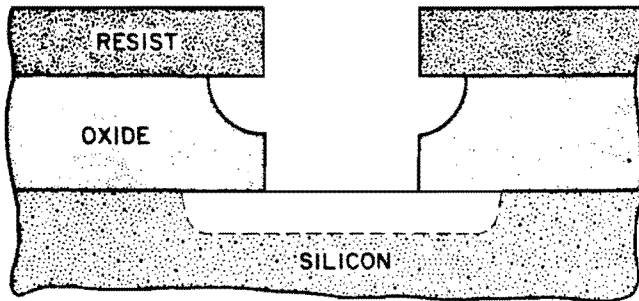
VIA TAPERING

ELIMINATES RE-FLOW PROBLEMS

DEMANDS RESIST PULL-BACK TO EXPOSE OXIDE.
DEPENDS ON RESIST PROFILE.

EXAMPLE PROCESS

1. WET FOR HALF FILM THICKNESS
2. DRY USING RESIST MASK TO PRESERVE X_c
3. WET FOR CLEAN-UP AND LOW R_c



PLASMA DEPOSITION

PLASMA PROVIDES REACTION ENERGY SO
THAT PROCESS CAN BE AT LOW TEMPERATURE

SILICON DIOXIDE

INTER-LEVEL DIELECTRIC



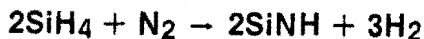
LOWER HYDROGEN INCORPORATION : 2-9 AT %

TYPICAL PROPERTIES OF SILICON DIOXIDE FILM

	PLASMA	SiH ₄ + O ₂	TEOS	SiCl ₄
TEMP(°C)	200	450	700	
COMPOSITION	SiO _{1.9} (H)	SiO ₂ (H)	SiO ₂	SiO ₂
STEP COVERAGE	NONCONFORMAL	NONCONFORMAL	CONFORMAL	CONFORMAL
THERMAL STABILITY	LOSES H	DENSIFIES	STABLE	LO
DENSITY (gm/cm ³)	2.3	2.1	2.2	
REFRACTIVE INDEX	1.47	1.44	1.46	
STRESS (10 ⁹ DYNES/cm ²)	3(c)-3(t)	3(t)	1(c)	
DIELECTRIC STRENGTH (10 ⁶ V/cm)	3-6	8	10	
ETCH RATE (Å/min)	400	60	30	
(100:1=H ₂ O:HF)				

SILICON NITRIDE

ENCAPSULATION / INTER-LEVEL INSULATOR



TYPICAL PROPERTIES OF SILICON NITRIDE FILM

	LPCVD	PLASMA
TEMP (°C)	700-800	250-3
COMPOSITION	Si ₃ N ₄ (H)	SiN _x (H)
Si/N	0.75	0.8-1.
AT % H	4-8	10-40
REFRACTIVE INDEX	2.01	1.8-2.
DENSITY (gm/cm ³)	2.9-3.1	2.4-2.
DIELECTRIC CONSTANT	6-7	6-9
RESISTIVITY (Ω-cm)	10 ¹⁶	10 ⁶⁻¹⁰
DIELECTRIC STRENGTH (10 ⁶ V/cm)	10	5
ENERGY GAP (eV)	5	4-5
STRESS (10 ⁹ dyne/cm ²)	10(t)	2(c)-5(t)

PARTICLE BOMBARDMENT DURING ION AND PLASMA ETCHING

TYPE OF PARTICLE	RF SPUTTER ETCHING	ION BEAM MILLING	TRIODE	DIODE
ELECTRONS	UP TO PEAK-TO-PEAK RF VOLTAGE	≤ 25 eV (FROM NEUTRALIZER)	INSIGNIFICANT	UP TO PEAK-TO-PEAK RF VOLTAGE ≈ 100 V
POSITIVE IONS	UP TO PEAK-TO-PEAK RF VOLTAGE	FEW eV LESS THAN ION ACCELERATING POTENTIAL	INSIGNIFICANT	A FEW eV
PHOTONS	UP TO PEAK-TO-PEAK RF VOLTAGE	\approx TENS OF eV FROM PLASMA DISCHARGE AND NEUTRALIZER ELECTRONS STRIKING CHAMBER WALLS	UP TO PEAK-TO-PEAK RF VOLTAGE	UP TO PEAK-TO-PEAK RF VOLTAGE

DAMAGE EFFECTS ON MOS PERFORMANCE

C-V CHARACTERISTICS CHANGE

ΔV_T , ΔV_{FB} , Q_{SS} , etc.

FORM OF DAMAGE

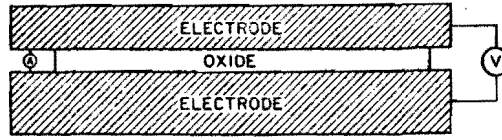
- ATOMIC DISPLACEMENT ($< 150 \text{ \AA}$)
- PRIMARY IONIZATION (ELECTRON-HOLE PAIRS)
- SECONDARY IONIZATION (ELECTRON--DEFECTS)

DAMAGE IS REVERSIBLE BY ANNEAL

- PHOTONS — 250-400 °C
- IONS — 500-750 °C
- X-RAYS — 800-1100 °C

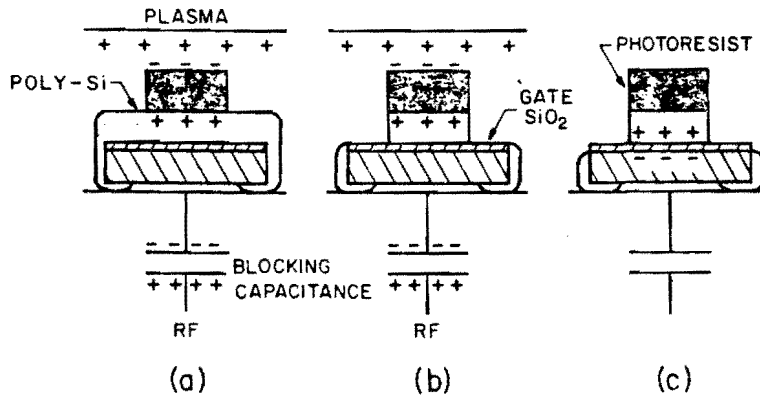
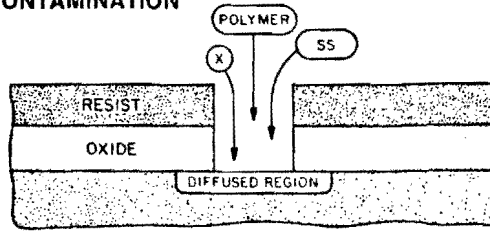
IRREVERSIBLE EFFECTS

A. ESD



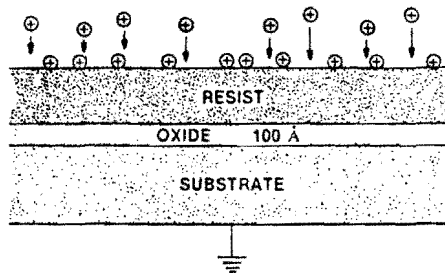
$\text{SiO}_2 V_{BD} \sim 12 \cdot 15 \text{ MV/cm}$
 for $d \sim 100 \text{ \AA}$, $V_{BD} \sim 12 \cdot 15 \text{ V}$

B. CONTAMINATION



Watanabe, Electro Chem Soc (1983)

ESD — RESIST STRIPPING



$\text{SiO}_2 V_{BD} \sim 12 \cdot 15 \text{ V}$

$V_f^{SS} \sim \frac{1}{2e} k T_e \ln [m/2M] \sim 5 \text{ V (OXYGEN)}$

BUT: $V_f^{\dagger} > 25 \text{ V}!$

SOLUTION: $\Delta V = 0$

IMMERSE WAFER IN PLASMA

TECHNIQUES TO REDUCE REACTION ENERGY

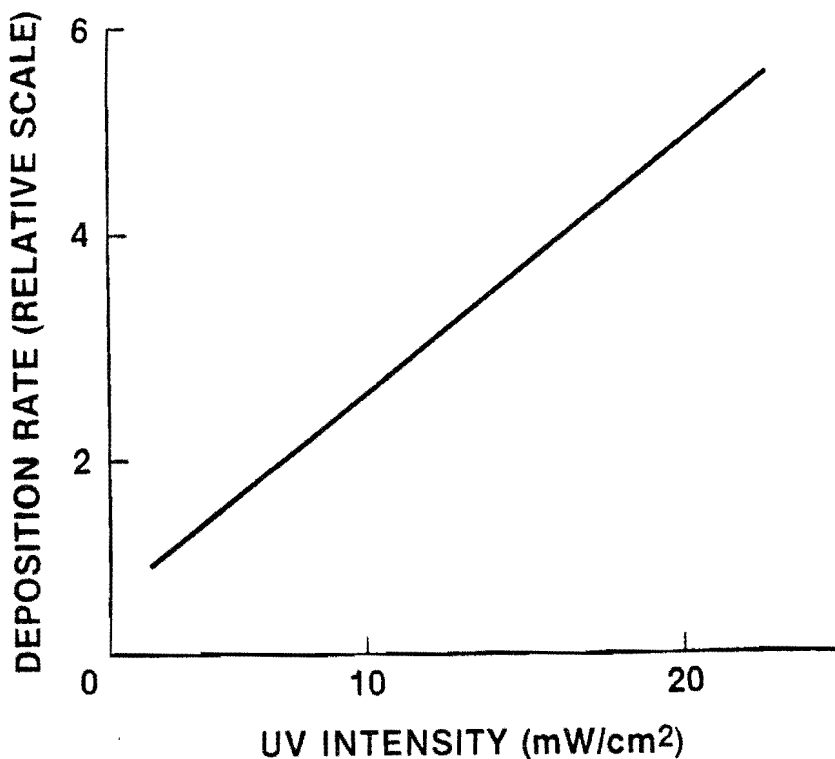
- PHOTON - ASSISTED PLASMA CHEMISTRY
- MAGNETRON SYSTEM

PHOTON - ASSISTED CHEMISTRY

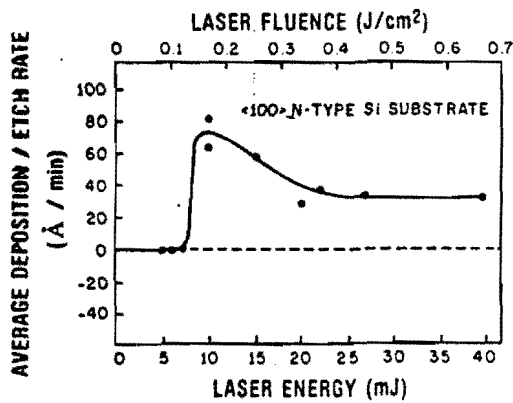
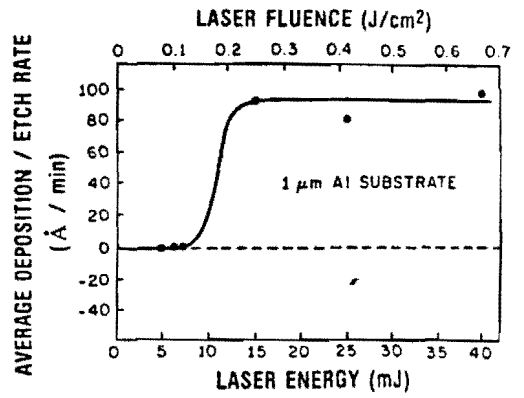
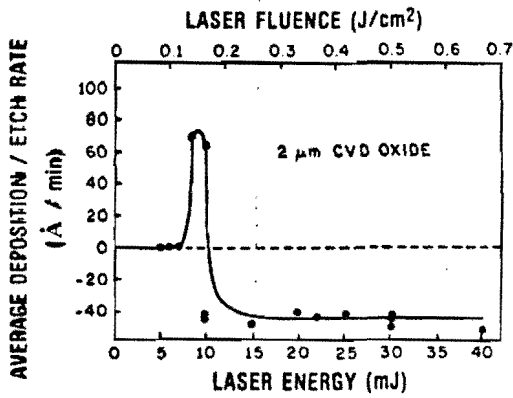
LASER ENERGY FOCUSED ONTO SUBSTRATE CAUSING LOCALIZED DEPOSITION, ETCHING, OR DOPING BY THERMALLY OR PHOTOCHEMICALLY DRIVEN REACTIONS.

DIRECT - WRITE PROCESS

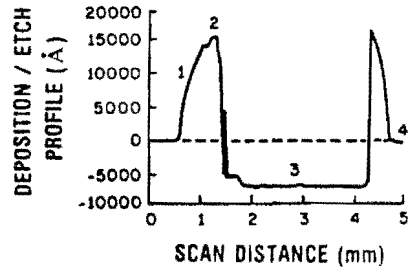
EFFECT OF INCREASE OF UV INTENSITY ON THE DEPOSITION RATE



PHOTON-ASSISTED PLASMA CHEMISTRY



PROFILE OF A CVD OXIDE SUBSTRATE ETCHED AT 0.25 J/cm² FOR 17 MINUTES.

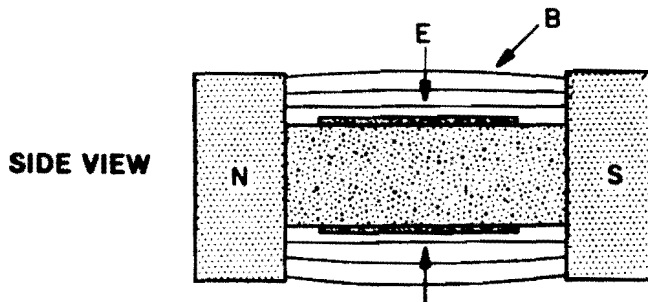


GEE & HARGIS, SPIE (1984)

MAGNETRON ENHANCED ETCHING

- INCREASED PLASMA REACTION
- RADICAL FORMATION FOR ETCHING OR PASSIVATION
- LOW ION BOMBARDMENT ENERGY
- MAGNETIC FIELD CONFINES PLASMA (ELECTRONS)
- LOWERS SUSTAINING VOLTAGE
- INCREASES ELECTRON DENSITY

MAGNETRON



LIN, ELECTRO CHEM. SOC. (1983)
 HORIIKE, ELECTRO CHEM. SOC. (1981)

PLASMA EQUIPMENT

BATCH vs. SWE

1. ANISOTROPY

BATCH : DIRECT IONS
SWE : RECOMBINANT CHEMISTRY

2. UNIFORMITY

BATCH : DIFFICULT WITHIN WAFER
SWE : GAS FLOW, ELECTRODE SHAPE

3. SELECTIVITY

BATCH : PHYSICAL SPUTTERING
SWE : ETCH RATE DOMINATES

4. THROUGHPUT (MMT JAN. 85, 125mm WAFERS)

BATCH : 30-80
SWE : 25-60

5. SCALE-UP FOR LARGER WAFERS

BATCH : DIFFICULT
SWE : EASY

6. MULTIPLE FILMS

BATCH : REDUCED EHO
SWE : ADDITIONAL MODULES

7. COST

BATCH : MED-HIGH
SWE : LOW-MEDIUM

8. FOOTPRINT

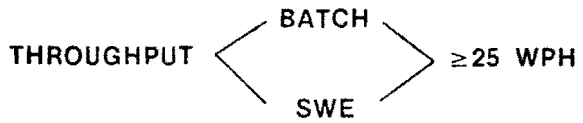
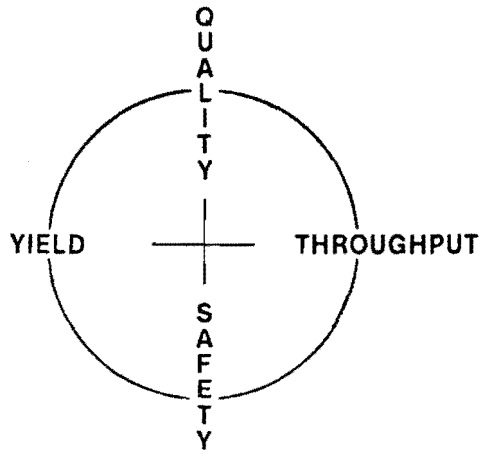
BATCH : MED-LARGE
SWE : LOW-MEDIUM

9. END-POINT AUTOMATION

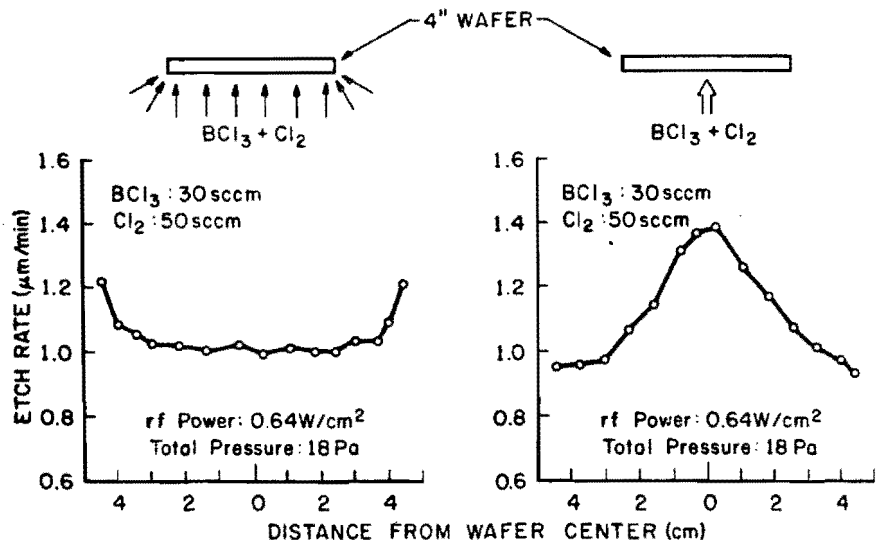
BATCH : DEPENDS ON W-W UNIFORMITY
SWE : DEPENDS ON WITHIN-W UNIFORMITY

10. CASSETTE-CASSETTE HANDLING

BATCH : SOME
SWE : ALL

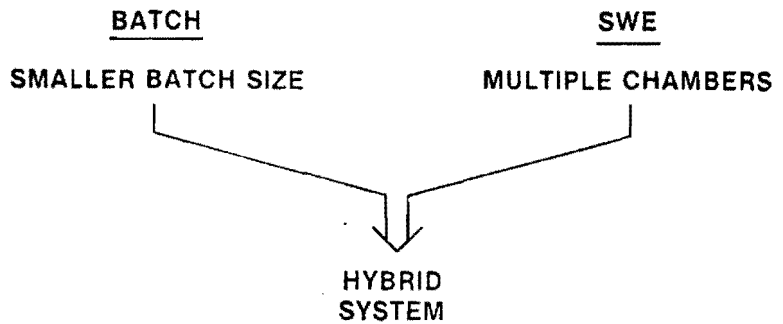


“SLOWER IS BETTER”



Horike, To be published

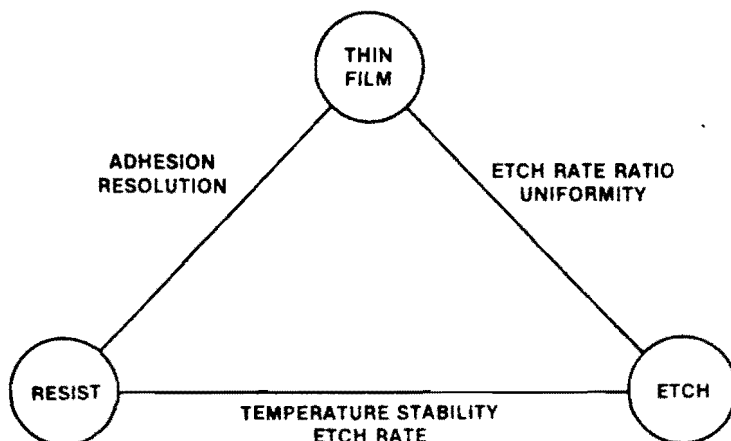
PLASMA EQUIPMENT FUTURE



FUTURE VLSI

ISSUES	REQUIREMENTS
FINER LINE DELINEATION	<ul style="list-style-type: none"> • $\Delta W < \text{PATTERN WIDTH} \times 1/10$ • NO "STRINGERS"
GATE OXIDE \longrightarrow 100 Å	<ul style="list-style-type: none"> • SELECTIVITY $> 30:1$ • UNIFORMITY $< \pm 5\%$ • NO OXIDE DAMAGE
PHOTO-LITHOGRAPHY	<ul style="list-style-type: none"> • $\Delta W < \text{PATTERN WIDTH} \times 1/10$ • PLANARIZATION
LARGE WAFER SIZE \longrightarrow 6 INCH	<ul style="list-style-type: none"> • UNIFORMITY $< \pm 5\%$ • THROUGHPUT ≥ 25 WAFERS/H
SUPER CLEAN ROOM \longrightarrow CLASS 10	<ul style="list-style-type: none"> • DECREASE IN OCCUPIED AREA • LOW PARTICULATES • AUTOMATION
MULTILEVEL METALLIZATION \longrightarrow 3-4 LAYERS	<ul style="list-style-type: none"> • NO INSULATOR INSTABILITY • PLANARIZATION • SELECTIVITY $> 20:1$ • LPCVD METAL

THE VLSI TRIANGLE



TOLLIVER, SOLID STATE TECHNOL (1980)

CAVEATAE DE PLASMUS

1. SAFETY FIRST! · NOT REGRETS LAST.
2. SLOWER IS BETTER!
3. F= ISOTROPY; CI= SPECIFICITY.
4. SWE= UNIFORMITY.
5. AVOID POLYMER AT ALL COSTS.
6. SIMPLE CHEMISTRIES ARE SOMEWHAT MORE TRACTABLE.
7. NO AMOUNT OF CLEVER PLASMATEERING CAN MAKE A POORLY CONCEIVED DESIGN MANAGEABLE.
8. A DEEP ABIDING FAITH IS NECESSARY TO CONNECT PLASMA PARAMETERS WITH MACHINE CONTROL KNOBS.
9. IF IT WERE EASY AND UNDERSTOOD, WE'D DO IT EVERY TIME.
10. PLASMA IS THE FINEST ENGRAVING TOOL IMAGINABLE.
11. PLASMA PATTERNING IS ONLY AS GOOD AS THE STENCIL AND MATERIAL QUALITIES OF THE MASK AND FILMS INVOLVED IN THE ETCH PROCESS.

REFERENCES

Articles

- D.L.Flamm and V.M.Donnely, PLASMA CHEM. and PLASMA PROCESSING, 1, 317(1981).
- J.W.Coburn, PLASMA CHEM. and PLASMA PROCESSING, 2, 1(1982).
- A.R.Reinberg, VLSI ELECTRONICS MICROSCIENCE, 2, 1(1981).
- R.H.Bruce, J. APPL. PHYS., 52, 7064(1981).
- H.F.Winters, J.W.Coburn and T.J.Chuang, J. VAC. SCI. TECH., 1, 469(1983).
- R.G.Poulsen, J. VAC. SCI. TECH., 14, 266(1977).
- R.L.Bersin, MICROELECTRONICS MANUFACT., p. 40, April 1984.
- J.L.Vossen, J. ELECTROCHEM. SOC., 126, 319(1979).
- L.M.Ephrath, J. ELECTROCHEM. SOC., 126, 1419(1979).
- C.J.Mogab and H.J.Levinstein, J. VAC. SCI. TECH., 17, 721(1980).

Books

- B.Chapman, GLOW DISCHARGE PROCESSING, John Wiley & Sons (1980).
- J.L.Vossen and W.Kern, THIN FLIM PROCESSES, Academic Press (1978).
- J.R.Hollahan and A.T.Bell, TECHNIQUES AND APPLICATIONS OF PLASMA CHEMISTRY, Wiley-Interscience (1974).
- 5 Monographs on Plasma Processing, Symposia Notes, Electrochemical Society, 1976-1985.

Journals

- Solid State Technology
 J. Vac. Sci. Tech.
 J. Electrochemical Soc.
 J. Appl. Phys.